INVESTIGATIONS ON THE IMPACT OF ELECTRIC VEHICLE CHARGING ON POWER DISTRIBUTION NETWORKS

A Thesis Submitted
In Partial Fulfillment of the Requirements
for the Degree of

DOCTOR OF PHILOSOPHY

by

SHEFALI PAINULI

(Roll No. 2K21/PHDEE/01)

Under the Supervision of

Prof. Suman Bhowmick and Prof. Radheshyam Saha



Department of Electrical Engineering

DELHI TECHNOLOGICAL UNIVERSITY

(Formerly Delhi College of Engineering)

Shahbad Daulatpur, Main Bawana Road, Delhi - 110042. INDIA

2026

©DELHI TECHNOLOGICAL UNIVERISITY, DELHI-2026
ALL RIGHTS RESERVED

DELHI TECHNOLOGICAL UNIVERSITY

(Formerly Delhi College of Engineering)
Shahbad Daulatpur, Main Bawana Road, Delhi-42

CANDIDATE'S DECLARATION

I hereby certify that the work which is being presented in the thesis entitled INVESTIGATIONS ON THE IMPACT OF ELECTRIC VEHICLE CHARGING ON POWER DISTRIBUTION NETWORKS in partial fulfillment of the requirements for the award of the degree of Doctor of Philosophy and submitted to the Department of Electrical Engineering, Delhi Technological University, is an authentic record of my own work carried out during the period from July, 2021 to December, 2025 under the supervision of Dr. Suman Bhowmick, Professor, Department of Electrical Engineering and Dr. Radheshyam Saha, Professor, Department of Electrical Engineering.

The matter presented in this thesis has not been submitted by me for the award of any other degree of this or any other Institute.

(Shefali Painuli)

DELHI TECHNOLOGICAL UNIVERSITY

(Formerly Delhi College of Engineering)
Shahbad Daulatpur, Main Bawana Road, Delhi-42

CERTIFICATE BY THE SUPERVISORS

Certified that **Shefali Painuli** (2K21/PHDEE/01) has carried out her work presented in this thesis entitled "**INVESTIGATIONS ON THE IMPACT OF ELECTRIC VEHICLE CHARGING ON POWER DISTRIBUTION NETWORKS**" for the award of **Doctor of Philosophy** from Department of Electrical Engineering, Delhi Technological University, Delhi, under our supervision. The thesis embodies results of original work, and studies are carried out by the student herself and the content of the thesis do not form the basis for the award of any other degree to the candidate or to anybody else from this or any other University/Institute.

(Prof. Suman Bhowmick)
Supervisor

(Prof. Radheshyam Saha)
Co-Supervisor

Date:

Abstract

Continuously depleting fossil fuels reserves, rising fuel costs and environmental concerns have led to the emergence of EVs as a popular choice of transportation. The rapid growth of EV adoption presents significant operational challenges for power distribution networks due to the stochastic, time-varying, and unbalanced nature of EV charging demand as it significantly affects power distribution network performance, causing distortions in the daily demand profile, increased power distribution network losses, and greater voltage magnitude deviations across the system. The concentrated and often uncoordinated charging load can place additional stress on network components, leading to reduced voltage stability and overall operational challenges. Accurate modeling of EV charging behavior and the development of effective mitigation strategies are therefore essential to ensure reliable and efficient grid operation under high EV penetration scenarios. The work in this thesis investigates the adverse effects of both slow residential and DC fast charging at public fast charging stations on power distribution network performance in detail and ways to improve the same.

Realistic models of slow residential charging and fast public charging are developed using travel behavior data from the 2017 National Household Travel Survey and operational data from a operator based in the US which provides fast charging services at the charging stations. The proposed models capture key characteristics such as the type of EV, charging start times, daily distance travelled, state-of-charge dependence, and charging duration. The impacts of EV charging demand are investigated on a real-world 240-bus radial power distribution network located in the Midwest United States. A key distinction of this distribution grid is the inclusion of one year's worth of smart meter data (hourly real and reactive power demands of all customers)for all nodes, thereby enabling realistic time-series analyses and facilitating more comprehensive planning and operational studies. The smart meter data spans from January 2017

to December 2017 which includes hourly energy consumption (kWh) for 1,079 customers. The network has 139 single-phase and 55 three-phase load buses. The customers allotted to each three-phase bus are distributed equally among the three single phases (A, B and C), in order to minimize the phase unbalance. Unlike standard IEEE and existing power distribution test systems, the 240-bus network provides the 24-hour real and reactive power demands of all the 1079 customers in the network. Simulation results demonstrate that slow residential charging increases network demand during afternoon and evening hours, while fast charging causes sharp morning demand spikes. Although slow charging leads to relatively smaller voltage magnitude deviations, fast charging results in severe voltage dips and increased network losses.

This underscores the need for practical demand-side management policy design, particularly time-of-use–based mechanisms, that can operate alongside realistic EV charging behavior while preserving system reliability. To mitigate the adverse effects, state-of-charge-based smart residential EV charging policies are proposed and evaluated by distributing EV loads across three network phases. The results show that coordinated charging significantly improves daily load profiles, reduces the network power losses, and enhances bus voltage profiles.

Beyond demand-side mitigation, the thesis explores network-side solutions through the optimal allocation of Distributed Generation resources. Appropriately sized distributed generation resources placed at suitable locations in the power distribution network have been reported to substantially improve the daily demand profile, bus voltage magnitude profile and also reduce distribution network losses. A novel human-based metaheuristic optimization algorithm, Driving Training-Based Optimization, is applied for the optimal siting and sizing of wind-based Distributed Generation units. The performance of driving training-based optimization is benchmarked against several established metaheuristic algorithms, demonstrating superior convergence behavior and solution quality. With single-objective driving training-based optimization formulation, the maximum reduction in the network real power loss is 45.65% whereas with multi-objective driving training-based optimization formulation, the maximum reductions in the network real power loss and voltage magnitude deviation are around 45.62% and 64.71% respectively.

Finally, a probabilistic planning framework is developed for the optimal deployment of solar photovoltaic and wind-based Distributed Generation units, incorporating uncertainties in EV charging demand, renewable energy generation, and seasonal variability. Real-world solar and wind datasets from NASA and specification from WT manufacturer and solar PV module manufacturer are utilized. The driving training-based optimization -based probabilistic planning approach results in reductions of approximately 54% in network Ohmic losses and 73% in voltage magnitude deviations, confirming the robustness and effectiveness of the proposed methodology.

Overall, this thesis demonstrates that realistic EV charging demand modeling, coordinated charging strategies, and optimally alocated renewable-based distributed generation resources are critical for enabling sustainable and reliable operation of future EV-integrated power distribution networks. The proposed frameworks provide valuable insights and practical tools for utility planners and policymakers to support large-scale EV integration.

Acknowledgements

First and foremost, my gratitude and appreciation must go to my advisors Prof. Suman Bhowmick and Prof. Radheshyam Saha, Department of Electrical Engineering, Delhi Technological University, for their invaluable support and guidance during the course of my Ph.D. studies. I consider this to be the highest degree of privilege to have completed my studies under their supervision.

I wish to express my deep sense of gratitude to Prof. Narendra Kumar II, Head of the Electrical Engineering Department, Delhi Technological University, for providing excellent facilities and a pleasant working atmosphere for the research work. I owe my deepest gratitude to my Ph.D. research committee for their valuable comments and input: Prof. Biswaroop Das, from the Department of Electrical Engineering, Indian Institute of Technology Roorkee; Dr. Arjun Tyagi, from the Department of Electrical Engineering, Delhi University; Prof. Rajiv Chaudhary, from the Department of Mechanical Engineering, Delhi Technological University, and Prof. S. T. Nagrajan, from the Department of Electrical Engineering, Delhi Technological University.

I extend my heartfelt gratitude to my parents, Dinesh Prasad Painuli and Sarita Painuli, whose unconditional love, sacrifices, and unwavering faith have been the cornerstone of my life and this journey. I am equally grateful to my brother, Shrey Painuli and best friend, Dr. Gade Kesava Rao, for their constant support, encouragement, and steadfast presence at every step. Their collective strength and belief in me have been my greatest source of inspiration, guiding me through every challenge and triumph.

I am also grateful to my dear friends - Divyanshu Khandelwal, Dr. Ganesh Jaiswal, Dr. Manvi Mishra, Dr. Shruti Prajapati, Arpana Singh, Dr. Poonam Kataria, Dr. Sudhanshu Mittal, Indrajeet Pal, Dr. Modassir Masoom, Dr. Brijender Senger, Dr. Arvind Goswami, Dhruv Kumar, Dr. Atul Awasthi, Dr. Deepak Kumar, Dr. Dipak Prasad, Dr. Ashutosh Gupta, Ayush, Divyansh Shelly, Dr. Rahma Aman, Nitisha Dharwade, Shilpa, Priya Rai, Kashika Baranwal, Dr. Meghna Srivastava, Apoorva Choumal, and, Dr. Komal - for their

companionship, encouragement, and countless moments of joy throughout the journey. Their presence has made this journey truly memorable and fulfilling.

I acknowledge the financial support provided by the Delhi Technological University – India, and the Department of Electrical Engineering, DTU, New Delhi, India, without which it would have been difficult to carry out the work.

I am also thankful to the Editor-in-Chiefs, Editors, and the reviewers of IEEE Transactions, Elsevier, and Springer for their constructive comments, which helped me gain deeper insights into the subject.

Finally, I thank, *Sarvocca Sarvaśaktimān Īśvara* for giving me strength at all times.

Date: Shefali Painuli

I dedicate this work to my grandfather, the Late Heeramani Painuli; parents, Dinesh Prasad Painuli and Sarita Painuli; and my brother, Shrey Painuli, for their boundless love, sacrifices, and unwavering support throughout my academic journey and life.

Contents

Abstract v
Acknowledgements viii
Table of Contents xii
List of Figures xvii
List of Tables xx
List of Acronyms xxiii
List of Symbols xxvi

1 Introduction 1
1.1 Power Distribution Networks 3
1.1.1 Overview of the Existing Power Distribution Networks 3
1.1.2 Description of the Time-Series Test System: 240-bus Iowa Power Distribution System 4
1.2 Electric Vehicles 6
1.2.1 Types of EVs 6
1.2.2 Hybrid Electric Vehicle 7
1.2.3 Plug-in Hybrid Electric Vehicle 8
1.2.4 Battery Electric Vehicle 9
1.2.5 Fuel-cell Electric Vehicle 10
1.3 Distributed Generation Resources 11
1.4 Effect of EV Charging on PDNs 12

2 Literature Review 17
2.1 Research Gaps 44
2.2 Motivation 46
2.3 Thesis Objectives 48

3 Modelling of EV Charging Demand and its Impact on PDNs 51
3.1 EV Charging Infrastructure 52
3.1.1 EV Charging Power Levels 52
3.2 EV Charging Technology 55
3.2.1 Battery Charging Methods for EVs 55
3.2.1 Constant Current 56
3.2.2 Constant Voltage 56
3.2.3 Constant Power 56
3.3 EV Charging Strategy 57
3.4 EV Charging Demand Modeling 58
3.4.1 Slow Charging 59
3.4.1 Charging Model of a PHEV 60
3.4.2 Charging Model of a BEV 61
3.4.2 Fast Charging 63
3.4.3 Estimating EV Demand Profiles Using the Data from the NHTS 65
3.4.4 Power Distribution Network 66
3.4.5 Direct Approach for Power-flow 67
3.5 Results and Discussions 69
3.6 Conclusions 72

4 Framing of EV Charging Policies to Mitigate EVCD Impact on PDNs 75
4.1 Methodology 76
4.1.1 Filtered NHTS 2009 Data 76
4.1.2 Charging strategy 77
4.1.3 Load Profile 78
4.2 Framework of Charging Policy 78
4.3 Results and Discussions 79
4.4 Conclusions 84

5 Impact Assessment of Residential EV Charging and Mitigation Using Optimal Allocation of Wind-Based DG Units 87
5.0.1 Chapter Contributions 88
5.1 Filtering NHTS 2017 Data 89

5.2 DG Operation 92
5.2.1 Power Output of a Wind Turbine 96
5.3 The DTBO Algorithm 99
5.3.1 Single-Objective DTBO Algorithm 101
5.3.2 Multi-Objective DTBO Algorithm 104
5.3.3 Sensitivity Analysis of DTBO 106
5.4 Case Studies and Results 109
5.4.1 Loss Sensitivity Factor 112
5.4.2 Analysis with Single-Objective DTBO 114
5.4.3 Analysis with Multi-Objective DTBO 116
5.4.4 Performance Evaluation of the Proposed Model Through Numerical Computations 117
5.4.5 Discussion 121
5.4.6 Practical Implementation Challenges and Future Work 123
5.5 Conclusions 123

6 A Probabilistic Framework for Optimal Allocation of Solar PV and Wind Turbine DGs in Distribution Networks with Residential and Fast EV Charging 125
6.0.1 Chapter Contributions 125
6.1 Framework For The Proposed Work 126
6.2 EVCD Model 127
6.3 Probabilistic Modelling of RBDG and Load 129
6.3.1 Processing of Historical Data 129
6.3.2 Modelling of WT Output Power 130
6.3.3 Modelling of SPV Module Output Power 131
6.3.4 Modelling of Load 134
6.4 System Overview 134
6.4.1 240-Bus PDN 134
6.4.2 EVCD Prediction Using Real Travel Survey Data 135
6.4.3 Structure of the TS-PFCS 136
6.4.4 Direct Approach for Load-Flow 136
6.4.5 Optimal Sizing and Siting of RBDG Units 137
6.5 Case Studies, Results and Discussions 137

6.6 Conclusions 148

7 Conclusions and Scope for Further Work 151
7.1 Conclusions of the Research 151
7.2 Social Impact of Research 153
7.3 Scope for Further Work 155

List of Publications 159

References 161

A Data for 240-Bus Power Distribution Network 181
A.1 Feeder C: Line Segment Data 183
A.2 Secondary Distribution Transformers 187

B NHTS Data 207

C NASA Data for Wind-speed and Solar-irradiance 209

D Manufacturer's Datasheet for Vestas 500 kW WT 211

E Manufacturer's Datasheet for SILFAB SOLAR 500kW SPV Module 213

List of Figures

1.1 240-Bus power distribution network [1] 5
1.2 Classification of EVs 7
1.3 Schematic diagram of EVs 8

3.1 Schematic diagram of charging ports and connectors developed according to various standards, [2] 53
3.2 CC-CV and CP-CV mode of charging [2, 3] 58
3.3 Arrival time probability for home based on NHTS 2017 Datasets 59
3.4 A generalized fast EV charging profile employing Tesla Supercharger [4] 62
3.5 Fast charging characteristics of EVs of different types at a PFCS [4, 5] 63
3.6 Arrival time probability for EVs at fast charging station based on NHTS 2017 Datasets 65
3.7 Topology of 240-bus PDN 66
3.8 A Simplified 6-Bus Distribution Network 67
3.9 Total per-phase demand of the network 70
3.10 Network total three-phase demand 71
3.11 Network bus voltage magnitude profiles for (a) Slow and (b) Fast charging 71

4.1 Total Demand Profile for 240-Bus Distribution System for Different Scenarios 79
4.2 Bus Voltage Magnitude Profile for 240-Bus Distribution System for Phase-A at 18:00 hrs for Different Scenarios 80
4.3 Bus Voltage Magnitude Profile for 240-Bus Distribution System for Phase-B at 18:00 hrs for Different Scenarios 81
4.4 Bus Voltage Magnitude Profile for 240-Bus Distribution System for Phase-C at 18:00 hrs for Different Scenarios 81

4.5 24-hours Bus Voltage Magnitude Profile for Single-Phase Bus 3147 without and with PHEV Charging Policy 82
4.6 24-hours Bus Voltage Magnitude Profile for Three-Phase Bus 3034 without and with PHEV Charging for Phase-A 82
4.7 24-hours Bus Voltage Magnitude Profile for Three-Phase Bus 3034 without and with PHEV Charging for Phase-B 83
4.8 24-hours Bus Voltage Magnitude Profile for Three-Phase Bus 3034 without and with PHEV Charging for Phase-C 84

5.1 Architecture of the proposed work. 89
5.2 Flowchart for the proposed work. 90
5.3 Vehicle arrival time pattern from NHTS 2017 data 92
5.4 Flowchart for distribution of EVs from NHTS data to the 240-bus PDN and estimation of EVCD 93
5.5 Daily demand profile for 240-bus PDN 94
5.6 Variation of network Ohmic losses with DG 95
5.7 Allocation of HOUSEIDs to PDN buses 95
5.8 Wind speed plot for a typical weekday of May 96
5.9 Various distribution fits for the annual windspeed data 97
5.10 Output power of wind-based DG for a typical May weekday 97
5.11 Convergence curves of DTBO and other popular algorithms with the Sphere function 98
5.12 Flowchart of the DTBO Algorithm 100
5.13 Convergence curves of DTBO and other popular algorithms with the Rastrigin function 105
5.14 Sensitivity analysis of the optimal DG capacity for wind energy using DTBO under varying wind speeds and EV demand 108
5.15 Comparison of P_{Tloss} and VD with w_1 111
5.16 Comparison of P_{Tloss} and VD with w_2 112
5.17 Bus voltage magnitude profile for phases 'A', 'B', and 'C' at 21:00 hours with (a) exactly 1 PHEV per house, (b) at most 2 PHEVs per house, and (c) at most 3 PHEVs per house 118
5.18 The comparison of the convergence based for Case I, II and III with single and multi-objective objective 120

6.1 Outline of the proposed work 128
6.2 Seasonal profiles of (a) windspeed and (b) solar irradiance at the site under study 130
6.3 Seasonal variation of the predicted output powers of a single (a) WT and (b) SPV module 132
6.4 Seasonal variation of the predicted base demand for the 240-bus PDN 135
6.5 Procedure for EVs modelling and allocation in the 240-bus PDN 136
6.6 Flowchart of the DTBO algorithm for optimal allocation of RBDGs 138
6.7 Predicted network demand profiles with EV charging 140
6.8 Normalized mean output of a single WT and SPV module 141
6.9 Convergence characteristics of DTBO, COA and IGWO 144
6.10 Boxplot of the objective function value for 30-runs obtained with: (a) DTBO, COA and IGWO; and (b) DTBO. 145
6.11 Bus voltage profile for Phase A, B and C at 07:00 hours 147

7.1 Alignment of the Research with SDGs 157

List of Tables

1.1 Overview of benchmark PDNs in the literature [6], [7] 14
1.3 Specifications Of Different EV Models 15

3.1 EV Charging Levels [2, 3] 54
3.3 PHEV40 battery capacities and ECPM for different types of vehicles [8] 60
3.4 EV Specifications for Slow Charging 62
3.6 EV Specifications for Fast Charging 64

4.1 Filtered NHTS 2009 Data 77

5.1 Sample of Filtered NHTS 2017 Data 91
5.3 Specifications of the wind turbine 98
5.4 Details of Benchmark Functions (BMFs) 107
5.6 DG Placement Results: Single-Objective DTBO 113
5.7 Fine-Tuned Control Parameters 114
5.8 DG-Placement Results: Multi-Objective DTBO (Network Power Loss) 115
5.10 DG-Placement Results: Multi-Objective DTBO (Voltage Deviation) 116
5.12 Comparative Performance Evaluation for Single and Multi-Objective Problem for the Proposed Case Studies 122

6.1 Overview of EVs Considered for Study 127
6.3 Selection of WT- and SPV-based DGs 142
6.5 Results for the Statistical Performance of DTBO, IGWO and COA for 30 Runs 145
6.7 Results of Multi-Objective Optimization Using DTBO 146

A.1 Line Segment Data for Feeder A 181
A.2 Line Segment Data for Feeder B 182

A.2 Line Segment Data for Feeder B 183
A.3 Line Segment Data for Feeder C 184
A.3 Line Segment Data for Feeder C 185
A.3 Line Segment Data for Feeder C 186
A.3 Line Segment Data for Feeder C 187
A.4 Circuit Breaker Data for 240-Bus Test System 187
A.6 Three-Phase Shunt Capacitor Bank 187
A.7 Equivalent Voltage Source 187
A.9 Tap Changer Settings 188
A.10 Substation Transformer 188
A.12 Line Configuration 1: OH_3p_type1 188
A.13 Line Configuration 2: OH_2p_type2 189
A.14 Line Configuration 3: OH_1p_type2 189
A.15 Line Configuration: OH_3p_type5 190
A.16 Line Configuration: OH_1p_type5 190
A.17 Line Configuration: UG_3p_type1 191
A.18 Line Configuration 5: UG_3p_type2 192
A.19 Line Configuration 6: UG_1p_type2 193
A.20 OH Neutral: #2/0 ACSR 6/1 193
A.21 OH Neutral: 1 ACSR 6/1 194
A.22 Geometric Mean Distance Parameters for Construction Type 1 194
A.23 Geometric Mean Distance Parameters for Construction Type 2 194
A.24 Three-phase Secondary Distribution Transformers 195
A.25 Single-phase Secondary Distribution Transformers 196
A.27 Single-Phase Center-tapped Secondary Distribution Transformer (cont.) 197
A.28 Spot Loads 199

D.1 Specifications of Vestas V39 WT [9] 211

E.1 Specifications of SIL-500 HM SPV Module [10] 213

List of Acronyms

EVs	Electric Vehicles
DG	Distributed Generation
DTBO	Driving Training-Based Optimization
PHEV	Plug-in Hybrid Electric Vehicles
ICEV	Internal Combustion Engine Vehicle
HEV	Hybrid Electric Vehicle
BEV	Battery Electric Vehicles
FCEV	Fuel Cell Electric Vehicles
CD	Charge depleting
CS	Charge sustaining
SoC	state of charge
CB	Charge blended
DER	Distributed Energy Resources
RES	Renewable Energy Sources
EVPL	EV Parking Lots
PDN	Power Distribution Network
EVCS	Electrical Vehicle Charging station
VSI	Voltage Stability Index

PEV Plug-in Electric Vehicles

EBCS Electric Bus Charging Stations

B2G Bus-to-Grid

NC-and-CG nested column-and-constraint generation

D-ST-GNN Dynamic Spatio temporal Graph Neural Networks

G2V Grid-to-Vehicle

AIMD Additive Increase–Multiplicative Decrease

GMM Gaussian Mixture Models

PCE Polynomial Chaos Expansion

EVDS Electric Vehicle Docking Stations

SPV Solar Photovoltaic

IGDT Information Gap Decision Theory

ADMM Alternating Direction Method of Multipliers

ToU Time-of-Use

PV Photovoltaic

CC Constant Current

CV Constant Voltage

CP Constant Power

EVCD EV Charging Demand

BIBC Bus-Injection to Branch-Current

BCBV Branch-Current to Bus-Voltage

DLF Distribution Load Flow

SAE	Society of Automotive Engineers
NHTS	National Household Travel Survey
WECS	Wind Energy Conversion System
GA	Genetic Algorithm
IGWO	Improved Grey Wolf Optimization
PSO	Particle Swarm Optimization
TLBO	Teaching Learning Based Optimization
COA	Coati Optimization Algorithm
IEM	Iowa Environmental Mesonet
PDF	Probability Distribution Function
BMF	Benchmark Mathematical Functions
VD	Voltage Deviation
WSM	Weighted Sum Model
PFCS	Public Fast Charging Stations
WT	Wind Turbine
ND	Network Demand
RBDG	Renewable Based Distributed Generation
CDF	Cumulative Density Function
TND	Total Network Demand

List of Symbols

C_{batt}	Usuable battery capacity of a PHEV	kWh
AER	All-Electric-Range of a PHEV	–
$ECPM$	Electrical energy consumption per mile	kWh
α	Percentage of distance travelled in electric mode	–
d	Distance travelled by EV in a day	miles
η	Efficiency of EV battery charging	–
E_g	Energy required for EV battery charging	kWh
ch_level	EV charging rate	kW
E_{cap}	EV battery capacity	kWh
$P(t)$	Power drawn by EV at time $'t'$ during fast-charging	kW
$S(t)$	State-of-charge of EV battery at time $'t'$	–
k_d	Exponential decay constant for TS	–
P_{max}	Initial charging power	kW
c	Scale indices of the Rayleigh distribution	–
ν	Wind speed	m/s
C_p	Turbine performance coefficient	–
ρ	Air density	kg/m^3
R	Radius of the turbine	m
$P_{w,r}$	Rated power output of wind turbine	kW
ν_w, ν	Wind speed	m/s
ν_r	Rated wind speed	m/s
ν_{ci}	Cut-in wind speed	m/s
ν_{co}	Cut-out wind speed	m/s
P_{Tloss}	Network Ohmic losses	kW
VD	Network voltage deviation	p.u.
I_j	Magnitude of current in the j^{th} branch	A

r_j	Resistance of branch in the j^{th} branch	Ω
V_z	Voltage magnitude at node z	p.u.
w_1, w_2	Weights related to PDN losses and VD	–
$P_{DG,z}$	Active output power of DG at node z	kW
$P_{DG,min}$	Minimum value of $P_{DG,z}$	kW
$P_{DG,max}$	Maximum value of $P_{DG,z}$	kW
V_{min}	Minimum voltage of V_z	p.u.
V_{max}	Maximum voltage of V_z	p.u.
$I_{max,j}$	Thermal limit of branch j	A
$P_{eff}[q]$	Total effective active power supplied beyond node q	kW
$\sigma_v, \sigma_s, \sigma_L$	Standard deviation of windspeed, solar irradiance, and load, respectively	–
μ_v, μ_s, μ_L	Mean of windspped, solar irradiance, and load respectively	–
$\Gamma(\cdot)$	Gamma function	–
r	Uniformly distributed random number on $[0, 1]$	
P_{WT_g}, P_{PV_g}	Power generation of WT and PV module for $v = v_g^t$ and $s = s_g^t$, respectively	kW
v_g^h, s_g^h, L_g^h	Windspeed, solar irradiance, and load at state $'g'$ and hour $'h'$	–
$\text{erf}(\cdot)$, $\text{erf}^{-1}(\cdot)$	Error and inverse error functions	–
$f_v(v_g^h), f_s(s_g^h), f_L(L_g^h)$	Probability of windspeed, solar irradiance, and load at state $'g'$ and hour $'h'$	–
P_{Tloss}^{base}	Base case network Ohmic losses	kW
b	Total number of network branches	–
$\frac{\partial P_{Tloss}}{\partial P_{eff}}$	Loss sensitivity factor	–
N	Population size of DTBO	–
m	Number of problem variables	–
t, T	Current and maximum number of iteration(s), respectively	–
F_i	Objective function value by i^{th} candidate	–

K_i	Randomly selected from $\{1, 2, \ldots, N_{DI}\}$	–
DI_i, $DI_{k_i,j}$	Driving instructor matrix and randomly selected DI to train the i^th member in the j^th dimension	–
$X_i^{P1}, X_i^{P2}, X_i^{P3}$	Newly calculated status of the i^{th} candidate solution in DTBO phases 1–3	–
$x_{i,j}^{P1}, x_{i,j}^{P2}, x_{i,j}^{P3}$	j^{th} dimension of $X_i^{P1}, X_i^{P2}, X_i^{P3}$, respectively	–
$F_i^{P1}, F_i^{P2}, F_i^{P3}$	Objective fumction value of the i^{th} candidate solution in phases 1–3 of DTBO	–
$F_{DI_{k,i}}$	Objective function value of $DI_{k,i}$	–
PI	Patterning Index	–

Chapter 1

Introduction

The primary objective of utility distribution systems is to deliver electrical energy to end-users in a reliable and economically efficient manner at the point of consumption. Effective power distribution system planning is therefore critical to ensure a cost-effective, reliable, and high-quality power supply. The distribution planning problem can be formulated to satisfy multiple design requirements, including the ability to efficiently meet load demand, minimize feeder losses, adapt to fluctuations in supply and demand, and maintain service continuity during outages. However, formulating an optimization problem that simultaneously satisfies all of these design constraints is inherently complex. To address this complexity, distribution network requirements are typically prioritized and the overall planning task is decomposed into a set of smaller optimization problems.

Traditionally, power distribution systems have been planned to minimize cost while providing reliable power to connected loads. Reliability of operation and quality of service have historically been achieved through the installation of additional equipment and protective systems, rather than being explicitly embedded in the distribution circuit design stage. Consequently, conventional distribution planning algorithms have not directly incorporated power quality and system reliability considerations into their core design framework [7].

However, in the past decade, the electric power grid has undergone transformative changes that require significant revisions in how distribution systems are designed, operated, and controlled. The electrification of transportation is emerging as one of the most disruptive transformations in modern power systems. Continuously depleting fossil fuels reserves, rising fuel

costs and environmental concerns have led to the emergence of EVs as a popular choice of transportation. However, with the rapid adoption of EVs, electricity demand profiles are experiencing fundamental changes. With increased EV penetration levels, the PDN may suffer distortion in the daily load profile, low bus voltage magnitudes, enhanced line losses, increased phase unbalance, poor power quality and voltage stability issues [11–15]. Large-scale EV charging demand also puts additional strain on distribution networks. These issues need to be addressed appropriately for proper PDN operation. Unlike traditional residential, commercial, and industrial loads, EV charging introduces large, stochastic, and often simultaneous demands on the distribution network [12], [14]. The planning of PDNs must therefore evolve to accommodate this new class of load while ensuring system reliability, efficiency, and sustainability. Moreover, the stochastic nature of renewable generation, coupled with the variability of EV charging demand, poses new challenges to the stability and reliability of traditional distribution systems. These challenges highlight the need to integrate emerging technologies and their impacts into modern PDN planning frameworks.

Recognizing that redesigning existing PDN circuits is often neither economical nor practical, the thesis develops methodologies to assess the impacts of EV integration and implement effective mitigation strategies within existing infrastructure of the PDNs. Additionally, the thesis explores the optimal allocation of distributed generation resources to meet the additional demand introduced by EV charging, thus enhancing the reliability of the system. To achieve these objectives, the thesis is structured around the following research tasks:

1. Modeling of emerging EV charging demand for both residential users and public fast-charging stations using realistic, data-driven datasets.

2. Performance assessment of existing utility distribution networks under EV charging demand, with emphasis on daily load dynamics, total network Ohmic losses, and bus voltage magnitude deviation.

3. Development of demand-side management strategies, such as time-of-use policies, to alleviate the additional stress imposed by EV charging and to preserve the system reliability.

4. Mitigation of the detrimental effects of both slow residential and public fast charging of EVs on PDNs through the optimal allocation of wind and solar photovoltaic-based distributed generation resources using different meta-heuristic techniques.

5. Formulation of a probabilistic planning model for the optimal siting and sizing of solar photovoltaic and wind turbine based distributed generation in PDNs with both residential and public fast EV charging demand, aiming to minimize PDN Ohmic losses and bus voltage magnitude deviations under operational and uncertainty constraints.

1.1 Power Distribution Networks

Benchmark test systems are essential tools for researchers in the field of PDNs. They serve as standardized models that enable the validation of new algorithms, comparative studies, and performance assessments under controlled conditions. By using well-established networks, researchers can test planning, operation, and control strategies while ensuring that their findings remain comparable to other studies in the literature.

1.1.1 Overview of the Existing Power Distribution Networks

Over the years, several benchmark networks have been developed and made available to the researchers, such as IEEE test feeders, UK Generic Distribution System, European low-voltage feeder, and other utility-based datasets [6], [7]. Each of these networks has its own structure, specifications, and modeling assumptions, making them suitable for different types of studies. However, a notable limitation is that most benchmark networks do not provide time-sequence load data, making it difficult to capture realistic load variations over a 24-hour period.

Despite their wide application, a major limitation of most benchmark distribution networks is the absence of time-sequence load data. Real-world power systems experience dynamic demand variations within a 24-hour cycle driven by consumer behavior, weather conditions, and economic activities. Without incorporating such time-dependent data, research is often restricted to

steady-state analysis, which cannot fully capture the operational complexities of modern distribution systems. Existing test feeders are typically static, single-snapshot models that lack real time-series measurements, thereby hindering their suitability for quasi-static time-series analyses that require capturing time-varying load behaviors. Among the widely used benchmark systems, the IEEE European Low Voltage Test Feeder is the only network that provides time-series load data; however, its application remains limited because the available dataset spans only a single day, which may be insufficient for long-term system behavior assessment.

To address the above limitations, this chapter reviews commonly adopted benchmark PDNs, highlights their specifications and research relevance which is presented in Table 1.1 [6]. Additionally, this section introduces the Iowa 240-bus power distribution test system. Unlike several standard distribution test systems (Table 1.1), the Iowa system provides smart meter-based 24-hour load profiles for every bus, thereby enabling realistic time-series analyses and facilitating more comprehensive planning and operational studies.

1.1.2 Description of the Time-Series Test System: 240-bus Iowa Power Distribution System

The 240-bus time-series test system represents a radial PDN comprising three feeders, incorporating 240 primary buses and approximately 23 miles of conductors, all supplied through a 69/13.8 kV three-phase step-down substation transformer as shown in Fig. 1.1. The substation transformer has a rating of 10,000 kVA. This power distribution system belongs to a municipal utility in the Midwestern state of Iowa, U.S.A. The network [1] has secondary side voltages of 120 V and 208 V and has smart meters installed at all the customer premises. The network has 139 single-phase and 55 three-phase load buses.

A key distinction of this distribution grid is the inclusion of one year's worth of smart meter data for all nodes, bridging the gap between current test feeders and quasi-static time series-based distribution system analysis. In this test system, the time-series data for each node is derived directly from customers' smart meter measurements, covering the period from January 2017 to December 2017. The dataset includes hourly active power consumption (kW), reactive

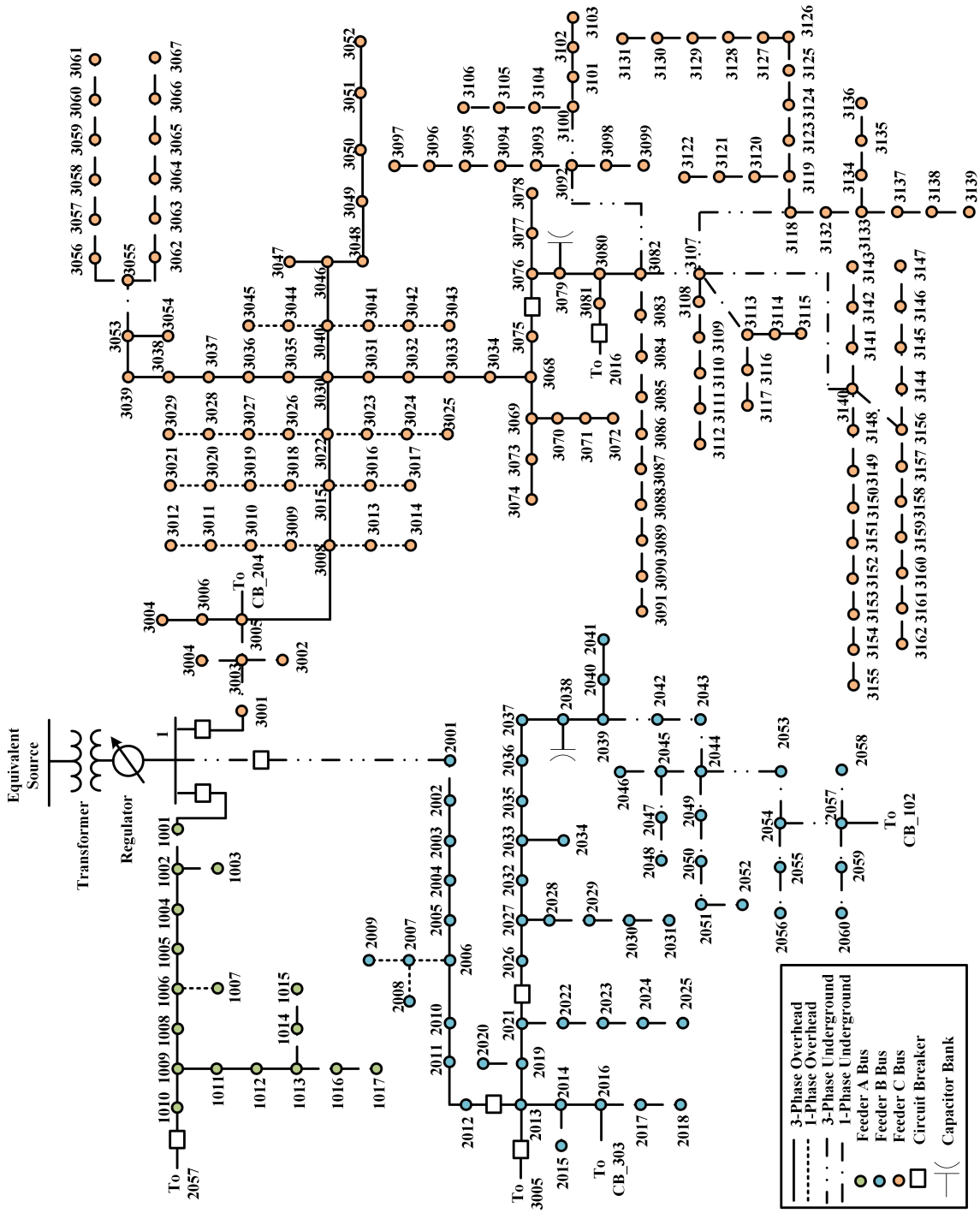


Fig. 1.1: 240-Bus power distribution network [1]

power consumption (kVar), and energy consumption (kWh) records from 1,079 customers. Unlike short-term demand profiles, the availability of a full year of load data of this network enables the capture of seasonal variations in customer behavior, thereby providing a more realistic representation of demand patterns.

1.2 Electric Vehicles

The transportation sector is undergoing a paradigm shift driven by the need to reduce greenhouse gas emissions, improve air quality, and energy security. At the forefront of this transformation are EVs, which offer a sustainable alternative to traditional ICE vehicles. Despite their early emergence, EVs remained a niche segment within the automotive market due to various technological and economic challenges. Recent advances in EV technologies have revived interest, with a growing adoption driven by key advantages such as zero tailpipe emissions, reduced dependence on fossil fuels, high energy efficiency, and low noise operation.

1.2.1 Types of EVs

EVs incorporate a combination of electrical and fuel energy that drives them. The electric motor provides propulsion either independently or in coordination with an ICE, depending on the vehicle architecture. In addition, the motor operates in regenerative mode during braking and deceleration, utilizing a bidirectional DC-AC converter to recover kinetic energy and charge the battery. During normal driving conditions, the converter facilitates the transfer of electrical energy from the battery to the motor. Battery recharging is achieved through an external electrical power source through the charging system. Based on the extent of electric power utilization, EVs are broadly categorized into two main types: hybrid vehicles and all-electric vehicles, as shown in Fig. 1.2. Moreover, the schematic diagram of these types is presented in Fig. 1.3.

Hybrid vehicles combine the design of a traditional ICE vehicle with a battery that powers the vehicle using both fuel and electric energy. The battery's capacity determines the vehicle's electric-only driving range. Hybrid Electric Vehicles and Plug-in Hybrid Electric Vehicles are two common types of hybrid

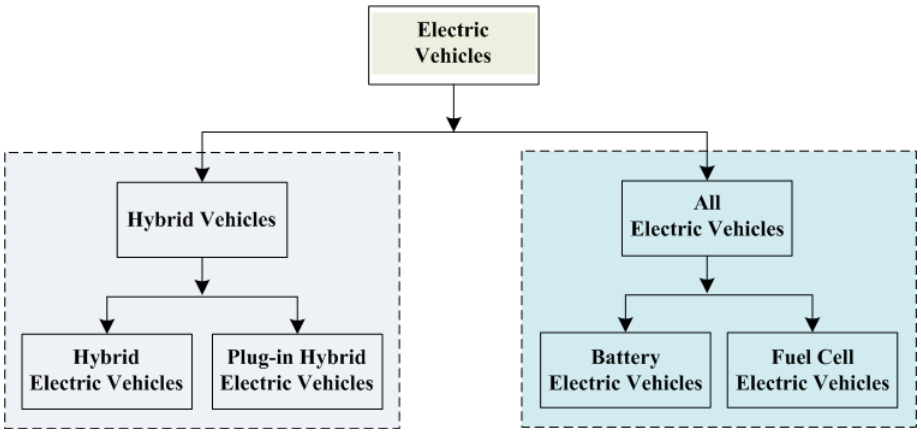


Fig. 1.2: Classification of EVs

vehicles. In contrast, AEVs are powered solely by electric motors, which are fueled by electrical sources. They can be divided into two categories: Battery Electric Vehicles and Fuel Cell Electric Vehicles.

1.2.2 Hybrid Electric Vehicle

HEVs include an ICE, a larger electric motor, and a battery. These vehicles operate similarly to standard ICE vehicles, but can also run on battery power for short distances. HEVs cannot be charged from the electric grid; instead, the battery charges automatically through regenerative braking, converting kinetic energy into electrical energy when the ICE is lightly loaded. Popular HEV models include Audi Q5 Hybrid, Acura ILX Hybrid, Cadillac Escalade Hybrid, BMW Active Hybrid 3, 5, and 7, Honda Civic Hybrid, and Honda CR-Z Hybrid.

Advantages of HEVs:

- Longer driving range than BEVs
- Reduced fuel consumption compared to conventional ICE vehicles
- Lower emissions than traditional ICE engines

Disadvantages of HEVs:

- Do not achieve zero tailpipe emissions
- More complex operational mechanisms

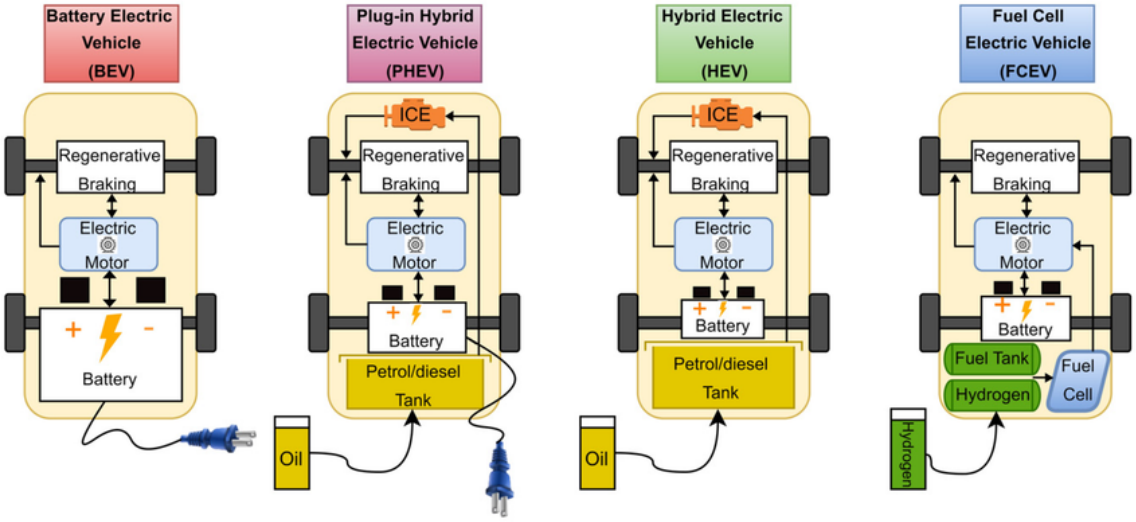


Fig. 1.3: Schematic diagram of EVs

- Higher operational costs compared to BEVs

1.2.3 Plug-in Hybrid Electric Vehicle

PHEVs function similarly to HEVs but feature a larger battery pack that can be charged via both regenerative braking and plugging into the power grid. PHEVs are equipped with a more powerful electric motor than HEVs, enabling them to run entirely on electricity with the ICE switched off. PHEVs primarily operate in two modes: CD and CS. In CD mode, the vehicle runs exclusively on battery power until the SoC, which indicates the remaining battery level, reaches a predefined minimum threshold. Once this point is reached, the vehicle switches to CS mode, where ICE takes over to power the vehicle and maintain the battery charge near the minimum SOC.

To further enhance fuel efficiency and reduce emissions, a third operating mode called CB has been introduced. In CB mode, both the electric motor and ICE are used in an optimized and dynamic manner throughout the drive cycle to achieve maximum efficiency and minimal environmental impact. Popular PHEV models include the BMW i3, BMW i8, Cadillac ELR, GM Chevy Volt, Porsche SE, Ford Fusion Energi, Ford C-Max Energi, and Toyota Prius Plug-in.

Advantages of PHEVs:

- Extended driving range
- Lower fuel consumption than traditional ICE vehicles
- Reduced environmental emissions

Disadvantages of PHEVs:

- Do not completely eliminate environmental pollution
- Generally, more expensive to operate than BEVs

1.2.4 Battery Electric Vehicle

A BEV operates solely using an electric motor and an onboard battery pack, without relying on a traditional ICE. BEVs are recharged by connecting to an electrical power source when their batteries are depleted. In addition, they can recover energy through regenerative braking, a process in which the electric motor helps slow the vehicle down and converts the kinetic energy, normally lost as heat through braking, back into stored electrical energy. Popular BEVs on the market include the Tesla Model S, Nissan Leaf, BMW i3, Mitsubishi iMiEV, Smart EV, and Ford Focus EV.

Advantages of BEVs:

- Zero tailpipe emissions
- No need for gasoline or oil refueling
- Convenient home charging
- Quick and smooth acceleration
- Generally lower operating costs

Disadvantages of BEVs:

- Shorter driving range compared to ICE vehicles
- Higher upfront cost, although fuel savings typically offset this within 2–3 years

1.2.5 Fuel-cell Electric Vehicle

FCEVs are EVs that generate electricity onboard using a hydrogen fuel cell instead of storing electricity in a battery like BEVs. The fuel cell combines hydrogen (stored in high-pressure tanks) with oxygen from the air to produce electricity, with only water vapor and heat as byproducts. FCEVs use this electricity to power an electric motor for propulsion, making them a clean alternative to traditional ICE vehicles. Popular FCEVs models include: Toyota Mirai, Hyundai NEXO, Honda Clarity Fuel Cell, Mercedes-Benz GLC F-CELL, BMW iX5 Hydrogen (limited release).

Advantages of FCEVs:

- Zero tailpipe emissions since only water vapor is emitted during operation
- Fast refueling time, Similar to gasoline cars (typically 3–5 minutes)
- Long driving range which is comparable to or greater than many BEVs
- Quiet and smooth ride
- Less dependence on the electric grid as hydrogen stations can operate independently

Disadvantages of FCEVs:

- Limited hydrogen refueling infrastructure, especially outside of major urban areas
- High production cost as fuel cells and hydrogen storage systems are expensive
- Hydrogen production challenges since mat present, most hydrogen is produced from fossil fuels
- Energy inefficiency since the hydrogen-to-electricity conversion process is less efficient compared to using electricity directly (as in BEVs)

The specifications of the popularly known electric vehicles are outlied in the Table 1.3.

1.3 Distributed Generation Resources

DERs or Distributed Generations DGs refer to small- to medium-scale energy generation, storage, and controllable load resources that are located close to electricity consumers and are connected directly to PDNs rather than centralized transmission systems [16–18]. Unlike conventional large-scale power plants, DERs enable decentralized electricity production and localized energy management, thereby transforming traditionally passive distribution networks into active and flexible systems. Solar PV and wind energy have gained particular prominence due to their environmental benefits, declining installation costs, and suitability for deployment within distribution networks [19, 20]. Energy storage systems and EVs further enhance DER functionality by providing temporal flexibility, allowing energy to be stored or shifted to periods of high demand [21].

The integration of DERs plays a critical role in modern PDNs. By generating electricity close to the point of consumption, DERs reduce the reliance on upstream transmission systems, lower power flows through distribution feeders, and decrease Ohmic losses [22, 23]. Additionally, DERs contribute to improved voltage regulation by supporting local voltage profiles, especially in networks experiencing high demand or significant load variability [24]. These capabilities are particularly valuable in PDNs facing increasing stress from electrification trends such as widespread EV adoption.

Proper sizing and siting of DERs are essential to fully realize their benefits within the PDNs. Inappropriately sized or poorly located DER units can lead to operational challenges such as voltage rise, reverse power flow, thermal overloading of feeders, and protection coordination issues [25, 26]. Conversely, optimally placed and correctly sized DERs can enhance system performance by balancing local generation and demand, maintaining voltage magnitudes within permissible limits, and reducing network losses [27, 28]. Strategic DER deployment also enables effective utilization of renewable energy while respecting network operational constraints.

DERs further contribute to grid resilience and operational flexibility. During peak demand periods or contingencies, DERs can supply local loads, reduce congestion, and support grid restoration efforts [29]. The combination of

renewable generation, energy storage, and flexible EV charging enables PDNs to respond dynamically to variations in load demand and generation availability [30]. This adaptability is increasingly important as power systems transition toward low-carbon and decentralized architectures.

In summary, distributed energy resources represent a foundational component of future-ready PDNs. Through localized generation, flexible operation, and coordinated planning, DERs enhance the efficiency, reliability, and sustainability of PDNs while supporting the integration of renewable energy and emerging electrified loads [18].

1.4 Effect of EV Charging on PDNs

The rapid adoption of EVs introduces a new and significant class of electrical load in PDNs. Unlike conventional residential or commercial loads, EV charging demand is highly variable in time, location, and magnitude, and is strongly influenced by user behavior, mobility patterns, and charging infrastructure availability [12, 24, 31, 32]. As EV penetration increases, their cumulative charging demand becomes a critical factor shaping the operational performance of PDNs.

Residential EV charging typically occurs during evening and nighttime hours when vehicles are parked at home. This coincides with existing peak demand periods in many distribution systems, leading to an increase in feeder loading and transformer utilization [33, 34]. Uncoordinated residential charging can significantly elevate daily peak demand, intensify load ramping, and increase thermal stress on distribution assets [35, 36]. These effects are particularly pronounced in low-voltage networks, where infrastructure was not originally designed to accommodate high-power charging loads [37].

Public and fast-charging stations introduce additional challenges due to their high power ratings and concentrated demand. Fast chargers can impose large, impulsive loads on the distribution network, resulting in localized voltage drops, increased current flows, and potential violations of thermal limits. The stochastic arrival of vehicles at public charging stations further amplifies uncertainty in network operation, complicating load forecasting and operational planning

[23, 38]. As a result, fast-charging infrastructure can significantly alter power flow patterns within PDNs.

Voltage regulation is one of the most critical concerns associated with widespread EV charging. Increased charging demand can cause voltage magnitude deviations, particularly at buses located far from substations or in weak network sections [22]. In extreme cases, sustained EV charging can lead to undervoltage conditions, reduced power quality, and customer service issues. The spatial distribution of EV charging loads plays a key role in determining the severity of voltage impacts across the network.

EV charging also contributes to increased PDN losses. Higher current flows during charging periods result in elevated Ohmic losses in feeders and transformers, reducing overall network efficiency [23, 39]. These losses become more significant under high EV penetration levels, especially when charging is concentrated in specific network locations. Additionally, fast charging can accelerate asset aging due to repeated high-load cycles [37].

From an operational perspective, EV charging introduces new sources of uncertainty and variability into the PDNs. Charging behavior depends on factors such as travel patterns, battery SoC, charging speed preferences, and tariff structures [40]. This uncertainty challenges traditional deterministic planning approaches and necessitates more adaptive operational strategies [25]. Nevertheless, EVs also present opportunities for enhanced flexibility when integrated with smart charging and vehicle-to-grid (V2G) capabilities [21].

Overall, EV charging fundamentally reshapes load characteristics in the PDNs. Its effects span increased peak demand, voltage deviations, higher network losses, and greater operational uncertainty. At the same time, EV charging demand—when properly managed—can be coordinated with advanced control strategies and distributed energy resources to support reliable and efficient PDN operation [30, 41].

Table 1.1: Overview of benchmark PDNs in the literature [6], [7]

Test System	Nominal Voltage (kV)	Radial or Meshed	Feeder Type	Dist. Transf.	Real Time-series Load Data
IEEE-4 Node	12.47, 4.16, 24.9	Radial	Four-wire wye	N	N
IEEE-13 Node	115, 4.16, 0.48	Radial	Four-wire wye	N	N
IEEE-34 Node	69, 24.9, 4.16	Radial	Four-wire wye	N	N
IEEE-37 Node	230, 4.8, 0.48	Radial	Three-wire delta	N	N
IEEE-123 Node	115, 34.5, 4.16, 0.48	Radial	Four-wire wye	N	N
IEEE Comp.	115, 24.9, 0.48, 0.24	Radial	Four-wire wye	Y	N
IEEE 8500	115, 12.47, 0.24	Radial	Four-wire wye	Y	N
IEEE NEV	12.47, 0.24	Radial	Four-wire wye	Y	N
IEEE-342 Node	230, 13.2, 0.48, 0.24	Meshed	Three-wire delta	Y	N
IEEE Euro LV	11, 0.416	Radial	Four-wire wye	Y	Y, one day
EPRI J1	69, 12.47, 0.48, 0.24	Radial	Four-wire wye	Y	N
EPRI K1	69, 13.2, 0.48, 0.24	Radial	Four-wire wye	Y	N
EPRI M1	69, 12.47, 0.48, 0.24	Radial	Four-wire wye	Y	N
EPRI Ckt5	115, 12.47, 0.48, 0.24	Radial	Four-wire wye	Y	N
EPRI Ckt7	115, 12.47, 0.48, 0.24	Radial	Four-wire wye	Y	N
EPRI Ckt24	230, 34.5, 13.2, 0.48, 0.24	Radial	Four-wire wye	Y	N

Table 1.3: Specifications Of Different EV Models

EV Model	**Type**	**Capacity (kWh)**	**Consumption (Wh/mile)**	**Connector Type**
Honda e	BEV	35.5	275	CCS, Type 2
Volkswagen e-Golf	BEV	35.8	245	CCS, Type 2
Nissan Leaf	BEV	40	330	CHAdeMO, Type 2
BMW i3	BEV	42.2	245	CCS, Type 2
Renault Zoe R110 ZE50	BEV	52	280	CCS, Type 2
Lexus UX 300e	BEV	54.3	270	CHAdeMO, Type 2
Tesla Model 3	BEV	55–82	225–265	Supercharger
SKODA Enyaq iv	BEV	62	252	CCS, Type 2
Kia Niro EV	BEV	64	255	CCS, Type 2
Nissan Leaf Plus	BEV	64	285	CHAdeMO, Type 2
Mercedes EQA	BEV	66.5	355	CCS, Type 2
Tesla Model S	BEV	75–100	305–310	Supercharger
Ford Mustang Mach-E	BEV	75.7	275	CCS, Type 2
Volvo XC40 Recharger	PHEV	78	380	CCS, Type 2
Polestar 2	BEV	78	305	CCS, Type 2
Porsche Taycan	BEV	79.2	335	CCS, Type 2
Volkswagen ID.4	BEV	82	290	CCS, Type 2
Jaguar I-PACE	BEV	90	354	CCS, Type 2
Audi E-Tron	BEV	95	426	CCS, Type 2
Tesla Model X	BEV	100	360–365	Supercharger

Chapter 2

Literature Review

As already discussed in Chapter 1, depleting fossil fuel reserves and increasing fuel prices are contributing to the growing proliferation of EVs. The increasing penetration of RES and EVs in distribution systems has introduced significant operational and planning challenges. High renewable penetration can negatively impact voltage profiles, increase energy losses, and compromise system reliability. To address these challenges, stochastic optimization techniques have been widely adopted to model uncertainties associated with load demand, renewable generation, and EV charging behavior. In particular, two-stage stochastic planning frameworks have proven effective in coordinating renewable integration and EV deployment to enhance hosting capacity while minimizing energy losses [42].

The electrification of the transportation sector further intensifies stress on distribution grids due to diverse EV charging speeds and charging strategies. Several studies have investigated the impact of residential and workplace charging of both light-duty and heavy-duty EVs, highlighting voltage violations and feeder congestion as major concerns. Sensitivity analyses indicate that uncoordinated charging significantly distorts load profiles and may exceed line capacity limits. Consequently, optimized charging strategies supported by renewable energy and distributed generation have been proposed to mitigate power quality issues [43].

It has been observed that [13, 19, 20] appropriately sized DGs at suitable nodes in the power distribution networks can mitigate the adverse efect of EV charging. The coordinated planning of fast charging stations (FCSs) and renewable-based DGs, particularly wind-based DGs, has attracted growing

research interest. Existing studies emphasize that renewable DGs can defer network upgrades and reduce energy losses. However, the stochastic nature of FCS demand and residential EV loads complicates planning decisions. To address this, stochastic planning models that consider investment costs, operational costs, and revenues have been proposed, along with practical geographical siting considerations for FCSs and DGs [27].

Comprehensive planning frameworks have been developed to balance the interests of EV users, charging infrastructure investors, and grid operators. Earlier EV planning studies often inadequately addressed grid-related issues, particularly voltage stability. Recent approaches incorporate voltage-dependent EV load modeling and renewable energy integration to accommodate increased EV penetration while maintaining acceptable voltage profiles and reliable grid operation [19].

Managing uncertainty in smart grids with high penetration of renewables and EVs remains a critical challenge. Prior studies identify variability in load demand, renewable generation, EV mobility patterns, and market price fluctuations as key uncertainty sources. Two-stage stochastic optimization models solved using Benders' decomposition have been shown to effectively minimize operational costs while improving computational tractability in large-scale energy resource management problems [44].

Accurate modeling of EV charging demand is another important research focus. Studies classify EV charging behavior into scenarios such as uncontrolled domestic charging, off-peak charging, smart charging, and public charging. The impact of electricity tariff structures—including fixed pricing, time-of-use tariffs, and real-time pricing—on EV charging behavior has been widely investigated. Results consistently show that high EV penetration under uncontrolled charging scenarios leads to significant peak load increases, highlighting the need for coordinated charging management [45].

Recent research emphasizes dynamic optimization techniques to mitigate the impact of EV charging stations on radial distribution systems. Considering hourly variations in demand is essential for realistic analysis. Advanced metaheuristic algorithms have been applied for the optimal placement of EV charging stations, renewable DGs, and compensating devices. Approaches using the Spotted Hyena Optimization Algorithm demonstrate improved voltage

stability and reduced power losses compared to conventional optimization methods [46].

Probabilistic and artificial intelligence-based optimization approaches have further advanced EV and RES integration studies. Probabilistic modeling effectively captures uncertainties in EV charging demand and renewable generation. Algorithms such as the Artificial Hummingbird Algorithm have been employed for optimal allocation of EV charging stations and solar DG units while considering charging speeds, voltage regulation, power losses, and system reliability [47].

Several review studies comprehensively analyze optimization-based approaches for the coordinated allocation of sustainable distributed generators and EV charging stations. These works compare conventional and advanced optimization techniques and emphasize the importance of coordinated planning in active distribution networks for improving efficiency, reliability, and sustainability [16].

Finally, recent studies indicate that traditional EV charging station planning methods based solely on peak demand assumptions often result in excessive grid upgrade costs. Modern approaches advocate multi-objective optimization frameworks that integrate renewable energy sources, battery energy storage systems, and real-time control strategies. Advanced algorithms and real-time charging control mechanisms enable dynamic adjustment of charging rates, reducing operational costs while enhancing system flexibility and reliability [48].

The coordinated allocation of EVCSs and RESs has been widely recognized as a critical factor in enhancing the operational performance of modern distribution networks. With the growing penetration of EVs, optimal placement of EVCSs is necessary to minimize system losses and improve voltage profiles. Renewable energy sources play a complementary role by supporting smart charging stations and reducing dependence on the main grid. Demand response programs, particularly time-of-use mechanisms, have been integrated into planning frameworks to smooth load curves. Advanced multi-objective optimization techniques, such as improved nondominated sorting genetic algorithms, have demonstrated superior performance compared to conventional genetic algorithms and particle swarm optimization methods in reducing losses, voltage drops, and total system costs [49].

The stochastic behavior of EV charging demand presents significant challenges for distribution system planning and operation. Prior studies emphasize that uncontrolled EV charging can increase peak demand and charging costs, necessitating the adoption of smart charging strategies. Research efforts have focused on realistic EV load modeling by incorporating parameters such as state of charge, travel distance, and user behavior. Metaheuristic optimization techniques, including the Jaya Algorithm, have been effectively employed for stochastic modeling and optimal integration of EVCSs, resulting in reduced power losses and improved voltage profiles under uncertain operating conditions [40].

Joint multi-objective planning of DERs and EVPLs has emerged as an important research direction in active distribution networks. The integration of RESs and EVs offers substantial environmental and economic benefits but also introduces additional demand and operational complexity. V2G technology enables EVs to act as distributed energy storage units, particularly beneficial during peak demand periods. Studies demonstrate that coordinated optimization of DERs and EVPLs, when combined with demand response programs, can significantly enhance technical performance, reduce operational costs, and improve environmental outcomes [50].

Several studies analyze distribution system performance in the presence of EVs while focusing on power loss reduction and voltage stability enhancement. Coordinated charging strategies are identified as essential for preventing network overloading. The classification of EVs based on charging capacity—such as cars, trucks, and buses—has been shown to facilitate effective charging and discharging strategies. VSI is frequently used to identify optimal locations for EV charging and discharging. Notably, some works propose integrating distributed generation units after EV placement, offering a novel planning sequence compared to traditional approaches that install DGs prior to EV integration [22].

The increasing number of EVs has driven the need for intelligent charging station placement strategies that address power quality issues. Conventional placement approaches often lead to increased power losses, voltage imbalance, and harmonic distortion. To overcome these challenges, intelligent data-driven methods have been introduced. Novel approaches such as Dove-based Recursive

Deep Networks have been proposed to optimize charging station placement while integrating hybrid renewable energy sources including wind, solar, and hydropower. Performance evaluations under balanced and unbalanced operating conditions demonstrate notable improvements over existing techniques [51].

Optimal energy modeling and planning in power systems with EVs and RESs have also been addressed using hybrid metaheuristic algorithms. EVs are increasingly viewed as flexible distributed generation resources capable of supporting grid loads and reducing operational costs. However, uncoordinated charging can lead to severe economic and technical issues. Studies highlight that coordinated charging strategies significantly reduce peak demand and operational costs. Hybrid optimization techniques, such as combined firefly and cuckoo algorithms, have demonstrated effectiveness in modeling EV behavior and optimizing energy planning, particularly in IEEE benchmark distribution systems [20].

The future growth of EV loads necessitates robust planning of FCSs and DGs. Improper placement and sizing of FCSs and DGs can negatively affect voltage profiles and increase system losses. Literature emphasizes the importance of multi-objective optimization frameworks that consider both present and future EV penetration levels. Various optimization algorithms have been explored, with hybrid algorithms showing improved convergence and solution quality when compared to traditional methods for optimal FCS and DG planning [52].

Fuzzy multi-objective optimization techniques have also been applied to address uncertainties associated with EV load growth and renewable generation. Two-stage fuzzy planning frameworks incorporating the Grasshopper Optimization Algorithm have been proposed for optimal sizing and placement of DGs, shunt capacitors, and EV charging stations. Compared to genetic algorithms and particle swarm optimization, grasshopper-based approaches exhibit faster convergence and improved solution robustness, particularly under uncertain operating conditions [28].

Multi-objective simultaneous planning of fast charging stations and DGs has been formulated as a mixed-integer nonlinear programming problem to address voltage stability and power quality issues. Inappropriate placement of FCSs and DGs can result in overvoltage and undervoltage conditions. Advanced

evolutionary algorithms such as NSGA-II have been widely adopted to minimize total system cost, power losses, voltage deviation, and EV charging costs. Large-scale test systems demonstrate the effectiveness of these methods while highlighting the need for further voltage profile improvement even after optimal placement [53].

Finally, recent studies emphasize the importance of simultaneously assessing the hosting capacity of distributed generation and electric vehicles in distribution systems. Existing approaches largely focus on residential-level simulations and often assess DG and EV hosting capacity separately. There remains a clear research gap in integrated hosting capacity assessment frameworks that consider both DGs and EVs concurrently at the system level, motivating further investigation into holistic planning methodologies [54].

The large-scale deployment of EVs and renewable distributed generation introduces significant uncertainty into distribution system planning. These uncertainties arise from stochastic EV charging demand, intermittent renewable generation, and load variability. To address these challenges, scenario-based stochastic planning approaches have been proposed for active distribution system reinforcement. Markovian modeling of historical EV charging behavior has been used to capture driving patterns and charging requirements, while scenario matrices are constructed to represent correlations among wind generation, photovoltaic output, conventional loads, and EV demand. Such expansion planning frameworks aim to minimize both investment and operational costs while optimally locating substations, feeders, EV charging stations, and renewable energy sources [25].

The increasing penetration of PEVs has also motivated research on optimal DG sizing and placement. Studies indicate that rising PEV penetration significantly affects energy consumption patterns and line losses in conventional distribution networks. Genetic algorithm-based optimization techniques have been widely applied to determine optimal DG locations and capacities under varying levels of PEV demand. Simulation results demonstrate that the number of connected PEVs directly influences DG sizing decisions, which in turn impacts total power losses and grid stability, highlighting the importance of coordinated DG planning in PEV-integrated networks [55].

In microgrid environments, the smart utilization of renewable energy sources

in the presence of PHEVs has been extensively investigated. Prior studies often assumed fixed PHEV battery capacities, which limits the realism of system modeling. More recent research emphasizes that battery capacity varies significantly among vehicles, and comprehensive modeling approaches are required to accurately represent PHEV behavior. The lack of integrated analysis combining renewable generation variability and PHEV operational characteristics remains a notable gap in earlier studies [56].

Optimizing EV charging strategies has become a key focus for enhancing both technical and economic performance of distribution networks. Traditional charging approaches are increasingly viewed as inefficient due to their inability to account for individual driving patterns and daily energy requirements. Intelligent charging optimization methods that tailor charging profiles to vehicle-specific trip data have been proposed. Novel bio-inspired algorithms, such as horse herd optimization, have demonstrated improved convergence speed and reduced computational burden. Comparative studies reveal substantial reductions in peak load and overall demand when intelligent charging is combined with load response programs, thereby improving network resilience and energy management efficiency [30].

Several review studies provide a comprehensive overview of modeling and optimization approaches for integrated electric vehicle–transportation–grid systems. These works discuss EV charging behavior models, transportation network interactions, and power system constraints, highlighting the complexity of coordinated management across multiple infrastructures. The reviews emphasize the need for integrated frameworks that jointly consider mobility patterns, grid constraints, and optimization strategies to enable efficient smart energy management [17].

V2G technology has been widely studied as a means to provide ancillary services such as frequency regulation and peak load shaving. Various charging coordination methodologies have been proposed, with mixed-integer linear programming emerging as a robust optimization framework. While V2G offers economic and operational benefits, studies caution that battery degradation can significantly offset these gains. Research indicates that effective EV charging coordination is feasible even under distribution system imbalances, but future solutions must incorporate dynamic scheduling and renewable-aware strategies

to fully exploit V2G potential [21].

The economic viability of V2G implementation has been further examined through cost-benefit analyses that explicitly consider battery degradation. As PEV market penetration increases, smart charging and discharging strategies become essential for maintaining economic feasibility. Stochastic methodologies have been applied to model uncertainties in charging behavior and renewable generation. Results suggest that V2G can be profitable under specific conditions, such as high wind-based distributed generation availability, but may become economically unattractive when battery degradation costs are fully accounted for in the absence of renewable support [57].

The transformation of the energy sector due to high renewable penetration has also driven the development of grid-aware energy management systems for distribution networks. Co-simulation approaches integrating power system models with communication and control layers have been proposed to improve system observability and control. Novel energy management strategies based on such frameworks enable more adaptive and resilient operation of distribution grids under uncertain and dynamic operating conditions [58].

The optimal placement and sizing of PEV charging stations in distribution networks with high photovoltaic penetration has been addressed using advanced stochastic modeling techniques. Correlations between PEV load demand and PV generation are captured using multivariate copula-based models. Evolutionary optimization algorithms, particularly particle swarm optimization, have been shown to effectively minimize voltage deviation and energy losses under uncertainty. Scenario-based approaches are commonly employed to represent variations in PEV demand and background grid load, reflecting a growing trend toward probabilistic planning methodologies [23].

Finally, the combined impact of distributed generation and PEV charging on power distribution systems has been investigated using queuing theory-based models. Queuing theory provides an effective means of estimating uncertain PEV charging demand, which is then integrated with optimization techniques such as differential evolution. Results demonstrate that coordinated optimization of DG sizing and PEV charging schedules significantly reduces total power losses. Comparative analyses indicate that differential evolution outperforms traditional methods such as genetic algorithms and simulated

annealing in terms of accuracy and convergence speed [59].

The increasing penetration of PEVs introduces reliability and operational challenges in power distribution systems due to stochastic and spatially concentrated charging demand. Aggregated control of PEV charging in PLs has been identified as an effective approach to alleviate these challenges by smoothing load profiles and reducing system losses. Existing literature emphasizes the importance of optimally determining both the location and size of PEV parking lots to enhance network reliability. To address uncertainty in PEV owners' behavior, stochastic optimization frameworks based on mixed-integer linear programming have been proposed, with kernel density estimation techniques employed to model temporal uncertainties without relying on restrictive assumptions [38].

Smart charging strategies have also been proposed to enable the optimal integration of PEVs within existing distribution system infrastructure. Grid-to-vehicle and vehicle-to-grid coordination frameworks are developed to minimize daily charging costs and reduce the peak-to-average ratio of load demand. Analytical studies demonstrate that smart charging strategies significantly increase the maximum PEV penetration level that existing networks can support. Comparative analyses reveal that both slow and fast charging modes can be effectively managed without requiring infrastructure reinforcement, underscoring the importance of optimizing existing assets rather than pursuing costly network upgrades [60].

The electrification of public transportation systems has further motivated research on stochastic energy management of EBCSs. Studies integrating photovoltaic systems and battery energy storage systems address the cost-effective charging of electric buses under uncertain operational conditions. Distributionally robust Markov decision process formulations have been employed to capture uncertainty in bus arrival times, charging demand, and energy prices. Event-based ambiguity sets are introduced to balance solution robustness and conservativeness. Case studies demonstrate that such approaches effectively minimize charging costs while mitigating adverse impacts on distribution networks, highlighting the benefits of B2G capabilities [29].

Several studies focus on quantifying the impacts of uncontrolled EV charging in low-voltage distribution grids. These works emphasize that increasing EV

adoption can significantly stress low-voltage networks, leading to voltage violations and transformer overloading. Stochastic simulation approaches incorporating household electricity consumption variability and EV usage patterns provide realistic assessments of worst-case operating conditions, underscoring the necessity of coordinated charging strategies [32].

The integration of EV charging stations with RES-based distributed generation has also been examined from a centralized management perspective. Literature reviews highlight the widespread deployment of RES-based DG and EV charging systems and their substantial impact on distribution grid planning. Centralized control by distribution system operators has been proposed to ensure optimal utilization of existing infrastructure. Optimal power flow-based frameworks tailored to DSO objectives demonstrate that coordinated integration of EV charging stations and RES-based DG can maintain operational limits while delaying or avoiding expensive grid reinforcements [61].

Robust planning approaches have been developed to accommodate uncertainties associated with large-scale EV charging demand and renewable generation. Distributed generation investment planning models based on two-stage robust optimization address the optimal sizing and siting of DG units while ensuring operational feasibility under worst-case scenarios. Real-life travel behavior data are used to model EV charging demand uncertainty, enhancing practical relevance. Simulation studies on benchmark distribution systems validate the effectiveness of robust DG investment in mitigating the adverse impacts of EV charging [26].

Accurate modeling of PEV energy consumption remains a critical research challenge. Existing models often neglect important factors such as vehicle usage diversity, trip purpose, ambient temperature, and multiple daily charging events. Recent studies advocate comprehensive modeling approaches based on Monte Carlo simulation to capture driver behavior and travel patterns more realistically. Improved PEV modeling enables more accurate assessment of network impacts and facilitates informed planning decisions for distribution system upgrades [36].

Temporal–spatial coordination of PEV charging has been identified as essential for reliable operation of active distribution networks with high penetration of distributed generation. Coordinated scheduling strategies jointly

optimize charging time and location to reduce system losses, mitigate voltage deviations, and enhance overall grid performance. The literature consistently highlights that uncoordinated charging undermines the environmental and operational benefits offered by PEVs and DGs [62].

Distributed coordination frameworks for EV charging have also been proposed for microgrids serving clusters of buildings. In urban environments with high-rise buildings, EV charging represents a substantial and dynamic load. Studies demonstrate that on-site renewable generation, such as wind power, can effectively support EV charging demands. Markov decision process formulations capture uncertainty in EV driving patterns and renewable generation, while distributed simulation-based policy improvement methods improve scalability and performance compared to centralized approaches [63].

Finally, the impact of EV charging on urban residential power distribution networks has been widely investigated. Global decarbonization initiatives have accelerated EV adoption, placing increasing stress on residential distribution infrastructure. Literature emphasizes the need for data-driven frameworks that utilize real residential load measurements and EV charging profiles. Consensus findings indicate that optimal charging management significantly reduces peak demand, improves voltage stability, and enhances system resilience under extreme operating conditions [24].

Probabilistic assessment of electric vehicle impacts on low-voltage residential distribution networks has gained increasing attention due to the rapid growth of EV adoption driven by decarbonization policies and technological advancements. Since most EV charging occurs at home, low-voltage residential feeders experience significant additional loading. Studies investigate different EV penetration levels using probabilistic charging models based on various probability distribution functions to capture user behavior. V2G technology is shown to provide flexibility and alleviate grid stress, while the integration of rooftop solar photovoltaic generation and volt–var control capabilities of PV inverters further mitigates voltage violations and transformer overloading caused by EV charging [33].

Distribution network planning approaches incorporating hourly load profiles have been proposed to better analyze EV charging strategies over realistic operating horizons. Literature reviews reveal that only a limited number of

studies explicitly address the impact of plug-in electric vehicles on distribution planning, highlighting a research gap. Economic feasibility is identified as a key factor influencing EV integration, with charging time and strategy significantly affecting network reinforcement costs. Rural networks are found to be constrained by feeder capacity, whereas urban networks are mainly limited by medium- and low-voltage transformer substations. To address these challenges, reference network models have been extended to include 24-hour profiles, enabling more accurate long-term planning analyses [34].

The proliferation of high-power domestic EV chargers presents additional technical challenges for distribution networks. Studies focusing on Ireland highlight regulatory constraints that currently limit residential charging to slow chargers, while fast chargers are restricted due to maximum import capacity limitations. Advances in battery technology have increased vehicle energy capacity, making long charging times with slow chargers impractical. Voltage unbalance factors and voltage magnitude violations are identified as the primary limiting factors for widespread EV adoption. While deterministic assessment methods remain common, recent trends emphasize probabilistic approaches to better capture the stochastic nature of EV charging behavior [37].

Adaptive charging management strategies have been proposed to address the integration of plug-in electric vehicles in renewable-rich distribution systems. Stochastic model predictive control frameworks are applied to manage uncertainties associated with renewable generation and PEV state-of-charge dynamics. Behavioral modeling of PEV drivers, influenced by socioeconomic factors and charging station accessibility, is incorporated to improve realism. Genetic algorithms are employed to solve the resulting complex optimization problems efficiently. These adaptive approaches aim to minimize operational costs while maintaining robustness against forecasting errors, underscoring the importance of flexibility in future energy management systems [64].

The interaction between electric vehicle energy consumption and distribution grids has also been analyzed using optimization-based methodologies. Studies highlight the increased electricity demand caused by large-scale EV adoption and the need for grid operators to prevent excessive losses and overloading. Case studies evaluating EV electricity consumption consider factors such as vehicle population, driving distance, and system efficiency. Steady-state

simulations of integrated distribution networks demonstrate that particle swarm optimization-based strategies can effectively manage EV charging demand while reducing dependence on the grid [39].

Dynamic scheduling strategies for plug-in electric vehicles have been developed to address multiple charging scenarios in smart grid environments. Literature reviews emphasize the growing importance of green transportation as a response to fossil fuel depletion and environmental concerns. Challenges related to the self-interested behavior of EV owners and information asymmetry between supply and demand necessitate advanced scheduling algorithms. Optimal energy management strategies are shown to improve grid efficiency, reduce greenhouse gas emissions, and enhance overall system security [41].

The technical impacts of EV penetration are further examined within the context of sustainable local energy communities. Reviews emphasize the role of active system management tools, including smart grid monitoring and active network management, in enabling higher EV penetration levels. Increased EV adoption intensifies load violations, requiring coordinated charging and load management strategies. Collaboration among distribution system operators, aggregators, and local energy community managers is identified as a key enabler for enhancing system flexibility and preventing critical grid events [65].

Optimal placement and sizing of electric vehicle charging stations have been studied under uncertainty using stochastic optimization frameworks. Monte Carlo simulation techniques are widely employed to model uncertainties related to EV arrival patterns, charging demand, and energy prices. Energy management strategies integrated with station planning are shown to improve system reliability and operational efficiency [66].

Deterministic methodologies have also been proposed to enhance distribution network performance in the presence of plug-in electric vehicles. Smart charging strategies are shown to increase EV hosting capacity; however, their effectiveness is often constrained by limited infrastructure. The integration of distributed generation is demonstrated to significantly improve voltage profiles and reduce losses in EV-dominated distribution networks [67].

Finally, comprehensive planning frameworks for EV charging stations with renewable energy integration have been developed. Literature reviews emphasize that optimal allocation of charging stations reduces power losses and

installation costs. Renewable-based distributed generation is shown to mitigate additional loading effects while improving voltage regulation. The uncertainties associated with EV traffic flow and renewable generation are addressed through established stochastic and robust optimization techniques, reinforcing the importance of integrated planning approaches [18].

The transformation of conventional gas stations into EV charging infrastructure has recently gained attention as a pragmatic pathway toward transportation electrification. Alyami [68] evaluates the controllability of such transformed charging facilities within distribution networks integrated with renewable energy sources. The study highlights the growing market penetration of EVs and the resulting shift from fossil-fuel-based refueling to electricity-based charging. By employing queuing theory, the work quantitatively models EV arrival and parking behaviors, establishing a strong linkage between charging stations and parking lot operations. An operational control model is formulated with clearly defined decision variables and constraints to manage charging demand effectively. The proposed time- and energy-based optimal control strategy enhances charging infrastructure controllability while exploiting synergies between EVs and renewable generation, thereby contributing to sustainable grid stability.

Shetty [69] investigates the operational impacts of PEV charging loads on distribution systems, with particular emphasis on optimal siting and sizing of charging stations. The study demonstrates that large-scale PEV integration significantly affects power generation dispatch, fuel consumption rates, and electricity prices. A detailed load modeling framework is developed to represent the additional demand imposed by PEV charging on distribution networks. The results underline the necessity of coordinated planning strategies to mitigate adverse operational impacts and ensure economic and reliable grid operation as PEV adoption increases.

Gan et al. [70] address the resilience challenges arising from the integration of EV charging infrastructure into coupled power distribution and transportation systems. The study emphasizes the importance of robust planning under severe contingencies and uncertain traffic demand conditions. EVs are modeled as flexible mobile energy storage resources capable of supporting grid operations during emergencies. The proposed robust optimization framework minimizes

both investment and operational costs while ensuring effective EV participation in resilience enhancement strategies. The use of a NC & CG algorithm is a key methodological contribution, enabling tractable solutions to large-scale, uncertainty-aware planning problems in interconnected energy and transportation networks.

The electrification of transportation introduces significant uncertainty into power system operations, necessitating accurate modeling of EV charging behavior. The work in [71] focuses on multivariate stochastic modeling of plug-in electric vehicle charging profiles to assess their grid impacts. Prior literature has addressed stochastic driving patterns and energy consumption; however, this study extends those efforts by capturing correlations among multiple stochastic variables. Grid impact analyses are conducted to identify potential vulnerabilities in distribution networks arising from high PEV penetration. The findings highlight the importance of techno-economic grid reinforcement measures to maintain voltage stability and ensure reliable operation of charging infrastructure under uncertain demand conditions.

Distribution network voltage performance under increasing EV penetration is examined in [72] using data-driven EV load profiles. The study analyzes the anticipated growth in EV adoption and its implications for voltage regulation in distribution systems. Distinct utilization patterns for residential, slow commercial, and fast public charging stations are identified, revealing heterogeneous impacts on network performance. Optimal power flow simulations, conducted with and without EV loads, demonstrate the timing and severity of voltage violations. The work further identifies peak violation periods and evaluates enabling technologies such as coordinated charging and renewable integration, confirming their effectiveness in mitigating voltage-related issues.

The dual functionality of EVs as both electrical loads and mobile storage assets is leveraged in [73] to enhance resilience in coupled traffic–electric networks. Two complementary strategies are proposed: rerouting power-deficient EVs to alternative charging stations and redispatching power-sufficient EVs to support the grid via V2G technology. A pricing-based coordination mechanism incorporating congestion tolls and charging fees is introduced under the user equilibrium principle. The integrated formulation

demonstrates how coordinated traffic and power system management can improve overall network resilience by exploiting sector coupling and EV flexibility.

Urban EV charging demand forecasting presents significant challenges due to spatial and temporal variability. The study in [74] introduces a spatiotemporal graph-based modeling framework using D-ST-GNNs to predict and manage EV charging demand. By incorporating traffic flows, charging station connectivity, and user behavior, the model captures complex interdependencies within urban charging networks. Validation results demonstrate high predictive accuracy, indicating the model's potential to improve infrastructure utilization, reduce queue times, and support real-time charging station management in dense urban environments.

The operational impacts of EV charging station loads on distribution networks are analyzed in [75]. The study identifies that EV charging demand adversely affects key operating parameters such as peak load, voltage levels, and reserve margins. Fast charging stations, in particular, are shown to significantly increase peak demand, exacerbating stress on distribution assets. These findings reinforce the need for strategic planning, demand management, and grid reinforcement to accommodate high-power charging infrastructure.

Accurate risk assessment of EV integration requires realistic modeling of charging behavior under uncertainty. The framework proposed in [76] addresses limitations in earlier works that relied on fixed EV penetration levels and deterministic charging assumptions. Previous approaches focused primarily on cost minimization while neglecting stochastic parameters such as charging duration, battery capacity, and driving frequency. By incorporating these factors, the proposed model enables a more comprehensive assessment of distribution network risks associated with large-scale EV adoption.

A comprehensive review and impact analysis of projected EV charging loads on low-voltage distribution systems is presented in [77]. The study synthesizes existing literature to highlight technical challenges such as voltage deviations, thermal overloading, and reliability degradation. The review also summarizes mitigation strategies including smart charging, network reinforcement, and renewable integration. By consolidating prior research, the work provides a strong foundation for planning and operational decision-making in EV-ready

low-voltage distribution networks.

A novel framework for incorporating EV evacuation behavior into power system resilience assessment, particularly during natural disasters is presented in [78]. The literature highlights the importance of accurately modeling EV charging demand under evacuation scenarios, as large-scale, time-sensitive charging can significantly stress distribution networks. The proposed approach integrates transportation and power system modeling, enabling operators to evaluate cascading impacts of evacuation-driven charging demand on grid performance. Furthermore, the use of geospatial visualization tools enhances situational awareness by allowing system operators to identify vulnerable grid locations and charging hotspots. Overall, the work contributes to resilience planning by bridging the gap between evacuation dynamics and power system operational analysis [78].

The optimal placement of EVCSs in active distribution networks to ensure efficient load management and system reliability is presented in [79]. The literature emphasizes that an optimized combination of charging station types and capacities can significantly reduce network stress caused by uncoordinated EV charging. The study also incorporates the impact of PV generation, demonstrating that local renewable energy sources can offset additional demand introduced by EVCSs. By jointly considering EV charging demand and distributed PV generation, the proposed framework enhances voltage regulation and reduces power losses. The findings underline the importance of integrated planning strategies for EVCS deployment in modern active distribution networks [79].

The coordinated allocation of RESs and EVCSs in distribution systems, recognizing the stochastic and dynamic nature of both resources is presented in [80]. The literature underscores the necessity of a multi-objective planning framework that simultaneously minimizes voltage deviations, energy losses, and EV users' dissatisfaction. Operational constraints of the grid, RESs, and EVCSs are explicitly considered to ensure feasible and reliable operation. Advanced control schemes, including G2V and V2G strategies, are highlighted as effective mechanisms for enhancing system flexibility. The proposed two-level optimization approach demonstrates substantial improvements over uncontrolled EV charging, reinforcing the consensus that structured planning

combined with intelligent control significantly improves distribution system performance [80].

An integrated planning strategy that jointly considers power network expansion and electric vehicle charging infrastructure deployment to enhance system resilience under extreme weather events is presented in [81]. The literature highlights that independent planning of power networks and EV infrastructure can lead to suboptimal resilience outcomes. To address this, the authors propose a robust two-stage/tri-level mixed-integer optimization framework that captures uncertainties and worst-case scenarios. Case studies on benchmark systems demonstrate that the integrated planning approach outperforms traditional transmission-only planning models by reducing operational costs and minimizing load shedding. The study emphasizes that coordinated expansion decisions are essential for maintaining reliable power supply during extreme and disruptive events [81].

A decentralized electric vehicle charging management using an AIMD control strategy adapted from Internet congestion control theory is presented in [82]. The literature identifies growing challenges associated with high EV penetration and increasing integration of low-cost renewable energy sources, which strain legacy grid control mechanisms. With the proliferation of power electronic interfaces, traditional centralized control approaches are shown to lack scalability and robustness. The proposed decentralized AIMD-based method enables autonomous, stable, and scalable EV charging coordination without extensive communication infrastructure. Comparative analysis demonstrates that the AIMD strategy effectively flattens peak loads under high EV penetration, highlighting its potential as a practical solution for future EV-dominated power systems [82].

Investigations on the role of EVs in mitigating load shedding in stressed distribution systems by leveraging their flexibility as controllable loads and mobile storage resources has been done in [83]. The literature emphasizes that appropriately incentivized EVs can provide valuable operational support during peak demand or contingency conditions. The authors propose a network equilibrium model that integrates electricity market clearing in distribution systems with traffic flow equilibrium in transportation networks. This framework captures decentralized interactions among EV users, charging

facilities, and system operators. To address computational complexity, a convex reformulation of the original non-convex model is developed, ensuring global convergence and tractability [83].

The critical role of spatial load distribution in assessing the impact of electric vehicle charging on voltage stability in distribution networks is presented in [84]. The literature demonstrates that the physical location of EV loads can significantly influence voltage profiles, with loads at electrically weak points having a disproportionate impact compared to multiple loads at stronger locations. The study focuses on small-disturbance voltage stability, which reflects the system's ability to maintain acceptable voltage levels under minor load variations. Voltage stability indices are widely used to identify vulnerable network locations and guide EV charging station placement. The paper also raises concerns regarding equity in charging access, suggesting that uniform charging rights may not be technically feasible due to location-dependent grid impacts [84].

The work presented in [85] reviews and extends studies on the optimal placement and sizing of electric vehicle charging stations in coordination with multiple distributed generation units. The literature indicates that integrating EVCS planning with distributed generators can significantly improve voltage profiles and reduce system losses. Various optimization methods and enabling technologies for incorporating EVs into distribution systems are discussed, reflecting the growing complexity of modern power networks. The study highlights the benefits of coordinated planning approaches that consider both EV charging demand and local generation capabilities, which enhance network efficiency and operational reliability [85].

A comprehensive review on existing methodologies for the allocation of electric vehicle charging stations in distribution networks is examined in [86]. The literature identifies the rapid growth of EV adoption driven by environmental concerns and fossil fuel depletion, alongside challenges such as inadequate charging infrastructure and uneven spatial distribution of charging stations. The review emphasizes the importance of optimal EVCS placement to support large-scale transport electrification while minimizing adverse grid impacts. A wide range of optimization techniques, from classical mathematical programming to advanced metaheuristic methods, are surveyed. The study also

evaluates traditional and emerging charging technologies, highlighting their effectiveness in mitigating voltage violations, power losses, and congestion in distribution systems [86].

The work presented in [87] investigates the optimal placement of DG units in radial distribution systems to mitigate the adverse impacts of electric vehicle charging stations. The literature underscores the growing reliance on alternative energy sources due to fossil fuel depletion, particularly in the transportation sector. The increasing penetration of plug-in electric vehicles presents challenges related to system reliability, power losses, and voltage instability. Various analytical and optimization-based approaches are discussed for evaluating EV impacts on distribution networks. The study concludes that integrating DGs, particularly solar photovoltaic units, at or near EV charging stations can significantly alleviate voltage deviations and power losses, thereby enhancing overall system performance [87].

The role of plug-in electric vehicles in addressing environmental and economic challenges while highlighting the necessity of robust planning models for fast-charging station deployment is investigated in [88]. The literature emphasizes minimizing expected planning costs across both transportation and distribution networks under uncertainty. To achieve this, a distributionally robust optimization framework based on -divergence is employed, allowing serviceability constraints to be established without assuming exact probability distributions. A modified capacitated flow refueling location model is proposed to formulate charging station location constraints, ensuring adequate coverage of transportation demand. Additionally, AC power flow constraints are incorporated to accurately represent the operational impacts of PEV penetration on the distribution network, reinforcing the importance of integrated power-transportation planning [88].

The adverse impacts of high plug-in electric vehicle penetration on residential distribution grids and proposes mitigation through smart charging strategies is examined in [89]. The literature utilizes data from the National Household Travel Survey to develop realistic PEV charging load models. An optimal charging control method is introduced to shift and coordinate charging demand, thereby reducing peak load and voltage violations. The results demonstrate that smart charging significantly alleviates grid stress compared to uncontrolled charging

scenarios. Overall, the study supports the consensus that data-driven smart charging strategies are essential for accommodating high PEV penetration in residential networks [89].

The challenges of uncertainty assessment in distribution systems with correlated electric vehicle charging demand and renewable energy generation are addressed in [90]. The literature notes that commonly used copulas, such as Gaussian, Clayton, and Frank, are insufficient to model the nonlinear correlations observed in real measurement data. To overcome this limitation, a data-driven approach based on GMM and PCE is proposed. The GMM clusters uncertain resources, enabling effective correlation modeling using Gaussian copulas, while k-medoids clustering is applied to select representative PCE samples. The results demonstrate high efficiency and accuracy in fast grid impact studies, highlighting the method's suitability for large-scale uncertainty analysis [90].

The study performed in [91] reviews and analyzes optimal sizing and placement strategies for EVDSs in smart grids. The literature highlights the rapid adoption of electric vehicles driven by rising fuel prices and environmental concerns, necessitating robust charging infrastructure planning. The integration of SPV systems into EVDSs is presented as a sustainable solution that reduces dependence on conventional grid supply. The review emphasizes that renewable-powered EVDSs improve charging reliability, particularly during peak demand and grid outages. Simulation results on the IEEE 69-bus distribution network demonstrate enhanced system efficiency and reduced charging times, supporting the role of renewable-integrated docking stations in future smart grids [91].

The optimal placement and capacity determination of electric vehicle charging stations under uncertainty is investigated in [92]. The literature highlights the growing impact of plug-in electric vehicles on distribution network performance, particularly in terms of voltage profiles and power losses. The study considers the perspectives of charging station investors, EV users, and distribution network operators in the planning process. Integrating renewable energy sources at charging stations is proposed as an effective solution to alleviate grid stress. Furthermore, energy management strategies incorporating battery storage systems and vehicle-to-grid operation are emphasized as key

tools for managing uncertainties in charging demand and power generation [92].

The impact of various charging models on the optimal integration of plug-in electric vehicles into distribution systems are analyzed in [93]. The literature discusses the rising environmental concerns and the anticipated high penetration of PEVs in future power networks. Multiple scheduling strategies, including load stabilization, cost-based charging, battery degradation minimization, and mixed-objective models, are evaluated. Their effects on operational parameters such as peak demand, transformer loading, and system losses are assessed. Comparative results on a 38-node distribution system demonstrate that coordinated charging strategies significantly outperform uncontrolled charging, both technically and economically [93].

A mathematical framework for modeling electric vehicle charging stations as smart loads capable of participating in demand response programs is presented in [94] . The literature employs queuing theory and neural networks to represent aggregate charging demand, with PEV arrivals modeled as a non-homogeneous Poisson process. The load model incorporates controllable parameters such as charging current and the number of simultaneously charging vehicles. The study evaluates smart charging operation from both the distribution utility's and charging station owner's perspectives. Comparative analysis demonstrates that smart EV charging stations significantly outperform uncontrolled stations by reducing peak demand and enhancing demand response capability [94] .

The increasing popularity of eco-friendly energy solutions and the anticipated rise in EV adoption, leading to higher demand for efficient charging schemes are discussed in [95] . The literature emphasizes that EVs must be connected to reliable power sources for charging, which introduces new challenges for distribution system operation. A key contribution of this work is the incorporation of actual operational data into the design of EV charging schemes, improving the realism and applicability of the proposed models. The study implies a growing consensus on the need for data-driven and sustainable charging strategies to support large-scale EV deployment while maintaining grid stability [95] .

The growing importance of effective distribution system operation in the presence of widespread EV adoption and renewable energy integration is highlighted in [96]. The literature outlines the benefits of EVs, including

improved efficiency, enhanced reliability, and reduced emissions, while also recognizing their potential to act as flexible loads or distributed storage during parking periods. The impact of controlled versus uncontrolled EV charging, renewable generation penetration, and EV driving behavior on load profiles is examined in detail. The findings underscore a consensus that understanding user behavior and adopting coordinated charging schedules are critical for optimizing distribution system performance under high EV penetration [96] .

The coordinated allocation of distributed energy resources, including plug-in electric vehicles, to enhance power system resilience is investigated in [97] . The literature emphasizes the importance of jointly planning wind farms, energy storage systems, and PEV parking lots to achieve optimal energy distribution. Demand response programs and hourly network reconfiguration are identified as essential tools for managing system flexibility and resilience. The proposed architecture aims to minimize power procurement costs while leveraging load flexibility. Simulation results on the IEEE 33-bus distribution system validate the feasibility and effectiveness of the resilience-oriented framework [97] .

An assessment framework to capture the interactions between electric vehicles and photovoltaic systems in emerging distribution networks is presented in [98] . The literature highlights the limitations of existing networks in accommodating high penetration levels of EVs and intermittent renewable energy sources. A strong emphasis is placed on developing new reference architectures and decentralized coordination mechanisms to manage distributed energy resources effectively. The study also identifies gaps in current research related to consumer engagement and responsiveness to price signals. Overall, the findings support the consensus that integrated EV-PV planning is essential for improving sustainability and reliability in future distribution systems [98].

The challenges associated with managing EV charging in grids with distributed generation systems are addressed in [99]. The literature highlights the probabilistic nature of EV energy consumption and renewable energy output, which necessitates advanced charge management strategies. The proposed approach models the combined effects of renewable generation and EV charging on system load curves, aiming to reduce peak demand. The integration of controlled charge-discharge strategies for EVs is shown to smooth load profiles and minimize peak power drawn from the upstream grid. The results

demonstrate improved technical performance, reduced losses, and enhanced utilization of distributed generation resources [99].

A comprehensive review on multilevel control and management strategies for electric vehicle infrastructure integrated with distributed energy resources is examined in [100] . The literature categorizes control approaches across different hierarchical levels, highlighting both conflicts and synergies among them. Particular attention is given to coordination challenges between EV charging control and renewable energy integration. The review synthesizes existing methodologies and identifies research gaps related to scalability, interoperability, and real-time implementation. Overall, the study provides a structured overview of current advancements and future research directions for EV-integrated smart grids [100] .

The integrated energy management strategies for plug-in electric vehicles operating in power grids with renewable energy sources is investigated in [101] . The literature emphasizes the importance of mathematical modeling for smart charging and V2G operations while considering distribution grid constraints. The proposed control algorithm minimizes total operating costs and supports frequency regulation through coordinated EV aggregation. Simulation results demonstrate that EVs located near wind power generators can effectively mitigate power fluctuations. The study reinforces the consensus that V2G-enabled EVs can significantly enhance grid stability and renewable energy utilization [101] .

The evolving role of electric vehicles and renewable energy sources in the decarbonization of electricity and transportation sectors is discussed in [102] . The literature highlights the need for new dispatching paradigms to manage medium- and low-voltage distribution grids affected by EV charging and dispersed generation. A novel dispatching model involving the distribution system operator and connected resources is proposed and validated using a real test case. The results demonstrate that the new paradigm effectively addresses operational challenges, indicating a shift toward innovative grid management strategies [102] .

The combined impact of electric vehicle penetration and demand management systems on electrical distribution networks is analyzed in [103] . The literature highlights rapid EV market growth and corresponding regulatory

adjustments aimed at facilitating integration. The need for smart network solutions to modernize aging distribution infrastructure is emphasized. The analysis focuses on technical indicators such as voltage levels and power losses, particularly in small urban networks. The findings underscore the importance of demand management systems in mitigating adverse impacts and enabling efficient adaptation to increasing EV penetration [103].

A cooperative energy management framework for an electric transportation system integrated with photovoltaic generation and energy storage is proposed in [104]. The literature highlights the challenges posed by heterogeneous EV loads, renewable intermittency, and variable grid conditions. A virtual energy hub concept is introduced to coordinate power flows among EVs, PV systems, and battery storage. A cooperative decision-making strategy is developed to optimize economic and operational performance. Simulation results across multiple scenarios demonstrate the effectiveness of the proposed approach in minimizing operational costs while satisfying grid constraints [104].

The work presented in [105] further elaborates the coordinated EV and renewable planning by emphasizing system-wide optimization of charging infrastructure deployment. The study reinforces the need for modeling heterogeneous EV charging behaviors and aggregating them into an economic dispatch framework. The MPC-based learning strategy enables adaptive planning by capturing spatiotemporal correlations between EV charging demand and renewable generation profiles. The results highlight the framework's effectiveness in supporting long-term planning decisions, particularly in determining charging capacity requirements across different regions. Overall, the study underscores the role of coordinated planning as a critical enabler for large-scale EV adoption and renewable integration [105].

A time- and energy-based EV charging prioritization strategy aimed at enhancing grid stability under high EV penetration is proposed in [106] . The literature highlights the limitations of conventional charging strategies in efficiently allocating limited grid capacity among competing EV demands. The proposed approach prioritizes EV charging based on both temporal urgency and energy requirements, enabling a larger number of EVs to meet their charging needs compared to existing methods. The results indicate that such prioritization schemes can significantly improve system-level utilization while maintaining

fairness and operational reliability, supporting sustainable EV integration [106] .

The congestion issues in distribution feeders caused by uncoordinated plug-in electric vehicle charging are addressed in [107] . The literature identifies charging coordination as a critical requirement for managing high PEV penetration, particularly when integrated with renewable energy sources. A coordinated charging strategy combining G2V and V2G operations is proposed. The use of gradient boosting regression trees for predicting PEV state-of-charge represents a novel contribution. The analysis evaluates maximum feasible PEV penetration levels under network constraints and demonstrates that solar-powered car parks can further mitigate congestion, highlighting the benefits of renewable-assisted charging coordination [107] .

A robust smart charging strategy for plug-in electric vehicles in renewable-rich smart distribution grids is propose4d in [108] . The literature emphasizes the techno-economic benefits of leveraging renewable energy sources to support coordinated charging and discharging of PEVs. Key challenges related to uncertainties in load demand, renewable generation, and electricity prices are acknowledged. To address these uncertainties, a non-deterministic optimization framework based on IGDT is developed. Simulation results on a test smart microgrid validate the effectiveness of the proposed approach in achieving robust charging schedules while maintaining system reliability under uncertainty [108] .

The role of demand response programs in energy management systems that incorporate renewable energy sources and electric vehicles is reviewed and examined in [109] . The literature synthesizes key benefits of demand response, including improved flexibility, reduced operational costs, and enhanced renewable utilization. Challenges related to consumer participation, communication infrastructure, and control complexity are also discussed. The review highlights the growing importance of coordinated demand response strategies in enabling effective integration of EVs and renewables within modern power systems [109] .

Distributed energy management as a core component of future distribution grid control architectures is investigated in [110]. The literature highlights the advantages of distributed energy management over centralized approaches, particularly in terms of scalability and resilience. However, achieving global

optimality remains challenging due to the non-convex nature of the underlying optimization problems. While the ADMM is widely used, its convergence guarantees are limited to convex problems. The study emphasizes the need for advanced distributed optimization techniques capable of addressing non-convexity in EV-integrated distribution systems [110] .

A hybrid management framework for coordinated EV fleet charging and load scheduling in active distribution systems is presented in [111]. The literature emphasizes decentralized optimization using the alternating direction method of multipliers to achieve fast and scalable solutions. Multiple EV charging strategies, including valley filling and peak shaving, are incorporated into the scheduling process. The framework also integrates real-time pricing signals to influence consumption behavior and reduce peak demand. Results indicate significant improvements in energy efficiency and operational performance compared to traditional centralized optimization approaches [111] .

The implications of integrating electric vehicles into distribution networks with high renewable energy penetration is examined in [112] . The literature indicates that EV adoption significantly alters electricity consumption patterns and demand profiles. A key research gap identified is the insufficient consideration of battery degradation and driver behavior in vehicle-to-grid applications. The study emphasizes the necessity of smart grid technologies to manage demand fluctuations and support renewable integration. Economic aspects, including the costs and benefits of EV adoption and vertical integration, are highlighted as critical areas for future research [112] .

The phase imbalance issues in three-phase distribution systems arising from increased renewable generation and plug-in electric vehicle penetration are addressed in [113]. The literature highlights the need for incentive mechanisms to encourage PEV owners to participate in phase balancing. A non-cooperative game-theoretic framework is proposed to model autonomous charging decisions influenced by charging costs and phase-balancing remuneration. The original non-smooth game is transformed into a smooth formulation to facilitate Nash equilibrium analysis. The results demonstrate that the proposed approach can simultaneously improve power quality, enhance system reliability, and provide financial benefits to both PEV owners and distribution system operators [113].

2.1 Research Gaps

Despite extensive research on the integration of EVs into the PDNs, a critical review of the existing literature reveals several unresolved gaps that limit the practical applicability and holistic understanding of EV–grid interactions. These gaps motivate the need for more comprehensive modeling, assessment, and planning frameworks of PDNs considering EV charging demand.

1. Lack of Unified, Data-Driven EV Charging Demand Modeling: Most existing studies model EV charging demand using simplified assumptions, fixed penetration levels, or synthetic probability distributions that do not fully represent real-world charging behaviors. While stochastic and probabilistic approaches have been proposed, they often rely on limited datasets or focus on either residential slow charging or public fast-charging stations independently. The simultaneous, data-driven modeling of both residential and public fast EV charging demand, capturing realistic temporal and spatial variations, remains insufficiently addressed. This limits the accuracy of impact assessments and planning decisions in practical PDNs.

2. Inadequate Consideration of Daily Load Dynamics in the PDN Performance Assessment: Although prior works analyze the impact of EV charging on PDNs, many evaluations are conducted under static or peak-load conditions, neglecting the time-varying daily dynamics of EV charging demand. Comprehensive assessments that jointly examine hourly load evolution, cumulative Ohmic losses, and voltage magnitude deviations over a full daily horizon are scarce. Consequently, the long-term operational stress imposed by mixed EV charging patterns is not adequately quantified.

3. Limited Integration of Demand-Side Management with Realistic EV Charging Behavior: Demand-side management strategies, such as time-of-use pricing and smart charging, have been widely studied to mitigate EV-induced network stress. However, most existing approaches assume idealized user participation. The effectiveness of DSM strategies under concurrent slow residential charging, considering realistic user

behavior and operational constraints, remains underexplored. Moreover, DSM is often studied independently of generation-side mitigation measures, reducing its overall impact.

4. Insufficient Joint Mitigation of EV Impacts Using Renewable-Based Distributed Generation: While numerous studies demonstrate the benefits of distributed generation in improving voltage profiles and reducing power losses, most works address either EV charging impacts or DG allocation in isolation. Integrated frameworks that jointly mitigate the detrimental effects of both residential and fast EV charging through optimal placement of wind and solar PV DGs are limited. Additionally, the comparative performance of different meta-heuristic optimization techniques under such integrated scenarios has not been systematically investigated.

5. Predominance of Deterministic Planning Approaches: A large portion of the literature employs deterministic models for EV load and DG planning, overlooking uncertainties associated with EV arrival times, charging duration, renewable generation variability, and load demand fluctuations. Although stochastic methods exist, few studies formulate comprehensive probabilistic planning models that simultaneously consider uncertainties in EV charging demand and renewable energy generation within operational constraints of distribution networks.

6. Limited Focus on Combined Residential and Public Fast-Charging Uncertainty: Existing probabilistic planning studies typically consider either residential EV charging or fast-charging stations separately. The combined uncertainty arising from both charging modes, which is increasingly relevant in modern urban and semi-urban distribution networks, has not been adequately captured. This results in suboptimal DG siting and sizing decisions that may not remain robust under real-world operating conditions.

7. Insufficient Multi-Objective Planning Targeting PDN Losses and Voltage Deviations: Although multi-objective optimization frameworks have been proposed, many focus on economic objectives or hosting capacity enhancement while giving limited attention to simultaneous minimization

of Ohmic losses and voltage magnitude deviations under uncertainty. Unified planning formulations that explicitly balance these technical objectives in EV-dominated distribution networks are still lacking.

In summary, the literature lacks a unified, data-driven, probabilistic planning framework that simultaneously:

- Models realistic residential and public fast EV charging demand,
- Assesses time-varying network performance,
- Incorporates practical demand-side management strategies,
- Optimally allocates renewable-based distributed generation under uncertainties, and
- Minimizes technical performance indices such as total PDN Ohmic losses and voltage deviations.

Addressing these gaps forms the core motivation and contribution of the present research.

2.2 Motivation

The global transition toward electrified transportation has positioned EVs as a cornerstone of sustainable energy and mobility systems. Extensive research over the past decade has demonstrated that increasing EV penetration significantly alters the operational characteristics of PDNs, introducing new challenges related to load growth, voltage regulation, thermal congestion, and network losses. Prior studies have analyzed these impacts under diverse contexts, including residential charging dominance, public fast-charging proliferation, stochastic user behavior, and renewable energy integration. However, despite this growing body of work, several critical gaps remain unresolved, motivating the present research.

A substantial portion of the existing literature models EV charging demand using simplified assumptions, fixed penetration levels, or synthetic load profiles that do not adequately reflect realistic charging behaviors. Although

probabilistic and stochastic approaches have been introduced to capture uncertainties in EV arrival times, state-of-charge, and charging duration, many studies rely on limited datasets or focus on either residential charging or public fast-charging stations in isolation. This fragmented modeling approach restricts the accurate representation of emerging EV charging ecosystems, where slow residential charging and high-power public fast charging coexist and interact dynamically. Consequently, there is a strong motivation to develop data-driven EV charging demand models that simultaneously represent residential users and public fast-charging stations using realistic temporal and spatial datasets.

From an operational perspective, previous investigations have clearly established that uncontrolled EV charging can exacerbate peak demand, increase Ohmic losses, and cause unacceptable voltage magnitude deviations, particularly in low- and medium-voltage distribution networks. While numerous studies assess network performance under EV penetration, most analyses are static or based on limited time snapshots, overlooking the daily load dynamics inherent in EV charging behavior. Furthermore, comparative evaluations of voltage deviation and loss patterns under mixed charging modes remain sparse. This motivates a comprehensive performance assessment framework that evaluates existing utility distribution networks under realistic, time-varying EV charging demand, with explicit emphasis on daily load evolution, total network losses, and voltage profile degradation.

To mitigate these adverse impacts, DSM strategies—such as ToU tariffs, smart charging, and coordinated scheduling—have been widely proposed. While prior works confirm the effectiveness of DSM in flattening load profiles and reducing congestion, many approaches assume idealized user compliance or neglect the interaction between DSM policies and high-power public fast-charging demand. Moreover, DSM strategies are often evaluated independently of generation-side solutions, limiting their ability to fully relieve network stress under high EV penetration. This underscores the need for practical DSM policy design, particularly time-of-use–based mechanisms, that can operate alongside realistic EV charging behavior while preserving system reliability.

Parallel to demand-side solutions, the integration of renewable-based DG, especially solar PV and wind energy, has emerged as a promising means to counterbalance EV-induced load growth. Numerous studies demonstrate that

optimally placed DG units can reduce power losses, improve voltage stability, and enhance hosting capacity. However, existing works frequently focus on either DG allocation or EV charging impacts separately, or they rely on deterministic planning approaches that fail to capture uncertainties in EV demand and renewable generation. Additionally, the comparative effectiveness of different meta-heuristic optimization techniques for mitigating the combined impacts of slow residential and public fast EV charging remains insufficiently explored. These limitations motivate the development of integrated mitigation frameworks that optimally allocate wind- and PV-based DG resources using advanced meta-heuristic methods.

Finally, although stochastic and probabilistic planning models have gained traction, many current formulations do not fully integrate the compounded uncertainties arising from EV charging behavior, renewable generation variability, and operational constraints of PDNs. There remains a notable lack of unified probabilistic planning frameworks that jointly optimize the siting and sizing of wind and solar PV DGs in networks experiencing both residential and public fast-charging demand, while explicitly minimizing Ohmic losses and voltage deviations. Addressing this gap is essential for enabling resilient, efficient, and future-ready distribution networks.

Motivated by these identified research gaps, the present work aims to develop a comprehensive, data-driven, and probabilistic planning framework that captures realistic EV charging demand, rigorously evaluates distribution network performance, incorporates demand-side management policies, and optimally integrates renewable-based distributed generation under uncertainty. By bridging demand modeling, operational assessment, DSM strategies, and probabilistic DG planning within a unified methodology, this research seeks to advance the state of the art in EV-integrated power distribution network planning and operation.

2.3 Thesis Objectives

Recognizing that redesigning existing PDNs is often neither economical nor practical, the thesis develops methodologies to assess the impacts of EV

integration and implement effective mitigation strategies within existing infrastructure of the PDNs. Additionally, the thesis explores the optimal allocation of renewable-based DG resources to meet the additional demand introduced by the EVCD, thus enhancing the reliability of the PDN. To achieve these objectives, the thesis is structured around the following research tasks:

1. Modeling of emerging EV charging demand for both residential users and public fast-charging stations using realistic, data-driven datasets.

2. Performance assessment of existing utility distribution networks under EV charging demand, with emphasis on daily load dynamics, total network Ohmic losses, and bus voltage magnitude deviation.

3. Development of demand-side management strategies, such as time-of-use policies, to alleviate the additional stress imposed by EV charging and to preserve the system reliability.

4. Mitigation of the detrimental effects of both slow residential and public fast charging of EVs on power distribution networks through the optimal allocation of wind and solar photovoltaic -based distributed generation resources using different meta-heuristic techniques.

5. Formulation of a probabilistic planning model for the optimal siting and sizing of solar photovoltaic and wind turbine based distributed generation in power distribution networks with both residential and public fast EV charging demand, aiming to minimize PDN Ohmic losses and bus voltage magnitude deviations under operational and uncertainty constraints.

Chapter 3

Modelling of EV Charging Demand and its Impact on PDNs

The rapid proliferation of EVs represents a paradigm shift in both the transportation and power sectors. Although adoption of EVs promises reduced greenhouse gas emissions and increased energy efficiency, it also introduces new, dynamic, and spatially distributed loads to PDNs. Unlike conventional residential, commercial or industrial loads, the demand for EV charging is highly stochastic, time-dependent, and behavior-driven, with magnitudes and durations varying significantly among users.

To accurately assess the technical impacts of EV integration-such as peak load growth, phase unbalancing, voltage regulation challenges, and increased losses-it is essential to develop realistic models of EV charging demand. Without these models, distribution system studies risk relying on oversimplified assumptions, potentially underestimating or overestimating the network reinforcements required.

The accuracy of EV charging demand models depends not only on the quality of mobility and behavioral data, but also on a comprehensive understanding of charging technologies, infrastructure types, and associated technical standards. These factors directly influence the magnitude, duration, timing, and location of EV charging loads, and therefore must be integrated into model development.

This chapter presents a comprehensive overview of EVs with a focus on their relevance to PDN studies. It begins with the classification of EVs, followed by an in-depth discussion of charging technologies, infrastructure types, and associated international standards. Various modeling approaches are reviewed,

from deterministic and stochastic methods to advanced data-driven techniques, to provide a holistic understanding of how the charging behavior of EVs can be realistically represented in power system analyzes.

3.1 EV Charging Infrastructure

EVs are developed with a range of charging technologies, capacities, and charging/discharging strategies to meet their specific requirements. As a result, standardized charging levels and models have been established to promote consistency and accelerate adoption within the industry. Different countries adhere to distinct EV charging standards, with the primary variation among them being the design of ports and connectors. Fig. 3.1 (a) and 3.1 (b), illustrate various charging ports and connectors developed according to these standards. To minimize incompatibility issues, manufacturers are actively working toward a universal connector solution. In the United States, the SAEJ1772 connector is widely used and supports AC and DC charging. Tesla has developed its own proprietary connector, also capable of AC and DC fast charging, along with an adapter that allows vehicles with SAEJ1772 connectors to use Tesla superchargers. Another widely adopted connector in Europe is the "Combo," which enhances existing AC connectors by adding separate DC charging pins. As shown in Fig. 3.1, current connectors on the market differ significantly in shape and design. Manufacturers of EV and charging equipment are striving to standardize these interfaces to achieve a globally compatible EV charging system.

3.1.1 EV Charging Power Levels

EV charging can be supplied using either AC or DC sources. AC charging operates at different voltage and frequency levels depending on the standards of the power system of the respective country. Based on voltage levels, AC charging is typically classified into Level 1, Level 2, and Level 3, with Level 3 providing the highest charging voltage. Level 1 and Level 2 chargers can generally be installed in private locations, while Level 3 chargers – requiring dedicated wiring and a separate transformer – require utility approval and are most often used at

	USA	JAPAN	EU	CHINA
Single Phase/ 3-Phase AC Charging	 SAE J1772 Level 1, Level 2 Single phase	 SAE J1772 Level 1, Level 2 Single phase	 IEC 62196 Level 1 Single Phase  IEC 62196-2 Level 2,3 Single/Three phase	 IEC 62196 Level 1,2 Single/Three Phase
DC Fast Charging /AC-DC Combo	 Level 1 + DC Level 2 + DC SAE J1772 Combo	 JEVS G105-1993 CHAdeMO DC Fast Charging	 IEC 62196-3 Hybrid Combo	 GB/T 20234.3-2011 DC Fast charging

(a) Charging Port

	USA	JAPAN	EU	CHINA
Single Phase/ 3-Phase AC Charging	 SAE J1772 Level 1, Level 2 Single phase	 SAE J1772 Level 1, Level 2 Single phase	 IEC 62196-2 Level 1, 2 Single/Three phase	 IEC 62196 Level 1,2 Single/Three Phase
DC Fast Charging /AC-DC Combo	 SAE J1772 Level 2 + DC Combo  Tesla Supercharger	 CHAdeMO DC Fast Charging	 IEC 62196-3 Hybrid Combo	 GB/T 20234.3-2011 DC Fast charging

(b) Charging Connector

Fig. 3.1: Schematic diagram of charging ports and connectors developed according to various standards, [2]

Table 3.1: EV Charging Levels [2, 3]

Power Level	**Level 1**	**Level 2**	**Level 3**
Voltage Level (V)	120 (AC)	208–240 (AC)	300–800 (DC)
Current Level (A)	12–16	12–80	250–500
Charging Power (kW)	1.44–1.9, Single-Phase	3.1–19.2, Single-phase/Split-Phase	20–350 Three-Phase
Charging Time	200 km: +/- 20 hours	200 km: +/- 5 hours	80% of 200 km: +/- 30 minutes
Supply Interface	Convenience Outlet	Dedicated EV Supply Equipment	Dedicated EV Supply Equipment
Charging Location	Residential	Private & Commercial	Commercial
Charger Type	On–board	On–board	Off–board

public charging stations. At an equivalent voltage level, DC charging offers faster charging rates and typically supports higher power capacities [72]. A summary comparison of different charging power levels, as specified by various international standards, is provided in Table 3.1.

According to the Electric Power Research Institute (EPRI), EV owners typically charge their vehicles overnight at home. Consequently, the most common options for residential charging are Level 1 and Level 2 equipment [3, 8]. Level 1 charging, the slowest method, operates using a standard household outlet and may employ a connector such as the J1722 for the AC port of the EV [2, 3]. This method requires no additional infrastructure at home or business locations and benefits from lower off–peak electricity rates during night–time hours.

Level 2 charging, which is widely used in both residential and public settings, offers faster charging times and typically involves dedicated charging equipment with a properly installed connection. By integrating certain power electronics onboard the vehicle, Level 2 systems reduce the complexity of external infrastructure.

Level 3 charging, intended primarily for commercial use, delivers the fastest charging rates, often under one hour–making it comparable to the refueling experience at petrol stations. These chargers are commonly installed at highway

rest areas and urban refueling hubs. They require off–board AC–DC conversion equipment and are not suited for residential deployment due to their high power requirements and infrastructure needs.

3.2 EV Charging Technology

The rapid growth of EVs has placed significant emphasis on the development of efficient and reliable charging technologies. As the performance and lifespan of EV batteries are directly influenced by the charging process, optimizing charging methods has become a critical research focus. Modern EV charging strategies aim to balance fast charging capability with battery safety, energy efficiency, and thermal management. This requires careful control of current, voltage, and power during the charging cycle to prevent degradation and ensure consistent performance. With advancements in charging algorithms and power electronics, innovative approaches are being explored to meet the increasing demand for faster charging while maintaining long-term battery health. A thorough understanding of these techniques provides the foundation for designing next-generation EV charging systems that can support the widespread adoption of electric mobility.

3.2.1 Battery Charging Methods for EVs

The rechargeable battery serves as the primary energy source for powering EVs. Significant advancements in battery technology have been a key driver behind the rapid growth and widespread adoption of EVs in recent years. Over time, the dominant battery technology for energy storage in EVs has shifted from traditional lead–acid batteries to modern lithium–ion batteries, while research efforts are also exploring high–energy–density alternatives such as lithium–sulfur batteries for various EV applications [3]. A range of charging techniques is employed for replenishing EV batteries, including:

- Constant Current
- Constant Voltage

- Constant Power

More recently, advanced charging strategies have emerged that combine these conventional methods to enhance control over the charging process, leading to hybrid approaches such as CC–CV and CP–CV charging methods.

3.2.1 Constant Current

The CC charging method is a straightforward approach in which the charging current supplied to the battery is maintained at a fixed level by adjusting the charging voltage. This process continues until the battery voltage reaches a predetermined threshold. In this method, a discharged battery typically receives a current equal to about 10% of its rated maximum capacity. CC charging is particularly suitable for nickel–metal hydride and nickel–cadmium batteries. However, without proper control, overcharging can lead to gassing, overheating, and even severe damage to the battery pack. Continuous overcharging or undercharging can significantly degrade battery performance, making it essential to regulate both current and voltage profiles—whether using CC, CV, or hybrid charging techniques [2]. In CC charging, batteries tend to draw higher power at the start of the process, and if this is not managed, excessive current injection during low-voltage conditions can shorten battery lifespan.

3.2.2 Constant Voltage

In contrast, the CV method maintains a fixed charging voltage while adjusting the current as needed, continuing until the charging current approaches zero. This approach mitigates the risk of excessive power draw and overcharging, as current naturally tapers off during charging. However, it often results in longer charging times compared to CC charging.

3.2.3 Constant Power

The CP charging method delivers a fixed amount of power to the battery throughout the charging process, adjusting the voltage and current dynamically to maintain the set power level. At the beginning of charging, when the battery voltage is relatively low, the current is high to meet the power requirement; as

the battery voltage rises, the current decreases proportionally to keep the power constant. This approach offers a balanced compromise between the CC and CV methods, potentially reducing overall charging time while avoiding excessive current injection at low voltages. However, precise control systems are essential to manage the rapid current changes and prevent thermal stress on the battery pack. CP charging is particularly advantageous in applications where fast and efficient energy transfer is prioritized, such as high-power EV charging stations, but careful thermal management and monitoring are required to preserve battery health and ensure safety.

3.3 EV Charging Strategy

Among the various charging strategies, current-voltage regulation plays a vital role in ensuring safe and reliable energy transfer to the battery. In particular, two widely adopted approaches – CC-CV and CP-CV charging are gaining prominence due to their balance between performance and protection [2, 3]. The CC–CV method, traditionally applied in lithium-ion battery charging, emphasizes stable current delivery followed by voltage regulation to prevent overcharging. On the other hand, the CP-CV approach offers a more optimized profile for fast-charging scenarios by maintaining constant power before transitioning to voltage control. A comprehensive understanding and comparison of these methods are essential for designing advanced charging systems that meet the growing demands of modern EV applications.

This study is undertaken with the objective of developing models that can accurately estimate realistic 24-hour EV charging demand profiles. The focus is placed on distinguishing between residential charging, which typically involves slow overnight charging, and public charging stations, where fast charging is more prevalent. By formulating separate demand profiles for these scenarios, the research aims to capture the variability in user behavior, charging patterns, and energy requirements associated with different charging contexts. The modeling framework is grounded in real-world data and transportation survey data, ensuring that the profiles reflect practical usage conditions rather than purely theoretical assumptions. Such an approach not only enhances the accuracy of

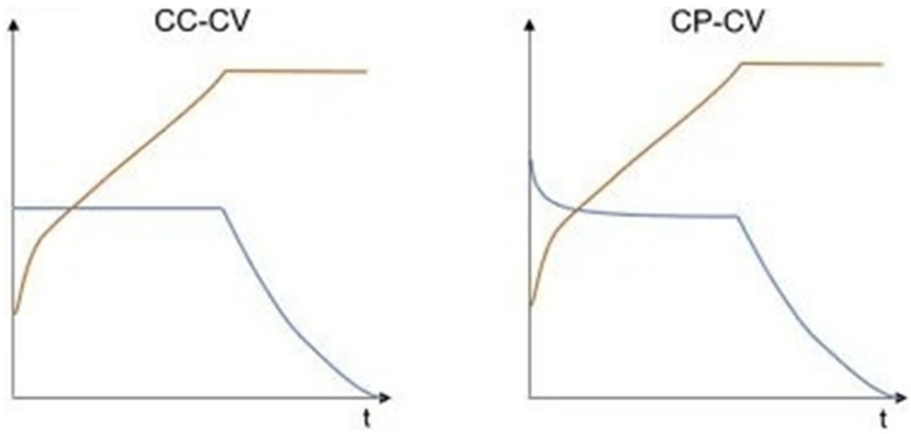


Fig. 3.2: CC-CV and CP-CV mode of charging [2, 3]

demand forecasting but also provides valuable insights for grid planning, infrastructure development, and policy formulation in the context of large-scale EV integration.

3.4 EV Charging Demand Modeling

Accurate modeling of EVCD is essential for the effective planning of charging infrastructure, minimizing grid impacts, and ensuring reliable service for EV users. To achieve this, transportation survey data can be leveraged to simulate the real–world travel patterns of EV owners, capturing details such as trip frequencies, travel distances, departure and arrival times. By incorporating these behavioral patterns into demand estimation models, planners can better predict when and where charging will be needed, leading to more precise infrastructure sizing, EVCD estimation, and improved integration of EVs into the power grid.

However, the development of reliable EVCD models requires more than just statistical representation of driver behavior or travel patterns. The physical characteristics of charging technologies, the deployment patterns of charging infrastructure, and the technical specifications defined by industry standards fundamentally shape when, where, and how EVs draw power from the grid. These factors dictate charging durations, load magnitudes, and simultaneity of demand. Without incorporating these technological and infrastructural realities,

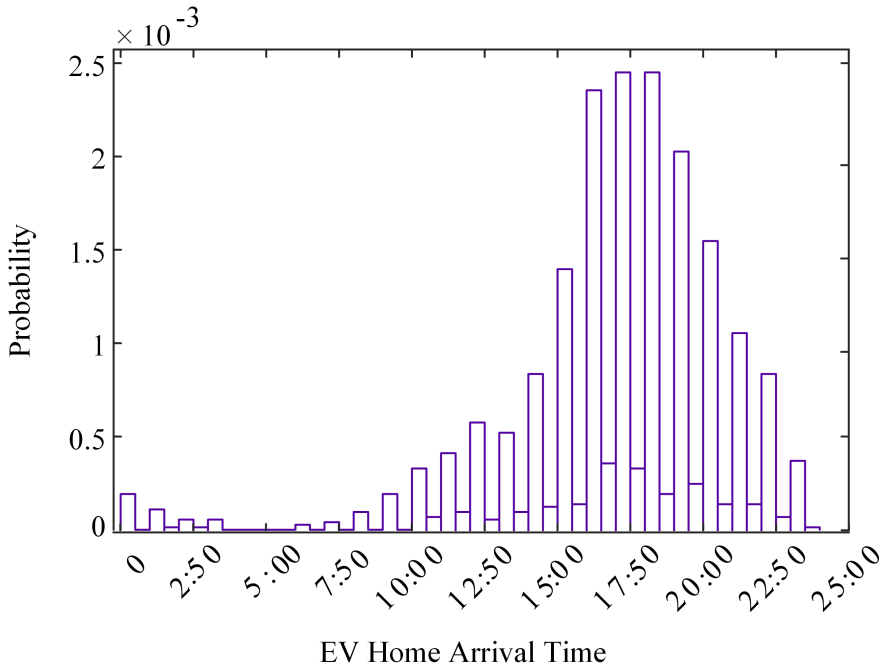


Fig. 3.3: Arrival time probability for home based on NHTS 2017 Datasets

demand models risk oversimplifying EV load behavior, potentially leading to inaccurate predictions of PDN impacts and suboptimal planning decisions.

3.4.1 Slow Charging

According to a 2017 survey [114], most EVs only go short distances and are primarily charged at home using slow AC charging. Charging at power level 1 is the slowest way to complete the EV charging procedure. A standard connector known as J1722 for the EV's AC port may be used for this kind of connection [2]. The most widely used domestic EV charging method is often slow charging with the CC–CV or CP–CV protocol.

The charging profile in CC–CV charging is generally divided into two main stages: an initial CC phase, followed by a CV phase. In the CC stage, the charging current is gradually increased in small increments to raise the battery voltage to a predetermined limit, referred to as the constant current threshold. This gradual increase ensures that power is delivered in a controlled manner

during the initial period, thereby minimizing the risk of battery damage. Once the voltage reaches the threshold, the charger maintains a higher constant current, enabling the battery to charge rapidly and reach approximately 80% of its SOC. At this point, to prevent overcharging and limit current flow, the charger transitions into the CV stage, where charging continues at a fixed voltage while the current progressively decreases [2, 3].

3.4.1 Charging Model of a PHEV

Multiple commercially viable charging standards are available worldwide which is outlined in Table 3.1. In our study, slow residential charging of EVs in the U.S. is considered and hence, it is assumed that the EV owners will charge their vehicles after reaching home using slow, level-1 charging with SAEJ1772 standard having 120V AC, 12A, 1.44 kW outlet [3]. EV parameters, such as battery capacity, SOC, amount of energy needed to charge the battery and charging level are crucial to assess the EV charging demand and its effects on the PDN. In this regard, PHEVs are broadly categorized into four segments in the study ranging from compact sedan EVs to full-size SUVs as presented in Table 3.3 [8, 115]. The modelling of charging demand of PHEVs is carried out using (3.1), (3.2), (3.3), and (3.4).

Table 3.3: PHEV40 battery capacities and ECPM for different types of vehicles [8]

Vehicle Type	ECPM (kWh/mile)	PHEV40 Battery Capacity (kWh)
Compact Sedan	0.26	10.4
Mid-size Sedan	0.30	12.0
Mid-size SUV	0.38	15.2
Full-size SUV	0.46	18.4

The usable battery capacity of a PHEV is the product of its AER and ECPM [8] as shown below,

$$C_{\text{batt}} = AER \times ECPM \tag{3.1}$$

The EV SOC is estimated as,

$$SOC = \begin{cases} \left(1 - \frac{\alpha \times d}{AER}\right) \times 100, & \alpha \times d \leq AER, \\ 0, & \alpha \times d \geq AER \end{cases} \tag{3.2}$$

The SOC determines how much energy is needed to charge the EV battery after the last trip. The electrical energy taken from the grid is calculated as,

$$E_g = \frac{\left(1 - \frac{SOC}{100}\right) \times C_{batt}}{\eta} \tag{3.3}$$

In this work, η is taken as 0.9 (90%) [115]. Finally, the total time required to charge the EV can be determined as

$$T_{ch} = \frac{E_g}{ch\_level} \tag{3.4}$$

The values of the parameters, *'d'* and *'Type of EV'*, in the above modelling equations are taken from the NHTS 2017 data, which is discussed in the further sub-section. Furthermore, changing the charging power level and battery charging efficiency will result in varied EV charging demand depending upon the battery capacity.

3.4.2 Charging Model of a BEV

To evaluate the demand for EV charging and its impact on PDNs, EV metrics like battery capacity, initial SOC, ECPM, and charging power level are essential. In this regard, BEVs are broadly divided into four groups, ranging from small city EVs to SUVs, as shown in Table 3.4 [4]. Thus, the estimation of slow BEV charging power demand is carried out using (3.5)-(3.7).

The battery SOC is estimated [45] as,

$$SOC = \left(1 - \frac{ECPM \times d}{E_{cap}}\right) \times 100 \tag{3.5}$$

The amount of energy required to charge the EV battery following the most recent trip is decided by the SOC. The electrical energy that is extracted from the

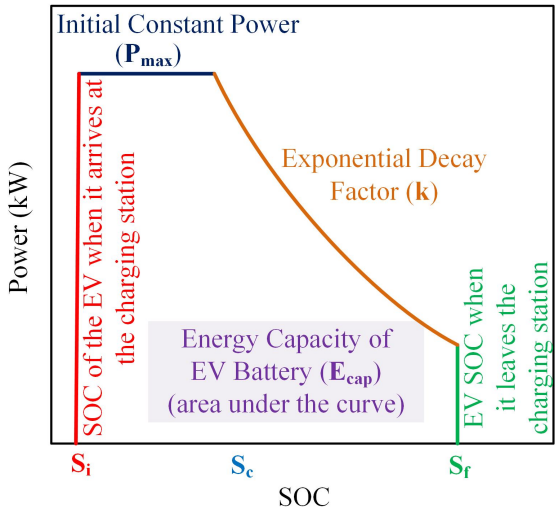


Fig. 3.4: A generalized fast EV charging profile employing Tesla Supercharger [4]

grid may be calculated as,

$$E_g = \frac{\left(1 - \frac{SOC}{100}\right) \times E_{cap}}{\eta} \tag{3.6}$$

Lastly, the time needed (in hours) to charge the EV may be calculated as,

$$T_{ch} = \frac{E_g}{ch\_level} \tag{3.7}$$

Table 3.4: EV Specifications for Slow Charging

Vehicle Type	ECPM (kWh/mile)	Battery Capacity (kWh)
Small	0.24955	42
Medium	0.25599	58
Large	0.29946	77
SUV	0.38157	70

With regard to level 1 charging of EVs in homes using the SAEJ1772 standard, *ch_level* is 1.44 kW [10]. In this study, the starting time of slow EV charging is taken as the trip end time of the EV.

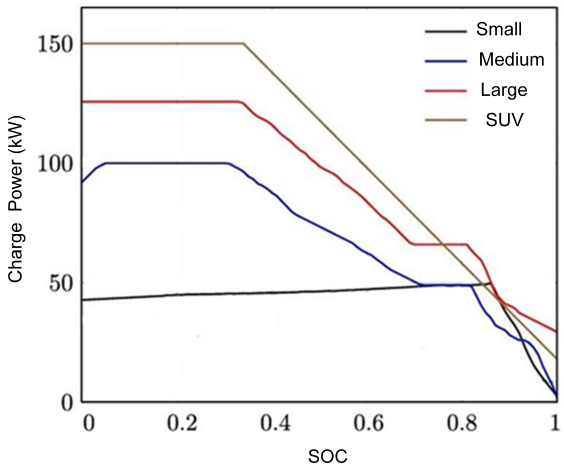


Fig. 3.5: Fast charging characteristics of EVs of different types at a PFCS [4, 5]

3.4.2 Fast Charging

In contrast to slow charging, which employs the CC-CV or CP-CV protocol, fast charging may experience phase transitions far earlier than 80% [4]. In this context, a generalized model that depicts the charging profile of the TS as shown in Fig. 3.4, is developed using datasets gathered from three Tesla superchargers (Fig. 3.5) [4, 5]. As demonstrated in Fig. 3.5, the Tesla supercharger does not use the CC-CV charging protocol; instead, it uses a maximum charging power phase from the beginning up to a specific SOC (usually 25%) and then transitioning to a phase where the power rapidly drops with the SOC. (3.8) and (3.9) provide the equations controlling the Tesla supercharger's charging power demand [116].

$$P(t) = \frac{P_{\max} e^{-k_d S(t)}}{e^{-k_d S_c}} \tag{3.8}$$

$$S(t) = \frac{1}{E_{\text{cap}}} \int_0^t P(t)\, dt \tag{3.9}$$

The value of k_d is taken as 2, and the value of S_c is obtained from Fastned [116]. Fig. 3.5 shows the practical charging characteristics for fast charging of different types of EVs [4].

From Fig. 3.4, it is observed that to model the fast EV charging power demand employing Tesla superchargers, six variables are required for all EV types which

are,

1. Energy capacity of the EV battery in kWh, E_{cap}
2. SOC of the EV when it arrives at the charging station, S_i
3. Initial constant power in kW, P_{max}
4. SOC at which the charging power switches (from constant to decaying mode), S_c
5. Exponential decay factor, k_d or k
6. SOC at which the EV leaves the charging station, S_f

Table 3.6: EV Specifications for Fast Charging

Vehicle Type	**Battery Capacity (kWh)**	**Maximum DC Charging Power (kW)**
Small	42	50
Medium	58	100
Large	77	125
SUV	70	150

The details of the EVs for fast charging is provided in Table 3.6. The value of k is set to 2 [116] and the value of S_c is sourced from Fastned [18], an operator that offers public-fast charging services to EVs. Fig. 3.5 illustrates the real-world charging characteristics of various types of EVs under fast charging [4, 5]. Fig. 3.6 depict the probability of EVs arriving at a charging station for fast charging [117].

The fast-charging station in this study consists of five charging ports, each with a power rating of 150 kW. In this study, the EV type (which determines battery capacity), and the initial SOC of the EVs arriving at the fast-charging station are both treated as independent random variables.

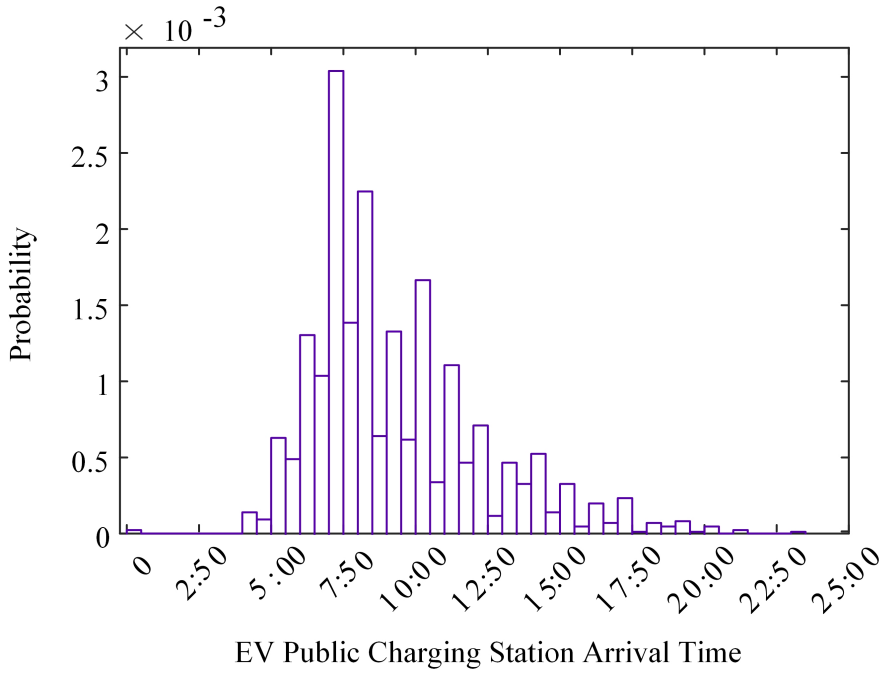


Fig. 3.6: Arrival time probability for EVs at fast charging station based on NHTS 2017 Datasets

3.4.3 Estimating EV Demand Profiles Using the Data from the NHTS

To assess the impact of EVs on the PDN, it is crucial to examine the behaviour patterns of EV owners, focusing on factors such as trip distance, arrival and departure times, EV type, and the travel day and date. Travel survey data are valuable resources for gathering these parameters, which can then be used to model charging demand profiles based on real world data. In this work, the NHTS data of the year 2017 is used. The detailed explanation about the filtering process of this data is explained in Chapter 5, subsection: 5.1.3.

The number of vehicles on the road during the day, the average commute distance of EV users to work, and statistical data on arrival and departure times are utilized to simulate the load demands for both slow and fast charging. In this study, the arrival time of the final vehicle trip is used as the charging start time for domestic, slow charging. However, for fast charging at the charging station(s), the charging start time is set as the average of EV departure and

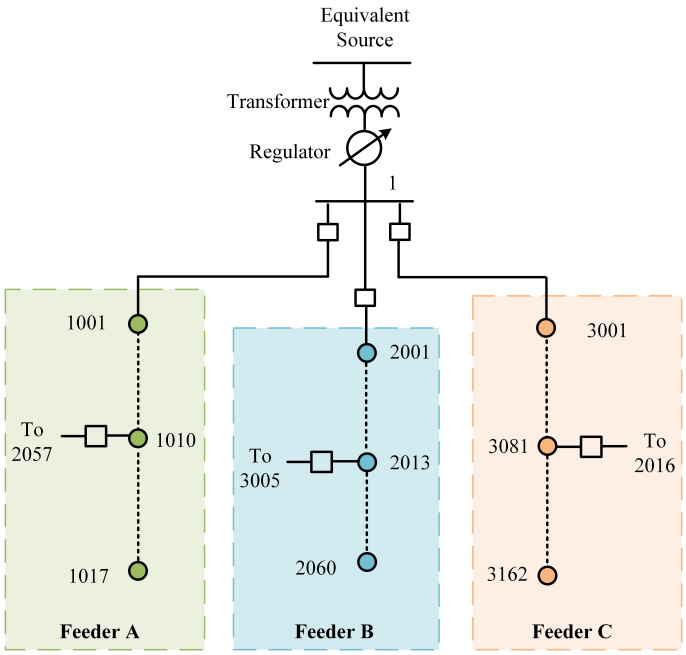


Fig. 3.7: Topology of 240-bus PDN

arrival time to represent the period when EVs are on the road and available to charge at the fast-charging station.

3.4.4 Power Distribution Network

The 240-bus power distribution test system represents a fully observable distribution grid in the Midwest U.S., where smart meters are installed at all end-user locations [1]. The topology of the 240-bus PDN is presented in Fig. 3.7. The complete single-line diagram of this PDN is presented in Chapter 1, Fig. 1.1. This time-series test system is a radial distribution network consisting of three feeders, all powered by a 69 kV substation. The three feeders in the test system are supplied by a 69/13.8 kV step-down, three-phase substation transformer with an on-load tap changer. The substation transformer has a rating of 10,000 kVA.

A key distinction of this distribution grid is the inclusion of one year's worth of smart meter data for all nodes, bridging the gap between current test feeders and quasi-static time series-based distribution system analysis. The smart meter data spans from January 2017 to December 2017 which includes hourly energy

consumption (kWh) for 1,079 customers. Unlike most of the standard IEEE distribution test systems, this network contains hourly real and reactive power demands of all customers from smart meters.

3.4.5 Direct Approach for Power-flow

A large number of PDNs are radially fed networks having low reactance-to-resistance ratio. In these kinds of configurations, the conventional power-flow techniques like Gauss-Seidel, Newton-Raphson are not suitable to apply. This article, therefore, uses a direct search-based approach for the power-flow analysis [118]. In this approach, two matrices have to be built – the BIBC matrix and the BCBV matrix. The power-flow solutions can be computed efficiently by multiplying these matrices. Fig. 3.8 shows a radial 6-bus distribution network. Here L_1 to L_5 are the branch currents and Z_{12} to Z_{56} are impedance of respective branches.

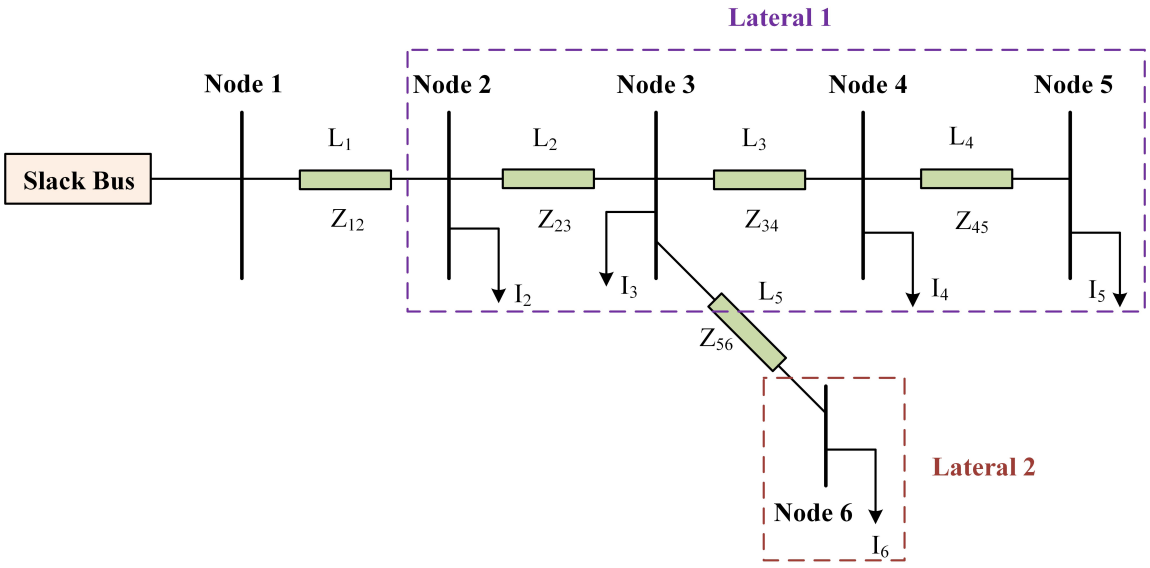


Fig. 3.8: A Simplified 6-Bus Distribution Network

At bus b, the complex load S_b is expressed by:

$$S_b = (P_b + jQ_b), \quad b = 1, 2, \ldots, 6 \tag{3.10}$$

whereas its corresponding equivalent current injection, I_b at k-th iteration is given by:

$$I_b^k = \left(\frac{P_b + jQ_b}{V_b^k} \right)^* \tag{3.11}$$

The branch current can be expressed as functions of equivalent current injections leading to the BIBC matrix as:

$$\begin{bmatrix} L_1 \\ L_2 \\ L_3 \\ L_4 \\ L_5 \end{bmatrix} = \begin{bmatrix} 1 & 1 & 1 & 1 & 1 \\ 0 & 1 & 1 & 1 & 1 \\ 0 & 0 & 1 & 1 & 0 \\ 0 & 0 & 0 & 1 & 0 \\ 0 & 0 & 0 & 0 & 1 \end{bmatrix} \begin{bmatrix} I_2 \\ I_3 \\ I_4 \\ I_5 \\ I_6 \end{bmatrix} \tag{3.12}$$

$$\mathbf{I}_{\text{branch}} = \mathbf{BIBC} \cdot \mathbf{I}_{\text{bus}} \tag{3.13}$$

Similarly, the relationship between branch currents and bus voltages can be expressed in the form of the BCBV matrix as:

$$\begin{bmatrix} V_1 \\ V_1 \\ V_1 \\ V_1 \\ V_1 \end{bmatrix} - \begin{bmatrix} V_2 \\ V_3 \\ V_4 \\ V_5 \\ V_6 \end{bmatrix} = \begin{bmatrix} Z_{12} & 0 & 0 & 0 & 0 \\ Z_{12} & Z_{23} & 0 & 0 & 0 \\ Z_{12} & Z_{23} & Z_{34} & 0 & 0 \\ Z_{12} & Z_{23} & Z_{34} & Z_{45} & 0 \\ Z_{12} & Z_{23} & 0 & 0 & Z_{56} \end{bmatrix} \begin{bmatrix} L_1 \\ L_2 \\ L_3 \\ L_4 \\ L_5 \end{bmatrix} \tag{3.14}$$

$$\mathbf{V} = \mathbf{BCBV} \cdot \mathbf{I}_{\text{branch}} \tag{3.15}$$

On combining (3.13) and (3.15),

$$\begin{aligned} [\Delta V] &= [BCBV]\,[BIBC]\,[I] \\ [\Delta V] &= [DLF]\,[I] \end{aligned} \tag{3.16}$$

where, the matrix DLF stands for Distribution Load Flow. DLF matrix is used to obtain the power-flow solutions efficiently.

3.5 Results and Discussions

For domestic charging, each household is assumed to receive power from a single-phase, 60 Hz, 120 V supply, in accordance with the SAEJ1772 charging protocol [2, 3]. Fast charging stations are assigned to three-phase buses 2058 and 3077 in the 240-bus PDN due to their higher transformer capacities [1]. In this work, slow charging refers to charging at home premises while fast charging refers to charging at a fast-charging station.

The dynamic EV charging demand for both domestic and fast charging is separately calculated using (3.5)-(3.7) and (3.8)-(3.9), respectively and then added to the base case demand of the PDN to obtain the 24-hour demand profile with EV charging. In this regard, two different penetration level of EVs are considered for both slow and fast charging as mentioned below,

- **Case I. Slow charging**
  - **SC, C1:** At least one EV per house
  - **SC, C2:** At most two EVs per house
- **Case II. Fast charging**
  - **FC, C1:** 5% EV penetration
  - **FC, C2:** 10% EV penetration

Fig. 3.10 shows the 240-bus power distribution network's total three-phase demand with different cases of slow and fast charging. The corresponding per-phase demand of the network is presented in Fig. 3.9. It may be noted that the EV charging demand for all phases are different, even with the same number of EVs connected, as the battery capacity, the distance travelled (indicative of the initial SOC), the trip end time are all random variables.

In Fig. 3.9 and Fig. 3.10, the green curve represents the network's base case demand profile (without any EV charging). The demand plots with slow charging (SC, C1, and SC, C2) show a significant increase during the evening hours. In contrast, fast charging exhibits a sharp spike in demand during the morning hours. This is because while EV owners usually charge their EVs after returning home in the evening whereas EVs recharge at fast charging stations

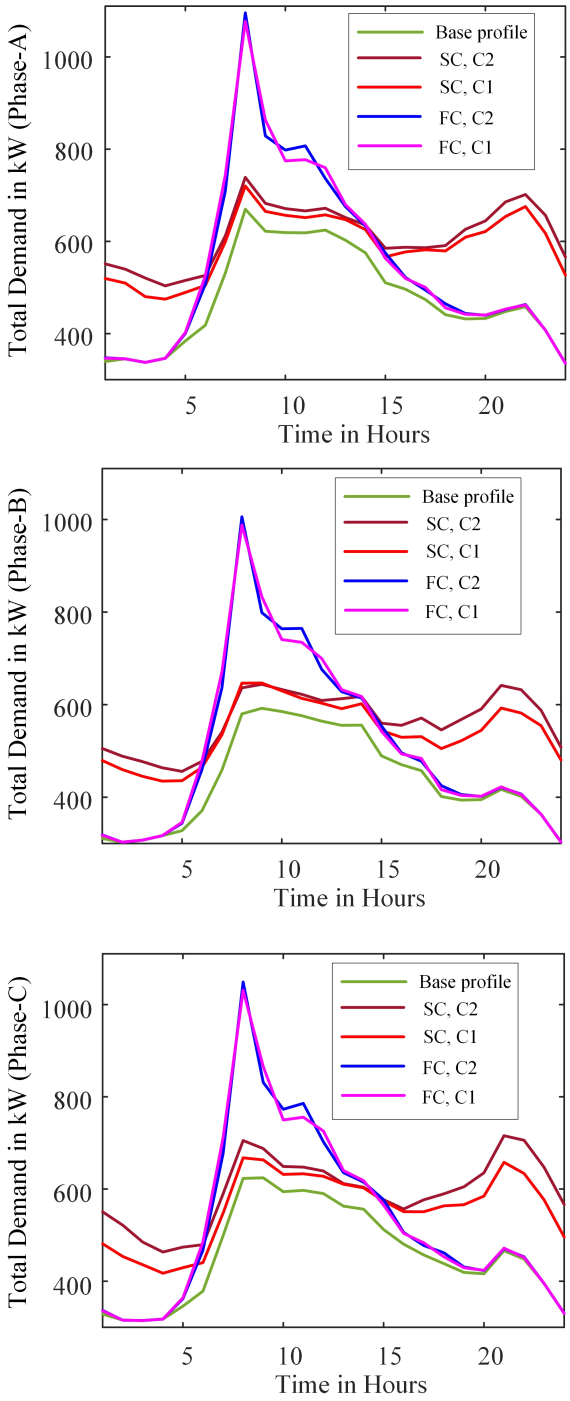


Fig. 3.9: Total per-phase demand of the network

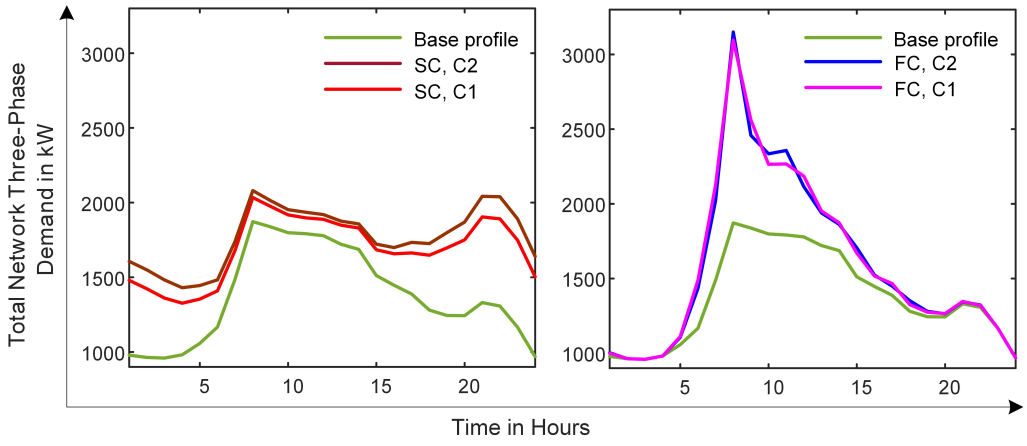
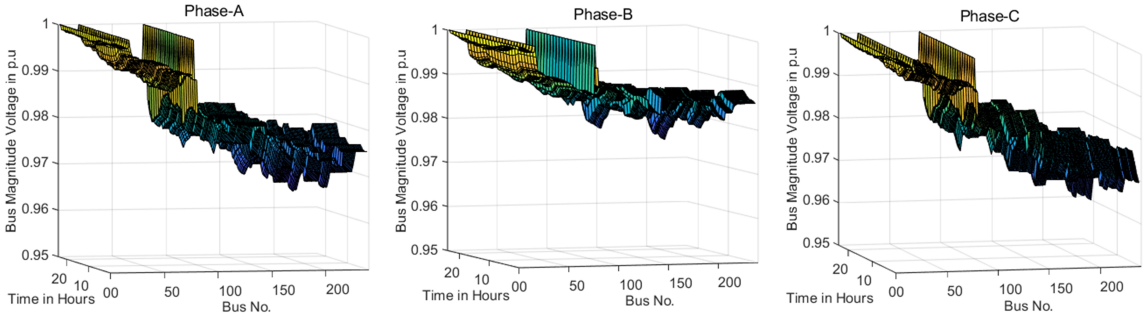
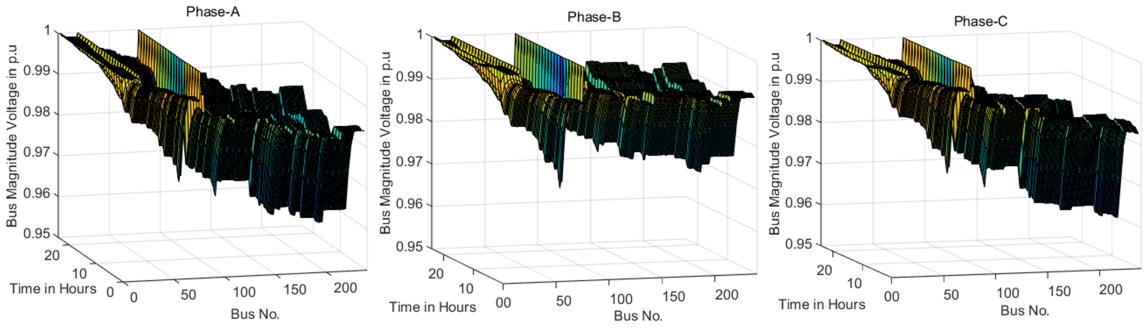


Fig. 3.10: Network total three-phase demand



(a) Slow Charging



(b) Fast Charging

Fig. 3.11: Network bus voltage magnitude profiles for (a) Slow and (b) Fast charging

when they are out for work. These results reflect practical scenarios, as they are based on data from the NHTS, which accounts for the probability of the EV arrival and departure times (Fig. 3.3 and Fig. 3.6), and as explained above in Section 3.4.3 of the chapter.

Fig. 3.11 depicts the 24-hour bus voltage magnitude profiles for slow and fast charging. The bus voltage magnitude profiles for slow charging (SC, C2) and fast charging (FC, C2) are shown in Fig. 3.11 (a) and Fig. 3.11 (b), respectively. These voltage profiles effectively corroborate the results presented in Fig. 3.9 and Fig. 3.10.

From Fig. 3.11 (a) and Fig. 3.11(b), it can be observed that for slow domestic charging (SC, C2), the bus voltage magnitude profile is smoother, with fewer fluctuations. Unlike slow domestic charging, where the voltage magnitude dips the incomer to the feeder ends are more predictable and lower, in fast charging, the voltage fluctuations are substantially higher and abrupt. In fact, the maximum voltage magnitude dips are observed to occur at and neighboring buses of buses 2058 and 3077 to which the fast-charging stations are connected (Fig. 3.11 (b). These buses were chosen for allocating fast charging stations because their transformer capacities are higher [20].

It is also observed from Fig. 3.11 (a) and Fig. 3.11 (b) that for phases A and C, the differences in the bus voltage magnitude dips with slow domestic and fast EV charging are substantially higher than that for phase B. It is due to the fact that the EV charging demand is observed to be lesser for phase B. It may be noted that the EV charging demand for all phases are different, even with the same number of EVs connected, as the battery capacity, the distance travelled (indicative of the initial SOC), the trip end time are all random variables.

Thus, bus voltage magnitude profiles suffer significantly more deterioration with fast charging of EVs, as compared to slow domestic charging.

3.6 Conclusions

This work presents the modeling of slow and fast EV charging based on real-world data from the NHTS 2017 travel survey and Fastned. The mathematical equations and parameters required for the modeling process are

thoroughly explained. Additionally, the practical challenges and impact of both slow and fast EV charging demand on a real-time 240-bus power distribution network is investigated. Two different EV penetration levels are considered for in-depth analysis. The results show that slow domestic charging increases the distribution network demand during noon and evening hours, while fast charging at charging stations causes a sharp demand spike in the morning. However, unlike slow domestic charging, which causes a relatively lower bus voltage magnitude dips, with fast charging, the bus voltage magnitude dips are substantially higher.

Chapter 4

Framing of EV Charging Policies to Mitigate EVCD Impact on PDNs

Uncoordinated and excessive charging demand can lead to several operational challenges within PDNs, including voltage instability, increased peak load, transformer overloading, higher power losses, and accelerated equipment aging. These impacts not only threaten the reliability and efficiency of power delivery but also impose additional costs on utilities in terms of infrastructure reinforcement and system upgrades. As EV penetration continues to grow, addressing these issues has become a priority for both researchers and policymakers.

To ensure the smooth integration of EVs without compromising grid performance, the formulation of effective EV charging policies has gained considerable attention. Such policies aim to regulate and optimize charging patterns through demand-side management strategies, time-of-use tariffs, and, controlled or smart charging mechanisms. By shaping user behavior and aligning charging demand with available grid capacity, these measures can significantly mitigate adverse impacts on PDNs while enhancing overall system resilience.

This research emphasizes the importance of framing structured EV charging policies that are informed by realistic demand profiles, grid conditions, and user behavior. The goal is to strike a balance between facilitating EV adoption and maintaining the stability and efficiency of PDNs. Ultimately, such policies will play a pivotal role in supporting the dual objectives of sustainable transportation and reliable power system operation, paving the way for a cleaner and more

resilient energy future.

4.1 Methodology

This section describes the data and the methodology utilized in the study of this chapter.

4.1.1 Filtered NHTS 2009 Data

In this study, NHTS 2009 data is used for extracting the trip characteristics of the vehicles. NHTS furnishes an encyclopedic travel pattern data in the U.S [117]. The database contains two Microsoft Excel files, VEHV2PUB.csv and DAYV2PUB.csv.

(a) VEHV2PUB.csv: This file demonstrates vehicle's characteristics and provides information related to more than three lakh vehicles. Eight attributes for each vehicle are used in this paper. They are: HOUSEID, TDAYDATE, TRAVDAY, PERSONID, VEHID, VEHTYPE, HHVEHCNT, BESTMILE. HOUSEID, PERSONID provides the trip characteristics covered by a specific member of a particular house. TDAYDATE and TRAVDAY stands for the date of travel and the day of the week respectively. HHVEHCNT indicates the count of vehicles in a household. Since BESTMILE is the best estimation of annual miles of each vehicle therefore, it is divided by 365 to extract daily miles travelled (DailyMile). VEHTYPE and VEHID indicates the type of the vehicle and the particular vehicle of a house used in a specific trip respectively.

(b) DAYV2PUB.csv: This file demonstrates trip characteristics and consists of more than 10 lakh trips. Nine attributes of each trip are used in this paper. They are: HOUSEID, TDAYDATE, TRAVDAY, PERSONID, VEHID, VEHTYPE, ENDTIME, TDTRPNUM and HHVEHCNT. ENDTIME indicates the time at which the trip ends. It is considered as the charging start time in this paper. TDTRPNUM indicates travel day trip number which is the number of trips covered by a vehicle in a day. VEHV2PUB.csv and DAYV2PUB.csv are merged to form a common file containing the required data. Table 4.1 presents a small portion of the filtered data.

Table 4.1: Filtered NHTS 2009 Data

HOUSE ID	TDAY DATE	TRAV DAY	PERSON ID	VEHID	VEH TYPE	END TIME	TRP NUM	VEH CNT	BEST MILE
20005517	200809	2	1	1	1	1800	1	1	10967.11
20006831	200804	2	3	1	1	2120	4	3	22183
20008273	200806	2	2	1	4	1845	6	2	18792.09
20024170	200808	2	1	1	1	1705	2	2	9192.44
20026482	200808	2	1	1	3	1745	4	3	24509.68
...	...	...	...	...	...	...	...	...	...

4.1.2 Charging strategy

In this study, residential charging (120 V) in U.S. is considered and hence, level 1 SAEJ1772 standard is used, with 120 V AC, 12 A, 1.44 kW outlet. The modelling of PHEVs is done using (3.1) to (3.4). The total number of customers in the PDN are 1079 [1] and each customer is considered as a household receiving single phase 120 V supply. The 240-bus system has 139 load buses which are single phase and customers allotted to each of them pertain to the phase (A, B or C) of that particular bus. The number of three-phase load buses are 55 and customers allotted to each of them are distributed equally among the three single phases (A, B and C), in order to minimize phase unbalance. It is assumed in this work that all customers charge their EVs from the confines of their home at 120 V, following the last trips of the vehicles.

To compute the charging demand due to the PHEVs, the following methodology is adopted:

(1) Each household (from the NHTS 2009 data) represents a single-phase customer. The number of customers allocated to the buses are carried out as per the customer data available in [1].

(2) The charging demand of each household (customer) is computed based on the number of PHEVs, type of the PHEV and its mileage using (3.1)-(3.4) and using the customer data of the PDN.

(3) The allocation of number of customers to each individual phase ('a', 'b' or 'c') is carried out using the customer data provided in [1] and as already detailed above.

(4) Finally, the charging demand of each phase is computed by summing the demands of all the customers pertaining to that phase. This is carried out for all the buses.

4.1.3 Load Profile

For obtaining the daily load curve, the smart meter data of all the customers of 240-bus PDN is taken into account [1]. On this basis, a 24-hour demand curve is plotted which is the base case for this study.

4.2 Framework of Charging Policy

To minimize the consequence of PHEV charging on the system demand profile and the bus voltages, practical charging policies are proposed in this work. Previously, many work has been done on coordinated/controlled/smart and non-coordinated/uncontrolled/non-smart charging of EVs for levelling the daily load curve [115, 119]. According to these strategies, the peak hours load is adjusted to off-peak hours and in this way the peak is shifted to valley thus levelling the 24-hour load of the distribution grid. Contrarily, these techniques are only time dependent since based on time interval, they shift the load of the system.

However, charging policies proposed in this chapter are time and SOC based since they are not only time dependent but also takes care of the SOC of the PHEVs. Therefore, the proposed policies are much practical and the description for the same is given below:

1. **Charging Policy 1:** As per this policy, vehicles having SOC greater than and equal to 50% and arriving home for charging between the interval 16:00 hrs to 05:00 hrs (next day) will be provided a commercially high incentive to charge their vehicles after 5 AM.

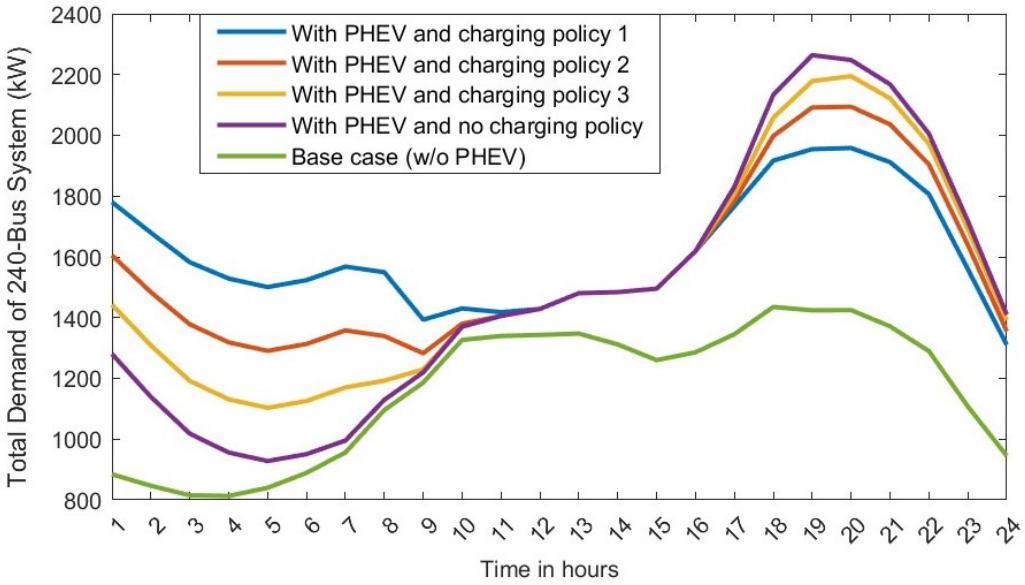


Fig. 4.1: Total Demand Profile for 240-Bus Distribution System for Different Scenarios

2. **Charging Policy 2:** As per this policy, vehicles having SOC greater than and equal to 60% and arriving home for charging between the interval 16:00 hrs to 05:00 hrs (next day) will be provided a commercially high incentive to charge their vehicles after 5 AM.

3. **Charging Policy 3:** As per this policy, vehicles having SOC greater than and equal to 70% and arriving home for charging between the interval 16:00 hrs to 05:00 hrs (next day) will be provided a commercially high incentive to charge their vehicles after 5 AM.

The proposed policy is aimed to make flat the daily load profile, reduce system losses and enhance bus voltage profile.

4.3 Results and Discussions

Fig. 4.1 shows the total hourly demand (three-phase) of the 240-bus PDN, on a typical summer weekday. From Fig. 4.1, it can be observed that the demand starts increasing from 3 p.m. onwards as residential customers start to plug in their vehicles after arriving home. Therefore, in order to counter this peak

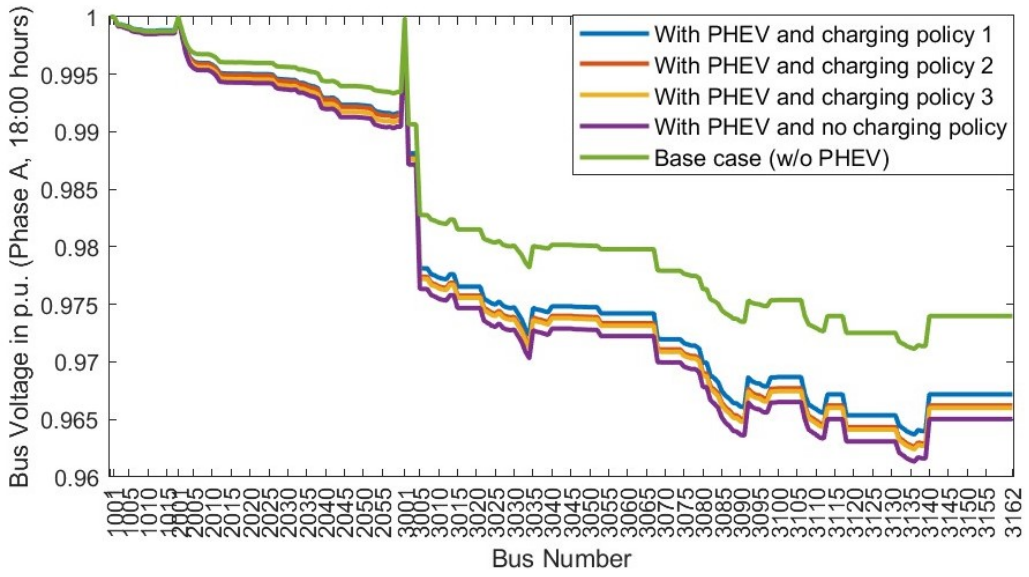


Fig. 4.2: Bus Voltage Magnitude Profile for 240-Bus Distribution System for Phase-A at 18:00 hrs for Different Scenarios

charging demand, practical PHEV charging policies are adopted which offer commercial disincentive for charging of vehicles between 16:00 to 05:00 hrs (next day) based on the SOC of the PHEV. It can be observed that with different charging policies, the total network demand (in purple) with PHEV charging has substantially flattened.

Fig. 4.2 – 4.4 shows the profile for bus voltages of the distribution system without and with PHEV charging at 18:00 hrs for phases A, B and C, respectively. It can be observed from all the plots that the bus voltage profiles with PHEV charging have deteriorated as compared to the case without PHEV. The system losses (at 18:00 hrs) for the base case (without any PHEV) and with PHEV (without any charging policy) are 31.06 kW and 71.43 kW, respectively. Thus, with PHEV charging, the system losses have increased substantially.

The system losses (at 18:00 hrs) with PHEVs but without any charging policy is 71.43 kW whereas with the proposed PHEV charging policies it's 56.5261 kW, 61.93 kW, 65.5409 kW for charging policy 1, 2 and 3 respectively. Thus, after the adoption of the PHEV charging policy, the system losses have decreased substantially.

Bus no. 3147 is a single-phase bus (Phase-C) with 17 connected customers and bus no. 3034 is a three-phase bus with 9 connected customers. These two

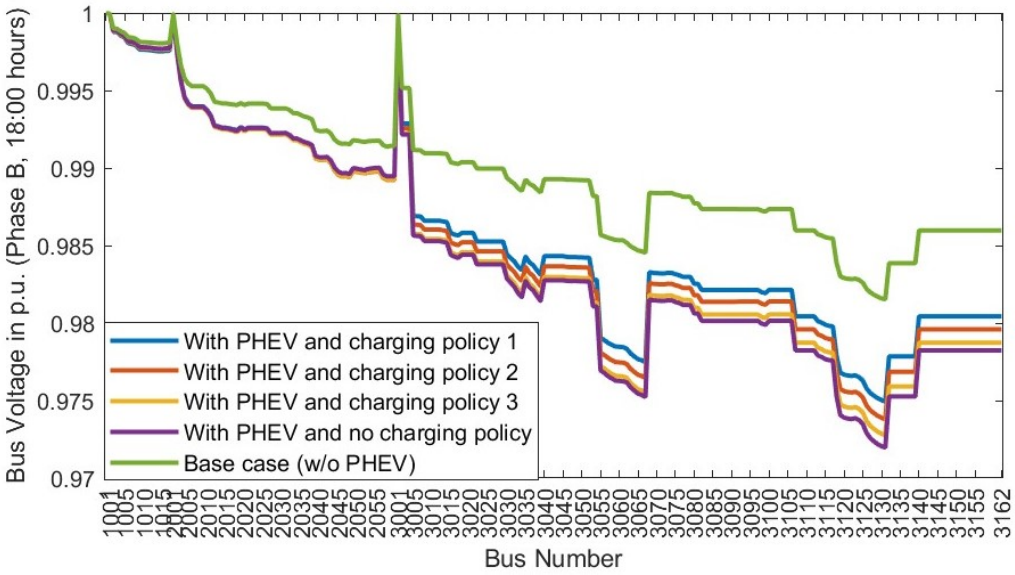


Fig. 4.3: Bus Voltage Magnitude Profile for 240-Bus Distribution System for Phase-B at 18:00 hrs for Different Scenarios

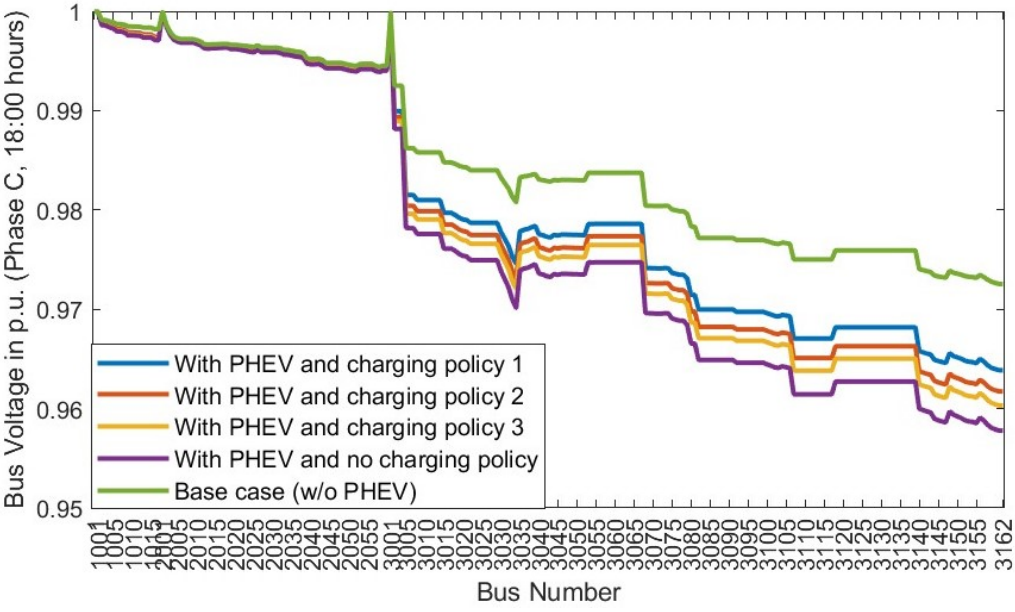


Fig. 4.4: Bus Voltage Magnitude Profile for 240-Bus Distribution System for Phase-C at 18:00 hrs for Different Scenarios

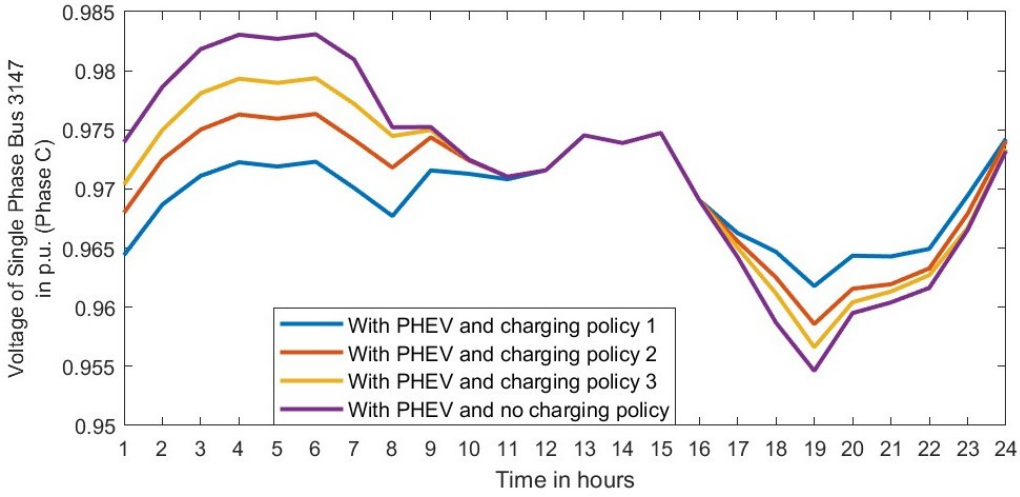


Fig. 4.5: 24-hours Bus Voltage Magnitude Profile for Single-Phase Bus 3147 without and with PHEV Charging Policy

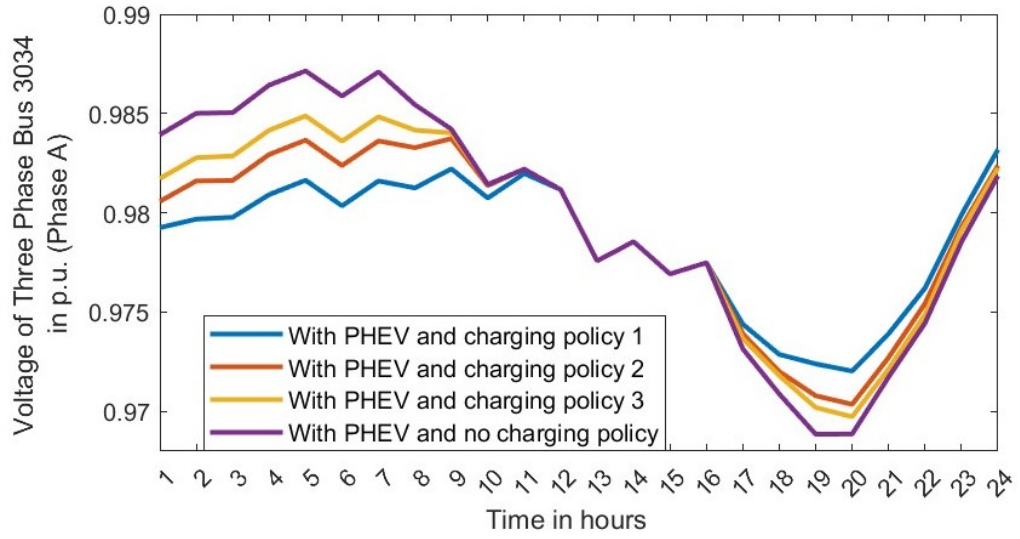


Fig. 4.6: 24-hours Bus Voltage Magnitude Profile for Three-Phase Bus 3034 without and with PHEV Charging for Phase-A

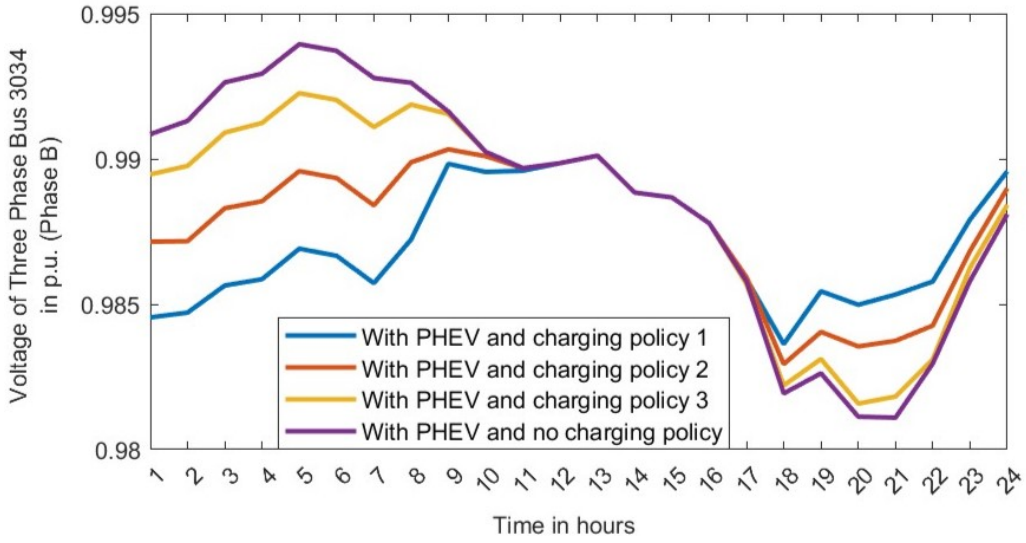


Fig. 4.7: 24-hours Bus Voltage Magnitude Profile for Three-Phase Bus 3034 without and with PHEV Charging for Phase-B

buses are targeted for further investigations as they have the maximum number of customers (and hence PHEVs) connected.

Fig. 4.5 shows both the 24-hour voltage profile for single phase bus 3147 with PHEV charging, without and with charging policies. It is observed that adoption of the proposed charging policies substantially improves the voltage profile during peak charging hours (1600-2100 hrs).

Subsequently, bus no. 3034 is considered for analysis, which is a three-phase bus with 9 customers (3 customers each for phase 'a', 'b' and 'c'). Figs. 4.6 – 4.8 presents the 24-hour voltage profile for bus no. 3034 without and with PHEV charging policy for phases A, B and C, respectively. Again, it's observed that adoption of the proposed charging policies substantially improves the bus voltage profile for all the three phases during peak charging hours (1600 - 2100 hrs).

From the above figures, it can be observed that all policies have their own advantages and disadvantages. While charging policy 1 results in the lowest maximum network demand, range anxiety will be more as PHEVs with SOC 50% has to wait until 5AM next day to charge and sufficient time for full charge before travel may not be available. On the other hand, the range anxiety with charging policy 3 will be minimum, but at the expense of a higher network maximum demand than with policies 1 and 2. Charging policy 2 offers a

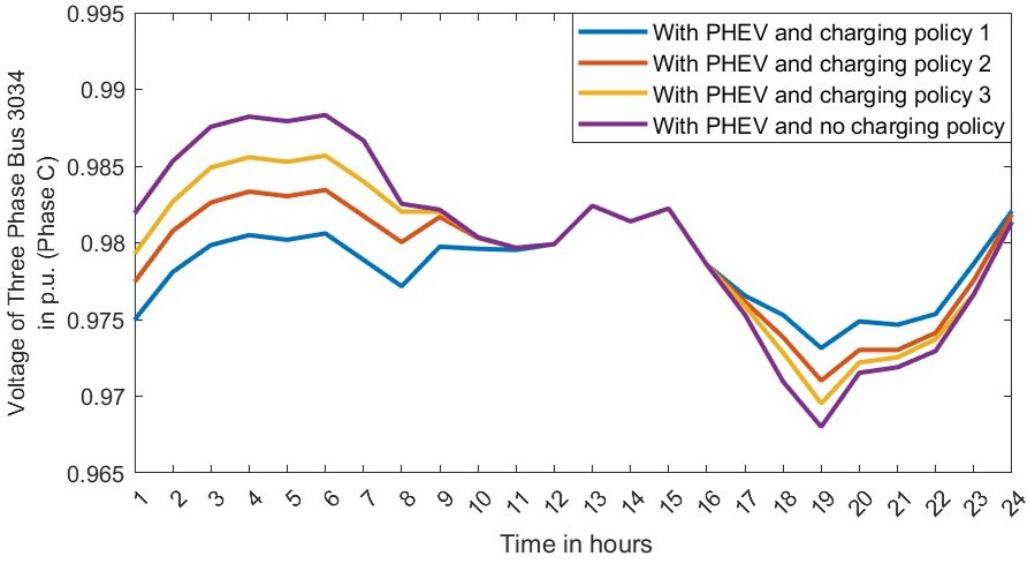


Fig. 4.8: 24-hours Bus Voltage Magnitude Profile for Three-Phase Bus 3034 without and with PHEV Charging for Phase-C

compromise between policies 1 and 3.

4.4 Conclusions

For power distribution systems, EV charging presents a random, unbalanced, dynamic load, which is a function of time. The charging load depends upon the number of charging EVs connected, the type of EV, the starting time of EV charging and the charging duration. Due to this, the PDN faces several challenges to meet the increased load requirement. The daily load profile is distorted, the bus voltages dip and the network losses increases. In this context, suitable EV charging policies can substantially improve the distribution system performance. The effect of domestic EV charging of more than 3000 U.S. residents is considered in the 240-bus radial distribution network situated in the Midwest U.S. For this, PHEV charging load is modelled as a function of time considering level-1 residential charging according to SAEJ1772 standard. Detailed analysis has been done by distributing the PHEV customers on three different phases and then evaluating their results on a the 240-bus network. Three SOC based PHEV charging policies are proposed in this paper. Multiple case studies on a 240-bus distribution network show that implementation of the

policies improves the network daily load profile, the system losses and the bus voltage profiles.

Chapter 5

Impact Assessment of Residential EV Charging and Mitigation Using Optimal Allocation of Wind-Based DG Units

Continuously depleting fossil fuels reserves, rising fuel costs and environmental concerns have led to the emergence of EVs as a popular choice of transportation. However, EV charging may affect the performance of distribution networks adversely. With increased EV penetration levels, the distribution network may suffer distortion in the daily load profile, low bus voltage magnitudes, enhanced line losses, increased phase unbalance, poor power quality and voltage stability issues [11–15]. Large-scale EV charging demand also puts additional strain on distribution networks. These issues need to be addressed appropriately for proper PDN operation.

This chapter examines how residential EV charging significantly impacts the PDN performance, leading to load profile distortions, reduced bus voltages, increased line losses, and challenges to voltage stability. This chapter addresses these challenges by proposing optimal allocation of wind power-based DG resources in a 240-bus PDN with residential EV charging. As EV charging peak is observed to occur during or after 21:00 hours (as shown in Fig. 5.5), solar-based DGs would not be able to address this problem. Therefore, in this chapter, only wind-based DGs are considered for the residential EVCD. The DTBO algorithm, with its dual-phase learning structure and dynamic adaptability, is used for the

optimal DG allocation in the PDN. DTBO balances exploration and exploitation effectively, offering a novel, intelligent optimization approach. Its performance is validated through benchmark tests and comparisons with algorithms like GA, IGWO, PSO, and TLBO. For case studies, wind speed data and turbine parameters are sourced from the IEM and manufacturer datasheets, while EV charging demand is modelled using NHTS 2017 data. Three different EV penetration levels are analyzed, showing reductions in network active power losses and voltage deviation of up to 45.6% and 64.7%, respectively. This validates the effectiveness of the proposed DTBO technique for optimal DG allocation.

5.0.1 Chapter Contributions

The main contributions of the proposed study are mentioned below:

- Unlike several existing studies, which considers static or probabilistic EV demand, in this chapter, 24-hour, dynamic EV charging demand is computed for different households based on the NHTS 2017 travel survey data [117] which details the number and type of EVs in a household, their distance travelled, trip end times etc. The residential charging of about 1500 EVs pertaining to a cluster of more than 800 U.S residents is considered. Three different EV penetration scenarios are proposed in this study.
- The effect of EV charging demand is analyzed on a real, 240-bus, PDN located in the mid-western state of Iowa, USA, having smart meter demand data is used [1]. To improve the performance of the PDN, wind-based DG resources are optimally allocated using DTBO, which is a human-based metaheuristic algorithm. This avoids the need for additional centralized fossil-fuel based power generation that may be required during the peak hours. The practical wind speed pattern data for a typical weekday of May is taken from the Iowa Environmental Mesonet [120] and the wind turbine parameters chosen for this study are taken directly from the manufacturer's data sheets. All case studies are implemented in the MATLAB platform.
- The performance of the single and multi-objective DTBO algorithm to improve the network performance indices like network daily demand

profile, bus voltage magnitude profile and network losses, is validated on different benchmark mathematical functions [121, 122] which proves the superiority of the DTBO over other existing algorithms. This is a maiden application of the DTBO for the optimal allocation of DGs in a PDN.

The general idea behind the Chapter is shown in Fig. 5.1 whereas the flowchart for the proposed work is presented in Fig. 5.2.

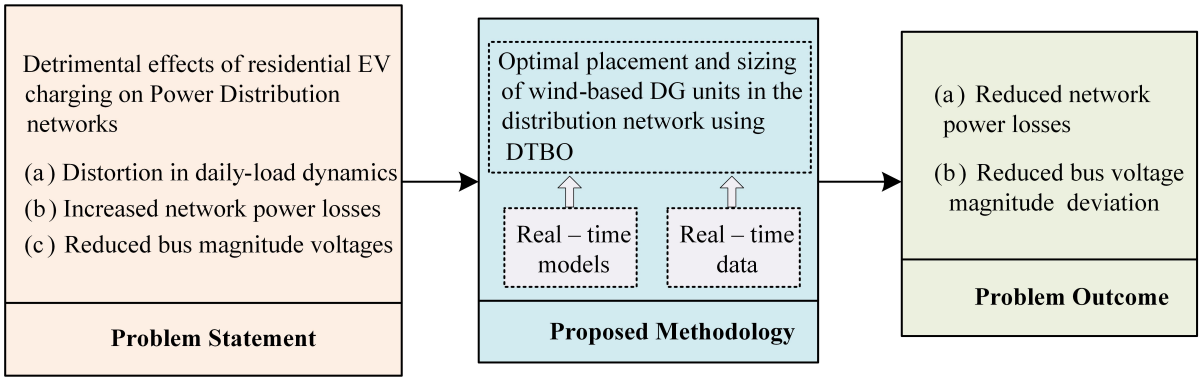


Fig. 5.1: Architecture of the proposed work.

5.1 Filtering NHTS 2017 Data

In this study, NHTS 2017 data is used for extracting the trip characteristics of the vehicles. NHTS furnishes an encyclopedic travel pattern data in the U.S. [117]. The NHTS data details the number and type of EVs in a household, the distance travelled, the trip end time, day and date of travel, etc. The database contains four Microsoft Excel files out of which two are filtered, sorted and merged to form a common file, whose format is shown in Table 5.1. Fig. 5.3 presents the frequency distribution of vehicles on the basis of their arrival times, for a typical weekday of May.

The detailed steps to understand the distribution of EVs from NHTS 2017 data to the 240-bus PDN along with the estimation of EV charging demand at each bus (node) of the PDN is presented in the flowchart at Fig. 5.4.

At first, the data about the number of customers at each bus of the PDN is extracted. Then, the distribution of customers is done on the basis of the nature

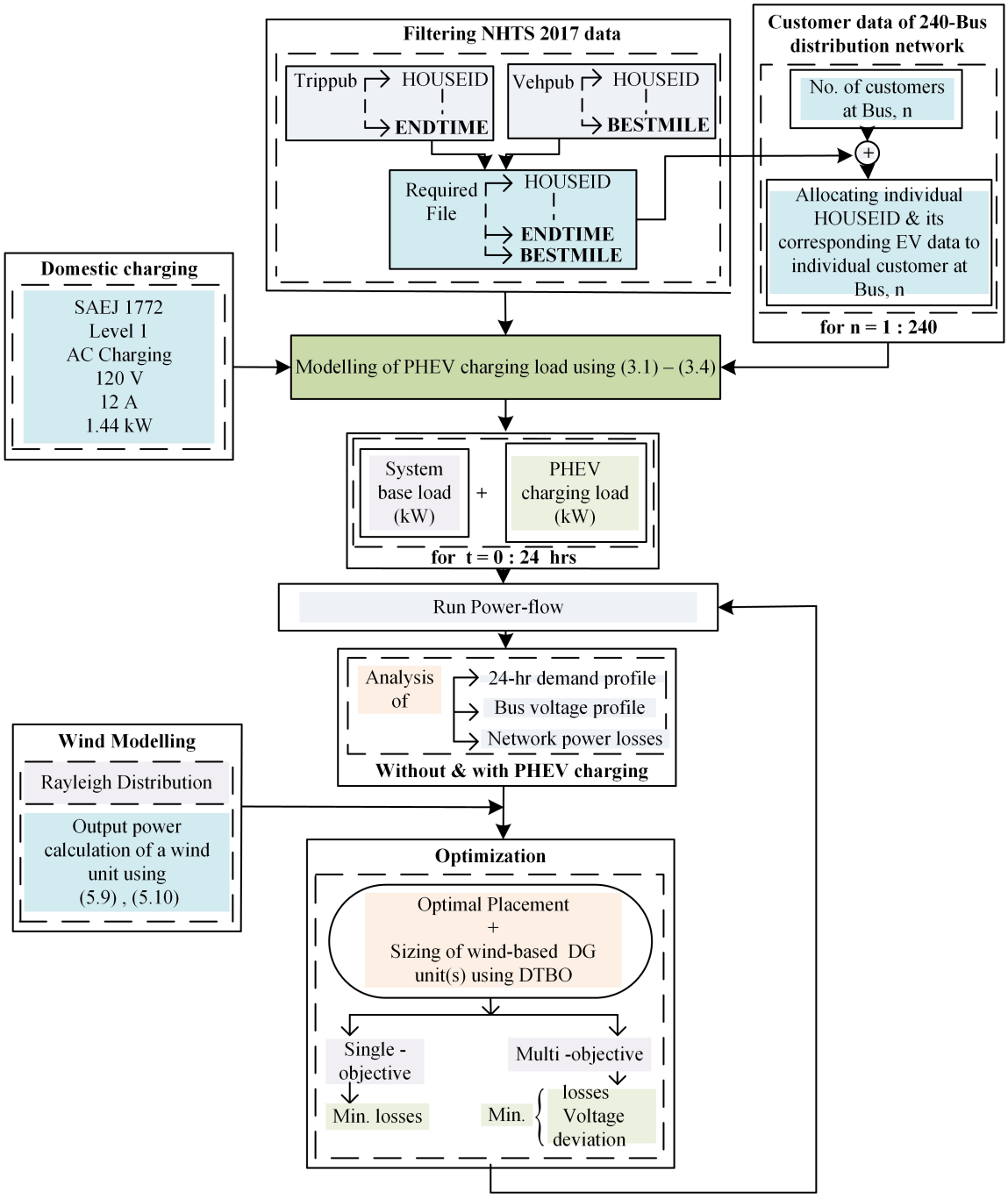


Fig. 5.2: Flowchart for the proposed work.

Table 5.1: Sample of Filtered NHTS 2017 Data

HOUSEID	30000007	30000008	300000012	300000019	300000029	...
TDAYDATE	201608	201608	201607	201605	201610	...
TRAVDAY	2	5	5	5	3	...
PERSONID	3	1	1	1	1	...
VEHID	1	4	2	1	1	...
VEHTYPE	1	4	3	1	3	...
ENDTIME	900	2340	605	1515	845	...
TDTRPNUM	1	2	1	1	1	...
HHVEHCNT	5	4	2	2	2	...
BESTMILE	14611.92	9192.44	4002.55	7027.68	14029.07	...

of the bus i.e. if the bus is single-phase, all the customers will be allocated to the phase at which this single-phase bus is connected whereas if the bus is three-phase, the customers at that bus are divided equally among the three phases. Now, each customer in the network is assigned an individual HOUSEID from the NHTS 2017 data. Depending upon the penetration level of EV and the type of the vehicle(s) of a particular bus (node), its charging demand is calculated using (3.1), (3.2), (3.3) and (3.4) on per-phase basis. Finally, the EVCD of individual three phase is estimated for the complete PDN. Subsequently, the dynamic EVCD of the complete PDN comprising of all the three-phases is computed and added to the base case demand to get the 24-hour demand curve with EV charging as shown in Fig. 5.5. However, for obtaining the network 24-hour demand curve for the base case (without any EV charging), the smart meter data of all the customers are used from [1].

In this perspective, three different cases, corresponding to three different levels of EV penetration, are proposed in this study (assuming the network base load demand to be the same) which is discussed in detail in section 5 of this chapter.

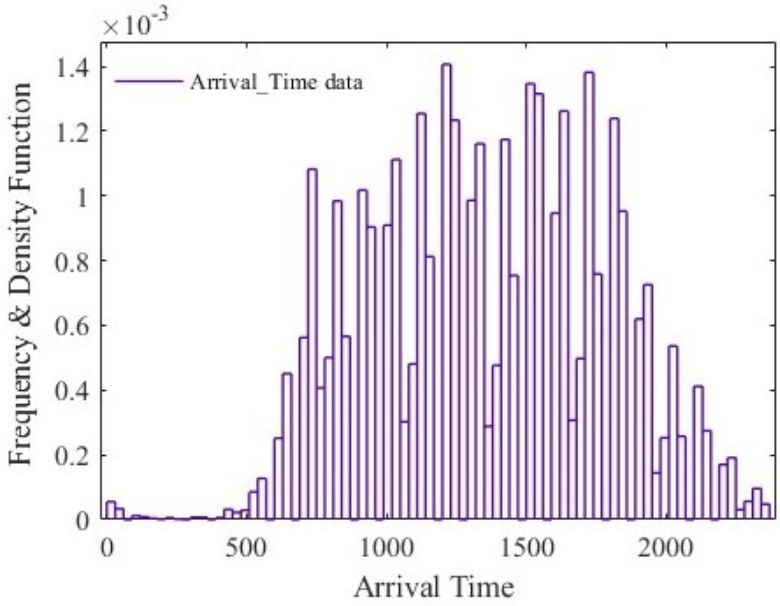


Fig. 5.3: Vehicle arrival time pattern from NHTS 2017 data

The pictorial representation of allocation of individual customers (HOUSEIDs) to the PDN buses along with the different EV penetration levels considered, is shown in Fig. 5.7. Three different EV penetration levels are considered:

(a) Exactly one EV per household

(b) At most two EVs per household

(c) At most three EVs per household

The daily demand plots pertaining to the base case and with EV charging are shown in Fig. 5.5. The corresponding bus voltage profiles are presented later in section 5 of this chapter. From Fig. 5.5, it is observed that with residential EV charging considered, the peak load demand in the system occurs at 21:00 hours and is almost twice that of the base load. It is also observed that the majority of EVs are not put on charging before 15:00-16:00 hours.

5.2 DG Operation

It is observed that EV charging demand distorts the PDN daily demand profile, deteriorates the PDN bus voltage magnitude profile and increases the network

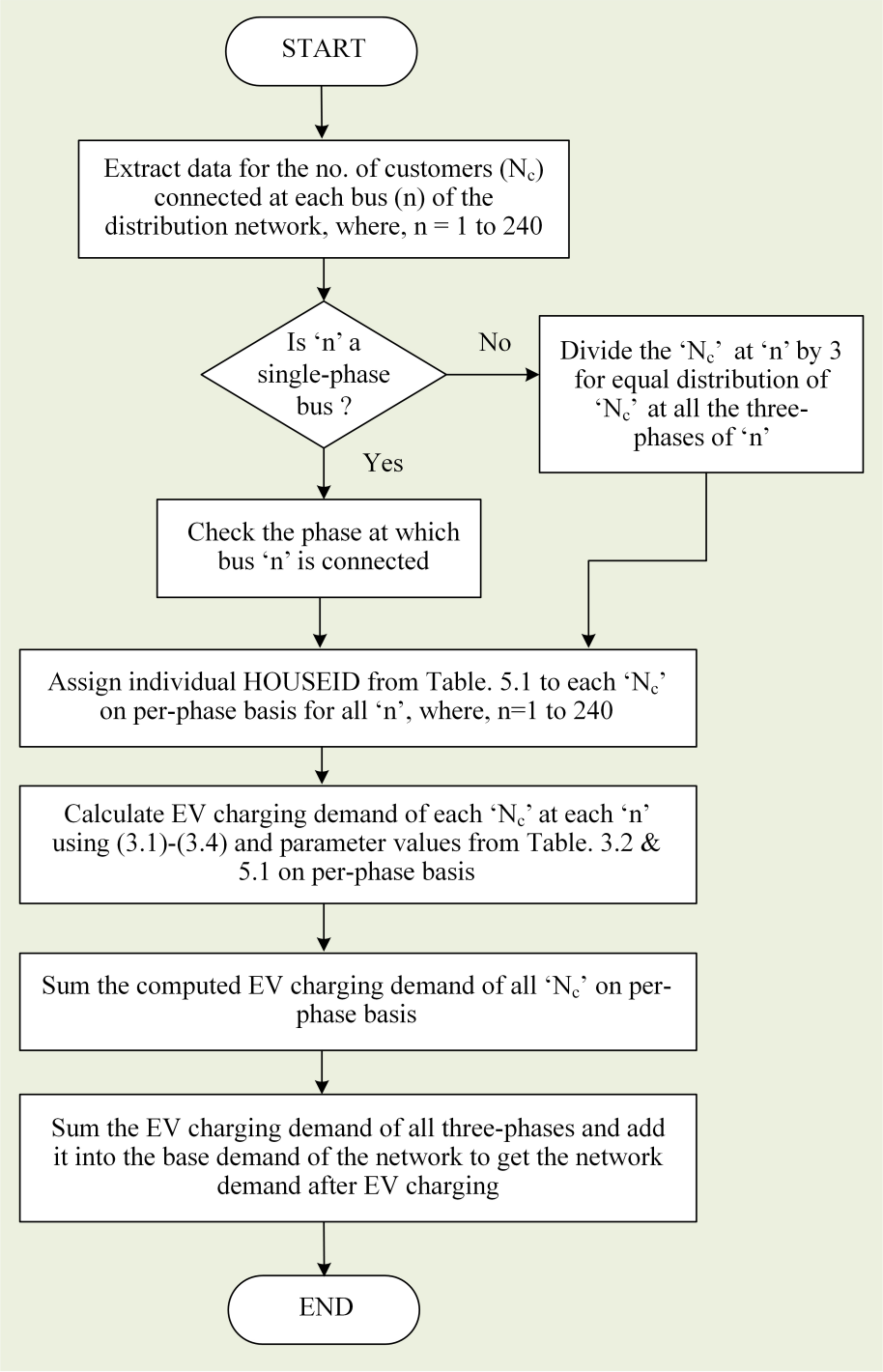


Fig. 5.4: Flowchart for distribution of EVs from NHTS data to the 240-bus PDN and estimation of EVCD

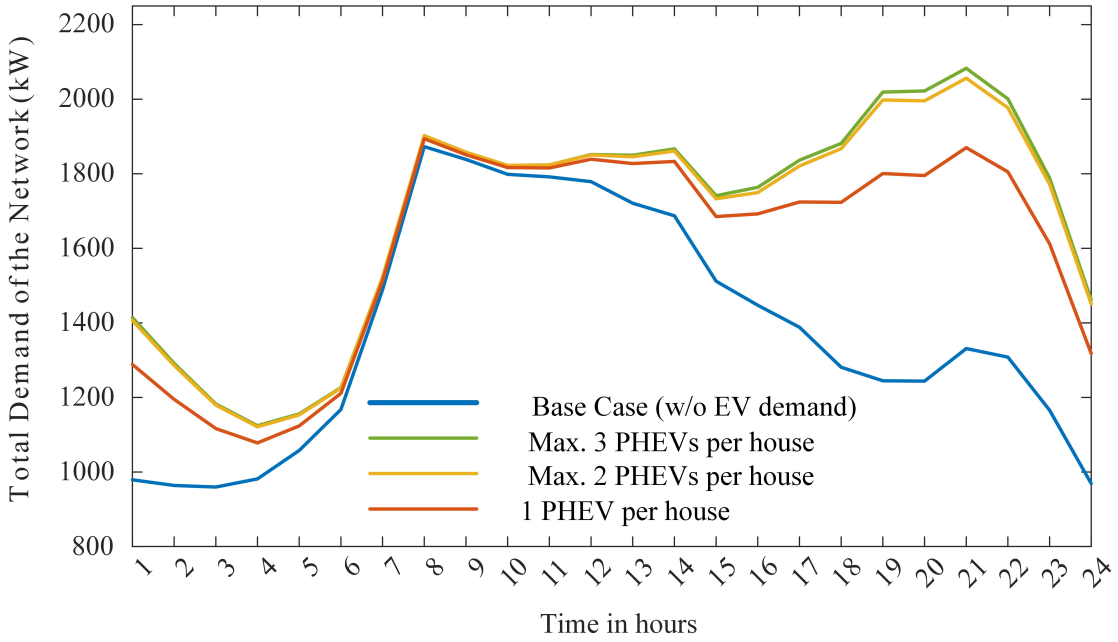


Fig. 5.5: Daily demand profile for 240-bus PDN

Ohmic losses. In this respect, DGs of appropriate size located at suitable nodes in the PDN have been reported [123–126] to improve bus voltage magnitude profile and decrease Ohmic losses of the PDN. The relationship between the system losses and DG capacity is depicted in Fig. 5.6. From Fig. 5.6, it can be observed that upto a certain DG capacity, the losses continue to reduce but start to increase if DG penetration is further increased. Therefore, it becomes extremely important to use DGs of appropriate capacity. In this thesis, this issue is addressed by the optimal allocation of wind turbine based DGs in the PDN by using a recent, human-based metaheuristic algorithm, DTBO.

To alleviate the detrimental effects of EV charging on the PDN performance, DGs are placed at suitable buses in the 240-bus PDN. Since the residential EV charging peak is observed to occur during or after 21:00 hours (as shown in Fig. 5.5), solar-based DGs would not be able to address this problem. Therefore, in this chapter, only wind-based DGs are considered for the residential EVCD. Fig. 5.8 shows the windspeed profile for a typical weekday of May [120].

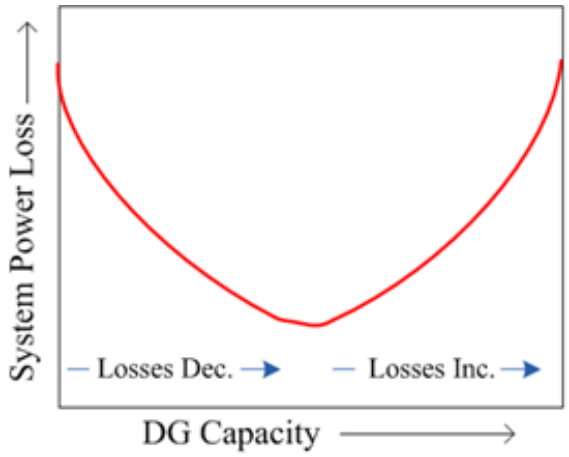


Fig. 5.6: Variation of network Ohmic losses with DG

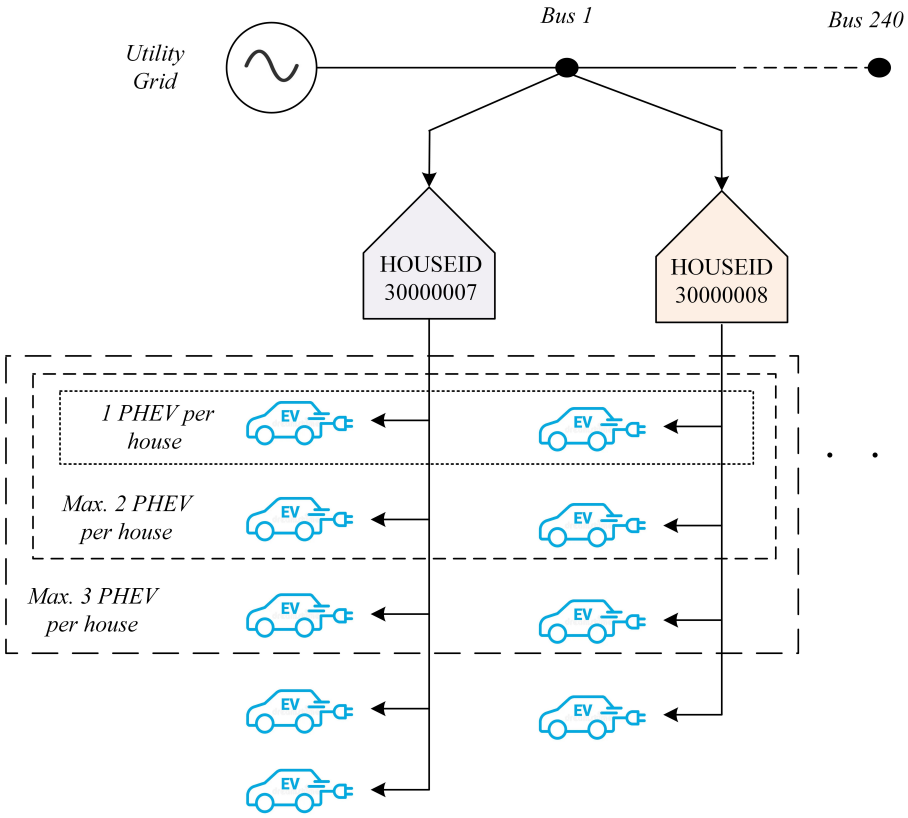


Fig. 5.7: Allocation of HOUSEIDs to PDN buses

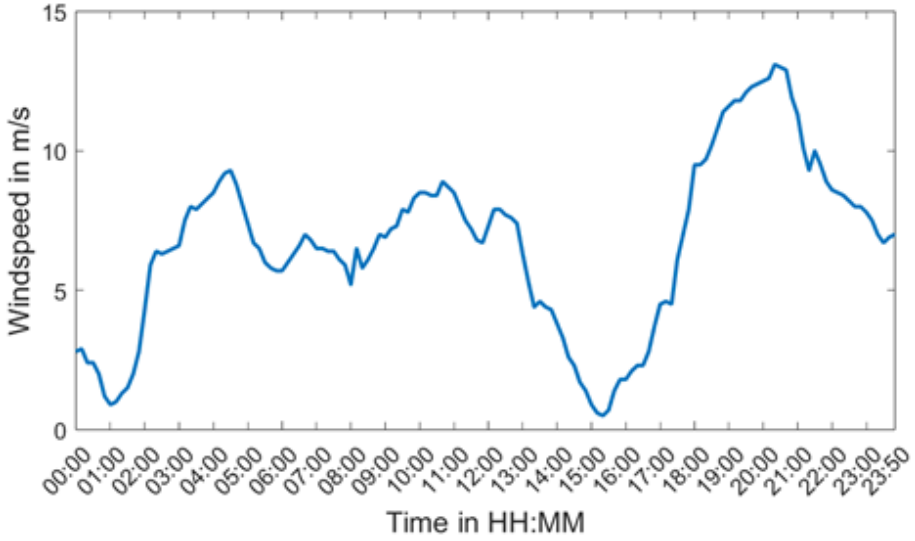


Fig. 5.8: Wind speed plot for a typical weekday of May

5.2.1 Power Output of a Wind Turbine

The output power of a wind turbine is influenced by the wind speed at its location. In this study, the Rayleigh statistical model is utilized for wind speed analysis because the annual wind speed pattern at the site aligns with a Rayleigh distribution, as illustrated in Fig. 5.9. To confirm this, the PDF for the annual wind speed data is first plotted. Subsequently, different distribution models (Rayleigh, Weibull, and Normal) are compared using MATLAB's Distribution Fitter Application, with the resulting plots shown in Fig. 5.9 based on which, it is determined that the wind speed at this site closely follows a Rayleigh distribution [127, 128] given as,

$$f(v) = \frac{2\,v}{c^2}\, e^{-\left(\frac{v}{c}\right)^2}, \quad 0 \leq v \leq \infty \tag{5.1}$$

The rated power delivered by the rotor is governed by the following equation [129]:

$$P_{w,r} = 0.5\, C_p\, \rho\, \pi\, R^2\, v_r^3 \tag{5.2}$$

There exist different mathematical models [130] for modelling the power output of a wind turbine. In this study, for all possible values of wind speed, the output power of the turbine is governed by [127]:

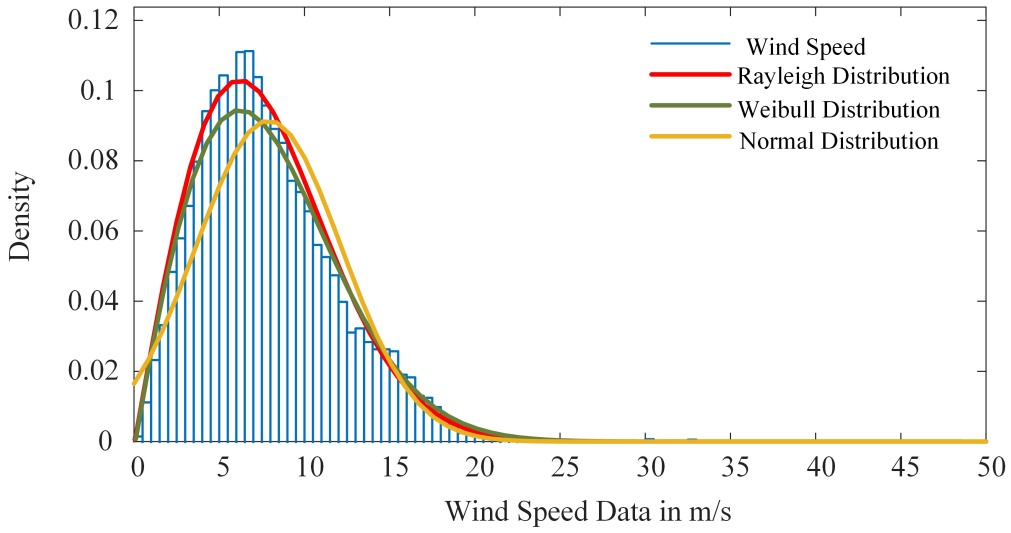


Fig. 5.9: Various distribution fits for the annual windspeed data

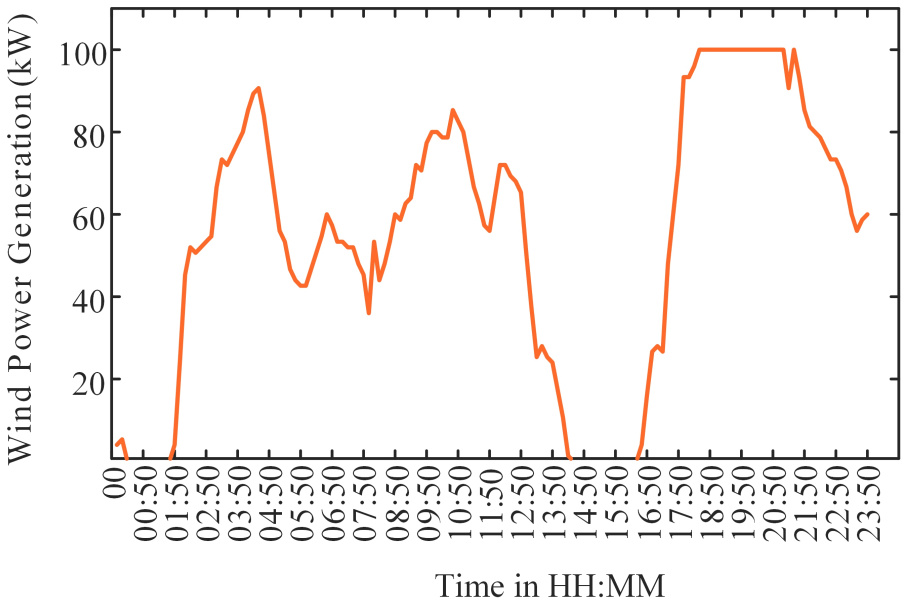


Fig. 5.10: Output power of wind-based DG for a typical May weekday

Table 5.3: Specifications of the wind turbine

Parameter	Value
C_p	0.3326
R	12.5 m
$P_{w,r}$	100 kW
v_r	10 m/s
v_{ci}	2.5 m/s
v_{co}	20 m/s
ρ	1.225 kg/m^3

$$P(v_w) = \begin{cases} 0, & v_w \leq v_{ci} \text{ or } v_w \geq v_{co} \\ P_{w,r}\dfrac{v_w - v_{ci}}{v_r - v_{ci}}, & v_{ci} < v_w < v_r \\ P_{w,r}, & v_r \leq v_w \leq v_{co} \end{cases} \tag{5.3}$$

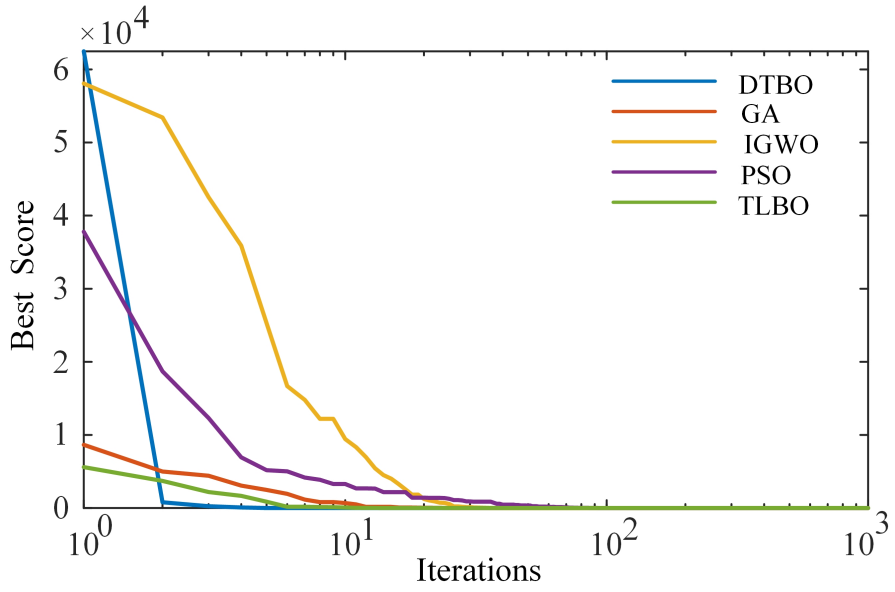


Fig. 5.11: Convergence curves of DTBO and other popular algorithms with the Sphere function

In this chapter, the case studies are carried out considering the fact that 20%

of the total PDN load is to be delivered by the wind turbine-based DGs while the rest 80% is to be supplied by the grid. The wind speed pattern shown in Fig. 5.8 is used to determine the WECS parameters to maximize the wind energy extraction potential and select the wind turbine rating suitable for the site [131]. Due to the distinctive geography of Midwest U.S.A, the turbines ideally suited are the medium sized ones [132]. The value of the parameters used in this study is provided in Table 5.3. Fig. 5.10 shows the power output of the wind-based DG based on Fig. 5.8 and (5.3). It should be noted that any surplus wind power after meeting the load demand (including EV load) will be injected to the grid and is to be accounted for using net metering principle. As such, any variation of the load demand on account of the EV load would be taken care of by the grid. It is further assumed that in case of any interruption of the grid to the consumer premises, EV charging would be held up. As discussed before (Fig. 5.5), it is observed that with EV charging, the network peak demand occurs at 21:00 hours. Hence, optimal DG allocation is carried out pertaining to the demand at this hour. Also, for the three different PHEV penetration levels considered, the total load at 21:00 hours in the system varies from 1870 kW to 2083 kW. Considering a wind power penetration of 20% as discussed earlier (rest to be provided by the grid), four units of 100 kW wind turbines are employed (specifications are detailed in Table 5.3) and are optimally placed using the DTBO algorithm. The DTBO algorithm is detailed in Section 5.4.

5.3 The DTBO Algorithm

DTBO is a metaheuristic algorithm in which a learner driver tries to learn driving skills by emulating the instructor [121]. Additionally, personal practice also improves the learner's driving skills. In order to provide both a local and global search, the DTBO updating process consists of three stages. The first phase of the update, termed 'training imparted by the driving instructor', involves scanning various parts of the search space based on the exploration capability of the DTBO. In the second phase, the DTBO implementation enhances exploration by introducing sudden shifts in the population position.

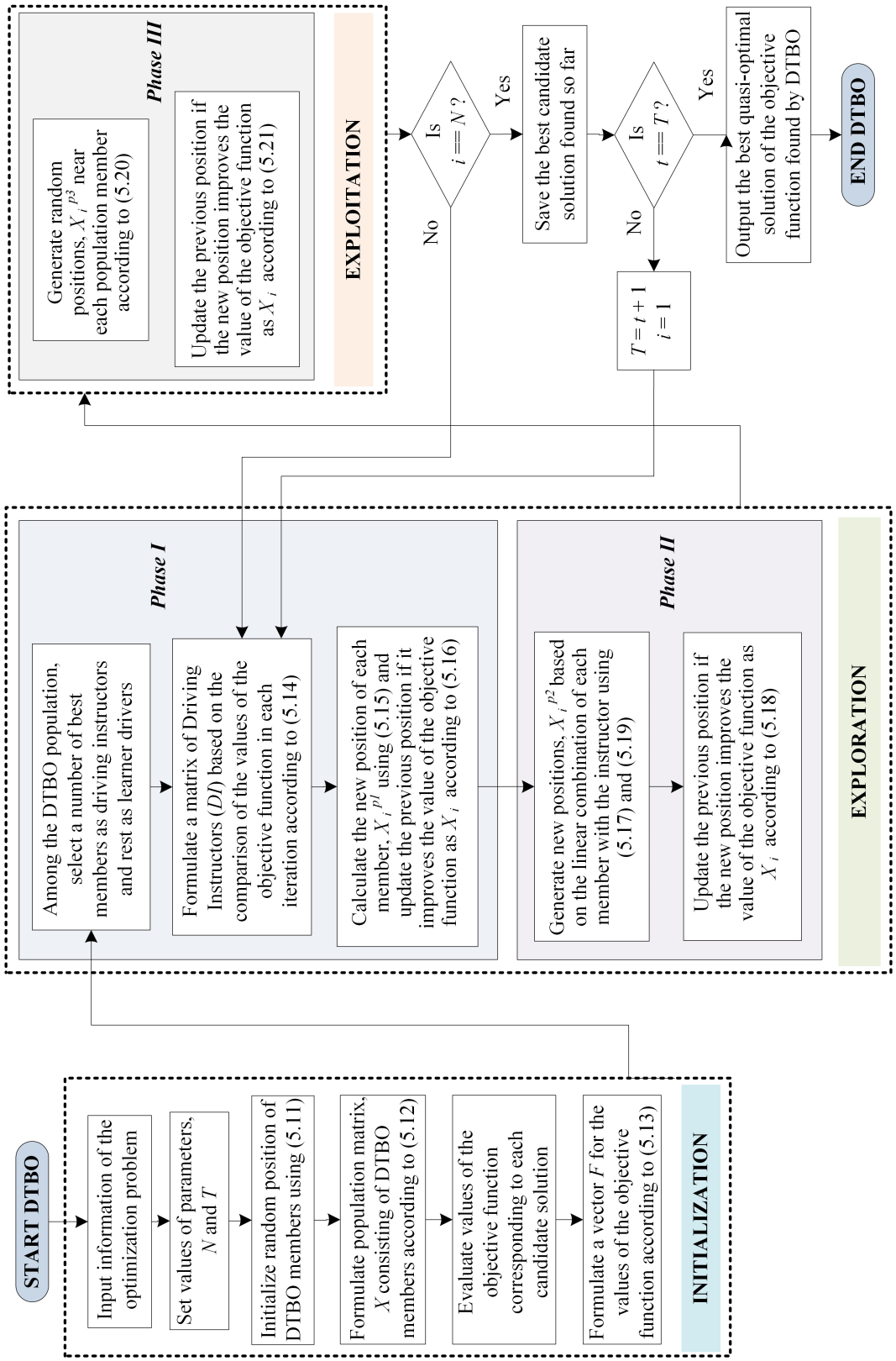


Fig. 5.12: Flowchart of the DTBO Algorithm

The third phase, known as 'personal practice', focuses on local search, thereby boosting DTBO's exploitation ability.

In the initial iterations, the DTBO algorithm exhibits a larger displacement range, facilitating effective exploration. As the algorithm progresses through more iterations, it becomes crucial for it to explore more promising areas of the search space and to refine the search around these areas with smaller and more precise steps. The update equations in the second and third phases are adjusted to yield smaller changes to the population as the number of iterations increases, enabling convergence to the optimal solution with greater precision. These strategies for updating the population members in DTBO contribute to the proposed approach, which not only excels in exploration and exploitation but also maintain a balanced performance between these two capabilities. Fig. 5.17 presents the flowchart for the DTBO algorithm explaining the importance of each step within a given phase of the algorithm.

5.3.1 Single-Objective DTBO Algorithm

The initial population is created from the following equation:

$$x_{i,j} = \mathrm{lb}_j + r\left(\mathrm{ub}_j - \mathrm{lb}_j\right), \quad i = 1, 2, \ldots, N_p; \quad j = 1, 2, \ldots, N \tag{5.4}$$

$$X = \begin{bmatrix} X_1 \\ \vdots \\ X_i \\ \vdots \\ X_{Np} \end{bmatrix} = \begin{bmatrix} x_{11} & \cdots & x_{11} & \cdots & x_{11} \\ \vdots & \ddots & \vdots & \ddots & \vdots \\ x_{11} & \cdots & x_{11} & \cdots & x_{11} \\ \vdots & \ddots & \vdots & \ddots & \vdots \\ x_{11} & \cdots & x_{11} & \cdots & x_{11} \end{bmatrix}_{N_p X\, N} \tag{5.5}$$

where X is the population of DTBO, X_i is the ith candidate solution, x_{ij} is the value of the j^{th} variable determined by the i^{th} candidate solution, N is the size of the population of DTBO, m is the number of problem variables, r is a random number from the interval $[0, 1]$, lb_j and ub_j are the lower and upper bounds of the j^{th} problem variable, respectively.

Each candidate solution assigns specific values to the problem variables, which are then substituted into the objective function for evaluation. This

process calculates an objective function value for each candidate solution. The values of the objective function are modelled in vector, F of (5.6) as:

$$F = \begin{bmatrix} F_1 \\ . \\ . \\ F_i \\ . \\ . \\ F_{N_p} \end{bmatrix}_{N_p \text{X} 1} = \begin{bmatrix} F(X_1) \\ . \\ . \\ F(X_i) \\ . \\ . \\ F\left(X_{N_p}\right) \end{bmatrix}_{N_p \text{X} 1} \tag{5.6}$$

where, F_i represents the value of the objective function delivered by the i^{th} candidate solution. The primary distinction among metaheuristic algorithms lies in the strategies used to update candidate solutions. In DTBO, candidate solutions are updated through the following three distinct phases:

Phase I (Training imparted by the driving instructor): The initial phase of the DTBO update involves the selection of a driving instructor by the learner driver, followed by skill training provided by the chosen instructor. Within the DTBO population, a subset of top-performing members is designated as driving instructors, while the remaining members act as learner drivers. By selecting instructors and adopting their skills, population members move to different regions within the search space, enhancing DTBO's ability to explore globally and identify optimal areas. This phase highlights the algorithm's exploration capability. During each iteration, depending upon the fitness function value, 'N_{DI}' population members are chosen as driving instructors, as described in (5.7).

$$\mathbf{DI} = \begin{bmatrix} DI_1 \\ \vdots \\ DI_i \\ \vdots \\ DI_{N_{DI}} \end{bmatrix}_{N_{DI} \times N} = \begin{bmatrix} DI_{11} & \cdots & DI_{1j} & \cdots & DI_{1N} \\ \vdots & \ddots & \vdots & \ddots & \vdots \\ DI_{i1} & \cdots & DI_{ij} & \cdots & DI_{iN} \\ \vdots & \ddots & \vdots & \ddots & \vdots \\ DI_{N_{DI}1} & \cdots & DI_{N_{DI}j} & \cdots & DI_{N_{DI}N} \end{bmatrix}_{N_p \times N} \tag{5.7}$$

where, DI denotes the matrix of driving instructors, DI_i is the i^{th} driving instructor, $DI_{i,j}$ is the j^{th} dimension, and

$$N_{DI} = 0.1 \times N \times \left(1 - \frac{t}{T}\right)$$

is the number of driving instructors, where, T and t are the maximum number of iterations and the current iteration, respectively. In this phase, the new position of the members is obtained by (5.8) and, using the greedy selection criteria [133], given by (5.9), is applied to update the old position with the new position.

$$x_{i,j}^{p1} = \begin{cases} x_{i,j} + r\left(DI_{k_{i,j}} - I \cdot x_{i,j}\right), & \text{if } F_{DI_{k_i}} < F_i, \\ x_{i,j} + r\left(x_{i,j} - DI_{k_{i,j}}\right), & \text{otherwise.} \end{cases} \tag{5.8}$$

$$X_i = \begin{cases} X_i^{p1}, & \text{if } F_i^{p1} < F_i, \\ X_i, & \text{otherwise.} \end{cases} \tag{5.9}$$

where, X_i^{p1} is the new calculated status of the i^{th} candidate solution, $x_{i,j}^{p1}$ is its j^{th} dimension, F_i^{p1} is its objective function value, $F_{DI_{k_i}}$ is a set of objective functions for the k^{th} driving instructor of the i^{th} learner driver, F_i is a set of objective functions for the i^{th} learner driver, I is a random number chosen between $[1, 2]$, and r is a random number chosen between $[0, 1]$.

Phase II (Patterning of the instructor skills of the learner driver): The second phase of the DTBO update involves the learner driver mimicking the instructor, where the learner strives to replicate the instructor's movements and skills. This imitation process redistributes DTBO members across the search space, enhancing the algorithm's exploration capabilities. Mathematically, this concept is represented by generating a new position as a linear combination of each member and the instructor, as defined by (5.10). If this new position yields an improved objective function value, it replaces the previous position, following the rule described in (5.11).

$$x_{i,j}^{p2} = P \cdot x_{i,j} + (1 - P) \cdot DI_{k_{i,j}} \tag{5.10}$$

$$X_i = \begin{cases} X_i^{p2}, & \text{if } F_i^{p2} < F_i, \\ X_i, & \text{otherwise.} \end{cases} \tag{5.11}$$

where, X_i^{p2} denotes the new calculated status of the i^{th} candidate solution based on the second phase of the DTBO, $x_{i,j}^{p2}$ is its j^{th} dimension, F_i^{p2} is its objective function value, and P is the patterning index given by,

$$P = 0.01 + 0.9\left(1 - \frac{t}{T}\right) \tag{5.12}$$

Phase III (Personal practice): The third phase of the DTBO update focuses on the individual practice of each learner driver, aiming to refine and enhance their driving skills. In this phase, each learner driver strives to achieve their optimal performance. It facilitates the discovery of improved positions through a local search around the current position of each member. This phase highlights the DTBO's ability to effectively exploit local search. Mathematically, this process involves generating a random position near each member of the population, as defined by (5.13). If the newly generated position improves the objective function value, it replaces the previous position, as described in (5.14).

$$x_{i,j}^{p3} = x_{i,j} + (1 - 2r) \cdot R \cdot \left(1 - \frac{t}{T}\right) \cdot x_{i,j} \tag{5.13}$$

$$X_i = \begin{cases} X_i^{p3}, & \text{if } F_i^{p3} < F_i \\ X_i, & \text{otherwise} \end{cases} \tag{5.14}$$

where, X_i^{p3} denotes the new calculated status of the i^{th} candidate solution based on the third phase of the DTBO, $x_{(i,j)}^{p3}$ is its j^{th} dimension, F_i^{p3} is its objective function value, and R denotes a tuning parameter.

5.3.2 Multi-Objective DTBO Algorithm

Multi-objective optimization problem consists of multiple objectives which are needed to be optimized simultaneously [132]. While formulating the multi-objective version of the DTBO, some modifications are required in the steps of the DTBO algorithm. Firstly, in the process of updating the old solution

with new solution in all the three phases. Unlike the single objective version, in the multi-objective version of the DTBO, both the old and the new solutions are combined and then a non-dominated sorting algorithm is applied to this combined population. After the non-dominated sorting, the best population members equal in size to the original population are extracted and are treated as a new population [134]. Secondly, in the multi-objective version, the population member is updated when the objective functions of the driving instructor dominate the objective functions of the learner driver, i.e., x_i^{p1}

$$x_{i,j}^{p1} = \begin{cases} x_{i,j} + r\left(DI_{k_{i,j}} - I \cdot x_{i,j}\right), & \text{if } F_{DI_{k_i}} < F_i, \\ x_{i,j} + r\left(x_{i,j} - DI_{k_{i,j}}\right), & \text{otherwise.} \end{cases} \tag{5.15}$$

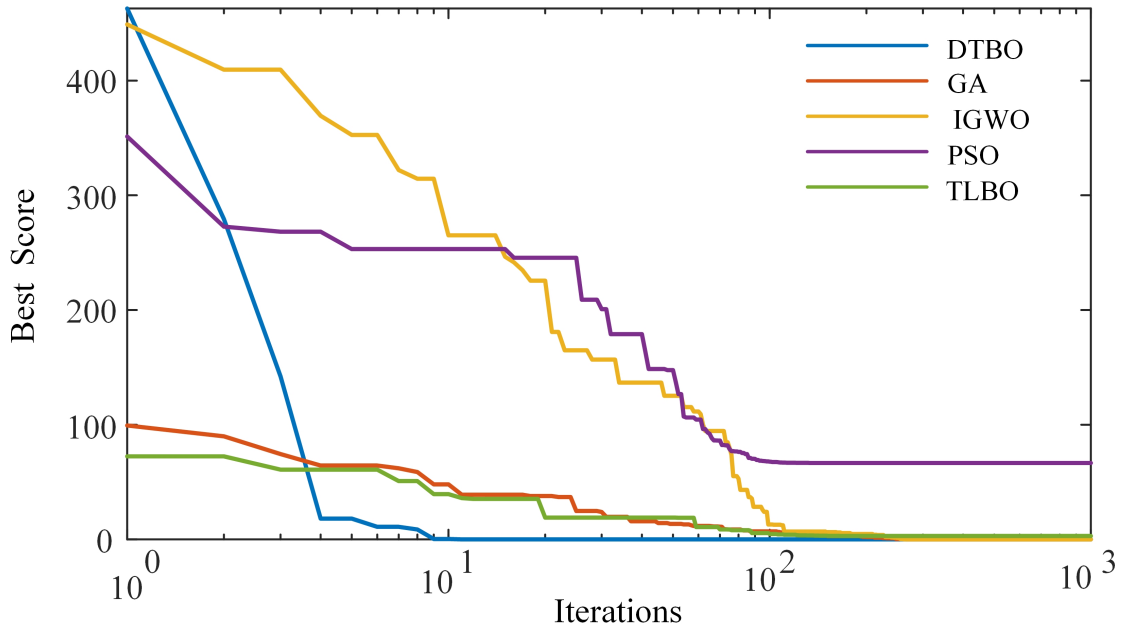


Fig. 5.13: Convergence curves of DTBO and other popular algorithms with the Rastrigin function

The pseudo-code for the DTBO algorithm is presented in Algorithm 1 in section 5.3.3 of this thesis. To test the efficacy of the proposed DTBO algorithm, one unimodal and one multimodal BMFs: the Sphere and the Rastrigin functions respectively, are considered. The convergence characteristics of both these functions with the DTBO algorithm is compared with four other popularly

well-known and widely-used algorithms namely, GA [135], IGWO [136], PSO [137] and TLBO [138], to validate the effectiveness of the DTBO. The convergence characteristics of the Sphere and Rastrigin functions are shown in Fig. 5.11 and 5.13, respectively with maximum number of iterations set to 1000. Moreover, the details of the parameters of BMFs are presented in Table 5.4.

As observed in Fig. 5.11 and Fig. 5.13, GA, IGWO, and TLBO demonstrate competitive performance, but they require more iterations to achieve results comparable to DTBO. Moreover, IGWO shows slower, stepwise convergence whereas GA and TLBO exhibit steady progress with balanced exploration and exploitation, making them reliable but less efficient than DTBO. PSO struggles with both convergence speed and solution accuracy, indicating inefficiency for this problem setup thus, consistently underperforms, converging the slowest and yielding suboptimal solutions. However, DTBO consistently outperforms all other algorithms in terms of convergence speed and solution accuracy, making it the most efficient and effective method for the given optimization problems. DTBO achieves rapid convergence in the early iterations, leveraging strong exploitation capabilities to identify optimal regions of the search space. The above observations conclude that GA, TLBO, and IGWO may be better suited for applications where computational cost is less of a constraint, as they still find competitive solutions whereas PSO may require significant adjustments or enhancements to improve its performance and suitability for the problem. However, DTBO is ideal for time-critical or high-accuracy applications due to its speed and precision which makes it the most promising algorithm in this case, demonstrating the best trade-off between convergence speed and accuracy.

Moreover, for the proposed optimization problem of the paper (minimization of network power loss and bus voltage magnitude deviation), the comparative study of DTBO with IGWO, TLBO and PSO is carried out in Sub-section 5.5 of this chapter.

5.3.3 Sensitivity Analysis of DTBO

Fig. 5.14, illustrates the sensitivity analysis [139] of the optimal DG capacity for wind energy using DTBO under varying wind speeds and EV demand,

Table 5.4: Details of Benchmark Functions (BMFs)

BMF	**Dim.**	**Range**	$f_{\min}$
$f(x) = \sum_{i=1}^{n} x_i^2$	30	$[-100, 100]$	0
$f(x) = 10n + \sum_{i=1}^{n} [x_i^2 - 10\cos(2\pi x_i)]$	30	$[-5.12, 5.12]$	0
Number of search agents, $N = 30$			
Maximum number of iterations, $T = 1000$			

Algorithm 1 : The DTBO Algorithm Pseudo-Code

Input: The optimization problem formulation
Adjust the size of population N and maximum number of iterations T
Initialize the DTBO population position and evaluate the objective function
for $t = 1$ to T **do**
    for $i = 1$ to N **do**
        Phase 1: Training by the driving instructor (Exploration)
        Compute the driving instructor matrix based on comparison of objective function values
        Select a driving instructor at random from the instructor matrix DI
        Calculate the new position for i^{th} DTBO member using (5.8)
        Update the position for i^{th} DTBO member using (5.9)
        Phase 2: Learner driver patterning from instructor skills (Exploration)
        Calculate the patterning index using (5.12)
        Calculate a new position for i^{th} DTBO member using (5.10)
        Update the position for i^{th} DTBO member using (5.11)
        Phase 3: Personal practice (Exploitation)
        Calculate the new position for i^{th} DTBO member using (5.13)
        Update the position for i^{th} DTBO member using (5.14)
    end for
    Update the best-found candidate solution
end for
Return: The global optimum solution

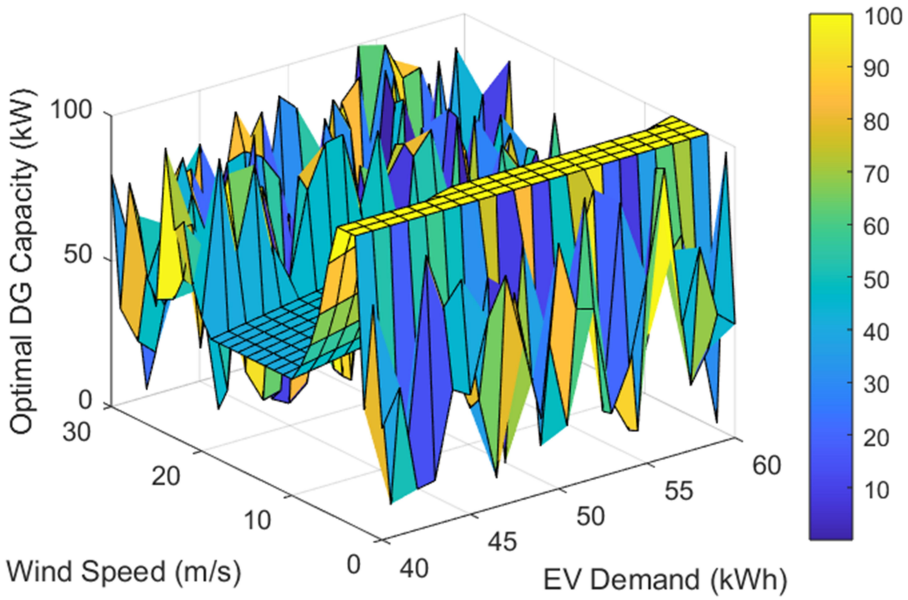


Fig. 5.14: Sensitivity analysis of the optimal DG capacity for wind energy using DTBO under varying wind speeds and EV demand

demonstrating that wind speed strongly influences the sizing of wind DG. It is observed that lower wind speeds (< 2 m/s) result in higher sensitivity to EV demand while higher EV demands necessitate larger DG capacities to maintain grid stability and to ensure sufficient power supply, particularly when wind speeds are low.

It is also observed from Fig. 5.14 that the optimal DG capacity increases with increasing EV demand as the system requires additional energy input to meet the load. At medium windspeed (4–11 m/s), the optimal DG capacity becomes more stable as wind turbines operate closer to their rated capacity. The increase in wind energy availability helps to meet the EV demand without requiring drastic changes in DG sizing which is clearly observed at high wind speeds (11–20 m/s), the optimal DG capacity shows a relatively linear trend, especially for moderate EV demands. As wind energy generation becomes more abundant, it can easily support the EV load, leading to reduced sensitivity to demand variations. However, a sharp increase in DG capacity occurs at lower wind speeds combined with higher EV demand. Regions of flat surfaces or gradual slopes indicate conditions where the system's capacity is less sensitive to changes in one or both parameters. This leads to a steep rise in DG capacity

requirements as wind speed approaches the cut-in threshold.

Furthermore, the plot surface in Fig. 5.14 is uneven, with sharp peaks and valleys. This indicates that the optimization process (using DTBO) is sensitive to both wind speed and EV demand. This highlights the importance of robust optimization to address uncertainties. Also, this sensitivity analysis is valuable for designing resilient energy systems that integrate renewable sources (e.g., wind) and manage dynamic EV demand. It supports grid operators in planning DG installations to ensure reliable energy supply under varying environmental and demand conditions for planning renewable energy integration into power systems

5.4 Case Studies and Results

As observed from Fig. 5.5, with residential EV charging, the network peak load occurs at 21:00 hours. Hence, the bus voltage magnitude profile of the 240-bus power distribution network is determined at 21:00 hours for both base case (without EV charging) and with EV charging. Subsequently, the optimal allocation of wind-based DGs is carried out in the 240-bus distribution network, with EV charging load, at 21:00 hours (considering the worst-case scenario).

The objective function for optimal DG allocation can be formulated in a number of ways. A single-objective function can be formulated by considering either the network ohmic loss per unit base case network ohmic loss, (P_{Tloss}) or the network VD [123], [140]. The objective functions are of the form as given in (5.16) and (5.17), respectively.

$$P_{\text{Tloss}} = \frac{\sum_{j=1}^{b} |I_j|^2 r_j}{P_{\text{Tloss}}^{\text{base}}} \quad (\text{kW}) \tag{5.16}$$

$$VD = \sum_{k=1}^{n} \left(|V_k| - V_{\text{nominal}}\right)^2 \quad (\text{p.u.}) \tag{5.17}$$

By including both the network ohmic loss and the voltage deviation from (5.16) and (5.17), we obtain a much more robust multi-objective function as follows,

$$F_{mo} = w_1 \cdot P_{\text{Tloss}} + w_2 \cdot VD \tag{5.18}$$

In this study, the values of both w_1 and w_2 are taken as 0.5 and $V_{nominal}$ as 1 p.u.

The goal is to minimize the objective function while adhering to the defined constraints. The constraints considered here are:

1) **DG-power capacity:**

$$P_{\text{DG,min}} \leq P_{\text{DG},n} \leq P_{\text{DG,max}}$$

2) **Node-voltage magnitude:**

$$V_{\text{min}} \leq V_n \leq V_{\text{max}}$$

3) **Thermal limit of each branch:**

$$I_j \leq I_{\text{max},j}$$

Here, V_n is the magnitude of voltage at nth node with DG, $P_{\text{DG,min}}$ and $P_{\text{DG,max}}$ is the minimum and maximum value of V_n in p.u and, V_{min} and V_{max} is the minimum and maximum value of V_n in p.u.

Multi-Criteria Decision Making (MCDM) approaches play a critical role in various fields by aiding decision-makers in evaluating and selecting the best alternatives among multiple, often conflicting, criteria. These methods are especially valuable in complex scenarios where decisions must consider trade-offs between diverse objectives. Consequently, MCDM plays a crucial role in the optimal allocation of DG resources in power systems, particularly because such allocation involves balancing multiple, often conflicting objectives as discussed in [141] and [142]. By systematically analyzing alternatives, MCDM methods enhance the quality and robustness of decisions.

The WSM is one of the simplest and most widely used methods in MCDM. It is a straightforward technique for evaluating and ranking alternatives when multiple criteria are involved. As discussed above, the study carried out in this paper has formulated a multi-objective optimization problem of minimizing

PT_{loss} and VD which are associated with weights w_1 and w_2, respectively, as shown in (5.18). To perform WSM, weights w_1 and w_2 in (5.18) are varied from 0 to 1 and 1 to 0, respectively, to observe the corresponding variation in PT_{loss} and VD, the results of which are shown in Fig. 5.15 and Fig. 5.16. From the figures, it is observed that at weights 0 and 1, both the parameters PT_{loss} and VD have their extreme values.

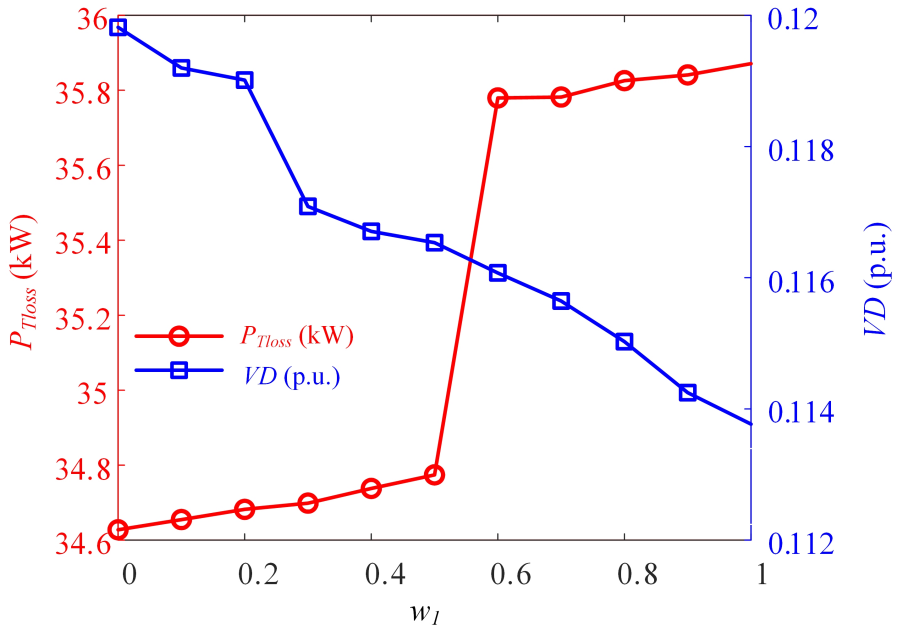


Fig. 5.15: Comparison of P_{Tloss} and VD with w_1

On comparing the results, it is observed that P_{Tloss} increases as w_2 increases and w_1 decreases, and VD decreases as w_2 increases and w_1 decreases. As the focus shifts more towards minimizing VD (w_2 increases), P_{Tloss} worsens slightly. Conversely, prioritizing lower P_{Tloss} (w_1 increases) leads to slightly higher VD. Thus, depending on the priority (i.e., minimizing losses or maintaining voltage stability), weights w_1 and w_2 can be adjusted. However, at $w_1 = w_2 = 0.5$, the output for P_{Tloss} and VD is balanced for both the parameters. Therefore, in this paper, the values of both weights w_1 and w_2 are taken as 0.5, which balances the trade-offs between PT_{loss} and VD based on system requirements.

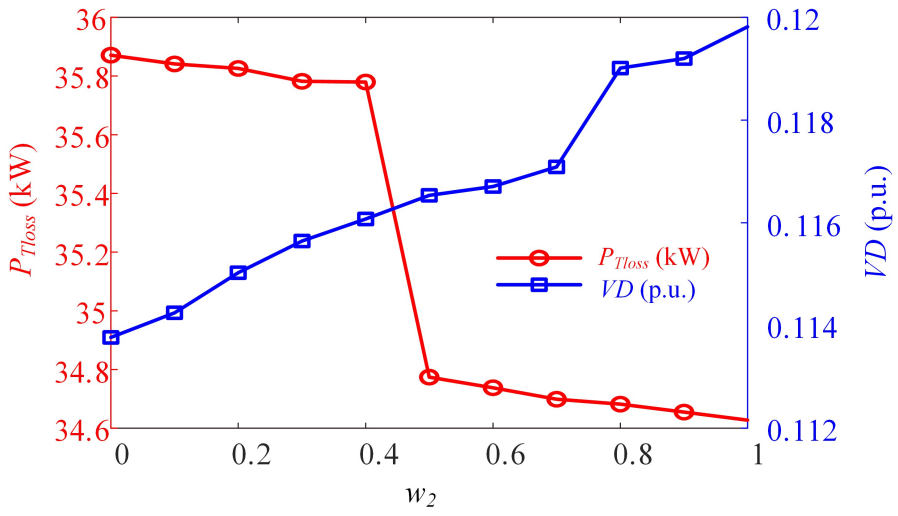


Fig. 5.16: Comparison of P_{Tloss} and VD with w_2

5.4.1 Loss Sensitivity Factor

For selection of the desirable network buses for DG placement, the preliminary selection is done by selecting all the three-phase buses in the network. The final selection to choose the most desirable locations among all the three-phase buses is carried out on the basis of the Loss Sensitivity Factor (LSF) [143] as shown below,

$$LSF = \frac{\partial P_{\text{loss}}}{\partial P_{\text{eff}}} = \frac{2 \cdot P_{\text{eff}}[q] \cdot r_j}{(V[q])^2} \tag{5.19}$$

where, P_{loss} is the line active power loss in kW.

The LSFs are computed from power flow analysis, and their values are arranged in descending order for all the lines of the system. A vector, `pos[i]`, is used to store the respective 'end' buses of the lines arranged by decreasing LSF values. The sequence of elements in the `pos[i]` vector determines the order in which buses are considered for DG placement. Additionally, for these buses, the normalized voltage magnitudes norm$[i]$ are calculated based on the network voltages $V[i]$ as,

$$\text{norm}\,[i] = \frac{V[i]}{0.95} \tag{5.20}$$

Buses with a '*norm*[i]' value less than 1.01pu are identified as candidate buses for DG placement and stored in a *rank_bus* vector. It is important to note that while

the *LSF* determines the evaluation sequence for DG placement, the *norm*[i] values decide whether a bus requires DG placement or not. If a bus in the sequence list has a healthy voltage (i.e., $norm[i] > 1.01$ pu), it does not need DG placement and is excluded from the *rank_bus* vector. The *rank_bus* vector provides information on potential candidate buses for DG placement. Finally, the sizing of DGs at the buses listed in the *rank_bus* vector is performed using the DTBO method.

Table 5.6: DG Placement Results: Single-Objective DTBO

Parameters	**Bus No.**	**Wind Turbine Output (kW)**	**Losses Before DG Placement (kW)**	**Losses After DG Placement (kW)**	**% Reduction in Losses**
Base Case (without EV, without DG)		–	31.06	–	–
Case I	3081 3078 3077 3074	85.58 88.31 73.43 97.18	49.14	26.71	45.65
Case II	3081 3078 3077 3074	92.93 99.90 87.19 84.31	60.37	34.77	42.41
Case III	3081 3078 3077 3074	100.00 100.00 100.00 100.00	62.18	36.07	42.00

Table 5.7: Fine-Tuned Control Parameters

Algorithm	Parameter	Value
DTBO	Random number	*rand* from $[0, 1]$
	Constant, R	0.05
GA	Mutation	Gaussian (Probability = 0.05)
	Crossover	Whole arithmetic (Probability = 0.8)
	Selection	Roulette wheel (Proportionate)
IGWO	Scale Factor of wolves updating, ε	5
	Crossover Probability, CR	0.7
PSO	Inertia weight	1
	Cognitive and social constant	$C_1 = 1.5,\ C_2 = 2$
TLBO	Random number	*rand* from $[0, 1]$
	Teaching Factor, T_F	$T_F = \text{round}(1 + rand)$
Number of search agents, $N = 30$ Maximum number of iterations, $T = 100$		

5.4.2 Analysis with Single-Objective DTBO

In this study, network Ohmic loss is considered as the objective function as presented in (5.16). Three different cases are considered, which are detailed below:

Case I: Each Household has Exactly One EV

The result for this case is shown in the third row of Table 5.6. It is observed that, on considering one EV per household, the losses in the network increase from 31.06 kW (base case) to 49.14 kW (Case I). To account for this, the total active power supplied by the wind turbines is computed as 344.5 kW. This accounts for 18.42% of the total network load. The network ohmic losses are reduced from 49.14 kW to 26.71 kW, resulting in a 45.65% decrement in the network losses.

Case II: Each Household has at Most Two EVs

The results for Case II are shown in the fourth row of Table 5.6. It is observed that the total active power supplied by the wind turbines is 364.33 kW, which accounts for 17.72% of the total network load. The network ohmic losses are reduced from 60.37 kW to 34.77 kW, accounting for a 42.41% decrement in the network power losses.

Table 5.8: DG-Placement Results: Multi-Objective DTBO (Network Power Loss)

Parameters	**Bus No.**	**Wind Turbine Output (kW)**	**Losses Before DG (kW)**	**Losses After DG (kW)**	**% Reduction in Losses**
Base Case (Without EV, without DG)	–	–	31.06	–	–
Case I	3081 3078 3077 3074	84.41 86.28 87.35 88.33	49.14	26.72	45.65
Case II	3081 3078 3077 3074	90.95 91.78 90.09 91.96	60.37	34.79	42.37
Case III	3081 3078 3077 3074	100 100 100 100	62.18	36.09	41.96

Case III: Each Household has at Most Three EVs

The results for this case are shown in the fifth row of Table 5.6. It is observed that the total active power supplied by the wind turbines is 400 kW for Case III, which accounts for 19.2% of the total network load. Also, the network ohmic losses are

Table 5.10: DG-Placement Results: Multi-Objective DTBO (Voltage Deviation)

Parameters	VD Before (p.u.)	VD After (p.u.)	% Reduction (p.u.)
Base Case (Without EV, without DG)	0.07	–	–
Case I	0.28	0.10	64.29
Case II	0.34	0.12	64.71
Case III	0.35	0.13	62.86

reduced from 62.18 kW to 36.07 kW, representing a 42% decrement in the network losses. From Table 5.6, it can be observed that the DG allocation using DTBO has reduced the network losses substantially.

5.4.3 Analysis with Multi-Objective DTBO

In this study, the network ohmic loss and voltage deviation are considered as the two objective functions as discussed in (5.16) and (5.17). Finally, equation (5.17) is used as the multi-objective problem accompanying equations (5.16) and (5.17) . Again, three different cases are considered, as detailed below:

Case I: Each Household is Allotted One EV

The results for this case are shown in the third rows of Tables 5.8 and 5.10. From the third row of Table 5.8 , it can be observed that the total active power supplied by the wind turbines is 346.37 kW, which accounts for 18.52% of the total network load. Also, with DGs, the network losses are reduced significantly from 49.14 kW to 26.72 kW, corresponding to a 45.62% decrease. From the third row of Table 5.10, it is observed that with DGs, the voltage deviation reduces drastically from 0.28 p.u. to 0.10 p.u., which is about a 64.29% decrease.

Case II: Each Household is Allocated a Maximum of Two EVs

From the fourth row of Table 5.8, it can be observed that the total active power supplied by the wind turbines is 364.78 kW, which accounts for 17.74% of the total network load. Also, the network losses are reduced from 60.37 kW to 34.79 kW, representing a 42.37% decrease. From the fourth row of Table 5.10, it is observed that with DGs, the voltage deviation is again reduced drastically from 0.34 p.u. to 0.12 p.u. (about 64.71% decrease).

Case III: Each Household is Allocated a Maximum of Three EVs

From the fifth row of Table 5.8 , it can be observed that the total active power supplied by the wind turbines is 400 kW, which accounts for 19.2% of the total network load. Also, with DGs, the network losses are reduced significantly from 62.18 kW to 36.09 kW, accounting for a 41.96% decrement in the network losses. From the fifth row of Table 5.10 , it is observed that with DGs, the voltage deviation is again reduced drastically from 0.35 p.u. to 0.13 p.u. (about 62.86% decrease).

The bus voltage magnitude profiles of the 240-bus network for the multi-objective case pertaining to phases A, B, and C (at 21:00 hours) for the proposed cases are shown in Fig. 5.17 . From Fig. 5.17 , it can again be observed that after optimal DG allocation using DTBO, the network bus voltage magnitude profiles with EV charging are substantially improved over those without DGs. This validates the effectiveness of the proposed methodology used in this paper.

5.4.4 Performance Evaluation of the Proposed Model Through Numerical Computations

To confirm the accuracy and effectiveness of the DTBO algorithm, a comparative analysis is performed with three other competitive metaheuristic algorithms – PSO, IGWO, and TLBO – for both the single and multi-objective problems discussed in (5.16) and (5.18) for the 240-bus PDN. The comparison of these three methods is presented individually for the proposed three cases I, II, and III, with a magnified illustration of each case on the right side, as shown in Fig. 5.18(a),

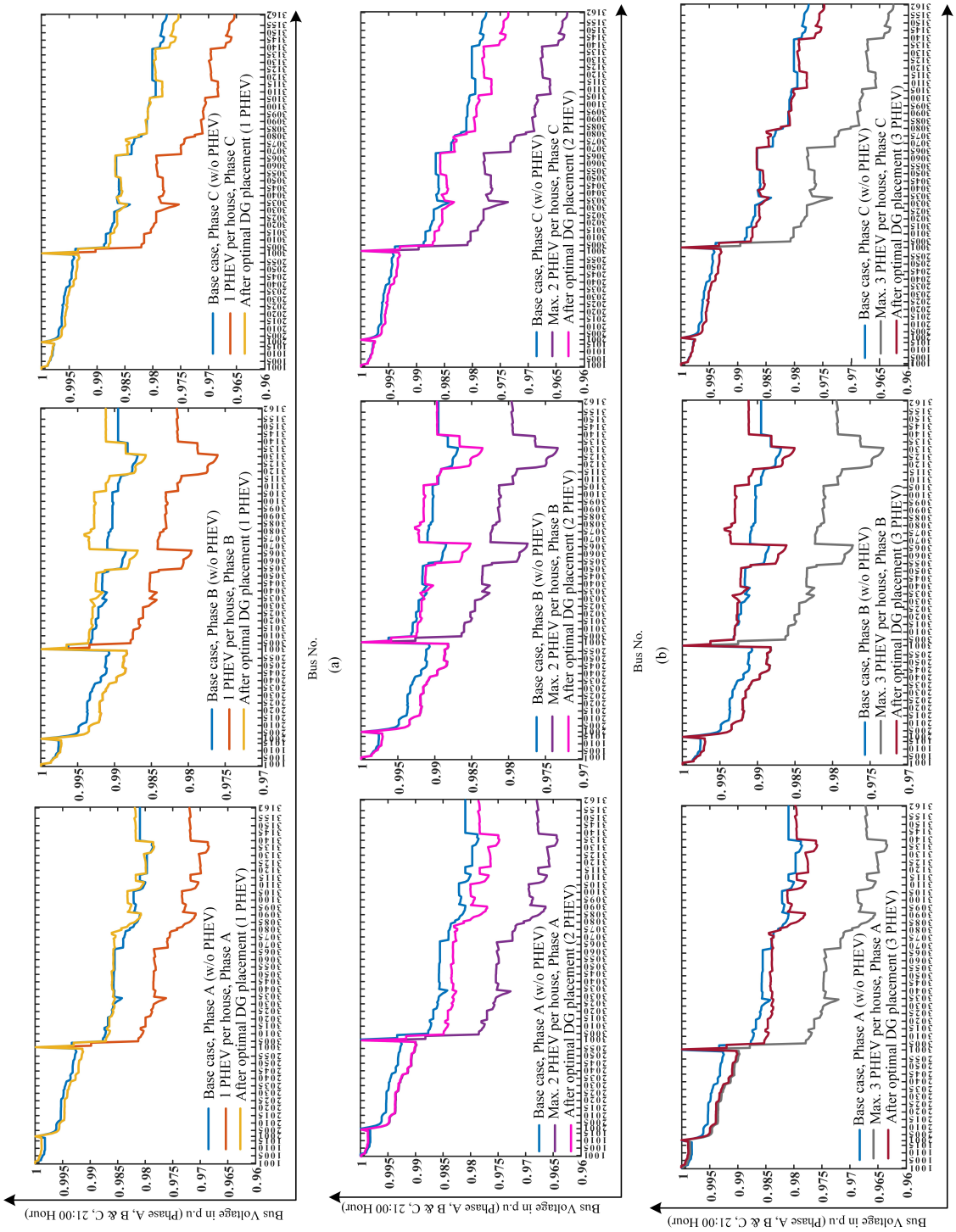
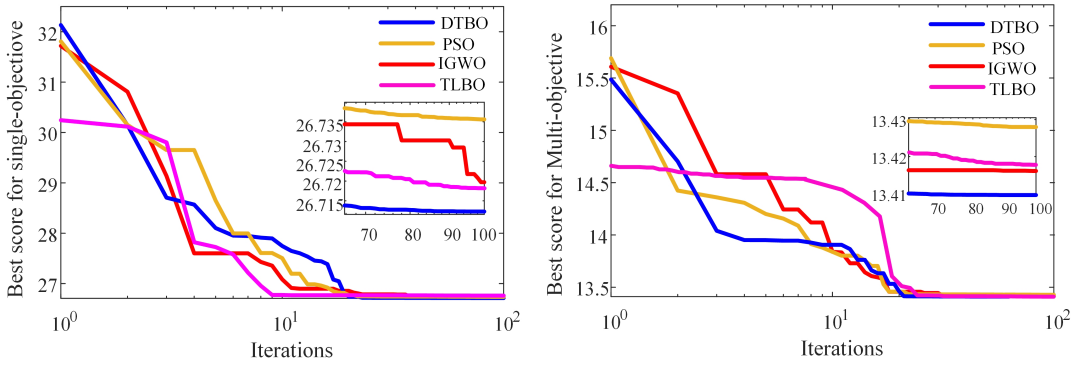


Fig. 5.17: Bus voltage magnitude profile for phases 'A', 'B', and 'C' at 21:00 hours with (a) exactly 1 PHEV per house, (b) at most 2 PHEVs per house, and (c) at most 3 PHEVs per house

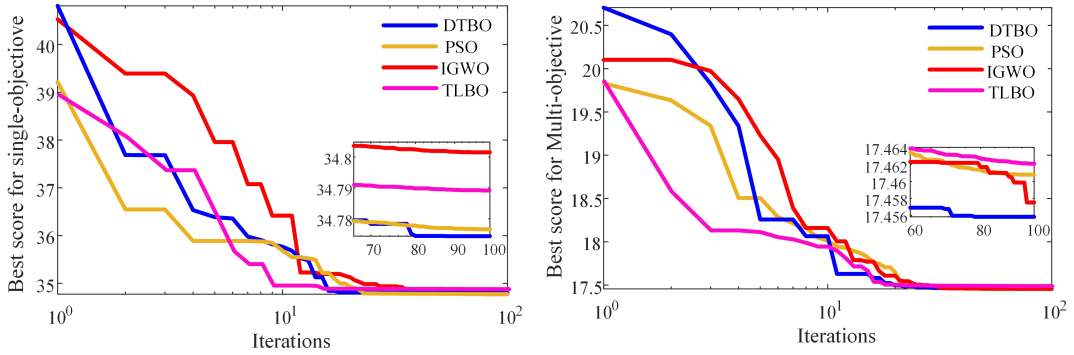
(b), and (c), respectively. All simulations were carried out in MATLAB, and the results are presented for 100 iterations. Moreover, the details of the parameters for each algorithm are provided in Table 5.7.

From Fig. 5.18, it is observed that for all three cases, IGWO, TLBO, and PSO struggle to provide the optimal solution, whereas DTBO performs significantly better by efficiently converging in less computational time and yielding the minimum fitness value for both the single and multi-objective problems of (5.16) and (5.18), respectively. The detailed results for the comparative analysis of DTBO with PSO, IGWO, and TLBO in terms of fitness value and computational time are provided in Table 5.12. It is observed from Table 5.12 that as the complexity of the system increases with the increasing number of EVs per household (from case I to III), both computational time and fitness score increase.

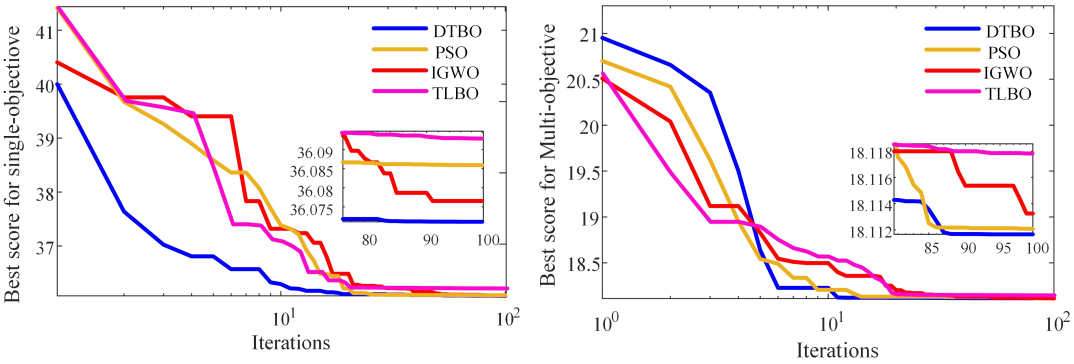
Although all four algorithms show competitive results, DTBO outperforms the other three in solving the proposed problems with better accuracy, lower fitness values, and less computational time, resulting in high exploration and exploitation ability to find the global optimum. The comparative results in Table 5.12 are displayed with arrows underneath each fitness and computational time value. An upward arrow indicates a superior value, while a downward arrow indicates an inferior value. The number of arrows denotes the degree of superiority of each value among the four. For instance, in case I of the single-objective analysis, PSO exhibits the poorest fitness value with three downward arrows, while DTBO demonstrates the best fitness value with four upward arrows compared to all four algorithms.approaches. In the same scenario, the IGWO fitness value is moderately positioned between the DTBO, TLBO and PSO fitness values, as indicated by a double downward arrow. The primary goal of the single-objective problem presented in this study is to minimize network real power losses. Thus, the fitness value that corresponds to the minimal or lowest value represents the best optimal solution, indicating the least network losses. Arrows are allocated to the results obtained in Table 5.12 based on this criterion. In the case of the multi-objective problem, the goal is to reduce both the network's real power losses and voltage deviation. Therefore, the lowest fitness value determines the best optimal objective value. The results indicate that the fitness values of PSO, IGWO and TLBO exhibit interchangeable outcomes for each scenario, whereas DTBO consistently achieves the best results



(a) Case I



(b) Case II



(c) Case III

Fig. 5.18: The comparison of the convergence based for Case I, II and III with single and multi-objective objective

among the three methods, hence denoted by four up-arrows. Moreover, DTBO demonstrates superior performance in terms of computational time required for convergence and finding the global optimum value, resulting in its assignment of four up-arrows. Thereby, the results in Fig. 5.18 and Table 5.12 suggest that among all the four algorithms, for both the single and multi-objective problems of optimal DG allocation in the 240-bus distribution network, the DTBO outperforms the other three which presents its superiority and robustness.

5.4.5 Discussion

The goal of the distribution system planning with wind-based DGs discussed in this chapter is to identify the optimal locations and sizes of DG units within a large 240-bus PDN, aiming to support the additional load from residential EV charging. In this respect, two minimization objective functions were defined in Equations (5.16)-(5.18) under specific network constraints. For the single-objective problem of minimizing network real power losses using the DTBO method, with optimal DG allocation, the network real power losses reduce by 45.65% to 42% for different cases. Similarly, for the multi-objective problem, the reduction in network real power losses is 45.62% to 41.96% and a reduction in voltage deviation by 64.29% to 62.86% for different case studies.

The improved bus voltage profiles for individual phases of the 240-bus distribution network are illustrated in Fig. 5.18 for the multi-objective problem. The bus voltage profile trends observed in Fig. 5.18 highlight the critical role of DG placement in maintaining voltage stability under increasing EV penetration. In the base case (without PHEVs), bus voltage magnitudes are relatively stable across all phases. However, as PHEVs are introduced (1, 2, and then 3 PHEVs per house), significant voltage dips occur, with the severity increasing as the number of PHEVs rises. This drop is most pronounced in Phase C, suggesting an uneven phase load distribution or system weaknesses in that phase.

The optimal placement of DGs mitigates these voltage dips effectively. For 1 PHEV per house, DG placement almost restores the voltages to their base case levels across all phases, showing high efficiency. For 2 PHEVs per house, DG still manages to stabilize the voltages substantially, though slight deviations from the base case start to appear. At 3 PHEVs per house, while DG placement improves

Table 5.12: Comparative Performance Evaluation for Single and Multi-Objective Problem for the Proposed Case Studies

Case	IGWO [136]		PSO [137]		TLBO [138]		DTBO [121]	
	Fitness Value	CPU Time (sec)	Fitness Value	CPU Time (sec)	Fitness Value	CPU Time (sec)	Fitness Value	CPU Time (sec)
Single-Objective								
Case I	26.7208 (↓↓)	292.755 (↓↓↓)	26.7358 (↓↓↓)	185.8211 (↓)	26.7201 (↓)	284.622 (↓↓)	26.7123 (↑↑↑↑)	101.972 (↑↑↑↑)
Case II	34.8015 (↓↓)	297.1026 (↓↓↓)	34.7766 (↓)	212.374 (↓)	34.8912 (↓↓↓)	288.3101 (↓↓)	34.7743 (↑↑↑↑)	121.4303 (↑↑↑↑)
Case III	36.0765 (↓)	340.413 (↓↓↓)	36.0859 (↓↓)	258.0349 (↓)	36.099 (↓↓↓)	291.325 (↓↓)	36.0711 (↑↑↑↑)	123.172 (↑↑↑↑)
Multi-Objective								
Case I	13.4161 (↓)	292.8011 (↓↓)	13.428 (↓↓↓)	210.3896 (↓)	13.4183 (↓↓)	295.6111 (↓↓↓)	13.4096 (↑↑↑↑)	102.9909 (↑↑↑↑)
Case II	17.4575 (↓)	303.2175 (↓↓↓)	17.4608 (↓↓)	227.8476 (↓)	17.4618 (↓↓↓)	230.2242 (↓↓)	17.4558 (↑↑↑↑)	114.0086 (↑↑↑↑)
Case III	18.1132 (↓↓)	347.297 (↓↓)	18.1121 (↓)	266.9919 (↓)	18.11767 (↓↓↓)	351.7891 (↓↓↓)	18.1117 (↑↑↑↑)	124.3729 (↑↑↑↑)

the voltage profiles considerably compared to the scenario without DG, the voltages remain below the base case for several buses, particularly in Phase C. This indicates that while DG placement is a highly efficient solution for moderate PHEV penetration, its effectiveness under high PHEV penetration can be enhanced with supplementary strategies such as load management and phase balancing. The observed trends demonstrate the importance of proactive planning and optimization in grid management to maintain stability under evolving load demands.

The results demonstrate that appropriately sizing and locating wind-based DG units using DTBO can lead to several benefits for the 240-bus PDN, including reduced network real power loss, improved bus voltage magnitude profile, and enhanced power supply reliability.

5.4.6 Practical Implementation Challenges and Future Work

The high accuracy, minimal fitness value, and rapid convergence of the DTBO in minimizing network real power losses and voltage deviation for a 240-bus PDN demonstrate its robustness and effectiveness for estimating the DG capacity and location in PDNs. However, as the network complexity increases, the computational time for the DTBO to find the optimal solution also rises. Therefore, future work will focus on developing a more robust and improved algorithm that better balances exploration and exploitation capabilities to achieve the global optimal value. Additionally, according to the No-Free-Lunch theorem, no optimization algorithm can claim to be universally superior. Consequently, new approaches may be developed in the future that perform better in addressing the problems proposed in this chapter.

5.5 Conclusions

1. In this chapter, DTBO, a human-based metaheuristic technique, is applied to the optimal DG allocation in a 240-bus power distribution network located in the Midwest U.S.A., to alleviate the detrimental effects of residential EV charging. About 1500 EVs pertaining to more than 1000 U.S. residents are considered, with three different EV penetration scenarios.

2. At first, the effectiveness and superiority of the DTBO algorithm over other commonly used metaheuristic algorithms like GA, IGWO, PSO, and TLBO is validated with respect to their convergence characteristics using different benchmark mathematical functions. Subsequently, the DTBO is applied to the optimal allocation of wind power-based DGs to improve the performance of a 240-bus distribution network subjected to residential EV charging. The wind speed patterns for the site are taken from the IEM data, and the dynamic EV charging demand is modeled using realistic 2017 NHTS travel survey data. Both single and multi-objective DTBO formulations are considered.

3. Three different EV penetration scenarios are analyzed, based on the level and acceptance of EVs by the general public. Multiple case studies conducted in the MATLAB platform demonstrate that with optimal DG allocation using the DTBO algorithm, the adverse effects of EV charging on the network performance are minimized. With the single-objective DTBO formulation, the maximum reduction in network real power loss is 45.65%, whereas with the multi-objective DTBO formulation, the maximum reductions in network real power loss and voltage deviation are around 45.62% and 64.71%, respectively. This validates the effectiveness of the proposed technique.

Chapter 6

A Probabilistic Framework for Optimal Allocation of Solar PV and Wind Turbine DGs in Distribution Networks with Residential and Fast EV Charging

Building upon the deterministic DG allocation approach presented in Chapter 5, this chapter introduces a probabilistic planning framework for the optimal siting and sizing of solar photovoltaic and wind-based DG units in a 240-bus PDN using a metaheuristic, human-based DTBO technique. This is accomplished by generating the stochastic RBDG outputs and the PDN demand profiles with EVCD for different seasons, using appropriate probabilistic models. The EVCD due to slow residential and Tesla Supercharger based PFCSs are generated from the U.S.-based 2017 NHTS and Fastned, a charging infrastructure provider, respectively. The windspeed and solar irradiance data are taken from the NASA website, while the WT and SPV module data are taken directly from the manufacturers' datasheets.The results demonstrate that with optimal RBDG allocation using DTBO, the maximum reductions in the PDN losses and network VD are 54% and 73%, respectively.

6.0.1 Chapter Contributions

In light of the above issues, the main contributions of this chapter are:

- A comprehensive probabilistic planning technique for optimal siting and sizing of SPV and WT-based DGs to improve the performance of a 240-bus PDN with slow residential and public fast EVCD is proposed in this paper. The primary objective of optimal RBDG allocation in the PDN is to minimize the Ohmic losses and the voltage deviation of the PDN with EVCD, subject to operational constraints.
- For estimating the 24-hour EVCD profiles for slow residential case, daily travel data from the 2017 NHTS, including number and type of EV, travel distance, trip arrival and departure timing is used.
- For EVCD estimation of public fast charging stations, practical EVCD profiles from Fastned, a leading EV charging infrastructure provider, is used. Both battery capacity and battery SOCs of individual EVs arriving for charging at PFCSs are considered stochastic quantities.
- Uncertainties in the solar irradiance and wind speed have been accounted for, using appropriate probabilistic models. In addition, seasonal variations in the RBDG outputs are considered for the estimation of their sizing.
- The RBDGs have been optimally allocated in the 240-bus PDN using DTBO algorithm. The DTBO algorithm is observed to outperform two recent algorithms, COA and IGWO, in terms of the convergence speed and the accuracy of the final objective function value.

6.1 Framework For The Proposed Work

Fig. 6.1 presents a framework of the proposed planning technique for the optimal allocation of WT- and SPV-based DGs in a 240-bus PDN to improve the PDN performance with EVCD. At first, it integrates multi-source annual data for 240-bus PDN base demand, NHTS 2017 EV travel patterns, wind speed, and solar irradiance data to build a realistic planning model.

Further, the approach includes:

1. Estimating EVCD due to residential and PFC,
2. Characterizing seasonal RBDG output from WT and SPV using PDFs, and

3. Probabilistic estimation of seasonal ND.

Uncertainties in the solar irradiance and wind speed are accounted for by appropriate probabilistic models to estimate the seasonal RBDG outputs. Subsequently, load-flow analysis of the 240-bus PDN is carried out, and the results are further fed into the DTBO optimization algorithm that minimizes PDN Ohmic losses and voltage deviations by optimally allocating the RBDGs into the PDN, subject to operational constraints.

6.2 EVCD Model

In this Chapter, the modelling of the 24-hour EVCD is carried out separately for both slow residential as well as PFC, using mathematical equations and travel survey data from NHTS 2017 as already explained in Chapter 3. For slow residential EVCD profiles, modelleling equations (3.5)-(3.7) were used. However, for generating the EVCD profiles PFCS, (3.8), (3.9) were used.

Table 6.1: Overview of EVs Considered for Study

Vehicle Type	ECPM (kWh/mile)	Battery Capacity (kWh)	Maximum DC Charging Power (kW)
Small	0.24955	42	50
Medium	0.25999	58	100
Large	0.29946	77	125
SUV	0.38157	70	150

Moreover, the PDF of EVs arriving home (residential charging) and at a TS-PFCS (fast charging) is shown in Fig. 3.5 [117]. Now, assuming that the daily EV mileage is a random variable and follows a lognormal PDF [45], the PDF f_S of the initial battery SOC is given as,

$$f_S(S) = \frac{1}{\frac{E_{\text{cap}}}{ECPM}(1-S)\sqrt{2\pi\sigma^2}} \exp\left(-\frac{\left(\ln(1-S) - \left(\mu - \ln\left(\frac{E_{\text{cap}}}{ECPM}\right)\right)\right)^2}{2\sigma^2}\right) \quad (6.1)$$

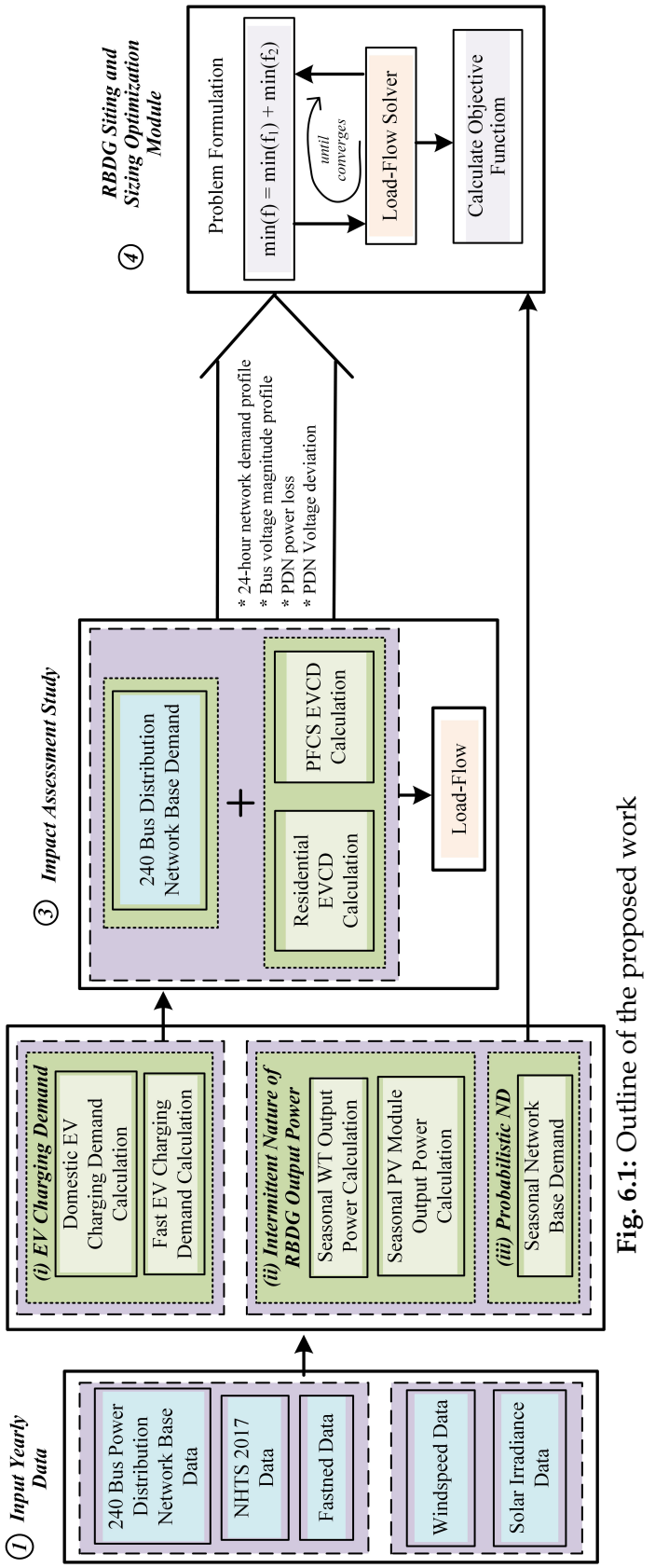


Fig. 6.1: Outline of the proposed work

where μ and σ are the mean and the standard deviation, respectively, of the PDF.

In a similar manner, assuming a normal distribution of EV type (which dictates E_{cap}), the PDF f_{batt} of the battery capacity of the whole EV fleet [117] is given by (6.2).

$$f_{\text{batt}}(E_{\text{cap}}) = \sum_{i=1}^{N_{\text{EV}}} M_i Y_i \cdot \frac{1}{\sigma_i \sqrt{2\pi}} \exp\left(-\frac{\left(E_{\text{cap}} - \mu_i\right)^2}{2\sigma_i^2} \right) \tag{6.2}$$

where i is the vehicle segment, M is the market share, Y is the normalized annual mileage, N_{EV} is the number of vehicle segments, while μ and σ are the mean and the standard deviation of the battery capacities. In this paper, it is assumed that $N_{\text{EV}} = 4$. The different EV segments (types) are shown in Table 6.1.

6.3 Probabilistic Modelling of RBDG and Load

6.3.1 Processing of Historical Data

In this study, yearly wind speed and solar irradiance data for 2024 are collected from [144] and are shown in Fig. 6.2 (a) and 6.2 (b), respectively. Each year is categorized into four seasons: spring (March to May), summer (June to August), autumn (September to November), and winter (December to February), comprising 92, 92, 91, and 90 days, respectively. These days are further divided into hours, serving as the fundamental time segments, denoted as h. Each time segment is then subdivided into different states, g, based on the sampling intervals of the measurements.

Based on the mean values and the standard deviations of wind speed and solar irradiance for each hour of a typical day, k and C of the Weibull PDF and α and β of the Gamma PDF are calculated, as explained in the subsequent subsections. By determining these statistical values for each of the 24 hours, a representative day for each season is constructed.

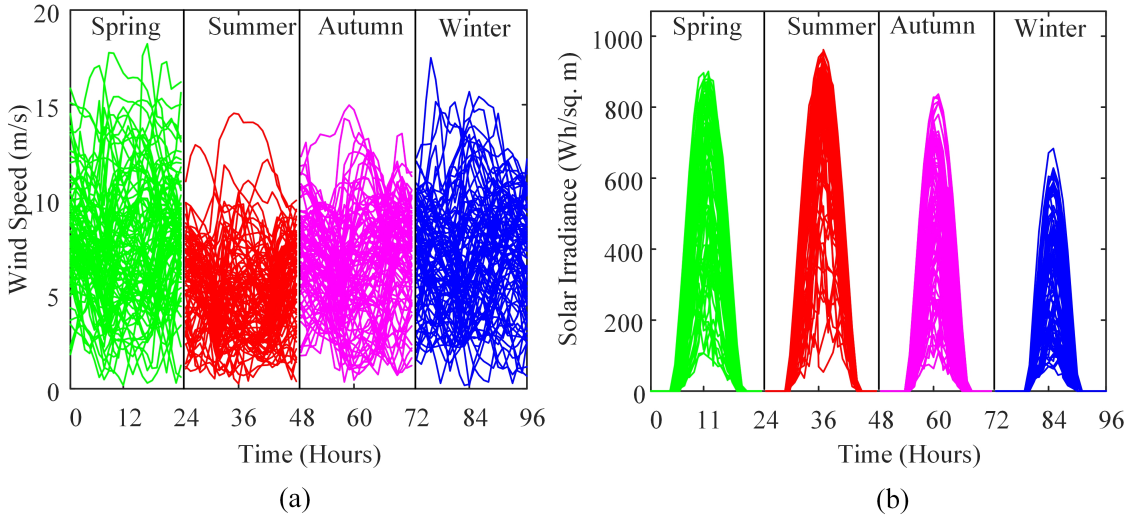


Fig. 6.2: Seasonal profiles of (a) windspeed and (b) solar irradiance at the site under study

6.3.2 Modelling of WT Output Power

The stochasticity of wind speed over a specified time period 'h' at a given site can typically be characterized using the Weibull PDF [145],

$$f_v(v) = \frac{k^h}{C^h}\left(\frac{v}{C^t}\right)^{k^h-1} \exp\left[-\left(\frac{v}{C^h}\right)^{k^h}\right] \tag{6.3}$$

In practice, the parameters 'C^h' and 'h^k' for a given time period 'h' can be determined [145] as,

$$k^h = \left(\frac{\sigma_v^h}{\mu_v^h}\right)^{-1.086} \tag{6.4}$$

$$C^h = \frac{\mu_v^h}{\Gamma\left(1+\frac{1}{k^h}\right)} \tag{6.5}$$

The CDF of Weibull distribution and its inverse, used to estimate the windspeed is given by (6.6) and (6.7), respectively [145].

$$F_v(v) = 1 - e^{-\left(\frac{v}{C^h}\right)^{k^h}} \tag{6.6}$$

$$v = C^h \left(-\ln(r)\right)^{\frac{1}{k^h}} \tag{6.7}$$

For all the possible values of wind speed, the output power of the turbine is governed by [145]:

$$P_{WT}(v) = \begin{cases} 0, & v \leq v_{ci} \text{ or } v \geq v_{co} \\ P_{w,r}\frac{v^2 - v_{ci}^2}{v_r^2 - v_{ci}^2}, & v_{ci} \leq v \leq v_r \\ P_{w,r}, & v_r \leq v \leq v_{co} \end{cases} \tag{6.8}$$

The specifications of the WT used in this study is detailed in Table D.1 [9].

To represent the Weibull PDF of each hour in discrete form, hour 'h' is divided into 'N_v' number of states as previously discussed. The corresponding wind speed and probability for each state 'g' are determined using equations (6.7) and (6.3), respectively. Finally, the WT's power generation is calculated by considering the probability of wind speed for each state during hour 'h' using (6.9) as shown in Fig. 6.3.

$$P_{WT}^h = \frac{\sum_{g=1}^{N_v} P_{WTg} f_v\left(v_g^h\right)}{\sum_{g=1}^{N_v} f_v\left(v_g^h\right)} \tag{6.9}$$

where, $f_v(v)$ is the probability of windspeed for state 'g' and hour 'h', and v_g^h is the windspeed at state 'g' and hour 'h'.

6.3.3 Modelling of SPV Module Output Power

The stochasticity of solar irradiance over a specified time period 'h' at a given site can typically be characterized using the Beta PDF [145],

$$f_s(s) = \begin{cases} \frac{\Gamma(\alpha+\beta)}{\Gamma(\alpha)\Gamma(\beta)} s^{\alpha+1}(1-s)^{\beta+1}, & 0 \leq s \leq 1,\ \alpha \geq 0,\ \beta \geq 0 \\ 0, & \text{otherwise} \end{cases} \tag{6.10}$$

Analogous to wind speed, the parameters 'α' and 'β' for a given time period 'h' can be determined [145] as,

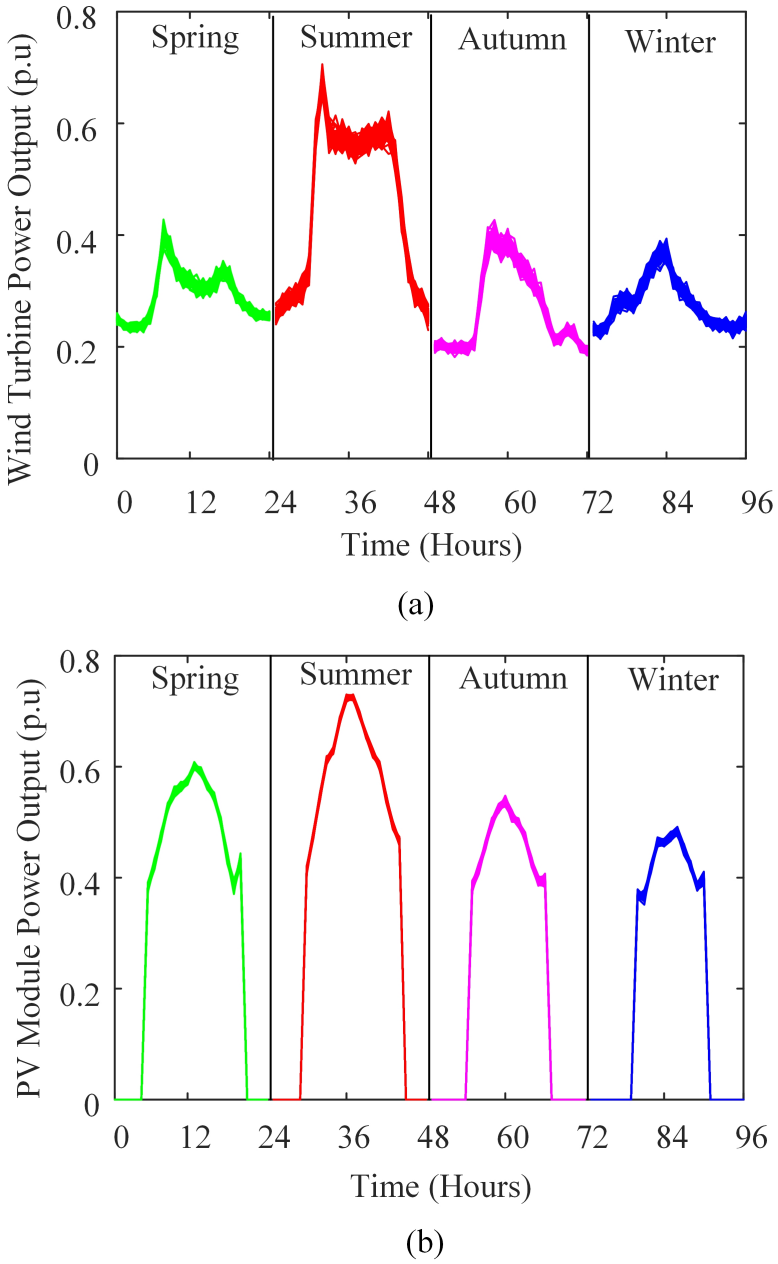


Fig. 6.3: Seasonal variation of the predicted output powers of a single (a) WT and (b) SPV module

$$\beta = (1 - \mu_s)\left[\frac{\mu_s(1+\mu_s)}{\sigma_s^2} - 1\right] \tag{6.11}$$

$$\alpha = \frac{\mu_s \beta}{1 - \mu_s} \tag{6.12}$$

The power output of the SPV module, based on its technical characteristics [10] (refer Table E.1), depends on the solar irradiance and ambient temperature. It can be described as,

$$T_{cg} = T_A + S_{ag}\left(\frac{N_{OT} - 20}{0.8}\right) \tag{6.13}$$

$$I_g = s_{ag}\left[I_{sc} + C_I(T_c - 25)\right] \tag{6.14}$$

$$V_g = V_{oc} - C_V \cdot T_{cg} \tag{6.15}$$

$$P_{PV,g} = N_M \cdot FF \cdot V_g \cdot I_g \tag{6.16}$$

$$FF = \frac{V_{MPP} * I_{MPP}}{V_{oc} * I_{sc}} \tag{6.17}$$

Here, T_{ce} is the cell temperature (°C) during state 'g', T_A is the ambient temperature (°C), s_{ag} is the average solar irradiance of state 'g' and FF is the fill factor.

To represent the Beta PDF of each hour in discrete form, hour 'h' is divided into 'N_s' number of states. Finally, the SPV module's power generation is calculated by considering the probability of solar irradiance for each state during hour 'h' using (6.18) as shown in Fig. 6.3 (a) and, (b).

$$P_{PV}^h = \frac{\sum_{g=1}^{N_s} P_{PV_g} f_s(s_g^h)}{\sum_{g=1}^{N_s} f_s(s_g^h)} \tag{6.18}$$

where, s_g^h is the solar irradiance at state 'g' and hour 'h', and $f_s(s_g^h)$ is the probability of solar irradiance for state 'g' and hour 'h'.

6.3.4 Modelling of Load

The randomness in load variations is represented by the normal PDF. Typically, the load is considered as a random variable 'L' that follows the same PDF within each hour of a given daily load dynamics.

$$f_L(L) = \frac{1}{\sigma_L\sqrt{2\pi}} e^{-\frac{(L-\mu_L)^2}{2\sigma_L^2}} \tag{6.19}$$

$$f_L(L) = \frac{1}{2}\left[1 + erf\left(\frac{L-\mu_L}{\sqrt{2}\,\sigma_L}\right)\right] \tag{6.20}$$

$$L = \mu_L + \sqrt{2}\,\sigma_L\, erf^{-1}(2r-1) \tag{6.21}$$

To obtain the discrete representation of the normal PDF for each hourly load, hour 'h' is divided into N_l number of states. The load and probability for each state 'g' are then determined using equations (6.21) and (6.19), respectively. Thereafter, by considering the probability of load for each state at hour 'h', the load level can be calculated using (6.22) as shown in Fig. 6.4.

$$L^h = \frac{\sum_{g=1}^{N_L} L_g f_L(L_g^h)}{\sum_{g=1}^{N_L} f_L(L_g^h)} \tag{6.22}$$

where, L_g^h is the load at state 'g' and hour 'h', and $f_L(L_g^h)$ is the probability of load for state 'g' and hour 'h'.

6.4 System Overview

6.4.1 240-Bus PDN

To investigate the impacts of both residential and PFC EVCD, a 240-bus radial PDN is used in this paper [1]. Unlike most of the IEEE standard distribution test systems, this PDN contains hourly real and reactive power demands of all customers from smart meters. The PDN is already shown in Fig. 1.1.

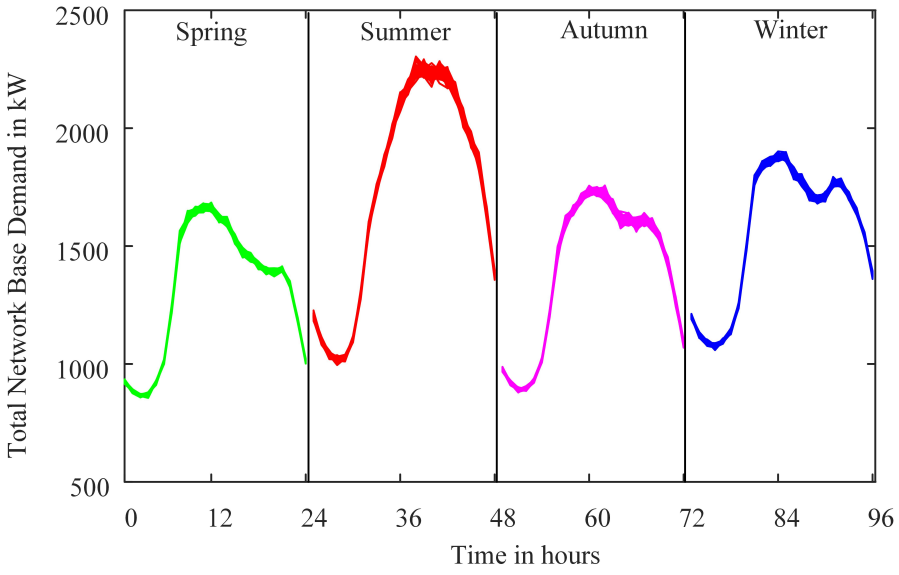


Fig. 6.4: Seasonal variation of the predicted base demand for the 240-bus PDN

6.4.2 EVCD Prediction Using Real Travel Survey Data

The number of vehicles on road during day-time, the average distance commuted by EV users to work each day, and the statistical data regarding arrival and departure times are used to simulate the load required for both residential and PFC. This information is extracted from the NHTS 2017 travel survey data (summarized in Fig. 6.5).

In this chapter, the `ENDTIME` of the final vehicle trip is used as the charging start time for residential charging. In contrast, for TS-PFCS, the charging start time is taken as the average of `STRTTIME` and `ENDTIME` to simulate the time when EVs are on road and available to use a PFCS.

The dynamic EVCD for both residential charging and PFC are individually computed and added to the base case ND, to get the 24-hour demand curve with EVCD. For residential charging, each household is assumed to be supplied from single-phase, 60 Hz, 120 V supply, pertaining to the SAE J1772 charging protocol [3]. The charging demands of the TS-PFCSs are allocated to three-phase buses 2058 and 3077 of the 240-bus PDN due to their higher transformer capacities [1].

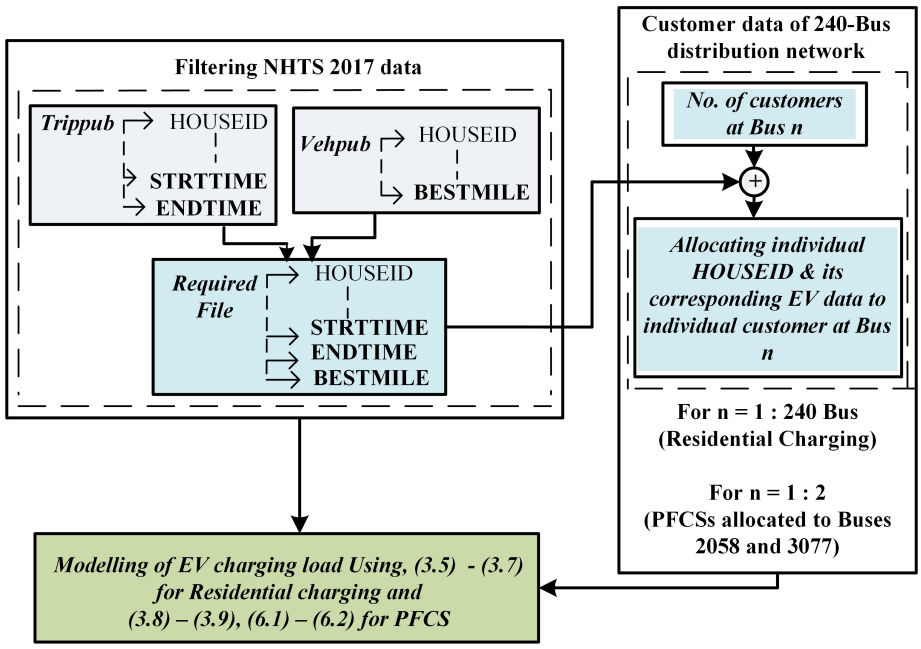


Fig. 6.5: Procedure for EVs modelling and allocation in the 240-bus PDN

6.4.3 Structure of the TS-PFCS

In this paper, we have categorized the EVs into four different segments ranging from city cars to SUVs as given in Table 6.1 [4]. The TS-PFCS used in this paper comprises five charging ports, each having a power rating of 150 kW. The type (which dictates battery capacity) and the initial SOC of the EV arriving at the TS-PFCS for charging are both considered independent random variables.

6.4.4 Direct Approach for Load-Flow

Most PDNs are built in a radial structure with a low ratio of reactance to resistance. Traditional power-flow methods like Gauss-Seidel and Newton-Raphson are ineffective in these cases. Therefore, in this paper, a direct search-based approach for load-flow analysis is used [118]. This approach involves creating two matrices: one for BIBC and another for BCBV. By multiplying these matrices together, the DLF matrix is obtained, using which, the load-flow solution is determined efficiently [118].

6.4.5 Optimal Sizing and Siting of RBDG Units

It has been reported that [146] a proper selection of the active power output P_{DG} of the DG reduces the line currents, lowers resistive losses, and improves bus voltages. In this study, RBDGs are optimally allocated in the 240-bus PDN with EVCD to improve the PDN performance vis-à-vis the total Ohmic losses and the VD of the PDN. As discussed earlier in Chapter 5, either the total Ohmic losses or the voltage deviation of the 240-bus PDN can be considered as a single-objective function [140].

These individual objective functions are of the form as given in (5.16) and (5.17), respectively. In this work, a multi-objective function is envisaged by including both the objectives from (5.16) and (5.17), as (5.18), already discussed in section-5.5 of chapter5.

The values of both w_1 and w_2 are taken as 0.5 in this work. Thus, the decision variable is the active power output 'P_{DG}' of the DG, subject to the operational constraints discussed in section-5.5 of chapter 5.

The optimization focuses on determining the optimal P_{DG} values that minimize (5.18) while adhering to the operational constraints.

The preliminary selection for RBDG placement is done by selecting all the three-phase buses in the 240-bus PDN. The final selection to choose the most desirable locations amongst all the three-phase buses is carried out on the basis of LSF as given in (5.19) at section-5.5.1 of chapter 5.

Subsequently, the active power rating of the DGs at the buses deemed suitable for their placement is carried out using the DTBO algorithm as detailed in Chapter 5. The steps for the optimal allocation of RBDG units in the 240-bus PDN using DTBO is outlined in the flowchart shown in Fig. 6.6. It may be noted that the optimal DG allocation results pertain to the peak ND at 07:00 hours, as detailed in Section 6.5

6.5 Case Studies, Results and Discussions

Case I: Base case 24-hour demand and bus voltage magnitude profiles of the 240-bus PDN

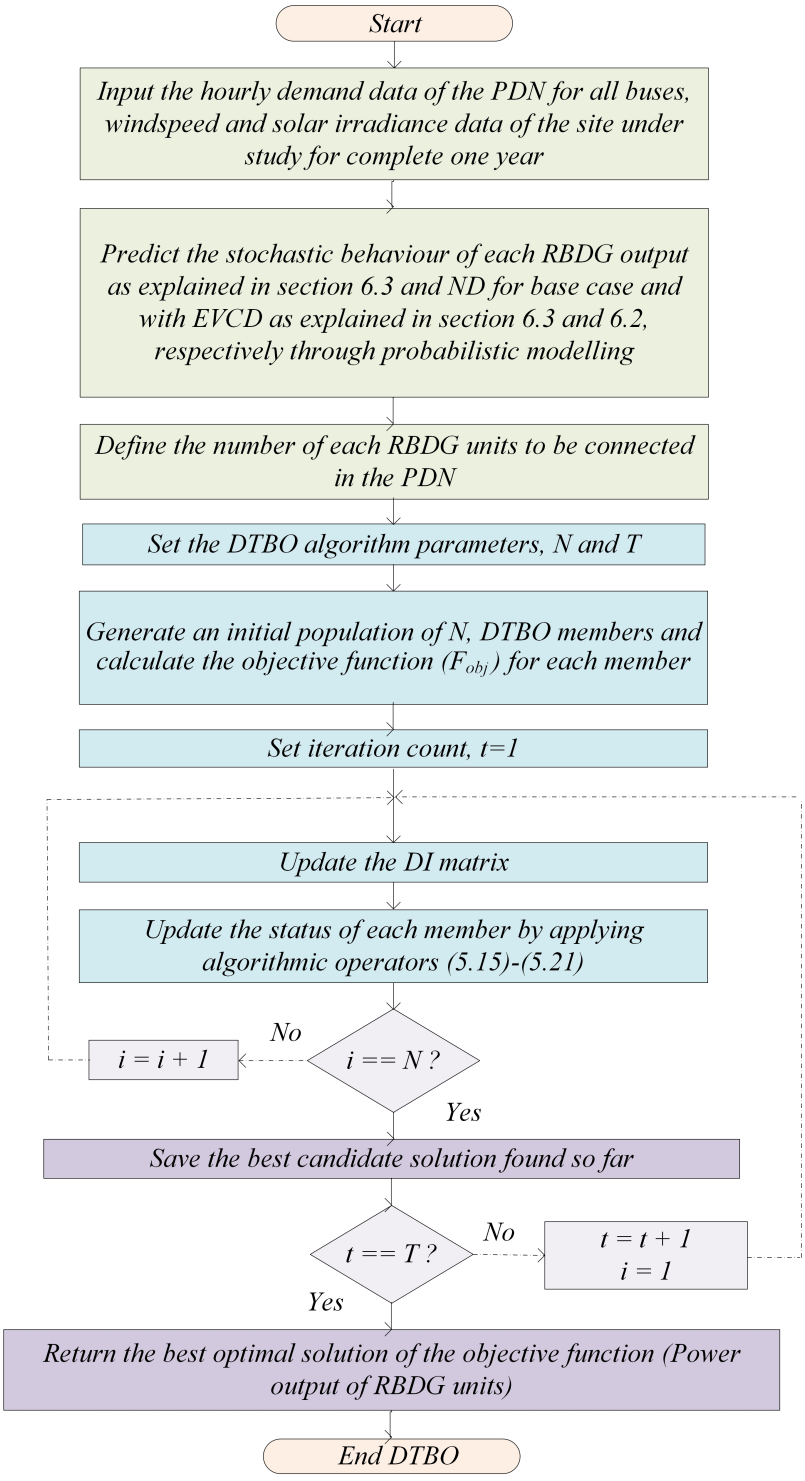


Fig. 6.6: Flowchart of the DTBO algorithm for optimal allocation of RBDGs

In this case study, the seasonal base case ND for the 240-bus PDN without EVCD is estimated using (6.14)–(6.17). It is stochastic in nature and is shown in Fig. 6.4. The PDN Ohmic losses and VD are 31.06 kW and 0.07 p.u., respectively (shown in rows 7 and 10, column 1, respectively, of Table 6.6). The corresponding bus voltage magnitude profiles for all the three phases (A, B and C) are shown in blue in Fig. 6.11. It pertains to the maximum TND occurring at 07:00 hours. From Fig. 6.11, it can be observed that buses located at the far ends of the feeder(s) have poorer voltage magnitude due to the radial structure of the PDN. Also, the bus voltage magnitude profiles for Phases A and C are slightly deteriorated as compared to Phase B.

Case II: 24-hour demand and bus voltage magnitude profiles of the 240-bus PDN with EV charging

In this case study, the effects of both slow residential and PFC of EVs on the performance of the 240-bus PDN is investigated. The case studies are carried out considering the charging of:

(i) 'At most two EVs per household'

(ii) '10% EV penetration', for residential and PFCs, respectively (x% EV penetration indicates that x% of all vehicles are EVs)

Fig. 6.7 illustrates the seasonal variations in the TND of the 240-bus PDN with EVCD. The PDN Ohmic losses and VD are now 112.76 kW and 0.412 p.u., respectively (shown in rows 7 and 10, column 2, respectively, of Table 6.7). It can be observed that with EVCD, both the PDN Ohmic losses and the VD have substantially increased, as compared to the base case values (31.06 kW and 0.07 p.u., respectively). The bus voltage magnitude profiles for all the three phases (A, B and C) with EVCD are shown in red in Fig. 6.11 (pertaining to the maximum TND occurring at 07:00 hours). From Fig. 6.11, it can be observed that with EVCD (red plot), the bus voltage magnitude profiles undergo marked deterioration as compared to the base case (blue plot), particularly for Phases A and C.

Selection of ratings and number of WT and SPV-based DGs

The total network demand of the 240-bus PDN with EVCD is shown in Fig. 6.7. The sizing of the WT and SPV-based DGs are carried out based on the mean of the

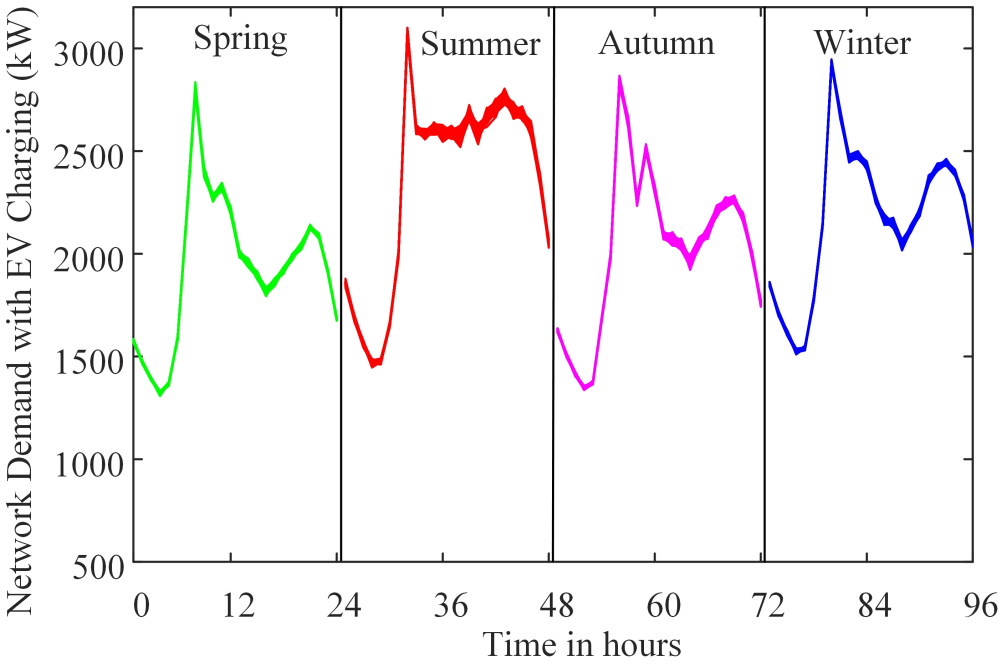


Fig. 6.7: Predicted network demand profiles with EV charging

above plot (not shown due to page limitations), wherein it is observed that for all four seasons, the peak TND (PTND) occur at 7:00 hours and 20:00 hours. This can be attributed to the peaks of the EV arrival time patterns at home and PFCSs, as shown in Fig. 3.5. Further, Fig. 6.8 depicts the normalized plots of the mean WT output (based on a single Vestas V39 WT of 500 kW capacity) and the mean SPV output (based on a single SILFAB SIL-500 HM SPV module of 500 W capacity). Table 6.3 details the values of the mean TND, the mean WT output and the mean SPV output at both 20:00 hours and 7:00 hours, for all four seasons [117].

Now, at 20:00 hours, SPV-based DGs are ineffective, while both SPV and WT-based DGs are available at 7:00 hours. Hence, the selection of WT-based DGs is considered first, based on the PTND at 20:00 hours. The selection of DGs is based on the assumption that 50% of the PTND is met by the DGs and the rest 50% by the power grid, as shown in Table 6.3. From Table 6.3 (row 7), it can be observed that at 20:00 hours, a maximum number of 10 WTs in summer and a minimum of 8 WTs in spring, are required. Thus, two cases are considered—(a) 10 WTs and (b) 8 WTs—each of 500 kW capacity, as detailed in row 8 of Table 6.3.

Subsequently, the number of SPV-based DGs are selected based on the PTND

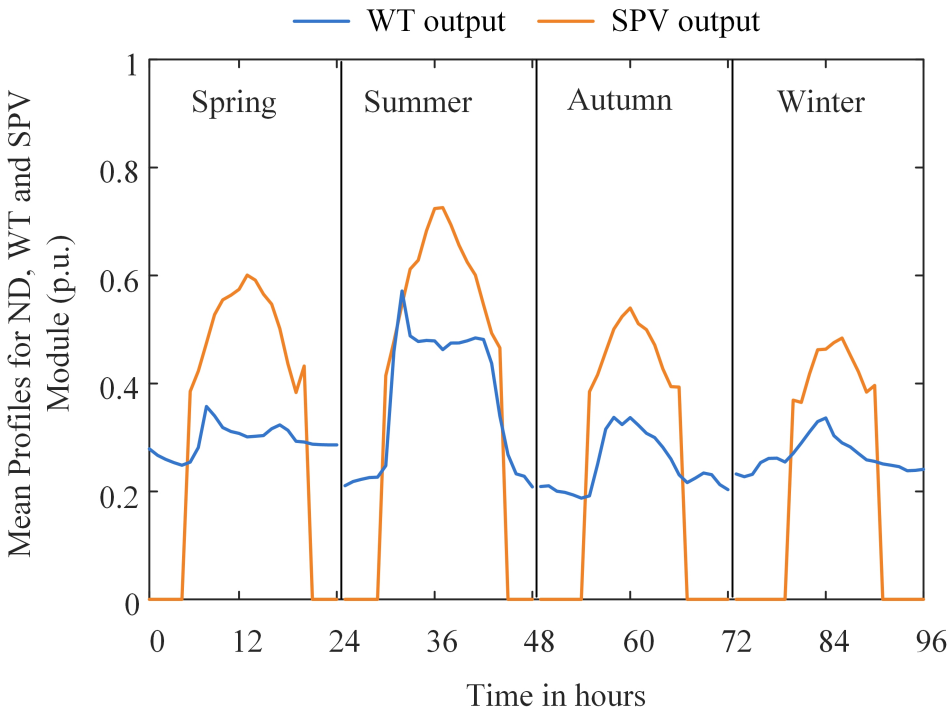


Fig. 6.8: Normalized mean output of a single WT and SPV module

occurring at 07:00 hours, when the SPV and the WT-based DGs together meet 50% of the PTND. The number of SPV modules is finally selected as 2000, as shown in rows 9–16 of Table 6.3. The fraction of the PTND as met by the DGs for cases (a) 8 WTs with 2000 SPV modules and (b) 10 WTs with 2000 SPV modules are shown in the last four rows of Table 6.3. Based on this, 8 WTs and 2 SPV panels (of 1000 modules each) are finally selected.

It may be noted for the above analysis that any surplus power from the RBDGs, after meeting the TND (including EVCD), will be injected into the power grid and is to be accounted for using the net metering principle. As such, any variation of the load demand on account of the EV load would be taken care of by the power grid.

Table 6.3: Selection of WT- and SPV-based DGs

Selection of number of WTs (each of 500 capacity)					
	Season	Spring	Summer	Autumn	Winter
	TND (kW)	2130	2680	2264	2444
20:00	50% TND	1065	1340	1132	1222
hrs	Each WT o/p (kW)	143.8	134	117.1	123
	SPV o/p (W)	—	—	—	—
	Required no of WT	7.41	10	9.67	9.94
No. of WTs considered: (a) 10 (b) 8					
Selection of number of SPV modules (each of 500 W capacity)					
	TND (kW)	2802	3076	2842	2930
	50% TND	1401	1538	1421	1465
	Each WT o/p (kW)	178.7	285.6	125.2	135.3
7:00	Total WT	(a) 1787	(a) 2856	(a) 1252	(a) 1353
hrs	o/p (kW)	(b) 1430	(b) 2285	(b) 1002	(b) 1082
	SPV o/p (W)	237.4	273	208	185
	No of SPV modules	(a) **	(a) **	(a) 813	(a) 606
	required	(b) **	(b) **	(b) 2015	(b) 2071
**** Only WT (without any SPV) sufficient to meet 50% of TND**					
% of TND met with (a) 10 WT with 2000 SPV modules and (b) 8 WT with 2000 SPV modules					
7:00	% of TND met by DG	Spring	Summer	Autumn	Winter
hrs	SPV+WT	(a) 80.7%	(a) 110.6%	(a) 58.7%	(a) 58.8%
		(b) 68%	(b) 92%	(b) 49.9%	(b) 49.6%
20:00	WT only	(a) 67.5%	(a) 50%	(a) 51.7%	(a) 50.3%
hrs		(b) 54%	(b) 40%	(b) 41.4%	(b) 40.3%
Hence, 8 WT and 2000 SPV modules (2 Panels of 1000 modules each) are finally selected.					

Case III:Optimal Allocation of DGs in 240-Bus PDN using DTBO

In this case study, subsequent to selection of the ratings and the number of WT and SPV-based DGs, the role of optimal DG allocation on the performance improvement of the 240-bus PDN with EVCD is investigated. which is lower than those achieved by COA and IGWO. This demonstrates that DTBO not only provides the best optimal solution among the tested algorithms but also ensures strong repeatability and robustness.

Further, a comparative analysis of the statistical performance of the three algorithms is summarized in Table. VII in terms of power loss minimization, voltage deviation and computational time. From Table 6.5, it is observed that as compared to COA and IGWO, DTBO achieved the lowest mean power loss (51.75 kW) with a very low standard deviation (0.0526), confirming its accuracy and stable convergence across runs. IGWO performed moderately, with a higher mean loss (56.00 kW) and noticeable variability, occasionally producing competitive results but also poor solutions (up to 60.84 kW). COA showed the least average performance (56.23 kW) with the largest variability, indicating low reliability, despite achieving a competitive best solution.

The optimal allocation of DGs is carried out using the DTBO algorithm. In this respect, Fig. 6.9 and 6.10 depict a comparison of the convergence characteristics (100 iterations) and the boxplot of the objective function values (30 runs) for the DTBO along with two recent optimization methods - COA and IGWO, respectively. To ensure a fair comparison of the computational performance of DTBO, IGWO, and COA, the algorithms were implemented and evaluated under the same computational conditions, including the population size (N = 30), stopping criterion/number of iterations (T = 100), and MATLAB implementation environment. The differences in computational time arise from the different mathematical operations and search mechanisms involved in the three algorithms. DTBO shows the fastest convergence and achieves the lowest objective function value (25.88) than both IGWO (26.22) and COA (26.29). The sub-plot in Fig. 6.9 presents a zoomed-in view of the convergence characteristics for iterations 65–100. For better visualization, Fig. 6.10 is used to depict a box-plot exclusively for the DTBO. It is observed that DTBO achieves the lowest objective function value with a very narrow spread, indicating that the algorithm consistently converges to nearly identical solutions across different trials. The

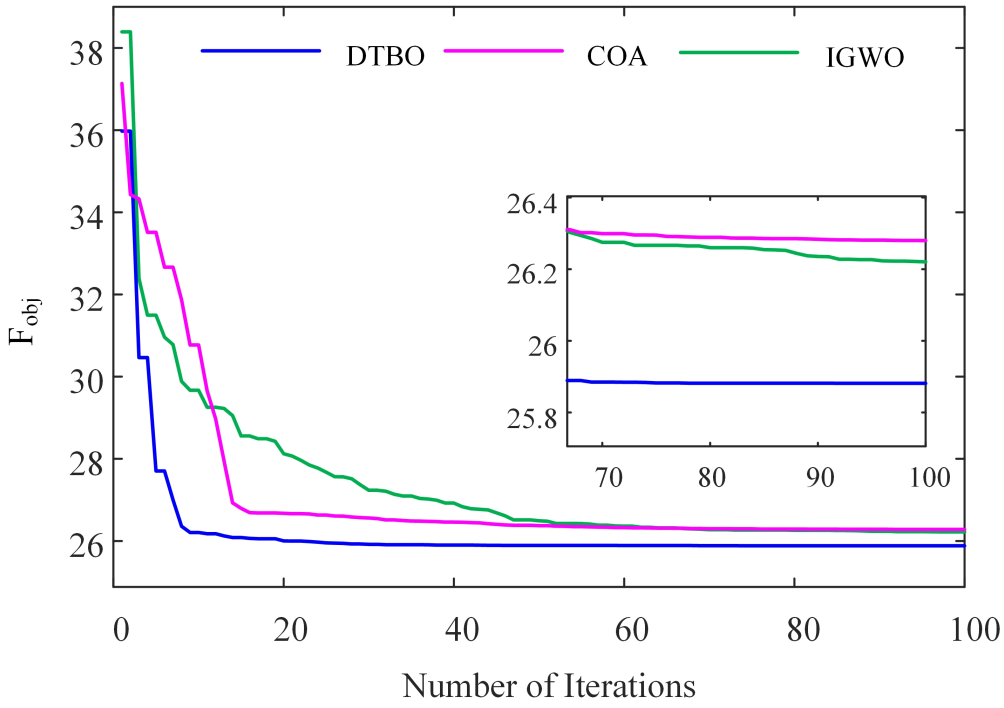


Fig. 6.9: Convergence characteristics of DTBO, COA and IGWO

median F_{obj} obtained by DTBO is 25.9311,

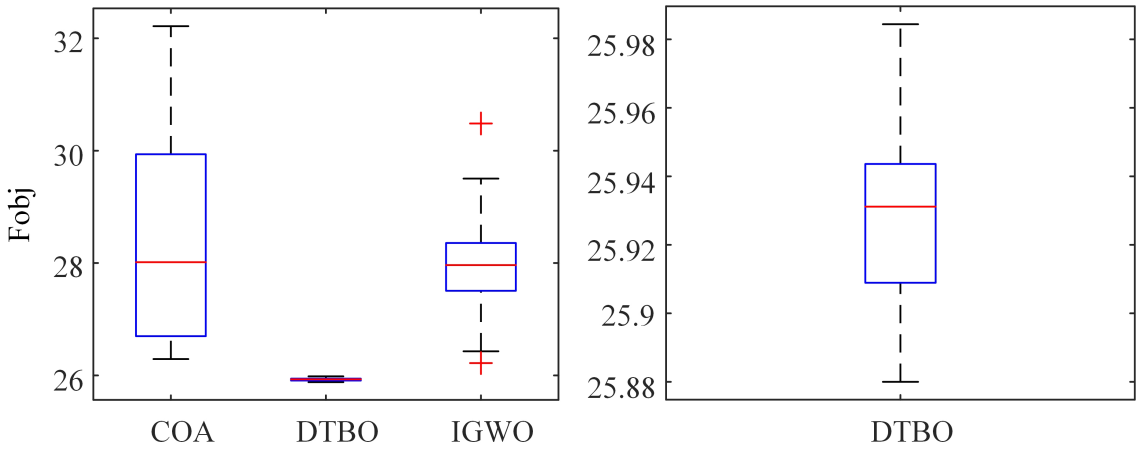


Fig. 6.10: Boxplot of the objective function value for 30-runs obtained with: (a) DTBO, COA and IGWO; and (b) DTBO.

Table 6.5: Results for the Statistical Performance of DTBO, IGWO and COA for 30 Runs

Parameters	Power Loss (kW)	Voltage Deviation (p.u)	Computational Time (sec)
DTBO			
Mean	51.75	0.1104	65.7372
Standard Deviation	0.0526	0.00096871	3.3999
Best Value	51.65	0.1084	58.5848
Worst Value	51.8573	0.1122	73.2906
IGWO			
Mean	56.00	0.1111	168.05
Standard Deviation	1.7889	0.0049	6.3305
Best Value	52.3255	0.1057	158.1296
Worst Value	60.8390	0.1281	189.4329
COA			
Mean	56.23	0.1129	227.1320
Standard Deviation	1.6541	0.0044	14.4382
Best Value	51.6505	0.1075	202.4652
Worst Value	64.3149	0.1229	256.4850

Table 6.7: Results of Multi-Objective Optimization Using DTBO

Bus No	3082	3079	3078	3075	3074
WT output (kW)	284.96	114.52	141.88	284.56	284.99
Bus No	3073	3072	3071	3055	3053
WT output (kW)	164.25	284.84	285.00	284.37	284.92
PDN Ohmic Losses					
Base Case	**With EV Charging without any DG**		**With EV Charging and with DG Allocation**		
31.06 kW	112.76 kW		51.65 kW (54.2% reduction)		
PDN Voltage Deviation					
Base Case	**With EV Charging without any DG**		**With EV Charging and with DG Allocation**		
0.07 p.u.	0.412 p.u.		0.11 p.u. (73.3% reduction)		

For voltage deviation study, DTBO again outperforms with the lowest mean deviation (0.1104 p.u.) and the smallest variance, while IGWO and COA exhibited higher deviations and instability. It is also observed that DTBO is the most computationally efficient (65.7 sec) method, outperforming both IGWO (168.05 sec) and COA (227.13 sec). Hence, DTBO is selected for the DG allocation process.

Subsequently, the DG active power outputs after optimal allocation of 10 RBDGs (8WTs and 2 SPV panels) in the 240-bus PDN using the DTBO algorithm are shown in Table 6.7. From Table 6.7, it is observed that for the base case, the PDN Ohmic loss is 31.06 kW, which increases to 112.76 kW with EVCD. However, after optimal allocation of DGs using DTBO algorithm, the corresponding PDN losses reduce to 51.65 kW (row 7, column 3), resulting in a 54.2% decrement. In a similar manner, it is observed that for the base case, the VD is 0.07 p.u., which increases to 0.412 p.u. with EVCD. However, after optimal allocation of DGs using DTBO algorithm, the corresponding VD reduces to 0.11 p.u. (row 10, column 3), resulting in a 73.3% decrement.

The bus voltage magnitude profiles for all the three phases (A, B and C) with

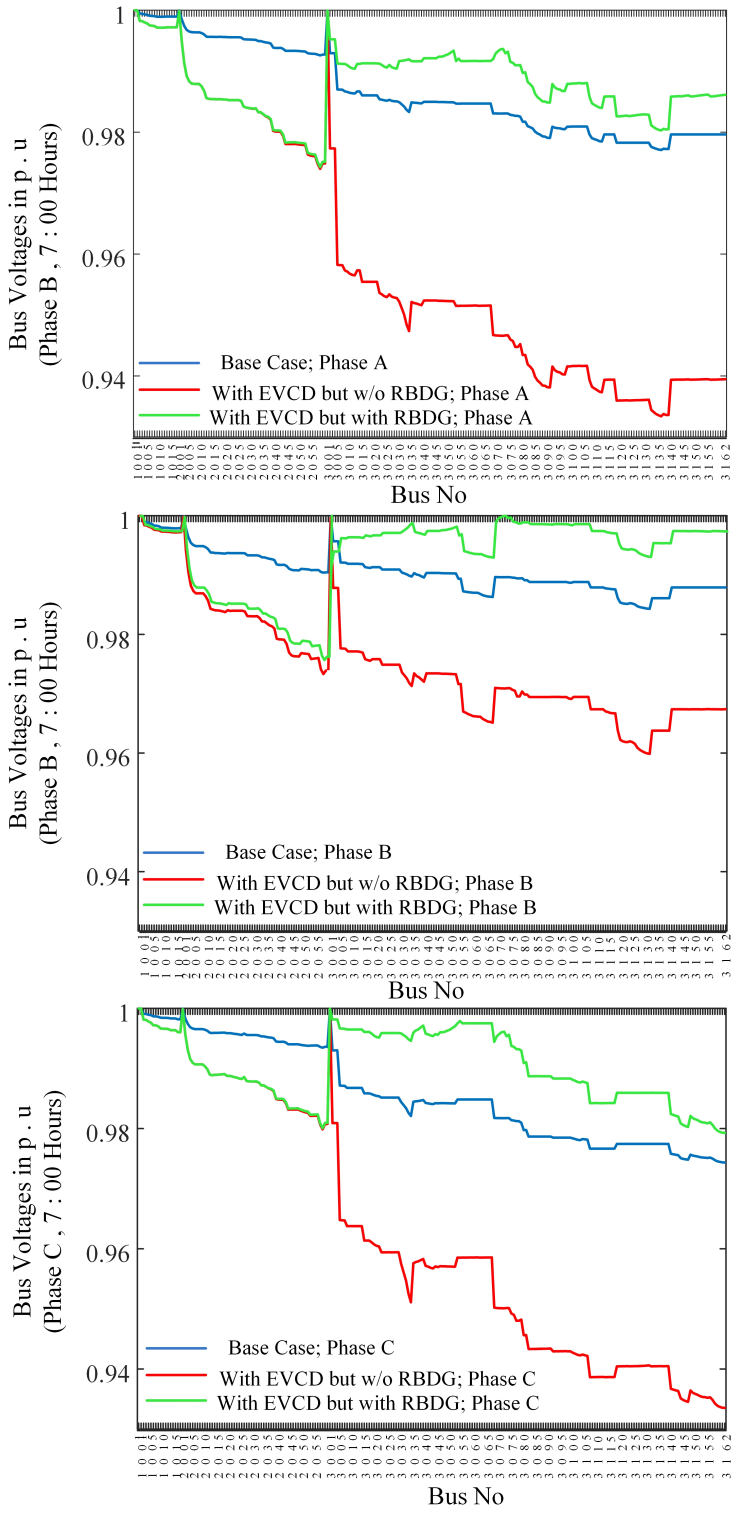


Fig. 6.11: Bus voltage profile for Phase A, B and C at 07:00 hours

both EVCD and optimal DG allocation are shown in green in Fig. 6.11 (pertaining to the maximum TND occurring at 07:00 hours). From Fig. 6.11, it can be observed that with optimal DG allocation, the bus voltage magnitude profiles (green plot) undergo substantial improvements as compared to that with EVCD but without any DG (red plot), particularly for Phases A and C. In fact, the bus voltage magnitude profiles with DG allocation (green plot) are even slightly better than the base case (blue plot). Also, for phase B, the bus voltage magnitude profile with DG allocation (green plot) is almost around 1.0 p.u and much better than phases A and C. This is because the bus voltage magnitude profile (with EVCD but without DG) of phase B (red plot) is better than that of phases A and C, leading to overcompensation by the three phase RBDGs, which results in the bus voltage magnitude profile of Phase B (green plot) being almost around 1.0 p.u.

6.6 Conclusions

1. This chapter presents a probabilistic planning framework for the optimal allocation of SPV and wind-based DG units to mitigate the adverse impacts of EVCD on a 240-bus PDN.

2. The EVCD estimation is modelled for both residential and PFC using real-world travel data such as EV type, trip distance, and timing from the 2017 NHTS.

3. The optimal siting and sizing of RBDG units are determined using the DTBO algorithm, incorporating uncertainties in solar irradiance and wind speed through probabilistic models, along with seasonal variability in renewable energy outputs. Solar and wind data are sourced from NASA, while WT and SPV specifications are taken from manufacturers' datasheets.

4. DTBO's performance in minimizing the PDN Ohmic losses and VDs is benchmarked against COA and IGWO, showing superior convergence speed and accuracy. The optimized RBDG deployment achieves 54% and 73% reductions in the PDN Ohmic losses and VDs, respectively. These

findings substantiate the efficacy and robustness of the proposed PDN planning methodology.

Chapter 7

Conclusions and Scope for Further Work

This chapter presents the overall conclusions derived from the research conducted in this thesis, along with its broader societal implications and potential directions for future work. The study focused on the comprehensive modeling and analysis of EV charging demand in PDNs, considering realistic charging behaviors, network operational constraints, and the growing penetration of EVs. Optimization techniques and probabilistic modeling approaches were employed to evaluate the impacts of EV integration and to develop effective mitigation strategies for maintaining system reliability and operational efficiency. The chapter first summarizes the major research findings related to EV charging demand modeling, its impacts on distribution network performance, and the effectiveness of coordinated charging policies and renewable-based DG planning. It then highlights the societal relevance of the research by discussing its alignment with global sustainability initiatives, particularly the United Nations Sustainable Development Goals (SDGs). Finally, the chapter outlines several potential research directions that can further enhance the planning, operation, and resilience of future EV-integrated power distribution networks.

7.1 Conclusions of the Research

This thesis comprehensively investigates the modeling, impact assessment, and mitigation of EVCD in PDNs using real-world data and advanced optimization

techniques. Slow and fast EV charging behaviors were accurately modeled using realistic travel patterns obtained from the 2017 NHTS and operational data from Fastned charging stations. The developed mathematical models effectively capture the temporal, stochastic, and unbalanced nature of EVCD, providing a robust foundation for power distribution network analysis.

The impact of EV charging was evaluated on a real-world 240-bus radial power distribution network located in the Midwest U.S. under multiple EV penetration scenarios. The results clearly indicate that slow residential charging significantly increases the network demand during noon and evening hours, while fast charging at PFCS causes sharp demand spikes during morning hours. Although slow charging results in comparatively smaller bus voltage magnitude dips, fast charging leads to severe voltage deviations due to its high-power and impulsive nature. Overall, EV charging distorts the daily load profile, increases system losses, and reduces bus voltage magnitude, highlighting the urgent need for effective charging coordination and network support mechanisms.

To address these challenges, SOC-based residential EV charging policies were proposed and evaluated by distributing EV loads across three phases of the PDN. The case studies demonstrate that the proposed charging policies significantly improve the daily load profile, reduce the system losses, and enhance bus voltage magnitude profiles. These findings confirm that intelligent charging strategies can play a critical role in alleviating the adverse impacts of large-scale EV integration without requiring extensive infrastructure upgrades.

Furthermore, the thesis investigates the application of DG as a mitigation measure for EV-induced network stress. A novel human-based metaheuristic optimization technique, the DTBO algorithm, was employed for the optimal allocation of wind-based DG units. The superiority of DTBO over widely used algorithms such as GA, PSO, IGWO, and TLBO was validated through benchmark mathematical functions and power system case studies. Under realistic EV penetration scenarios, optimal DG placement using DTBO achieved up to 45.65% reduction in network real power losses in the single-objective formulation and simultaneous reductions of approximately 45.62% in power losses and 64.71% in voltage deviation in the multi-objective formulation. In comparison, the DTBO algorithm-based DG allocation resulted in relatively superior performance, confirming the robustness and effectiveness of the

algorithm.

Finally, a probabilistic planning framework was developed for the optimal siting and sizing of SPV and wind-based DG units to mitigate the combined impacts of residential and public fast-charging EV demand. The framework incorporates uncertainties in the EV charging behavior, renewable energy generation, and seasonal variability using probabilistic models and real-world datasets from NASA and manufacturer specifications. The DTBO-based planning approach demonstrated superior convergence characteristics and solution quality compared to COA and IGWO. The optimized renewable-based DG deployment achieved reductions of approximately 54% in network Ohmic losses and 73% in voltage deviations, underscoring the effectiveness and resilience of the proposed planning methodology.

In summary, this thesis establishes that accurate EV charging demand modeling, coordinated charging policies, and optimally planned renewable-based distributed generation are essential for maintaining the operational reliability and efficiency of future power distribution networks with high EV penetration. The proposed methodologies provide a scalable and practical framework for utilities and planners to facilitate sustainable EV integration while minimizing adverse technical impacts on distribution systems.

7.2 Social Impact of Research

This research aligns with the global sustainability framework established by the United Nations through the SDGs. These goals provide a comprehensive roadmap for achieving sustainable development by addressing social, economic, and environmental challenges worldwide. The proposed research on optimal integration of renewable-based DG for EV charging in PDNs contributes to several SDGs by promoting cleaner energy systems, improving energy efficiency, and supporting sustainable urban development as outlined in Fig. 7.1.

1. **SDG 3: Good Health and Well-being:** The research contributes to 'Good Health and Well-being', by enabling cleaner electricity supply for EV charging through the optimal integration of renewable-based distributed generation in power distribution networks. Conventional electricity

generation often relies on fossil fuels, which produce greenhouse gases and harmful air pollutants that negatively affect human health. By reducing reliance on fossil-fuel-based electricity and improving overall energy efficiency, the proposed system helps reduce emissions associated with power generation. Consequently, the approach supports improved urban air quality and contributes to healthier living environments by lowering health risks related to air pollution.

2. **SDG 7: Affordable and Clean Energy:** The study strongly supports 'Affordable and Clean Energy', by enhancing the penetration of renewable energy sources in power distribution networks through the optimal allocation and sizing of distributed generation units. The proposed methodology improves voltage stability, minimizes power losses, and facilitates the efficient integration of EV charging demand into the grid. These improvements contribute to a reliable, sustainable, and cost-effective electricity supply while accelerating the transition from fossil-fuel-based energy systems to clean and renewable energy solutions.

3. **SDG 9: Industry, Innovation, and Infrastructure:** The research aligns with 'Industry, Innovation and Infrastructure', by introducing innovative planning strategies for modern power distribution networks facing increasing EV charging demand. The developed optimization framework enhances the operational efficiency and resilience of power infrastructure by enabling effective integration of renewable-based distributed energy resources. This contributes to the modernization of electricity networks and supports the development of smart, sustainable, and technologically advanced energy systems.

4. **SDG 11: Sustainable Cities and Communities:** The proposed work contributes to 'Sustainable Cities and Communities', by promoting the integration of renewable-powered EV charging infrastructure within urban electricity networks. Rapid urbanization and increasing transportation demand place significant stress on power systems and contribute to environmental degradation. By optimizing distributed generation placement and supporting cleaner transportation electrification, the study

helps reduce emissions associated with electricity generation while ensuring reliable energy services for urban mobility. This supports the development of environmentally sustainable and resilient cities.

5. **SDG 12: Responsible Consumption and Production:** The research supports 'Responsible Consumption and Production', by encouraging efficient utilization of energy resources within distribution networks. Through the proposed SOC and time-based EV charging policies and the optimal placement and sizing of renewable-based distributed generation units, the proposed framework reduces the network Ohmic losses and enhances the management of electricity demand for EV charging. This results in improved energy efficiency and promotes more sustainable patterns of electricity consumption within the power systems.

6. **SDG 13: Climate Action:** The study contributes to 'Climate Action', by facilitating low-carbon electricity supply for transportation electrification. The integration of renewable energy sources into distribution networks significantly reduces dependence on fossil-fuel-based power generation and lowers greenhouse gas emissions associated with EV charging infrastructure. By enabling a cleaner and more sustainable electricity supply, the proposed approach supports global climate mitigation efforts and contributes to the transition toward sustainable energy and transportation systems.

7.3 Scope for Further Work

Future research may consider the following directions to enhance the comprehensiveness and applicability of the complete study:

1. **Incorporation of DG investment cost, land availability, protection coordination, communication requirements, and utility/customer economics:** The present study primarily focuses on the technical assessment of EV charging impacts and optimal renewable-based DG allocation in terms of network power losses and voltage deviation.

However, several practical and economic aspects, including DG investment cost, land availability, protection coordination, reverse power flow, voltage-regulation equipment, communication requirements, and utility/customer economics, could be investigated as future research work.

2. **Use of conventional optimization techniques:** Future work may investigate deterministic mathematical optimization methods such as Mixed-Integer Nonlinear Programming (MINLP), Mixed-Integer Linear Programming (MILP), and Nonlinear Programming (NLP), for the planning and operation of EV-integrated distribution networks, enabling guaranteed optimality and systematic comparison with metaheuristic approaches in terms of solution quality, computational efficiency, scalability, and robustness under uncertainty.

3. **Integration of demand response and smart EV charging:** Future work can explore coordinated demand response and smart EV charging strategies to reshape load profiles, reduce peak PDN demand, and enhance system flexibility under high EV penetration.

4. **Assessment of grid power quality issues due to EVCD:** Further studies may analyze power quality impacts such as harmonics, voltage flicker, and phase imbalance introduced by large-scale EVCD, especially from fast-charging stations.

5. **Smart EV charging with dynamic time-of-use (TOU) tariffs:** Development of intelligent EV charging schemes linked with dynamic ToU and real-time pricing can encourage off-peak charging, improve economic efficiency, and support grid reliability.

6. **Inclusion of EV queuing and waiting time in EVCD analysis:** Incorporating EV queuing behavior and waiting times at public charging stations can improve the accuracy of EVCD modeling and support optimal charging infrastructure planning.



Fig. 7.1: Alignment of the Research with SDGs

List of Publications

Journal Publications

[1] Shefali Painuli, Suman Bhowmick, and Radheshyam Saha. Mitigation of the effects of electric vehicle charging on distribution networks by optimal allocation of distributed generation resources. *IEEE Transactions on Industrial Informatics*, 22(1):474–485, 2026. doi: 10.1109/TII.2025.3611697.

[2] Shefali Painuli, Divyanshu Khandelwal, Suman Bhowmick, and Radheshyam Saha. Effects of residential ev charging on power distribution networks and their mitigation by optimal allocation of wind-based dg resources. *Electric Power Systems Research, Elsevier*, 241:111395, 2025. ISSN 0378-7796. doi: https://doi.org/10.1016/j.epsr.2024.111395.

[3] Shefali Painuli, Suman Bhowmick, and Radheshyam Saha. Mitigation of residential ev charging effects on power distribution networks with optimal allocation of dgs using coati optimization. *Arabian Journal for Science and Engineering, Springer*, 50:10731–10750, 2025. doi: https://doi.org/10.1007/s13369-024-09782-0.

[4] Shefali Painuli, Suman Bhowmick, and Radheshyam Saha. Optimal allocation of distributed generation resources to alleviate the effects of slow residential and dc fast charging of electric vehicles on power distribution systems. *Sadhana, Springer*, (Under Review).

International Conference Publications

[1] Shefali Painuli, Suman Bhowmick, and Radheshyam Saha. A comprehensive analysis of the impacts of ev charging on a power distribution network. In *2025 IEEE 5th International Conference on Sustainable Energy and Future Electric Transportation (SEFET)*, pages 1–6, 2025. doi: 10.1109/SEFET65155.2025.11255184.

[2] Shefali Painuli, Suman Bhowmick, and Radheshyam Saha. Impact of residential phev charging on utility distribution networks and its mitigation. In *2023 IEEE International Conference on Power Electronics, Smart Grid, and Renewable Energy (PESGRE)*, pages 1–6, 2023. doi: 10.1109/PESGRE58662.2023.10405065.

[3] Divyanshu Khandelwal, Suman Bhowmick, Shefali Painuli, and Radheshyam Saha. A practical phev charging policy to improve performance of power distribution systems. In *2023 International Conference on Power, Instrumentation, Energy and Control (PIECON)*, pages 1–6, 2023. doi: 10.1109/PIECON56912.2023.10085850.

[4] Divyanshu Khandelwal, Shefali Painuli, Suman Bhowmick, and Radheshyam Saha. A comparison of practical electric vehicle charging policies to improve the performance of power distribution systems. In *2023 International Conference on Recent Advances in Electrical, Electronics Digital Healthcare Technologies (REEDCON)*, pages 7–12, 2023. doi: 10.1109/REEDCON57544.2023.10151097.

References

[1] Iowa State University, Department of Electrical and Computer Engineering. Test system website. [Online]. Accessed: Oct. 11, 2025. [Online]. Available: http://wzy.ece.iastate.edu/Testsystem.html

[2] S. Habib, M. M. Khan, F. Abbas, L. Sang, M. U. Shahid, and H. Tang, "A comprehensive study of implemented international standards, technical challenges, impacts and prospects for electric vehicles," *IEEE Access*, vol. 6, pp. 13 866–13 890, 2018.

[3] M. Yilmaz and P. T. Krein, "Review of battery charger topologies, charging power levels, and infrastructure for plug-in electric and hybrid vehicles," *IEEE Trans. on Power Electron.*, vol. 28, no. 5, pp. 2151–2169, May 2013.

[4] S. Schoenberg, D. S. Buse, and F. Dressler, "Siting and sizing charging infrastructure for electric vehicles with coordinated recharging," *IEEE Transactions on Intelligent Vehicles*, vol. 8, no. 2, pp. 1425–1438, February 2023.

[5] Tesla Motors Club LLC, "Tesla motors club," 2016, accessed 16 March 2016. [Online]. Available: https://teslamotorsclub.com/tmc/

[6] K. P. Schneider, B. A. Mather, B. C. Pal, C.-W. Ten, G. J. Shirek, H. Zhu, J. C. Fuller, J. L. R. Pereira, L. F. Ochoa, L. R. de Araujo, R. C. Dugan, S. Matthias, S. Paudyal, T. E. McDermott, and W. Kersting, "Analytic considerations and design basis for the ieee distribution test feeders," *IEEE Transactions on Power Systems*, vol. 33, no. 3, pp. 3181–3188, 2018.

[7] K. Ma, L. Fang, and W. Kong, "Review of distribution network phase unbalance: Scale, causes, consequences, solutions, and future research directions," *CSEE Journal of Power and Energy Systems*, vol. 6, no. 3, pp. 479–488, 2020.

[8] S. Shafiee, M. F. Firuzabad, and M. Rastegar, "Investigating the impacts of plug-in hybrid electric vehicles on power distribution systems," *IEEE Trans. Smart Grid*, vol. 4, no. 3, pp. 1351–1360, Sept 2013.

[9] "Vestas v39 turbine data," https://en.wind-turbine-models.com/turbines/383-vestas-v39, accessed 2025.

[10] "Silfab sil-500-hm data sheet," https://silfabsolar.com/wp-content/uploads/2024/04/Silfab-SIL-500-HM-Data-Generic-20231221.pdf, 2024.

[11] C. Ziras, M. Thingvad, T. Fog, G. Yousefi, and T. Weckesser, "An empirical analysis of electric vehicle charging behavior based on real danish residential charging data," *Electric Power Systems Research*, vol. 234, p. 110556, 2024.

[12] A. Srivastava, M. Manas, and R. K. Dubey, "Integration of power systems with electric vehicles: A comprehensive review of impact on power quality and relevant enhancements," *Electric Power Systems Research*, vol. 234, p. 110572, 2024.

[13] K. Gholami, S. Karimi, A. Rastgou, A. Nazari, and V. Moghaddam, "Voltage stability improvement of distribution networks using reactive power capability of electric vehicle charging stations," *Computers and Electrical Engineering*, vol. 116, p. 109160, 2024.

[14] M. M. Rahman, E. A. Al-Ammar, H. S. Das, and W. Ko, "Comprehensive impact analysis of electric vehicle charging scheduling on load-duration curve," *Computers & Electrical Engineering*, vol. 85, p. 106673, 2020.

[15] A. R. Battula and S. Vuddanti, "Distributed control strategy for secondary frequency regulation with ev demand aggregation and delay compensation in ac unbalanced microgrid," *Electric Power Systems Research*, vol. 225, 2023.

[16] A. Aljumah, A. Darwish, D. Csala, and P. Twigg, "A review on the allocation of sustainable distributed generators with electric vehicle charging stations," *Sustainability*, vol. 16, no. 15, 2024. [Online]. Available: https://www.mdpi.com/2071-1050/16/15/6353

[17] G. Alkawsi, Y. Baashar, U. Abbas, A. A. Alkahtani, and S. K. Tiong, "Toward efficient smart management: A review of modeling and optimization approaches in electric vehicle-transportation network-grid integration," *Energies*, vol. 16, no. 3, p. 1303, 2023.

[18] V. K. B. Ponnam and K. Swarnasri, "Planning of electric vehicle charging station with integration of renewables in distribution network," in *2021 7th International Conference on Electrical Energy Systems (ICEES)*. IEEE, 2021, pp. 452–457.

[19] C. H. Dharmakeerthi, N. Mithulananthan, and T. K. Saha, "A comprehensive planning framework for electric vehicle charging infrastructure deployment in the power grid with enhanced voltage stability," *International Transactions on Electrical Energy Systems*, vol. 25, no. 6, pp. 1022–1040, 2015. [Online]. Available: https://doi.org/10.1002/etep.1886

[20] H. Lotfi, "Optimal energy modeling and planning in the power system via a hybrid firefly and cuckoo algorithm in the presence of renewable energy sources and electric vehicles," *Journal of Ambient Intelligence and Humanized Computing*, vol. 14, pp. 11 749–11 768, 2023.

[21] L. Galván, J. C. López, S. Martínez, I. Isaac, and J. W. González, "A new methodology for the optimal charging coordination of electric vehicles considering vehicle-to-grid technology," *IEEE Latin America Transactions*, vol. 18, no. 01, pp. 73–81, 2020.

[22] S. K. Injeti and V. K. Thunuguntla, "Optimal integration of DGs into radial distribution network in the presence of plug-in electric vehicles to minimize daily active power losses and to improve the voltage profile of the system using bioinspired optimization algorithms," *Protection and Control of Modern Power Systems*, vol. 5, no. 1, pp. 1–15, 2020.

[23] R. Ebadi, A. Ghaffari, and N. Ghadimi, "Optimal placement and sizing of plug in electric vehicles charging stations within distribution networks with high penetration of photovoltaic panels," *Journal of Ambient Intelligence and Humanized Computing*, vol. 11, pp. 5621–5634, 2020.

[24] M. Nour, J. P. Chaves, and A. Sanchez-Miralles, "Impact of electric vehicles charging on urban residential power distribution networks," *Applied Sciences*, vol. 10, no. 12, p. 4303, 2020.

[25] H. Yuan, J. Huang, W. Zhang, and K. Zhang, "Active distribution system reinforcement planning with EV charging stations—Part I: Uncertainty modeling and problem formulation," *IEEE Transactions on Transportation Electrification*, vol. 7, no. 1, pp. 73–84, 2021.

[26] A. A. Shehata, C. Ghenai, M. E. Nassar, and A. Abd El Satar, "Robust distributed generation investment accommodating electric vehicle charging in a distribution network," *IEEE Access*, vol. 9, pp. 131 238–131 252, 2021.

[27] A. Amer, M. A. Azzouz, A. Azab, and A. S. A. Awad, "Stochastic planning for optimal allocation of fast charging stations and wind-based dgs," *IEEE Systems Journal*, vol. 15, no. 3, pp. 4589–4599, 2021. [Online]. Available: https://doi.org/10.1109/JSYST.2020.3012939

[28] S. R. Dash, S. Mishra, A. Y. Abdelaziz, J. Hong, and Z. W. Geem, "Grasshopper optimization algorithm based two stage fuzzy multiobjective approach for optimum sizing and placement of distributed generations, shunt capacitors and electric vehicle charging stations," *Energies*, vol. 15, no. 13, p. 4551, 2022.

[29] Y. He, Z. Liu, and C. Gu, "Stochastic energy management of electric bus charging stations with renewable energy integration and B2G capabilities," *IEEE Transactions on Intelligent Transportation Systems*, vol. 22, no. 10, pp. 6563–6573, 2021.

[30] R. Sharma and S. Prakash, "Intelligent electric vehicle charging optimization and horse herd-inspired power generation for enhanced energy management," *Scientific Reports*, vol. 14, no. 1, p. 2451, 2024.

[31] G. A. Abiassaf and A. A. Arkadan, "Impact of ev charging, charging speed, and strategy on the distribution grid: A case study," *IEEE Journal of Emerging and Selected Topics in Industrial Electronics*, vol. 2, no. 4, pp. 531–542, 2024. [Online]. Available: https://ieeexplore.ieee.org/document/10387566

[32] N. B. G. Brinkel, W. L. Schram, T. A. AlSkaif, I. Lampropoulos, and W. G. J. H. M. van Sark, "Simulating the impacts of uncontrolled electric vehicle charging in low voltage grids," in *2020 IEEE 17th International Conference on the European Energy Market (EEM)*. IEEE, 2020, pp. 1–6.

[33] M. Nour, A. Ali, and C. Farkas, "Impact of electric vehicles on low-voltage residential distribution networks: A probabilistic analysis," *International Journal of Energy Research*, vol. 44, no. 12, pp. 9566–9588, 2020.

[34] A. Perez-Diaz, F. Barreras, and E. Schaltz, "Distribution planning with hourly profiles for analysing electric vehicle charging strategies," *Electric Power Systems Research*, vol. 190, p. 106646, 2021.

[35] K. Qian, C. Zhou, M. Allan, and Y. Yuan, "Modeling of load demand due to ev battery charging in distribution systems," *IEEE Transactions on Power Systems*, vol. 26, no. 2, pp. 802–810, 2011. [Online]. Available: https://doi.org/10.1109/TPWRS.2010.2057456

[36] S. Deb, K. Kalita, and P. Mahanta, "PEVs modeling and impacts mitigation in distribution networks," *International Transactions on Electrical Energy Systems*, vol. 31, no. 1, p. e12689, 2021.

[37] M. Muthusamy, S. Ravishankar, S. Kumar, and K. R. Salkuti, "Impact assessment of high-power domestic EV charging proliferation of a distribution network," *International Journal of Power Electronics and Drive Systems (IJPEDS)*, vol. 12, no. 2, pp. 1089–1098, 2021.

[38] S. S. Amiri, S. Jadid, and H. Saboori, "Stochastic optimal sizing of plug-in electric vehicle parking lots in reconfigurable power distribution systems," *Electric Power Systems Research*, vol. 181, p. 106176, 2020.

[39] R. Asghar, F. Rehman, Z. Ullah, A. Qamar, K. Ullah, K. S. Abdul-Kadir, and N. M. Sahar, "Energy consumption and grid interaction analysis of electric vehicles based on particle swarm optimisation method," *Energies*, vol. 14, no. 20, p. 6541, 2021.

[40] S. Vuddanti and K. R. Salkuti, "Stochastic modelling and integration of electric vehicles in the distribution system using the jaya algorithm,"

International Journal of Renewable Energy Research (IJRER), vol. 10, no. 1, pp. 270–277, 2020.

[41] Y. Saleem, M. Al-Saffar, A. Al-Saffar, and A. Al-Obaidi, "A dynamic optimal scheduling strategy for multi-charging scenarios of plug-in-electric vehicles over a smart grid," *International Journal of Integrated Engineering*, vol. 13, no. 4, pp. 253–264, 2021.

[42] T. Rawat, J. Singh, V. C. Pandey, and S. Sharma, "Planning renewables in distribution system with electric vehicles to improve hosting capacity and energy losses: Two-stage stochastic optimization framework," *Sustainable Energy, Grids and Networks*, vol. 39, p. 101445, 2024. [Online]. Available: https://doi.org/10.1016/j.segan.2024.101445

[43] G. A. Abiassaf and A. A. Arkadan, "Impact of ev charging, charging speed, and strategy on the distribution grid: A case study," *IEEE Journal of Emerging and Selected Topics in Industrial Electronics*, vol. 5, no. 2, pp. 531–542, April 2024.

[44] J. ao Soares, B. Canizes, M. A. F. Ghazvini, Z. Vale, and G. K. Venayagamoorthy, "Two-stage stochastic model using benders' decomposition for large-scale energy resource management in smart grids," *IEEE Transactions on Industry Applications*, vol. 53, no. 6, pp. 5905–5914, 2017. [Online]. Available: https://doi.org/10.1109/TIA.2017.2723339

[45] K. Qian, C. Zhou, A. Malcolm, and Y. Yuan, "Load model for prediction of electric vehicle charging demand," *IEEE Transactions on Power Systems*, vol. 26, pp. 802–810, 2011.

[46] T. Yuvaraj, N. Prabaharan, C. John De Britto, M. Thirumalai, M. Salem, and M. A. Nazari, "Dynamic optimization and placement of renewable generators and compensators to mitigate electric vehicle charging station impacts using the spotted hyena optimization algorithm," *Sustainability*, vol. 16, no. 19, 2024. [Online]. Available: https://www.mdpi.com/2071-1050/16/19/8458

[47] M. Bilal, S. Gupta, P. N. Bokoro, and G. Sharma, "A probabilistic approach for optimal integration of evs and res using artificial hummingbird algorithm in distribution network," *IET Renewable Power Generation*, vol. 18, no. 14, pp.

2305–2325, 2024. [Online]. Available: https://ietresearch.onlinelibrary.wiley.com/doi/abs/10.1049/rpg2.13074

[48] M. Alizadeh, A. M. Amani, L. Meegahapola, M. Jalili, and O. Hill, "Optimal integration of ev charging stations into distribution network planning and operation," *IEEE Transactions on Industrial Informatics*, vol. 21, no. 9, pp. 7120–7130, 2025.

[49] M. Farjamipur, H. Lotfi, and M. H. Nikkhah, "Simultaneous optimal allocation of EVCSs and RESs using an improved genetic method," *IET Circuits, Devices & Systems*, vol. 18, no. 1, pp. 12–25, 2024.

[50] L. Bagherzadeh and I. Kamwa, "Joint multi-objective allocation of parking lots and DERs in active distribution network considering demand response programs," *Energies*, vol. 16, no. 23, p. 7805, 2023.

[51] S. P. R. Polisetty, R. Jayanthi, and M. Sai Veerraju, "An intelligent optimal charging stations placement on the grid system for the electric vehicle application," *Energy*, vol. 285, p. 129500, 2023.

[52] V. K. B. Ponnam and K. Swarnasri, "Multi-objective optimal allocation of electric vehicle charging stations and distributed generators in radial distribution systems using metaheuristic optimization algorithms," *Engineering, Technology & Applied Science Research*, vol. 10, no. 3, pp. 5837–5844, 2020.

[53] G. Battapothula, C. Yammani, and S. Maheswarapu, "Multi-objective simultaneous optimal planning of electrical vehicle fast charging stations and dgs in distribution system," *Journal of Modern Power Systems and Clean Energy*, vol. 7, no. 4, pp. 923–934, 2019.

[54] D. Mendoza-Grisales, O. D. Montoya, L. F. Grisales-Noreña, and J. C. Hernández, "Simultaneous distributed generation and electric vehicles hosting capacity assessment in electric distribution systems," *IEEE Access*, vol. 9, pp. 109 341–109 356, 2021.

[55] A. Fathy and A. Y. Abdelaziz, "Optimal DG sizing and location in modern power grids using PEVs load demand probability," *Electric Power Components and Systems*, vol. 48, no. 11, pp. 1141–1155, 2020.

[56] E. Shahrabi, H. Abdi, M. Jalali, and N. Ghadimi, "Smart utilization of renewable energy sources in a microgrid system integrated with plug-in hybrid electric vehicles," *International Journal of Energy Research*, vol. 45, no. 11, pp. 16 362–16 379, 2021.

[57] S. Singh, P. Chauhan, and N. Singh, "Cost-benefit analysis of V2G implementation in distribution networks considering PEVs battery degradation," *International Transactions on Electrical Energy Systems*, vol. 31, no. 11, p. e13103, 2021.

[58] C. D. Korkas, S. Baldi, I. Michailidis, and E. B. Kosmatopoulos, "Grid-aware energy management system for distribution grids based on a co-simulation approach," *IEEE Transactions on Control Systems Technology*, vol. 28, no. 5, pp. 1811–1824, 2020.

[59] E. L. Karfopoulos and N. D. Hatziargyriou, "Integration of distributed generation and plug-in electric vehicles on power distribution system by using queuing theory," *IEEE Transactions on Power Systems*, vol. 35, no. 1, pp. 321–330, 2020.

[60] S. Deb, K. Kalita, and P. Mahanta, "Smart charging strategies for optimal integration of plug-in electric vehicles within existing distribution system infrastructure," *IEEE Access*, vol. 9, pp. 114 321–114 335, 2021.

[61] G. Battapothula, C. Yammani, and S. Maheswarapu, "EV charging stations and RES-based DG: a centralized approach for smart integration in active distribution grids," *Journal of Electrical Engineering & Technology*, vol. 16, pp. 1245–1256, 2021.

[62] M. J. Moghaddam, A. Kalam, S. A. T. Nowdeh, and A. Ahmadi, "Optimal temporal-spatial PEV charging scheduling in active power distribution networks," *International Journal of Electrical Power & Energy Systems*, vol. 114, p. 105395, 2020.

[63] Y. Zheng, D. W. Gao, and L. Lin, "Distributed coordination of EV charging with renewable energy in a microgrid of buildings," *IEEE Transactions on Smart Grid*, vol. 12, no. 3, pp. 2239–2248, 2021.

[64] A. H. El-Metwaly, A. A. El-Desouky, and A. A. Sallam, "An adaptive approach for PEVs charging management and reconfiguration of electrical distribution system penetrated by renewables," *IEEE Access*, vol. 10, pp. 56 781–56 795, 2022.

[65] M. Moncecchi, C. Brivio, and M. Merlo, "Assessment of the technical impacts of electric vehicle penetration in distribution networks: A focus on system management strategies integrating sustainable local energy communities," *Energies*, vol. 15, no. 1, p. 321, 2022.

[66] I. Alotaibi, A. Malik, M. Malik, and N. Ghadimi, "Placement and capacity of EV charging stations by considering uncertainties with energy management strategies," *Journal of Ambient Intelligence and Humanized Computing*, vol. 12, pp. 1–16, 2021.

[67] A. Ali, I. Shayea, M. Ergen, and M. Nour, "Effective deterministic methodology for enhanced distribution network performance and plug-in electric vehicles," *IEEE Access*, vol. 10, pp. 25 121–25 134, 2022.

[68] S. Gao, J. Wu, and B. Xu, "Controllability evaluation of ev charging infrastructure transformed from gas stations in distribution networks with renewables," *Energies*, vol. 12, no. 8, 2019. [Online]. Available: https://www.mdpi.com/1996-1073/12/8/1577

[69] S. Shetty, "Impact of pev charging loads on distribution system operations and optimal siting and sizing of pev charging stations," Master of Applied Science, University of Waterloo, Waterloo, Ontario, Canada, 2015. [Online]. Available: https://core.ac.uk/download/pdf/144148906.pdf

[70] J. Wen, W. Gan, C.-C. Chu, L. Jiang, and J. Luo, "Robust resilience enhancement by ev charging infrastructure planning in coupled power distribution and transportation systems," *IEEE Transactions on Smart Grid*, vol. 16, no. 1, pp. 491–504, 2025.

[71] A. Tariq, S. A. A. Kazmi, G. Ali, and A. H. U. Bhatti, "Multivariate stochastic modeling of plugin electric vehicles charging profile and grid impact analysis," *Sustainable Energy, Grids and Networks*, vol. 36, p. 101155, 2023. [Online]. Available: https://www.sciencedirect.com/science/article/pii/S2352467723001637

[72] K. N. Hasan, K. M. Muttaqi, P. Borboa, J. Scira, Z. Zhang, and M. thew Leishman, "Distribution network voltage analysis with data-driven electric vehicle load profiles," *Sustainable Energy, Grids and Networks*, vol. 36, p. 101216, 2023. [Online]. Available: https://www.sciencedirect.com/science/article/pii/S2352467723002242

[73] W. Gan, J. Wen, M. Yan, Y. Zhou, and W. Yao, "Enhancing resilience with electric vehicles charging redispatching and vehicle-to-grid in traffic-electric networks," *IEEE Transactions on Industry Applications*, vol. 60, no. 1, pp. 953–965, 2024.

[74] Z. Xi, G. Guo, X. Yang, J. Sun, X. Shi, and X. Xiao, "Forecasting and managing urban ev charging demand with spatiotemporal graph models," *Journal of Renewable and Sustainable Energy*, vol. 17, no. 1, p. 015502, January 2025. [Online]. Available: https://doi.org/10.1063/5.0244546

[75] S. Deb, K. Tammi, K. Kalita, and P. Mahanta, "Impact of electric vehicle charging station load on distribution network," *Energies*, vol. 11, no. 1, 2018. [Online]. Available: https://www.mdpi.com/1996-1073/11/1/178

[76] S. Habib, M. M. Khan, F. Abbas, M. Numan, Y. Ali, H. Tang, and X. Yan, "A framework for stochastic estimation of electric vehicle charging behavior for risk assessment of distri-bution networks," *Frontiers in Energy*, vol. 14, no. 2, pp. 298–317, June 2020. [Online]. Available: https://doi.org/10.1007/s11708-019-0648-5

[77] S. Rahman, I. A. Khan, A. A. Khan, A. Mallik, and M. F. Nadeem, "Comprehensive review impact analysis of integrating projected electric vehicle charging load to the exist-ing low voltage distribution system," *Renewable and Sustainable Energy Reviews*, vol. 153, p. 111756, 2022.

[Online]. Available: https://www.sciencedirect.com/science/article/pii/S1364032121010273

[78] D. L. Donaldson, M. S. Alvarez-Alvarado, and D. Jayaweera, "Integration of electric vehicle evacuation in power system resilience assessment," *IEEE Transactions on Power Systems*, vol. 38, no. 4, pp. 3085–3096, July 2023.

[79] M. Z. Zeb, K. Imran, A. Khattak, A. K. Janjua, A. Pal, M. Nadeem, J. Zhang, and S. Khan, "Optimal placement of electric vehicle charging stations in the active distribution network," *IEEE Access*, vol. 8, pp. 68 124–68 134, 2020.

[80] A. Ali, M. F. Shaaban, A. S. A. Awad, M. A. Azzouz, M. Lehtonen, and K. Mahmoud, "Multi-objective allocation of ev charging stations and ress in distribution systems considering ad-vanced control schemes," *IEEE Transactions on Vehicular Technology*, vol. 72, no. 3, pp. 3146–3160, March 2023.

[81] F. Yao, J. Wang, F. Wen, C.-L. Tseng, X. Zhao, and Q. Wang, "An integrated planning strategy for a power network and the charging infrastructure of electric vehicles for power system resilience enhancement," *Energies*, vol. 12, no. 20, 2019. [Online]. Available: https://www.mdpi.com/1996-1073/12/20/3918

[82] E. Ucer, M. C. Kisacikoglu, and M. Yuksel, "Decentralized additive increase and multiplicative decrease-based electric vehicle charging," *IEEE Systems Journal*, vol. 15, no. 3, pp. 4272–4280, 2021.

[83] S. Baghali, Z. Guo, W. Wei, and M. Shahidehpour, "Electric vehicles for distribution system load pickup under stressed conditions: A network equilibrium approach," *IEEE Transactions on Power Systems*, vol. 38, no. 3, pp. 2304–2317, May 2023.

[84] J. de Hoog, V. Muenzel, D. C. Jayasuriya, T. Alpcan, M. Brazil, D. A. Thomas, I. Mareels, G. Dahlenburg, and R. Jegatheesan, "The importance of spatial distribution when analysing the impact of electric vehicles on voltage stability in distribution networks," *Energy Systems*, vol. 6, no. 1, pp. 63–84, March 2025. [Online]. Available: https://doi.org/10.1007/s12667-014-0122-8

[85] D. Chippada and M. D. Reddy, "Optimal planning of electric vehicle charging station along with multiple distributed generator units," *International Journal of Intelligent Systems and Applications (IJISA)*, vol. 14, no. 2, pp. 40–53, April 2022. [Online]. Available: https://doi.org/10.5815/ijisa.2022.02.04

[86] T. Yuvaraj, K. R. Devabalaji, J. A. Kumar, S. B. Thanikanti, and N. I. Nwulu, "A comprehensive review and analysis of the allocation of electric vehicle charging stations in distribu-tion networks," *IEEE Access*, vol. 12, pp. 5404–5461, 2024.

[87] G. Pedda and P. S. Raju, "Optimal placement of dg in the radial distribution system for mitigating the impact of ev charging sta-tions," in *2021 IEEE Bombay Section Signature Conference (IBSSC)*, 2021, pp. 1–6.

[88] B. Zhou, G. Chen, T. Huang, Q. Song, and Y. Yuan, "Planning pev fast-charging stations using data-driven distributionally robust optimization approach based on -divergence," *IEEE Transactions on Transportation Electrification*, vol. 6, no. 1, pp. 170–180, 2020.

[89] C. Cao, L. Wang, and B. Chen, "Mitigation of the impact of high plug-in electric vehicle penetration on residential distribution grid us-ing smart charging strategies," *Energies*, vol. 9, no. 12, 2016. [Online]. Available: https://www.mdpi.com/1996-1073/9/12/1024

[90] Y. Jiang, T. Ortmeyer, and M. Fan, "Data-driven fast uncertainty assessment of distribution systems with correlated ev charging demand and renewable generation," *IEEE Transactions on Sustainable Energy*, vol. 14, no. 3, pp. 1446–1456, July 2023.

[91] S. S., S. T., P. N., and G. C., "Charging station sizing and placement for ev docking station in smart grid," *International Journal of Energy Research*, vol. 2025, p. 9520314, 2025, 19 pages. [Online]. Available: https://doi.org/10.1155/er/9520314

[92] F. Ahmad, A. Iqbal, I. Asharf, M. Marzband, and I. Khan, "Placement and capacity of ev charging stations by considering uncertainties with energy

management strategies," *IEEE Transactions on Industry Applications*, vol. 59, no. 3, pp. 3865–3874, May 2023.

[93] J. Singh and R. Tiwari, "Impact analysis of different charging models for optimal integration of plug-in electric vehicles in distribu-tion system," *The Journal of Engineering*, vol. 2019, no. 18, pp. 4728–4733, 2019. [Online]. Available: https://ietresearch.onlinelibrary.wiley.com/doi/abs/10.1049/joe.2018.9374

[94] O. Hafez and K. Bhattacharya, "Integrating ev charging stations as smart loads for demand response provisions in distribution sys-tems," *IEEE Transactions on Smart Grid*, vol. 9, no. 2, pp. 1096–1106, March 2018.

[95] J.-H. Kim and C.-H. Kim, "Demand power with ev charging schemes considering actual data," *Journal of International Council on Electrical Engineering*, vol. 6, no. 1, pp. 235–241, 2016. [Online]. Available: https://doi.org/10.1080/22348972.2016.1254080

[96] G. J. Osório, M. Shafie-khah, P. D. L. Coimbra, M. Lotfi, and J. P. S. Catalão, "Distribution system operation with electric vehicle charging schedules and renewable energy re-sources," *Energies*, vol. 11, no. 11, 2018. [Online]. Available: https://www.mdpi.com/1996-1073/11/11/3117

[97] E. Kianmehr, S. Nikkhah, V. Vahidinasab, D. Giaouris, and P. C. Taylor, "A resilience-based architecture for joint distributed energy resources allocation and hourly network reconfiguration," *IEEE Transactions on Industrial Informatics*, vol. 15, no. 10, pp. 5444–5455, Oct 2019.

[98] A. Chaouachi, E. Bompard, G. Fulli, M. Masera, M. De Gen-naro, and E. Paffumi, "Assessment framework for ev and pv synergies in emerging distribution systems," *Renewable and Sustainable Energy Reviews*, vol. 55, pp. 719–728, 2016. [Online]. Available: https://www.sciencedirect.com/science/article/pii/S1364032115010631

[99] S. Abazari and A. Khalili, "Charge management of electric vehicles in grids with distributed generation (dg) systems for reducing grid peak and improvement in its technical parameters," *Indian Journal of*

Science and Technology, vol. 9, no. 7, pp. 1–8, 2016. [Online]. Available: http://dx.doi.org/10.17485/ijst/2016/v9i7/87860

[100] T. U. Solanke, P. K. Khatua, V. K. Ramachandaramurthy, J. Y. Yong, and K. M. Tan, "Control and management of a multilevel electric vehicles infrastructure integrated with distributed re-sources: A comprehensive review," *Renewable and Sustainable Energy Reviews*, vol. 144, p. 111020, 2021. [Online]. Available: https://www.sciencedirect.com/science/article/pii/S1364032121003105

[101] S. Gao, K. T. Chau, C. Liu, D. Wu, and C. C. Chan, "Integrated energy management of plug-in electric vehicles in power grid with renewables," *IEEE Transactions on Vehicular Technology*, vol. 63, no. 7, pp. 3019–3027, Sep. 2014.

[102] F. Cazzato, M. Di Clerico, M. C. Falvo, S. Ferrero, and M. Vivian, "New dispatching paradigm in power systems including ev charging stations and dispersed genera-tion: A real test case," *Energies*, vol. 13, no. 4, 2020. [Online]. Available: https://www.mdpi.com/1996-1073/13/4/944

[103] M. Oliinyk, J. Džmura, M. Kolcun *et al.*, "Impact of electric vehicles and demand management systems on electrical distribution networks," *Electrical Engineering (Electr Eng)*, vol. 104, pp. 667–680, 2022. [Online]. Available: https://doi.org/10.1007/s00202-021-01327-0

[104] A. Zahedmanesh, K. M. Muttaqi, and D. Sutanto, "A cooperative energy management in a virtual energy hub of an electric transportation system powered by pv generation and energy storage," *IEEE Transactions on Transportation Electrification*, vol. 7, no. 3, pp. 1123–1133, Sep. 2021.

[105] B. Wang, P. Dehghanian, and D. Zhao, "Coordinated planning of electric vehicle charging infrastructure and renewables in power grids," *IEEE Open Access Journal of Power and Energy*, vol. 10, pp. 233–244, 2023.

[106] S. Alyami, "Ensuring sustainable grid stability through effective ev charging management: A time and energy-based approach," *Sustainability*, vol. 16, no. 14, 2024. [Online]. Available: https://www.mdpi.com/2071-1050/16/14/6149

[107] S. Deb, A. K. Goswami, P. Harsh, J. P. Sahoo, R.-h. L. Chetri, R. Roy, and A. S. Shekhawat, "Charging coordination of plug-in electric vehicle for congestion management in distribution system inte-grated with renewable energy sources," *IEEE Transactions on Industry Applications*, vol. 56, no. 5, pp. 5452–5462, 2020.

[108] M. Ahmadigorji and M. Mehrasa, "A robust renewable energy source-oriented strategy for smart charging of plug-in electric vehicles considering diverse uncertainty resources," *International Journal of Engineering. Transactions A: Basics*, vol. 36, no. 4, pp. 693–702, January 2023. [Online]. Available: https://doi.org/10.5829/ije.2023.36.04a.10

[109] B. Chatuanramtharnghaka, S. Deb, K. R. Singh, T. S. Ustun, and A. Kalam, "Reviewing demand response for energy management with consideration of renewable energy sources and electric vehicles," *World Electric Vehicle Journal*, vol. 15, no. 9, 2024. [Online]. Available: https://www.mdpi.com/2032-6653/15/9/412

[110] P. H. Hoang, G. Ozkan, P. R. Badr, B. Papari, C.-t. S. Edrington, M. A. Zehir, B. Hayes, L. Mehigan, D. A. Kez, and A. M. Foley, "A dual distributed optimal energy management method for distribution grids with electric vehicles," *IEEE Transactions on Intelligent Transportation Systems*, vol. 23, no. 8, pp. 13 666–13 677, 2022.

[111] A. I. Aygun, M. S. Hasan, A. Joshi, and S. Kamalasadan, "An optimal hybrid management of electric vehicle fleet charging and load scheduling in active electric distribution system," *IEEE Transactions on Industry Applications*, vol. 60, no. 4, pp. 5304–5316, 2024.

[112] J. Ibrahimov, T. Aliyev, I. Marufov, and N. Mammadov, "A solution to renewable energy source integration challenges: integrating electric vehicles into distribution networks," *Przegląd Elektrotechniczny*, vol. 100, no. 9, 2024, rocznik 2024 - zeszyt 9. [Online]. Available: https://doi.org/10.15199/48.2024.09.08

[113] S. Chen, Z. Guo, Z. Yang, Y. Xu, and R. S. Cheng, "A game theoretic approach to phase balancing by plug-in electric vehicles in the smart grid," *IEEE Transactions on Power Systems*, vol. 35, no. 3, pp. 2232–2244, 2020.

[114] M. Neaimeh, S. D. Salisbury, G. A. Hill, P. T. Blythe, D. R. Scoffield, and J. E. Francfort, "Analysing the usage and evidencing the importance of fast chargers for the adoption of battery electric vehicles," *Energy Policy*, vol. 108, pp. 474–486, 2017. [Online]. Available: https://www.sciencedirect.com/science/article/pii/S0301421517303877

[115] M. K. Gray and W. G. Morsi, "Power quality assessment in distribution systems embedded with plug-in hybrid and battery electric vehicles," *IEEE Trans. Power Syst.*, vol. 30, no. 2, pp. 663–671, Mar 2015.

[116] T. S. Bryden, A. J. Cruden, G. Hilton, B. H. Dimitrov, C. P. de León, and A. Mortimer, "Off-vehicle energy store selection for high-rate ev charging station," in *6th Hybrid and Electric Vehicles Conference (HEVC 2016)*, London, UK, 2016, pp. 1–9.

[117] "National household travel survey," online. Available: http://nhts.ornl.gov.

[118] J.-H. Teng, "A direct approach for distribution system load flow solutions," *IEEE Trans. on Power Delivery*, vol. 18, no. 3, pp. 882–887, Jul 2003.

[119] A. Dubey and S. Santoso, "Electric vehicle charging on residential distribution systems: Impacts and mitigations," *IEEE Access*, vol. 3, pp. 1871–1893, 2015.

[120] "Mesonet iowa state university data," online. Available: https://mesonet.agron.iastate.edu/request/download.phtml.

[121] M. Dehghani, E. Trojovská, and P. Trojovský, "A new human-based metaheuristic algorithm for solving optimization problems on the base of simulation of driving training process," *Sci Rep*, vol. 12, p. 9924, 2022.

[122] X. Yao, Y. Liu, and G. Lin, "Evolutionary programming made faster," *IEEE Trans. Evol. Comput.*, vol. 3, pp. 82–102, 1999.

[123] X. D. et al., "A charging pricing strategy of electric vehicle fast charging stations for the voltage control of electricity distribution networks," *Applied Energy*, vol. 225, pp. 857–868, 2018.

[124] J. Mutale, G. Strbac, S. Curcic, and N. Jenkins, "Allocation of losses in distribution systems with embedded generation," *Proc. Inst. Elect. Eng., Gen. Transm. Dist.*, vol. 147, no. 1, Jan 2000.

[125] V. H. M. Quezada, J. R. Abbad, and T. G. S. Roman, "Assessment of energy distribution losses for increasing penetration of distributed generation," *IEEE Trans. on Power Systems*, vol. 21, no. 2, pp. 533–540, May 2006.

[126] L. F. Ochoa and G. P. Harrison, "Minimizing energy losses: Optimal accommodation and smart operation of renewable distributed generation," *IEEE Trans. Power Syst.*, vol. 26, no. 1, pp. 198–205, Feb 2011.

[127] Z. Liu, F. Wen, and G. Ledwich, "Optimal siting and sizing of distributed generators in distribution systems considering uncertainties," *IEEE Trans. on Power Delivery*, vol. 26, no. 4, pp. 2541–2551, Oct 2011.

[128] A. E. Feijoo, J. Cidras, and J. L. G. Dornelas, "Wind speed simulation in wind farms for steady-state security assessment of electrical power systems," *IEEE Trans. on Energy Conversion*, vol. 14, no. 4, pp. 1582–1588.

[129] G. M. Masters, *Renewable and Efficient Electric Power Systems*. John Wiley & Sons, Inc, 2004, accessed: July 28, 2004.

[130] W. C. Wong and C. Y. Chung, "Coordinated damping control design for dfig-based wind generation considering power output variation," *IEEE Trans. on Power Systems*, vol. 27, no. 4, pp. 1916–1925, Nov 2012.

[131] "Hummer h25.0-100kw wind turbine models," online. Available: https://en.wind-turbine-models.com/turbines/1682-hummer-h25.0-100kwmodels.

[132] "Wind turbines: Bigger and better," online. Available: https://www.energy.gov/eere/articles/wind-turbines-bigger-better.

[133] T. Nagata, K. Yamada, K. Nakai, Y. Saito, and T. Nonomura, "Randomized group-greedy method for large-scale sensor selection problems," *IEEE Sensors Journal*, vol. 23, no. 9, pp. 9536–9548, May 1 2023.

[134] K. Deb, A. Pratap, S. Agarwal, and T. Meyarivan, "A fast and elitist multiobjective genetic algorithm: Nsga-ii," *IEEE Trans. on Evolutionary Computation*, vol. 6, no. 2, pp. 182–197, Apr 2002.

[135] J. H. Holland, *Adaptation in Nature and Artificial Systems*. MIT Press, 1992.

[136] J. S. Wang and S. X. Li, "An improved grey wolf optimizer based on differential evolution and elimination mechanism," *Sci Rep*, vol. 9, p. 7181, 2019.

[137] J. Kennedy and R. Eberhart, "Particle swarm optimization," in *Proceedings of ICNN'95 - International Conference on Neural Networks*, vol. 4, Perth, WA, Australia, 1995, pp. 1942–1948.

[138] R. V. Rao, V. J. Savsani, and D. P. Vakharia, "Teaching–learning-based optimization: An optimization method for continuous non-linear large-scale problems," *Inf. Sci.*, vol. 183, no. 1, pp. 1–15, 2012.

[139] M. Emmanuel, R. Rayudu, and I. Welch, "Grid incremental capacity evaluation with an optimally deployed photovoltaic system in distribution network," in *2017 IEEE Power & Energy Society General Meeting*, Chicago, IL, USA, 2017, pp. 1–5.

[140] R. S. Rao, K. Ravindra, K. Satish, and S. V. L. Narasimham, "Power loss minimization in distribution system using network reconfiguration in the presence of distributed generation," *IEEE Trans. on Power Systems*, vol. 28, no. 1, pp. 317–325, Feb 2013.

[141] M. Khani, R. Ghazi, and B. Nazari, "An unsupervised learning based mcdm approach for optimal placement of fault indicators in distribution networks," *Engineering Applications of Artificial Intelligence*, vol. 125, p. 106751, 2023.

[142] T. S. Haque, A. Chakraborty, S. P. Mondal, and S. Alam, "Approach to solve multi-criteria group decision-making problems by exponential operational

law in generalised spherical fuzzy environment," *CAAI Transactions on Intelligence Technology*, vol. 5, no. 2, pp. 106–114, 2020. [Online]. Available: https://ietresearch.onlinelibrary.wiley.com/doi/abs/10.1049/trit.2019.0078

[143] K. Prakash and M. Sydulu, "Particle swarm optimization based capacitor placement on radial distribution systems," in *2007 IEEE Power Engineering Society General Meeting*, Tampa, FL, USA, 2007, pp. 1–5.

[144] "Nasa power data access viewer," https://power.larc.nasa.gov/data-access-viewer/, accessed 2025.

[145] J. Radosavljević, N. Arsić, M. Milovanović, and A. Ktena, "Optimal placement and sizing of renewable distributed generation using hybrid metaheuristic algorithm," *Journal of Modern Power Systems and Clean Energy*, vol. 8, no. 3, pp. 499–510, May 2020.

[146] S. R. Ghatak, S. Sannigrahi, and P. Acharjee, "Multiobjective framework for optimal integration of solar energy source in three-phase unbalanced distribution network," *IEEE Transactions on Industry Applications*, vol. 56, no. 3, pp. 3068–3078, May-June 2020.

Appendix A

Data for 240-Bus Power Distribution Network

Table A.1: Line Segment Data for Feeder A

Name	Bus A	Bus B	Length(ft.)	Phases	Config.
L_1001_1002	1001	1002	2967	ABC	UG_3p_type1
L_1002_1003	1002	1003	372	ABC	UG_3p_type2
L_1002_1004	1002	1004	638	ABC	OH_3p_type1
L_1004_1005	1004	1005	394	ABC	OH_3p_type1
L_1005_1006	1005	1006	1049	ABC	OH_3p_type1
L_1006_1007	1006	1007	2000	AB	OH_2p_type2
L_1006_1008	1006	1008	454	ABC	OH_3p_type1
L_1008_1009	1008	1009	1082	ABC	OH_3p_type1
L_1009_1010	1009	1010	169	ABC	OH_3p_type1
L_1009_1011	1009	1011	60	ABC	UG_3p_type2
L_1011_1012	1011	1012	60	ABC	UG_3p_type2
L_1012_1013	1012	1013	306	ABC	UG_3p_type2
L_1013_1014	1013	1014	208	B	UG_1p_type2
L_1014_1015	1014	1015	126	B	UG_1p_type2
L_1013_1016	1013	1016	468	C	UG_1p_type2
L_1016_1017	1016	1017	71	C	UG_1p_type2

Table A.2: Line Segment Data for Feeder B

Name	Bus A	Bus B	Length(ft.)	Phase	Config.
L_2001_2002	2001	2002	1388	ABC	UG_3p_type1
L_2002_2003	2002	2003	1281	ABC	OH_3p_type1
L_2003_2004	2003	2004	798	ABC	OH_3p_type1
L_2004_2005	2004	2005	317	ABC	OH_3p_type1
L_2005_2006	2005	2006	145	ABC	OH_3p_type1
L_2006_2007	2006	2007	245	A	OH_1p_type5
L_2007_2008	2007	2008	125	A	UG_1p_type2
L_2007_2009	2007	2009	161	A	OH_1p_type2
L_2006_2010	2006	2010	170	ABC	OH_3p_type1
L_2010_2011	2010	2011	275	ABC	OH_3p_type1
L_2011_2012	2011	2012	503	ABC	OH_3p_type1
L_2013_2014	2013	2014	268	ABC	OH_3p_type1
L_2014_2015	2014	2015	120	B	UG_1p_type2
L_2014_2016	2014	2016	257	ABC	OH_3p_type1
L_2016_2017	2016	2017	174	ABC	UG_3p_type2
L_2017_2018	2017	2018	447	ABC	UG_3p_type2
L_2013_2019	2013	2019	45	ABC	OH_3p_type1
L_2019_2020	2019	2020	642	B	UG_1p_type2
L_2019_2021	2019	2021	43	ABC	OH_3p_type1
L_2021_2022	2021	2022	205	C	UG_1p_type2
L_2022_2023	2022	2023	150	C	UG_1p_type2
L_2023_2024	2023	2024	408	C	UG_1p_type2
L_2024_2025	2024	2025	331	C	UG_1p_type2
L_2026_2027	2026	2027	369	ABC	OH_3p_type1
L_2027_2028	2027	2028	285	ABC	UG_3p_type2
L_2028_2029	2028	2029	131	ABC	UG_3p_type2
L_2029_2030	2029	2030	165	ABC	UG_3p_type2
L_2030_2031	2030	2031	245	ABC	UG_3p_type2
L_2027_2032	2027	2032	149	ABC	OH_3p_type1
L_2032_2033	2032	2033	289	ABC	OH_3p_type1
L_2033_2034	2033	2034	185	ABC	OH_3p_type5

Table A.2: Line Segment Data for Feeder B

Name	Bus A	Bus B	Length(ft.)	Phase	Config.
L_2033_2035	2033	2035	160	ABC	OH_3p_type1
L_2035_2036	2035	2036	160	ABC	OH_3p_type1
L_2036_2037	2036	2037	80	ABC	OH_3p_type1
L_2037_2038	2037	2038	192	ABC	OH_3p_type1
L_2038_2039	2038	2039	800	ABC	OH_3p_type1
L_2039_2040	2039	2040	309	ABC	OH_3p_type1
L_2040_2041	2040	2041	383	ABC	OH_3p_type1
L_2039_2042	2039	2042	35	ABC	UG_3p_type2
L_2042_2043	2042	2043	158	ABC	UG_3p_type2
L_2043_2044	2043	2044	342	ABC	UG_3p_type2
L_2044_2045	2044	2045	323	B	UG_1p_type2
L_2045_2046	2045	2046	330	B	UG_1p_type2
L_2045_2047	2045	2047	189	B	UG_1p_type2
L_2047_2048	2047	2048	259	B	UG_1p_type2
L_2044_2049	2044	2049	130	ABC	UG_3p_type2
L_2049_2050	2049	2050	124	ABC	UG_3p_type2
L_2050_2051	2050	2051	139	ABC	UG_3p_type2
L_2051_2052	2051	2052	134	ABC	UG_3p_type2
L_2044_2053	2044	2053	464	ABC	UG_3p_type2
L_2053_2054	2053	2054	139	ABC	UG_3p_type2
L_2054_2055	2054	2055	156	ABC	UG_3p_type2
L_2055_2056	2055	2056	204	ABC	UG_3p_type2
L_2053_2057	2053	2057	761	ABC	UG_3p_type2
L_2057_2058	2057	2058	407	ABC	UG_3p_type2
L_2057_2059	2057	2059	685	ABC	UG_3p_type2
L_2059_2060	2059	2060	304	ABC	UG_3p_type2

A.1 Feeder C: Line Segment Data

Table A.3: Line Segment Data for Feeder C

Name	Bus A	Bus B	Length (ft.)	Phase	Config.
L_3001_3003	3001	3003	2307	ABC	UG_3p_type1
L_3003_3002	3003	3002	85	ABC	UG_3p_type2
L_3003_3004	3003	3004	81	ABC	UG_3p_type2
L_3003_3005	3003	3005	1997	ABC	UG_3p_type1
L_3005_3006	3005	3006	311	ABC	OH_3p_type1
L_3006_3007	3006	3007	370	ABC	OH_3p_type1
L_3005_3008	3005	3008	136	ABC	OH_3p_type1
L_3008_3009	3008	3009	161	A	OH_1p_type5
L_3009_3010	3009	3010	347	A	OH_1p_type5
L_3010_3011	3010	3011	265	A	OH_1p_type5
L_3011_3012	3011	3012	312	A	OH_1p_type5
L_3008_3013	3008	3013	170	B	OH_1p_type5
L_3013_3014	3013	3014	295	B	OH_1p_type5
L_3008_3015	3008	3015	322	ABC	OH_3p_type1
L_3015_3016	3015	3016	210	B	OH_1p_type5
L_3016_3017	3016	3017	259	B	OH_1p_type5
L_3015_3018	3015	3018	181	C	OH_1p_type5
L_3018_3019	3018	3019	281	C	OH_1p_type5
L_3019_3020	3019	3020	307	C	OH_1p_type5
L_3020_3021	3020	3021	303	C	OH_1p_type5
L_3015_3022	3015	3022	289	ABC	OH_3p_type1
L_3022_3023	3022	3023	181	A	OH_1p_type5
L_3023_3024	3023	3024	320	A	OH_1p_type5
L_3024_3025	3024	3025	331	A	OH_1p_type5
L_3022_3026	3022	3026	164	A	OH_1p_type5
L_3026_3027	3026	3027	368	A	OH_1p_type5
L_3027_3028	3027	3028	241	A	OH_1p_type5
L_3028_3029	3028	3029	317	A	OH_1p_type5
L_3022_3030	3022	3030	304	ABC	OH_3p_type1
L_3030_3035	3030	3035	103	ABC	OH_3p_type1
L_3035_3036	3035	3036	271	ABC	OH_3p_type1

Table A.3: Line Segment Data for Feeder C

Name	Bus A	Bus B	Length (ft.)	Phase	Config.
L_3036_3037	3036	3037	136	ABC	OH_3p_type1
L_3037_3038	3037	3038	252	ABC	OH_3p_type1
L_3038_3039	3038	3039	235	ABC	OH_3p_type1
L_3039_3053	3039	3053	263	ABC	OH_3p_type1
L_3053_3054	3053	3054	280	ABC	UG_3p_type2
L_3053_3055	3053	3055	1335	B	UG_1p_type2
L_3030_3040	3030	3040	332	ABC	OH_3p_type1
L_3040_3046	3040	3046	329	ABC	OH_3p_type1
L_3050_3051	3050	3051	360	ABC	OH_3p_type1
L_3082_3092	3082	3092	185	ABC	UG_3p_type2
L_3107_3118	3107	3118	2267	ABC	UG_3p_type1
L_3108_3109	3108	3109	136	A	UG_1p_type1
L_3109_3110	3109	3110	152	A	UG_1p_type2
L_3110_3111	3110	3111	276	A	UG_1p_type2
L_3111_3112	3111	3112	328	A	UG_1p_type2
L_3107_3113	3107	3113	245	B	UG_1p_type2
L_3113_3114	3113	3114	149	B	UG_3p_type2
L_3114_3115	3114	3115	331	B	UG_1p_type2
L_3113_3116	3113	3116	456	B	UG_1p_type2
L_3116_3117	3116	3117	112	B	UG_1p_type2
L_3118_3119	3118	3119	464	B	UG_1p_type2
L_3119_3120	3119	3120	350	B	UG_1p_type2
L_3120_3121	3120	3121	206	B	UG_1p_type2
L_3121_3122	3121	3122	177	B	UG_1p_type2
L_3119_3123	3119	3123	91	B	UG_1p_type2
L_3123_3124	3123	3124	67	B	UG_1p_type2
L_3124_3125	3124	3125	151	B	UG_1p_type2
L_3125_3126	3125	3126	343	B	UG_1p_type2
L_3126_3127	3126	3127	234	B	UG_1p_type2
L_3127_3128	3127	3128	238	B	UG_1p_type2
L_3128_3129	3128	3129	243	B	UG_1p_type2

Table A.3: Line Segment Data for Feeder C

Name	Bus A	Bus B	Length (ft.)	Phase	Config.
L_3129_3130	3129	3130	230	B	UG_1p_type2
L_3130_3131	3130	3131	194	B	UG_1p_type2
L_3118_3132	3118	3132	501	A	UG_1p_type2
L_3132_3133	3132	3133	145	A	UG_1p_type2
L_3133_3134	3133	3134	281	A	UG_1p_type2
L_3134_3135	3134	3135	240	A	UG_1p_type2
L_3135_3136	3135	3136	367	A	UG_1p_type2
L_3133_3137	3133	3137	252	A	UG_1p_type2
L_3137_3138	3137	3138	351	A	UG_1p_type2
L_3138_3139	3138	3139	289	A	UG_1p_type2
L_3107_3140	3107	3140	255	C	UG_1p_type2
L_3140_3141	3140	3141	134	C	UG_1p_type2
L_3141_3142	3141	3142	193	C	UG_1p_type2
L_3142_3143	3142	3143	202	C	UG_1p_type2
L_3140_3148	3140	3148	147	C	UG_1p_type2
L_3148_3149	3148	3149	253	C	UG_1p_type2
L_3149_3150	3149	3150	139	C	UG_1p_type2
L_3150_3151	3150	3151	156	C	UG_1p_type2
L_3151_3152	3151	3152	260	C	UG_1p_type2
L_3152_3153	3152	3153	139	C	UG_1p_type2
L_3153_3154	3153	3154	119	C	UG_1p_type2
L_3154_3155	3154	3155	505	C	UG_1p_type2
L_3140_3156	3140	3156	319	C	UG_1p_type2
L_3156_3144	3156	3144	122	C	UG_1p_type2
L_3144_3145	3144	3145	178	C	UG_1p_type2
L_3145_3146	3145	3146	178	C	UG_1p_type2
L_3146_3147	3146	3147	178	C	UG_1p_type2
L_3156_3157	3156	3157	153	C	UG_1p_type2
L_3157_3158	3157	3158	295	C	UG_1p_type2
L_3158_3159	3158	3159	257	C	UG_1p_type2
L_3159_3160	3159	3160	243	C	UG_1p_type2

Table A.3: Line Segment Data for Feeder C

Name	Bus A	Bus B	Length (ft.)	Phase	Config.
L_3160_3161	3160	3161	237	C	UG_1p_type2
L_3161_3162	3161	3162	176	C	UG_1p_type2

Table A.4: Circuit Breaker Data for 240-Bus Test System

Name	Bus A	Bus B	R_1	R_0	X_1	X_0	C_1	C_0	Status
CB_101	bus1	bus1001	0.0001	0.0001	0	0	0	0	Closed
CB_102	bus1010	bus2057	0.0001	0.0001	0	0	0	0	Open
CB_201	bus1	bus2001	0.0001	0.0001	0	0	0	0	Closed
CB_202	bus2012	bus2013	0.0001	0.0001	0	0	0	0	Closed
CB_203	bus2021	bus2026	0.0001	0.0001	0	0	0	0	Closed
CB_204	bus2013	bus3005	0.0001	0.0001	0	0	0	0	Open
CB_301	bus1	bus3001	0.0001	0.0001	0	0	0	0	Closed
CB_302	bus3075	bus3076	0.0001	0.0001	0	0	0	0	Closed
CB_303	bus3081	bus2016	0.0001	0.0001	0	0	0	0	Open

Table A.6: Three-Phase Shunt Capacitor Bank

Name	Bus	kV Rating	Connection	kVAr	Status
CAP_201	bus2038	13.8	Y–Grd.	50	Closed
CAP_301	bus3079	13.8	Y–Grd.	50	Closed

Table A.7: Equivalent Voltage Source

Nom. Volt.	p.u.	Angle (°)	R_1 (Ω)	X_1 (Ω)	R_0 (Ω)	X_0 (Ω)
69 kV	1	0	4.5426	10.5274	7.3655	24.5046

A.2 Secondary Distribution Transformers

Table A.9: Tap Changer Settings

Parameter	Sub_Reg. A	Sub_Reg. B	Sub_Reg. C
kVA rating	3500	3500	3500
Phase	A	B	C
Bus A	bus_Xfmr	bus_Xfmr	bus_Xfmr
Bus B	bus1	bus1	bus1
Connection	Grd–Wye	Grd–Wye	Grd–Wye
Monitoring bus	Bus 1, Ph. A	Bus 1, Ph. B	Bus 1, Ph. C
Primary voltage (kV)	7.9677	7.9677	7.9677
Secondary voltage (kV)	7.9677	7.9677	7.9677
PT ratio	66.3953	66.3953	66.3953
Voltage setting (V)	123	123	123
Voltage bandwidth (V)	2	2	2
Max voltage limit (V)	129	129	129
No. of taps	32	32	32

Table A.10: Substation Transformer

Name	Bus A	Bus B	kVA	Pri. (kV)	Sec. (kV)	R %	X %
Sub_eq_source_Xfmr	source_bus	bus_Xfmr	10000	69–Delta	13.8 GrdWye	0.6266	6.2659

Table A.12: Line Configuration 1: OH_3p_type1

Parameter	Phase A	Phase B	Phase C
R_{matrix} (Ω/mile)	0.615927	0.170927	0.170927
	0.170927	0.615927	0.170927
	0.170927	0.170927	0.615927
X_{matrix} (Ω/mile)	1.209389	0.433188	0.433188
	0.433188	1.209389	0.433188
	0.433188	0.433188	1.209389
Size	4/0		
Material	ACSR		
Current Carrying Capacity (A)	340		
Resistance @ 25°C (Ω/mile)	0.445		
Resistance @ 50°C (Ω/mile)	0.592		
Geometric Mean Radius (ft)	0.00814		
Conductor Diameter (in)	0.563		
Preferred Neutral Construction	#2/0 ACSR 6/1		

Table A.13: Line Configuration 2: OH_2p_type2

Parameter	Phase A	Phase B
R_{matrix} (Ω/mile)	0.589255	0.169495
	0.169495	0.589255
X_{matrix} (Ω/mile)	1.074856	0.387876
	0.387876	1.074856
Size	4/0	
Material	ACSR	
Current Carrying Capacity (A)	357	
Resistance @ 25°C (Ω/mile)	0.41976	
Resistance @ 50°C (Ω/mile)	0.62832	
Geometric Mean Radius (ft)	0.0255	
Conductor Diameter (in)	0.502	
Preferred Neutral Construction	#2/0 ACSR 6/1	
Construction	2	

Table A.14: Line Configuration 3: OH_1p_type2

Parameter	Value
R_{matrix} (Ω/mile)	0.592473
X_{matrix} (Ω/mile)	1.065821
Size	4/0
Material	ACSR
Current Carrying Capacity (A)	357
Resistance @ 25°C (Ω/mile)	0.41976
Resistance @ 50°C (Ω/mile)	0.62832
Geometric Mean Radius (ft)	0.0255
Conductor Diameter (in)	0.502
Preferred Neutral	2/0 ACSR 6/1
Construction	2

Table A.15: Line Configuration: OH_3p_type5

Parameter	Phase A	Phase B	Phase C
R_{matrix} (Ω/mile)	1.191602	0.234849	0.234849
	0.234849	1.191602	0.234849
	0.234849	0.234849	1.191602
X_{matrix} (Ω/mile)	1.209452	0.489263	0.489263
	0.489263	1.209452	0.489263
	0.489263	0.489263	1.209452
Size	1/0		
Material	ACSR		
Current Carrying Capacity (A)	242		
Resistance @ 25°C (Ω/mile)	0.956753		
Resistance @ 50°C (Ω/mile)	1.051257		
Geometric Mean Radius (ft)	0.012915		
Conductor Diameter (in)	0.398		
Preferred Neutral	1 ACSR 6/1		
Construction	1		

Table A.16: Line Configuration: OH_1p_type5

Parameter	Value
R_{matrix} (Ω/mile)	1.19426
X_{matrix} (Ω/mile)	1.20542
Size	1/0
Material	ACSR
Current Carrying Capacity (A)	242
Resistance @ 25°C (Ω/mile)	0.956753
Resistance @ 50°C (Ω/mile)	1.051257
Geometric Mean Radius (ft)	0.012915
Conductor Diameter (in)	0.398
Preferred Neutral	1 ACSR 6/1
Construction	1

Table A.17: Line Configuration: UG_3p_type1

Parameter	**Phase A**	**Phase B**	**Phase C**
R_{matrix} (Ω/mile)	1.009423	0.409732	0.409732
	0.409732	1.009423	0.409732
	0.409732	0.409732	1.009423
X_{matrix} (Ω/mile)	0.493164	0.100849	0.100849
	0.100849	0.493164	0.100849
	0.100849	0.100849	0.493164
C_{matrix} (nF/mile)	286.101593	0	0
	0	286.101593	0
	0	0	286.101593
Property		**Value**	
Size		4/0	
Material		AA	
Current Carrying Capacity (A)		326	
Phase Conductor Resistance (Ω/1k ft)		0.105	
GMR of Phase Conductor (ft)		0.0167	
Type Neutral		Concentric	
Eq. Resistance Neut. (Ω/1k ft)		0.3	
Number of Strands		11	
OD of Cable Incl. Neutral (in)		1.218	
Diameter Under Neutral (in)		1.09	
OD of Insulation (in)		1.01	
Diameter of Conductor (in)		0.512	
Dielectric Constant		2.75	
Construction Type		1	

Table A.18: Line Configuration 5: UG_3p_type2

Parameter	**Phase A**	**Phase B**	**Phase C**
R_{matrix} (Ω/mile)	1.692577	0.550087	0.550087
	0.550087	1.692577	0.550087
	0.550087	0.550087	1.692577
X_{matrix} (Ω/mile)	0.791756	0.344931	0.344931
	0.344931	0.791756	0.344931
	0.344931	0.344931	0.791756
C_{matrix} (nF/mile)	207.880539	0	0
	0	207.880539	0
	0	0	207.880539
Property		**Value**	
Size		1/0	
Material		AA	
Current Carrying Capacity (A)		228	
Phase Conductor Resistance (Ω/1k ft)		0.211	
GMR of Phase Conductor (ft)		0.111	
Type Neutral		Concentric	
Eq. Resistance Neutral (Ω/1k ft)		0.55	
Number of Strands		6	
Outside Diameter incl. Neutral (in)		1.068	
Diameter Under Neutral (in)		0.94	
Outside Diameter of Insulation (in)		0.86	
Diameter of Conductor (in)		0.362	
Dielectric Constant of Insulation		2.75	
Construction Type		1	

Table A.19: Line Configuration 6: UG_1p_type2

Parameter	Value
R_{matrix} (Ω/mile)	1.675338
X_{matrix} (Ω/mile)	1.210007
C_{matrix} (nF/mile)	207.880539
Size	1/0
Material	AA
Current Carrying Capacity (A)	228
Phase Conductor Resistance (Ω/1k ft)	0.211
GMR of Phase Conductor (ft)	0.111
Type Neutral	Concentric
Eq. Resistance of Neutral (Ω/1k ft)	0.55
Number of Strands	6
OD of Cable Including Neutral (in)	1.068
Diameter Under Neutral (in)	0.94
OD of Cable Insulation (in)	0.86
Diameter of Conductor (in)	0.362
Dielectric Constant of Insulation	2.75
Construction Type	1

Table A.20: OH Neutral: #2/0 ACSR 6/1

Parameter	Value
Size	2/0
Material	ACSR
Current Carrying Capacity (A)	270
Resistance @ 25°C (Ω/mile)	0.706
Resistance @ 50°C (Ω/mile)	0.895
Geometric Mean Radius (ft)	0.0051
Conductor Diameter (in)	0.447

Table A.21: OH Neutral: 1 ACSR 6/1

Parameter	Value
Size	1
Material	ACSR
Current Carrying Capacity (A)	212
Resistance @ 25°C (Ω/mile)	1.181612
Resistance @ 50°C (Ω/mile)	1.298326
Geometric Mean Radius (ft)	0.011487
Conductor Diameter (in)	0.354

Table A.22: Geometric Mean Distance Parameters for Construction Type 1

Configuration	GMDP (in)	GMDPN (in)
3-phase OH	58.6	53.6
V-phase OH	88	55.8
Single-phase OH	51	51
UG All phase	3	0

Table A.23: Geometric Mean Distance Parameters for Construction Type 2

Configuration	GMDP (in)	GMDPN (in)
3-phase OH	58.6	53.6
V-phase OH	88	55.8
Single-phase OH	51	51
UG All phase	3	0

Table A.24: Three-phase Secondary Distribution Transformers

Name	Connection	Bus W1	Bus W2	Pri kV	Sec kV	kVA	%R	X/R
T_1003	Grd. Y – Grd. Y	bus1003	T_bus1003_L	13.8	0.208	112.5	2.43	3.87
T_1004	Grd. Y – Grd. Y	bus1004	T_bus1004_L	13.8	0.208	75	2.27	1.91
T_1005	Grd. Y – Grd. Y	bus1005	T_bus1005_L	13.8	0.208	75	2.27	1.91
T_1008	Grd. Y – Grd. Y	bus1008	T_bus1008_L	13.8	0.208	45	2.52	1.73
T_1009	Grd. Y – Grd. Y	bus1009	T_bus1009_L	13.8	0.208	75	2.27	1.91
T_1010	Grd. Y – Grd. Y	bus1010	T_bus1010_L	13.8	0.208	45	2.52	1.73
T_1013	Grd. Y – Grd. Y	bus1013	T_bus1013_L	13.8	0.208	45	2.52	1.73
T_202	Grd. Y – Grd. Y	bus2002	T_bus2002_L	13.8	0.208	300	1.8	4.5
T_2003	Grd. Y – Grd. Y	bus2003	T_bus2003_L	13.8	0.208	75	2.27	1.91
T_2005	Grd. Y – Grd. Y	bus2005	T_bus2005_L	13.8	0.208	45	2.52	1.73
T_2010	Grd. Y – Grd. Y	bus2010	T_bus2010_L	13.8	0.208	45	2.52	1.73
T_2011	Grd. Y – Grd. Y	bus2011	T_bus2011_L	13.8	0.208	45	2.52	1.73
T_2029	Grd. Y – Grd. Y	bus2029	T_bus2029_L	13.8	0.208	75	2.27	1.91
T_2030	Grd. Y – Grd. Y	bus2030	T_bus2030_L	13.8	0.208	75	2.27	1.91
T_2032	Grd. Y – Grd. Y	bus2032	T_bus2032_L	13.8	0.208	45	2.52	1.73
T_2034	Grd. Y – Grd. Y	bus2034	T_bus2034_L	13.8	0.208	45	2.52	1.73
T_2035	Grd. Y – Grd. Y	bus2035	T_bus2035_L	13.8	0.208	75	2.27	1.91
T_2037	Grd. Y – Grd. Y	bus2037	T_bus2037_L	13.8	0.208	45	2.52	1.73
T_2040	Grd. Y – Grd. Y	bus2040	T_bus2040_L	13.8	0.208	300	1.8	4.5
T_2041	Grd. Y – Grd. Y	bus2041	T_bus2041_L	13.8	0.208	45	2.52	1.73
T_2042	Grd. Y – Grd. Y	bus2042	T_bus2042_L	13.8	0.208	75	2.27	1.91
T_2043	Grd. Y – Grd. Y	bus2043	T_bus2043_L	13.8	0.208	75	2.27	1.91
T_2052	Grd. Y – Grd. Y	bus2052	T_bus2052_L	13.8	0.208	225	2.2	4.65
T_2053	Grd. Y – Grd. Y	bus2053	T_bus2053_L	13.8	0.208	225	2.2	4.65
T_2058	Grd. Y – Grd. Y	bus2058	T_bus2058_L	13.8	0.208	300	1.8	4.5
T_3002	Grd. Y – Grd. Y	bus3002	T_bus3002_L	13.8	0.208	45	2.52	1.73
T_3004	Grd. Y – Grd. Y	bus3004	T_bus3004_L	13.8	0.208	45	2.52	1.73
T_3006	Grd. Y – Grd. Y	bus3006	T_bus3006_L	13.8	0.208	75	2.27	1.91
T_3007	Grd. Y – Grd. Y	bus3007	T_bus3007_L	13.8	0.208	45	2.52	1.73
T_3031	Grd. Y – Grd. Y	bus3031	T_bus3031_L	13.8	0.208	45	2.52	1.73
T_3032	Grd. Y – Grd. Y	bus3032	T_bus3032_L	13.8	0.208	45	2.52	1.73
T_3033	Grd. Y – Grd. Y	bus3033	T_bus3033_L	13.8	0.208	45	2.52	1.73
T_3034	Grd. Y – Grd. Y	bus3034	T_bus3034_L	13.8	0.208	45	2.52	1.73

Table A.24 – Continued from previous page

Name	Connection	Bus W1	Bus W2	Pri kV	Sec kV	kVA	%R	X/R
T_3035	Grd. Y – Grd. Y	bus3035	T_bus3035_L	13.8	0.208	45	2.52	1.73
T_3036	Grd. Y – Grd. Y	bus3036	T_bus3036_L	13.8	0.208	45	2.52	1.73
T_3037	Grd. Y – Grd. Y	bus3037	T_bus3037_L	13.8	0.208	45	2.52	1.73
T_3038	Grd. Y – Grd. Y	bus3038	T_bus3038_L	13.8	0.208	45	2.52	1.73
T_3039	Grd. Y – Grd. Y	bus3039	T_bus3039_L	13.8	0.208	45	2.52	1.73
T_3047	Grd. Y – Grd. Y	bus3047	T_bus3047_L	13.8	0.208	45	2.52	1.73
T_3048	Grd. Y – Grd. Y	bus3048	T_bus3048_L	13.8	0.208	45	2.52	1.73
T_3049	Grd. Y – Grd. Y	bus3049	T_bus3049_L	13.8	0.208	45	2.52	1.73
T_3050	Grd. Y – Grd. Y	bus3050	T_bus3050_L	13.8	0.208	45	2.52	1.73
T_3051	Grd. Y – Grd. Y	bus3051	T_bus3051_L	13.8	0.208	45	2.52	1.73
T_3052	Grd. Y – Grd. Y	bus3052	T_bus3052_L	13.8	0.208	45	2.52	1.73
T_3054	Grd. Y – Grd. Y	bus3054	T_bus3054_L	13.8	0.208	45	2.52	1.73
T_3070	Grd. Y – Grd. Y	bus3070	T_bus3070_L	13.8	0.208	45	2.52	1.73
T_3071	Grd. Y – Grd. Y	bus3071	T_bus3071_L	13.8	0.208	45	2.52	1.73
T_3072	Grd. Y – Grd. Y	bus3072	T_bus3072_L	13.8	0.208	45	2.52	1.73
T_3073	Grd. Y – Grd. Y	bus3073	T_bus3073_L	13.8	0.208	45	2.52	1.73
T_3074	Grd. Y–Grd. Y	bus3074	T_bus3074_L	13.8	0.208	45	2.52	1.73
T_3077	Grd. Y–Grd. Y	bus3077	T_bus3077_L	13.8	0.208	500	1.6	5.9
T_3078	Grd. Y–Grd. Y	bus3078	T_bus3078_L	13.8	0.208	45	2.52	1.73
T_3081	Grd. Y–Grd. Y	bus3081	T_bus3081_L	13.8	0.208	45	2.52	1.73

Table A.25: Single-phase Secondary Distribution Transformers

Name	Conn.	Phs	Bus Winding 1	Bus Winding 2	Pri. (kV)	Sec. (kV)	kVA Rating	%R	%X
T_1006	D–D	AB	bus1006	T_bus1006_L	13.8	0.208	75	1.0	2.1
T_1007	D–D	AB	bus1007	T_bus1007_L	13.8	0.208	25	1.33	1.88

Table A.27: Single-Phase Center-tapped Secondary Distribution Transformer (cont.)

Name	Bus W1	Ph W1	V-Rat W1	kVA W1	Bus W2	Node W2	V-Rat W2	kVA W2	Bus W3	Node W3	V-Rat W3	kVA W3	%R1	%R2	%R3	%X12	%X13	%X23
T_1011	bus1011	A	7.97	25.0	b1011_L	1	0.12	25.0	b1011_L	2	0.12	25.0	0.67	1.33	1.33	2.26	2.26	1.50
T_1012	bus1012	B	7.97	37.5	b1012_L	1	0.12	37.5	b1012_L	2	0.12	37.5	0.60	1.19	1.19	2.08	2.08	1.38
T_1014	bus1014	B	7.97	25.0	b1014_L	1	0.12	25.0	b1014_L	2	0.12	25.0	0.67	1.33	1.33	2.26	2.26	1.50
T_1015	bus1015	B	7.97	25.0	b1015_L	1	0.12	25.0	b1015_L	2	0.12	25.0	0.67	1.33	1.33	2.26	2.26	1.50
T_1016	bus1016	C	7.97	50.0	b1016_L	1	0.12	50.0	b1016_L	2	0.12	50.0	0.55	1.10	1.10	2.16	2.16	1.44
T_1017	bus1017	C	7.97	37.5	b1017_L	1	0.12	37.5	b1017_L	2	0.12	37.5	0.60	1.19	1.19	2.08	2.08	1.38
T_2008	bus2008	A	7.97	25.0	b2008_L	1	0.12	25.0	b2008_L	2	0.12	25.0	0.67	1.33	1.33	2.26	2.26	1.50
T_2009	bus2009	A	7.97	25.0	b2009_L	1	0.12	25.0	b2009_L	2	0.12	25.0	0.67	1.33	1.33	2.26	2.26	1.50
T_2014	bus2014	B	7.97	37.5	b2014_L	1	0.12	37.5	b2014_L	2	0.12	37.5	0.60	1.19	1.19	2.08	2.08	1.38
T_2015	bus2015	B	7.97	25.0	b2015_L	1	0.12	25.0	b2015_L	2	0.12	25.0	0.67	1.33	1.33	2.26	2.26	1.50
T_2016	bus2016	B	7.97	25.0	b2016_L	1	0.12	25.0	b2016_L	2	0.12	25.0	0.67	1.33	1.33	2.26	2.26	1.50
T_2017	bus2017	B	7.97	25.0	b2017_L	1	0.12	25.0	b2017_L	2	0.12	25.0	0.67	1.33	1.33	2.26	2.26	1.50
T_2018	bus2018	B	7.97	25.0	b2018_L	1	0.12	25.0	b2018_L	2	0.12	25.0	0.67	1.33	1.33	2.26	2.26	1.50
T_2020	bus2020	B	7.97	25.0	b2020_L	1	0.12	25.0	b2020_L	2	0.12	25.0	0.67	1.33	1.33	2.26	2.26	1.50
T_2022	bus2022	C	7.97	25.0	b2022_L	1	0.12	25.0	b2022_L	2	0.12	25.0	0.67	1.33	1.33	2.26	2.26	1.50
T_2023	bus2023	C	7.97	15.0	b2023_L	1	0.12	15.0	b2023_L	2	0.12	15.0	0.83	1.66	1.66	1.54	1.54	1.02
T_2024	bus2024	C	7.97	25.0	b2024_L	1	0.12	25.0	b2024_L	2	0.12	25.0	0.67	1.33	1.33	2.26	2.26	1.50
T_2025	bus2025	C	7.97	25.0	b2025_L	1	0.12	25.0	b2025_L	2	0.12	25.0	0.67	1.33	1.33	2.26	2.26	1.50
T_2028	bus2028	A	7.97	25.0	b2028_L	1	0.12	25.0	b2028_L	2	0.12	25.0	0.67	1.33	1.33	2.26	2.26	1.50
T_2031	bus2031	A	7.97	25.0	b2031_L	1	0.12	25.0	b2031_L	2	0.12	25.0	0.67	1.33	1.33	2.26	2.26	1.50
T_2045	bus2045	B	7.97	15.0	b2045_L	1	0.12	15.0	b2045_L	2	0.12	15.0	0.83	1.66	1.66	1.54	1.54	1.02
T_2046	bus2046	B	7.97	50.0	b2046_L	1	0.12	50.0	b2046_L	2	0.12	50.0	0.55	1.10	1.10	2.16	2.16	1.44
T_2047	bus2047	B	7.97	50.0	b2047_L	1	0.12	50.0	b2047_L	2	0.12	50.0	0.55	1.10	1.10	2.16	2.16	1.44
T_2048	bus2048	B	7.97	50.0	b2048_L	1	0.12	50.0	b2048_L	2	0.12	50.0	0.55	1.10	1.10	2.16	2.16	1.44
T_2049	bus2049	C	7.97	37.5	b2049_L	1	0.12	37.5	b2049_L	2	0.12	37.5	0.60	1.19	1.19	2.08	2.08	1.38
T_2050	bus2050	C	7.97	37.5	b2050_L	1	0.12	37.5	b2050_L	2	0.12	37.5	0.60	1.19	1.19	2.08	2.08	1.38
T_2051	bus2051	C	7.97	37.5	b2051_L	1	0.12	37.5	b2051_L	2	0.12	37.5	0.60	1.19	1.19	2.08	2.08	1.38
T_2054	bus2054	A	7.97	37.5	b2054_L	1	0.12	37.5	b2054_L	2	0.12	37.5	0.60	1.19	1.19	2.08	2.08	1.38
T_2055	bus2055	A	7.97	50.0	b2055_L	1	0.12	50.0	b2055_L	2	0.12	50.0	0.55	1.10	1.10	2.16	2.16	1.44
T_2056	bus2056	A	7.97	25.0	b2056_L	1	0.12	25.0	b2056_L	2	0.12	25.0	0.67	1.33	1.33	2.26	2.26	1.50
T_2059	bus2059	B	7.97	25.0	b2059_L	1	0.12	25.0	b2059_L	2	0.12	25.0	0.67	1.33	1.33	2.26	2.26	1.50
T_2060	bus2060	B	7.96	25.0	b2060_L	1	0.12	25.0	b2060_L	2	0.12	25.0	0.68	1.33	1.33	2.25	2.25	1.50
T_3009	bus3009	A	7.96	37.5	b3009_L	1	0.12	37.5	b3009_L	2	0.12	37.5	0.59	1.19	1.19	2.07	2.07	1.38
T_3010	bus3010	A	7.96	37.5	b3010_L	1	0.12	37.5	b3010_L	2	0.12	37.5	0.59	1.19	1.19	2.07	2.07	1.38
T_3011	bus3011	A	7.96	37.5	b3011_L	1	0.12	37.5	b3011_L	2	0.12	37.5	0.59	1.19	1.19	2.07	2.07	1.38
T_3012	bus3012	A	7.96	50.0	b3012_L	1	0.12	50.0	b3012_L	2	0.12	50.0	0.55	1.10	1.10	2.16	2.16	1.44
T_3017	bus3017	B	7.96	100.0	b3017_L	1	0.12	100.0	b3017_L	2	0.12	100.0	0.56	1.12	1.12	2.68	2.68	1.79
T_3041	bus3041	C	7.96	50.0	b3041_L	1	0.12	50.0	b3041_L	2	0.12	50.0	0.55	1.10	1.10	2.16	2.16	1.44
T_3056	bus3056	B	7.96	37.5	b3056_L	1	0.12	37.5	b3056_L	2	0.12	37.5	0.59	1.19	1.19	2.07	2.07	1.38
T_3061	bus3061	B	7.96	37.5	b3061_L	1	0.12	37.5	b3061_L	2	0.12	37.5	0.59	1.19	1.19	2.07	2.07	1.38
T_3019	bus3019	C	7.96	37.5	b3019_L	1	0.12	37.5	b3019_L	2	0.12	37.5	0.59	1.19	1.19	2.07	2.07	1.38
T_3020	bus3020	C	7.96	100.0	b3020_L	1	0.12	100.0	b3020_L	2	0.12	100.0	0.56	1.12	1.12	2.68	2.68	1.79
T_3021	bus3021	C	7.96	37.5	b3021_L	1	0.12	37.5	b3021_L	2	0.12	37.5	0.59	1.19	1.19	2.07	2.07	1.38
T_3023	bus3023	A	7.96	50.0	b3023_L	1	0.12	50.0	b3023_L	2	0.12	50.0	0.55	1.10	1.10	2.16	2.16	1.44
T_3024	bus3024	A	7.96	37.5	b3024_L	1	0.12	37.5	b3024_L	2	0.12	37.5	0.59	1.19	1.19	2.07	2.07	1.38
T_3025	bus3025	A	7.96	50.0	b3025_L	1	0.12	50.0	b3025_L	2	0.12	50.0	0.55	1.10	1.10	2.16	2.16	1.44

Name	Bus W1	Ph	V-Rat1	kVA1	Bus W2	Nd2	V-Rat2	kVA2	Bus W3	Nd3	V-Rat3	kVA3	%R1	%R2	%R3	%X12	%X13	%X23
T_3026	bus3026	A	7.96	37.5	b3026_L	1	0.12	37.5	b3026_L	2	0.12	37.5	0.59	1.19	1.19	2.07	2.07	1.38
T_3027	bus3027	A	7.96	100.0	b3027_L	1	0.12	100.0	b3027_L	2	0.12	100.0	0.56	1.12	1.12	2.68	2.68	1.79
T_3028	bus3028	A	7.96	100.0	b3028_L	1	0.12	100.0	b3028_L	2	0.12	100.0	0.56	1.12	1.12	2.68	2.68	1.79
T_3029	bus3029	A	7.96	37.5	b3029_L	1	0.12	37.5	b3029_L	2	0.12	37.5	0.59	1.19	1.19	2.07	2.07	1.38
T_3042	bus3042	C	7.96	37.5	b3042_L	1	0.12	37.5	b3042_L	2	0.12	37.5	0.59	1.19	1.19	2.07	2.07	1.38
T_3043	bus3043	C	7.96	37.5	b3043_L	1	0.12	37.5	b3043_L	2	0.12	37.5	0.59	1.19	1.19	2.07	2.07	1.38
T_3044	bus3044	C	7.96	37.5	b3044_L	1	0.12	37.5	b3044_L	2	0.12	37.5	0.59	1.19	1.19	2.07	2.07	1.38
T_3045	bus3045	C	7.96	37.5	b3045_L	1	0.12	37.5	b3045_L	2	0.12	37.5	0.59	1.19	1.19	2.07	2.07	1.38
T_3057	bus3057	B	7.96	37.5	b3057_L	1	0.12	37.5	b3057_L	2	0.12	37.5	0.59	1.19	1.19	2.07	2.07	1.38
T_3058	bus3058	B	7.96	37.5	b3058_L	1	0.12	37.5	b3058_L	2	0.12	37.5	0.59	1.19	1.19	2.07	2.07	1.38
T_3059	bus3059	B	7.96	37.5	b3059_L	1	0.12	37.5	b3059_L	2	0.12	37.5	0.59	1.19	1.19	2.07	2.07	1.38
T_3060	bus3060	B	7.96	37.5	b3060_L	1	0.12	37.5	b3060_L	2	0.12	37.5	0.59	1.19	1.19	2.07	2.07	1.38
T_3062	bus3062	B	7.97	37.5	b3062_L	1	0.12	37.5	b3062_L	2	0.12	37.5	0.60	1.19	1.19	2.08	2.08	1.38
T_3063	bus3063	B	7.97	37.5	b3063_L	1	0.12	37.5	b3063_L	2	0.12	37.5	0.60	1.19	1.19	2.08	2.08	1.38
T_3064	bus3064	B	7.97	37.5	b3064_L	1	0.12	37.5	b3064_L	2	0.12	37.5	0.60	1.19	1.19	2.08	2.08	1.38
T_3065	bus3065	B	7.97	37.5	b3065_L	1	0.12	37.5	b3065_L	2	0.12	37.5	0.60	1.19	1.19	2.08	2.08	1.38
T_3066	bus3066	B	7.97	37.5	b3066_L	1	0.12	37.5	b3066_L	2	0.12	37.5	0.60	1.19	1.19	2.08	2.08	1.38
T_3067	bus3067	B	7.97	37.5	b3067_L	1	0.12	37.5	b3067_L	2	0.12	37.5	0.60	1.19	1.19	2.08	2.08	1.38
T_3083	bus3083	A	7.97	37.5	b3083_L	1	0.12	37.5	b3083_L	2	0.12	37.5	0.60	1.19	1.19	2.08	2.08	1.38
T_3084	bus3084	A	7.97	37.5	b3084_L	1	0.12	37.5	b3084_L	2	0.12	37.5	0.60	1.19	1.19	2.08	2.08	1.38
T_3085	bus3085	A	7.97	37.5	b3085_L	1	0.12	37.5	b3085_L	2	0.12	37.5	0.60	1.19	1.19	2.08	2.08	1.38
T_3086	bus3086	A	7.97	37.5	b3086_L	1	0.12	37.5	b3086_L	2	0.12	37.5	0.60	1.19	1.19	2.08	2.08	1.38
T_3087	bus3087	A	7.97	37.5	b3087_L	1	0.12	37.5	b3087_L	2	0.12	37.5	0.60	1.19	1.19	2.08	2.08	1.38
T_3088	bus3088	A	7.97	37.5	b3088_L	1	0.12	37.5	b3088_L	2	0.12	37.5	0.60	1.19	1.19	2.08	2.08	1.38
T_3089	bus3089	A	7.97	37.5	b3089_L	1	0.12	37.5	b3089_L	2	0.12	37.5	0.60	1.19	1.19	2.08	2.08	1.38
T_3090	bus3090	A	7.97	37.5	b3090_L	1	0.12	37.5	b3090_L	2	0.12	37.5	0.60	1.19	1.19	2.08	2.08	1.38
T_3091	bus3091	A	7.97	25.0	b3091_L	1	0.12	25.0	b3091_L	2	0.12	25.0	0.67	1.33	1.33	2.26	2.26	1.50
T_3093	bus3093	A	7.97	37.5	b3093_L	1	0.12	37.5	b3093_L	2	0.12	37.5	0.60	1.19	1.19	2.08	2.08	1.38
T_3094	bus3094	A	7.97	37.5	b3094_L	1	0.12	37.5	b3094_L	2	0.12	37.5	0.60	1.19	1.19	2.08	2.08	1.38
T_3095	bus3095	A	7.97	37.5	b3095_L	1	0.12	37.5	b3095_L	2	0.12	37.5	0.60	1.19	1.19	2.08	2.08	1.38
T_3096	bus3096	A	7.97	37.5	b3096_L	1	0.12	37.5	b3096_L	2	0.12	37.5	0.60	1.19	1.19	2.08	2.08	1.38
T_3097	bus3097	A	7.97	37.5	b3097_L	1	0.12	37.5	b3097_L	2	0.12	37.5	0.60	1.19	1.19	2.08	2.08	1.38
T_3098	bus3098	B	7.97	50.0	b3098_L	1	0.12	50.0	b3098_L	2	0.12	50.0	0.55	1.10	1.10	2.16	2.16	1.44
T_3099	bus3099	B	7.97	37.5	b3099_L	1	0.12	37.5	b3099_L	2	0.12	37.5	0.60	1.19	1.19	2.08	2.08	1.38
T_3101	bus3101	C	7.97	37.5	b3101_L	1	0.12	37.5	b3101_L	2	0.12	37.5	0.60	1.19	1.19	2.08	2.08	1.38
T_3102	bus3102	C	7.97	37.5	b3102_L	1	0.12	37.5	b3102_L	2	0.12	37.5	0.60	1.19	1.19	2.08	2.08	1.38
T_3103	bus3103	C	7.97	50.0	b3103_L	1	0.12	50.0	b3103_L	2	0.12	50.0	0.55	1.10	1.10	2.16	2.16	1.44
T_3104	bus3104	C	7.97	100.0	b3104_L	1	0.12	100.0	b3104_L	2	0.12	100.0	0.56	1.12	1.12	2.69	2.69	1.79
T_3105	bus3105	C	7.97	37.5	b3105_L	1	0.12	37.5	b3105_L	2	0.12	37.5	0.60	1.19	1.19	2.08	2.08	1.38
T_3106	bus3106	C	7.97	100.0	b3106_L	1	0.12	100.0	b3106_L	2	0.12	100.0	0.56	1.12	1.12	2.69	2.69	1.79
T_3108	bus3108	A	7.97	37.5	b3108_L	1	0.12	37.5	b3108_L	2	0.12	37.5	0.60	1.19	1.19	2.08	2.08	1.38
T_3109	bus3109	A	7.97	37.5	b3109_L	1	0.12	37.5	b3109_L	2	0.12	37.5	0.60	1.19	1.19	2.08	2.08	1.38
T_3110	bus3110	A	7.97	50.0	b3110_L	1	0.12	50.0	b3110_L	2	0.12	50.0	0.55	1.10	1.10	2.16	2.16	1.44
T_3111	bus3111	A	7.97	50.0	b3111_L	1	0.12	50.0	b3111_L	2	0.12	50.0	0.55	1.10	1.10	2.16	2.16	1.44
T_3112	bus3112	A	7.97	50.0	b3112_L	1	0.12	50.0	b3112_L	2	0.12	50.0	0.55	1.10	1.10	2.16	2.16	1.44
T_3114	bus3114	B	7.97	37.5	b3114_L	1	0.12	37.5	b3114_L	2	0.12	37.5	0.60	1.19	1.19	2.08	2.08	1.38
T_3115	bus3115	B	7.97	50.0	b3115_L	1	0.12	50.0	b3115_L	2	0.12	50.0	0.55	1.10	1.10	2.16	2.16	1.44
T_3116	bus3116	B	7.97	37.5	b3116_L	1	0.12	37.5	b3116_L	2	0.12	37.5	0.60	1.19	1.19	2.08	2.08	1.38
T_3117	bus3117	B	7.97	37.5	b3117_L	1	0.12	37.5	b3117_L	2	0.12	37.5	0.60	1.19	1.19	2.08	2.08	1.38
T_3120	bus3120	B	7.97	37.5	b3120_L	1	0.12	37.5	b3120_L	2	0.12	37.5	0.60	1.19	1.19	2.08	2.08	1.38

Name	Bus W1	Ph	V-Rat1	kVA1	Bus W2	Nd2	V-Rat2	kVA2	Bus W3	Nd3	V-Rat3	kVA3	%R1	%R2	%R3	%X12	%X13	%X23
T_3121	bus3121	B	7.97	37.5	b3121_L	1	0.12	37.5	b3121_L	2	0.12	37.5	0.60	1.19	1.19	2.08	2.08	1.38
T_3122	bus3122	B	7.97	37.5	b3122_L	1	0.12	37.5	b3122_L	2	0.12	37.5	0.60	1.19	1.19	2.08	2.08	1.38
T_3123	bus3123	B	7.97	37.5	b3123_L	1	0.12	37.5	b3123_L	2	0.12	37.5	0.60	1.19	1.19	2.08	2.08	1.38
T_3124	bus3124	B	7.97	37.5	b3124_L	1	0.12	37.5	b3124_L	2	0.12	37.5	0.60	1.19	1.19	2.08	2.08	1.38
T_3125	bus3125	B	7.97	15.0	b3125_L	1	0.12	15.0	b3125_L	2	0.12	15.0	0.83	1.66	1.66	1.54	1.54	1.02
T_3126	bus3126	B	7.97	37.5	b3126_L	1	0.12	37.5	b3126_L	2	0.12	37.5	0.60	1.19	1.19	2.08	2.08	1.38
T_3127	bus3127	B	7.97	37.5	b3127_L	1	0.12	37.5	b3127_L	2	0.12	37.5	0.60	1.19	1.19	2.08	2.08	1.38
T_3128	bus3128	B	7.97	37.5	b3128_L	1	0.12	37.5	b3128_L	2	0.12	37.5	0.60	1.19	1.19	2.08	2.08	1.38
T_3129	bus3129	B	7.97	37.5	b3129_L	1	0.12	37.5	b3129_L	2	0.12	37.5	0.60	1.19	1.19	2.08	2.08	1.38
T_3130	bus3130	B	7.97	37.5	b3130_L	1	0.12	37.5	b3130_L	2	0.12	37.5	0.60	1.19	1.19	2.08	2.08	1.38
T_3131	bus3131	B	7.97	37.5	b3131_L	1	0.12	37.5	b3131_L	2	0.12	37.5	0.60	1.19	1.19	2.08	2.08	1.38
T_3132	bus3132	A	7.97	50.0	b3132_L	1	0.12	50.0	b3132_L	2	0.12	50.0	0.55	1.10	1.10	2.16	2.16	1.44
T_3134	bus3134	A	7.97	50.0	b3134_L	1	0.12	50.0	b3134_L	2	0.12	50.0	0.55	1.10	1.10	2.16	2.16	1.44
T_3135	bus3135	A	7.97	37.5	b3135_L	1	0.12	37.5	b3135_L	2	0.12	37.5	0.60	1.19	1.19	2.08	2.08	1.38
T_3136	bus3136	A	7.97	50.0	b3136_L	1	0.12	50.0	b3136_L	2	0.12	50.0	0.55	1.10	1.10	2.16	2.16	1.44
T_3137	bus3137	A	7.97	50.0	b3137_L	1	0.12	50.0	b3137_L	2	0.12	50.0	0.55	1.10	1.10	2.16	2.16	1.44
T_3138	bus3138	A	7.97	50.0	b3138_L	1	0.12	50.0	b3138_L	2	0.12	50.0	0.55	1.10	1.10	2.16	2.16	1.44
T_3139	bus3139	A	7.97	37.5	b3139_L	1	0.12	37.5	b3139_L	2	0.12	37.5	0.60	1.19	1.19	2.08	2.08	1.38
T_3141	bus3141	C	7.97	37.5	b3141_L	1	0.12	37.5	b3141_L	2	0.12	37.5	0.60	1.19	1.19	2.08	2.08	1.38
T_3142	bus3142	C	7.97	37.5	b3142_L	1	0.12	37.5	b3142_L	2	0.12	37.5	0.60	1.19	1.19	2.08	2.08	1.38
T_3143	bus3143	C	7.97	37.5	b3143_L	1	0.12	37.5	b3143_L	2	0.12	37.5	0.60	1.19	1.19	2.08	2.08	1.38
T_3144	bus3144	C	7.97	15.0	b3144_L	1	0.12	15.0	b3144_L	2	0.12	15.0	0.83	1.66	1.66	1.54	1.54	1.02
T_3145	bus3145	C	7.97	37.5	b3145_L	1	0.12	37.5	b3145_L	2	0.12	37.5	0.60	1.19	1.19	2.08	2.08	1.38
T_3146	bus3146	C	7.97	37.5	b3146_L	1	0.12	37.5	b3146_L	2	0.12	37.5	0.60	1.19	1.19	2.08	2.08	1.38
T_3147	bus3147	C	7.97	37.5	b3147_L	1	0.12	37.5	b3147_L	2	0.12	37.5	0.60	1.19	1.19	2.08	2.08	1.38
T_3148	bus3148	C	7.97	50.0	b3148_L	1	0.12	50.0	b3148_L	2	0.12	50.0	0.55	1.10	1.10	2.16	2.16	1.44
T_3149	bus3149	C	7.97	37.5	b3149_L	1	0.12	37.5	b3149_L	2	0.12	37.5	0.60	1.19	1.19	2.08	2.08	1.38
T_3150	bus3150	C	7.97	25.0	b3150_L	1	0.12	25.0	b3150_L	2	0.12	25.0	0.67	1.33	1.33	2.26	2.26	1.50
T_3151	bus3151	C	7.97	25.0	b3151_L	1	0.12	25.0	b3151_L	2	0.12	25.0	0.67	1.33	1.33	2.26	2.26	1.50
T_3152	bus3152	C	7.97	25.0	b3152_L	1	0.12	25.0	b3152_L	2	0.12	25.0	0.67	1.33	1.33	2.26	2.26	1.50
T_3153	bus3153	C	7.97	37.5	b3153_L	1	0.12	37.5	b3153_L	2	0.12	37.5	0.60	1.19	1.19	2.08	2.08	1.38
T_3154	bus3154	C	7.97	25.0	b3154_L	1	0.12	25.0	b3154_L	2	0.12	25.0	0.67	1.33	1.33	2.26	2.26	1.50
T_3155	bus3155	C	7.97	25.0	b3155_L	1	0.12	25.0	b3155_L	2	0.12	25.0	0.67	1.33	1.33	2.26	2.26	1.50
T_3157	bus3157	C	7.97	50.0	b3157_L	1	0.12	50.0	b3157_L	2	0.12	50.0	0.55	1.10	1.10	2.16	2.16	1.44
T_3158	bus3158	C	7.97	50.0	b3158_L	1	0.12	50.0	b3158_L	2	0.12	50.0	0.55	1.10	1.10	2.16	2.16	1.44
T_3159	bus3159	C	7.97	50.0	b3159_L	1	0.12	50.0	b3159_L	2	0.12	50.0	0.55	1.10	1.10	2.16	2.16	1.44
T_3160	bus3160	C	7.97	25.0	b3160_L	1	0.12	25.0	b3160_L	2	0.12	25.0	0.67	1.33	1.33	2.26	2.26	1.50

Table A.28: Spot Loads

Load Name	XMR Type	Bus	V (V)	Connection & Model	Customers
Load_1003	3Ø XFMR	T_bus1003_L	208	wye-PQ	4
Load_1004	3Ø XFMR	T_bus1004_L	208	wye-PQ	2
Load_1005	3Ø XFMR	T_bus1005_L	208	wye-PQ	2

Continued on next page

Load Name	XMR Type	Bus	V (V)	Connection & Model	Customers
Load_1006	1Ø XFMR	T_bus1006_L	208	delta-PQ	2
Load_1007	1Ø XFMR	T_bus1007_L	208	delta-PQ	2
Load_1008	3Ø XFMR	T_bus1008_L	208	wye-PQ	3
Load_1009	3Ø XFMR	T_bus1009_L	208	wye-PQ	2
Load_1010	3Ø XFMR	T_bus1010_L	208	wye-PQ	4
Load_1011	1Ø CT XFMR	T_bus1011_L	120	wye-PQ	13
Load_1012	1Ø CT XFMR	T_bus1012_L	120	wye-PQ	7
Load_1013	3Ø XFMR	T_bus1013_L	208	wye-PQ	3
Load_1014	1Ø CT XFMR	T_bus1014_L	120	wye-PQ	2
Load_1015	1Ø CT XFMR	T_bus1015_L	120	wye-PQ	3
Load_1016	1Ø CT XFMR	T_bus1016_L	120	wye-PQ	7
Load_1017	1Ø CT XFMR	T_bus1017_L	120	wye-PQ	7
Load_2002	3Ø XFMR	T_bus2002_L	208	wye-PQ	4
Load_2003	3Ø XFMR	T_bus2003_L	208	wye-PQ	3
Load_2005	3Ø XFMR	T_bus2005_L	208	wye-PQ	2
Load_2008	1Ø CT XFMR	T_bus2008_L	120	wye-PQ	4
Load_2009	1Ø CT XFMR	T_bus2009_L	120	wye-PQ	2
Load_2010	3Ø XFMR	T_bus2010_L	208	wye-PQ	5
Load_2011	3Ø XFMR	T_bus2011_L	208	wye-PQ	7
Load_2014	1Ø CT XFMR	T_bus2014_L	120	wye-PQ	4
Load_2015	1Ø CT XFMR	T_bus2015_L	120	wye-PQ	2
Load_2016	1Ø CT XFMR	T_bus2016_L	120	wye-PQ	3
Load_2017	1Ø CT XFMR	T_bus2017_L	120	wye-PQ	6
Load_2018	1Ø CT XFMR	T_bus2018_L	120	wye-PQ	4
Load_2020	1Ø CT XFMR	T_bus2020_L	120	wye-PQ	2
Load_2022	1Ø CT XFMR	T_bus2022_L	120	wye-PQ	3
Load_2023	1Ø CT XFMR	T_bus2023_L	120	wye-PQ	2
Load_2024	1Ø CT XFMR	T_bus2024_L	120	wye-PQ	4
Load_2025	1Ø CT XFMR	T_bus2025_L	120	wye-PQ	4
Load_2028	1Ø CT XFMR	T_bus2028_L	120	wye-PQ	1
Load_2029	3Ø XFMR	T_bus2029_L	208	wye-PQ	2
Load_2030	3Ø XFMR	T_bus2030_L	208	wye-PQ	3
Load_2031	1Ø CT XFMR	T_bus2031_L	120	wye-PQ	3

Continued on next page

Load Name	XMR Type	Bus	V (V)	Connection & Model	Customers
Load_2032	3Ø XFMR	T_bus2032_L	208	wye-PQ	4
Load_2034	3Ø XFMR	T_bus2034_L	208	wye-PQ	5
Load_2035	3Ø XFMR	T_bus2035_L	208	wye-PQ	3
Load_2037	3Ø XFMR	T_bus2037_L	208	wye-PQ	4
Load_2040	3Ø XFMR	T_bus2040_L	208	wye-PQ	4
Load_2041	3Ø XFMR	T_bus2041_L	208	wye-PQ	2
Load_2042	3Ø XFMR	T_bus2042_L	208	wye-PQ	2
Load_2043	3Ø XFMR	T_bus2043_L	208	wye-PQ	6
Load_2045	1Ø CT XFMR	T_bus2045_L	120	wye-PQ	2
Load_2046	1Ø CT XFMR	T_bus2046_L	120	wye-PQ	8
Load_2047	1Ø CT XFMR	T_bus2047_L	120	wye-PQ	8
Load_2048	1Ø CT XFMR	T_bus2048_L	120	wye-PQ	7
Load_2049	1Ø CT XFMR	T_bus2049_L	120	wye-PQ	4
Load_2050	1Ø CT XFMR	T_bus2050_L	120	wye-PQ	3
Load_2051	1Ø CT XFMR	T_bus2051_L	120	wye-PQ	6
Load_2052	3Ø XFMR	T_bus2052_L	208	wye-PQ	3
Load_2053	3Ø XFMR	T_bus2053_L	208	wye-PQ	1
Load_2054	1Ø CT XFMR	T_bus2054_L	120	wye-PQ	8
Load_2055	1Ø CT XFMR	T_bus2055_L	120	wye-PQ	7
Load_2056	1Ø CT XFMR	T_bus2056_L	120	wye-PQ	4
Load_2058	3Ø XFMR	T_bus2058_L	208	wye-PQ	4
Load_2059	1Ø CT XFMR	T_bus2059_L	120	wye-PQ	2
Load_2060	1Ø CT XFMR	T_bus2060_L	120	wye-PQ	2
Load_3002	3Ø XFMR	T_bus3002_L	208	wye-PQ	5
Load_3004	3Ø XFMR	T_bus3004_L	208	wye-PQ	4
Load_3006	3Ø XFMR	T_bus3006_L	208	wye-PQ	6
Load_3007	3Ø XFMR	T_bus3007_L	208	wye-PQ	8
Load_3009	1Ø CT XFMR	T_bus3009_L	120	wye-PQ	7
Load_3010	1Ø CT XFMR	T_bus3010_L	120	wye-PQ	8
Load_3011	1Ø CT XFMR	T_bus3011_L	120	wye-PQ	7
Load_3012	1Ø CT XFMR	T_bus3012_L	120	wye-PQ	9
Load_3013	1Ø CT XFMR	T_bus3013_L	120	wye-PQ	5
Load_3014	1Ø CT XFMR	T_bus3014_L	120	wye-PQ	7

Continued on next page

Load Name	XMR Type	Bus	V (V)	Connection & Model	Customers
Load_3016	1Ø CT XFMR	T_bus3016_L	120	wye-PQ	9
Load_3017	1Ø CT XFMR	T_bus3017_L	120	wye-PQ	12
Load_3018	1Ø CT XFMR	T_bus3018_L	120	wye-PQ	11
Load_3019	1Ø CT XFMR	T_bus3019_L	120	wye-PQ	9
Load_3020	1Ø CT XFMR	T_bus3020_L	120	wye-PQ	9
Load_3021	1Ø CT XFMR	T_bus3021_L	120	wye-PQ	7
Load_3023	1Ø CT XFMR	T_bus3023_L	120	wye-PQ	9
Load_3024	1Ø CT XFMR	T_bus3024_L	120	wye-PQ	9
Load_3025	1Ø CT XFMR	T_bus3025_L	120	wye-PQ	9
Load_3026	1Ø CT XFMR	T_bus3026_L	120	wye-PQ	9
Load_3027	1Ø CT XFMR	T_bus3027_L	120	wye-PQ	12
Load_3028	1Ø CT XFMR	T_bus3028_L	120	wye-PQ	8
Load_3029	1Ø CT XFMR	T_bus3029_L	120	wye-PQ	5
Load_3031	3Ø XFMR	T_bus3031_L	208	wye-PQ	8
Load_3032	3Ø XFMR	T_bus3032_L	208	wye-PQ	9
Load_3033	3Ø XFMR	T_bus3033_L	208	wye-PQ	7
Load_3034	3Ø XFMR	T_bus3034_L	208	wye-PQ	9
Load_3035	3Ø XFMR	T_bus3035_L	208	wye-PQ	8
Load_3036	3Ø XFMR	T_bus3036_L	208	wye-PQ	5
Load_3037	3Ø XFMR	T_bus3037_L	208	wye-PQ	7
Load_3038	3Ø XFMR	T_bus3038_L	208	wye-PQ	7
Load_3039	3Ø XFMR	T_bus3039_L	208	wye-PQ	6
Load_3041	1Ø CT XFMR	T_bus3041_L	120	wye-PQ	9
Load_3042	1Ø CT XFMR	T_bus3042_L	120	wye-PQ	8
Load_3043	1Ø CT XFMR	T_bus3043_L	120	wye-PQ	7
Load_3044	1Ø CT XFMR	T_bus3044_L	120	wye-PQ	9
Load_3045	1Ø CT XFMR	T_bus3045_L	120	wye-PQ	6
Load_3047	3Ø XFMR	T_bus3047_L	208	wye-PQ	6
Load_3048	3Ø XFMR	T_bus3048_L	208	wye-PQ	3
Load_3049	3Ø XFMR	T_bus3049_L	208	wye-PQ	5
Load_3050	3Ø XFMR	T_bus3050_L	208	wye-PQ	6
Load_3051	3Ø XFMR	T_bus3051_L	208	wye-PQ	4
Load_3052	3Ø XFMR	T_bus3052_L	208	wye-PQ	5

Continued on next page

Load Name	XMR Type	Bus	V (V)	Connection & Model	Customers
Load_3054	3Ø XFMR	T_bus3054_L	208	wye-PQ	2
Load_3056	1Ø CT XFMR	T_bus3056_L	120	wye-PQ	4
Load_3057	1Ø CT XFMR	T_bus3057_L	120	wye-PQ	4
Load_3058	1Ø CT XFMR	T_bus3058_L	120	wye-PQ	5
Load_3059	1Ø CT XFMR	T_bus3059_L	120	wye-PQ	3
Load_3060	1Ø CT XFMR	T_bus3060_L	120	wye-PQ	4
Load_3061	1Ø CT XFMR	T_bus3061_L	120	wye-PQ	4
Load_3062	1Ø CT XFMR	T_bus3062_L	120	wye-PQ	3
Load_3063	1Ø CT XFMR	T_bus3063_L	120	wye-PQ	4
Load_3064	1Ø CT XFMR	T_bus3064_L	120	wye-PQ	6
Load_3065	1Ø CT XFMR	T_bus3065_L	120	wye-PQ	7
Load_3066	1Ø CT XFMR	T_bus3066_L	120	wye-PQ	3
Load_3067	1Ø CT XFMR	T_bus3067_L	120	wye-PQ	8
Load_3070	3Ø XFMR	T_bus3070_L	208	wye-PQ	5
Load_3071	3Ø XFMR	T_bus3071_L	208	wye-PQ	9
Load_3072	3Ø XFMR	T_bus3072_L	208	wye-PQ	7
Load_3073	3Ø XFMR	T_bus3073_L	208	wye-PQ	4
Load_3074	3Ø XFMR	T_bus3074_L	208	wye-PQ	4
Load_3077	3Ø XFMR	T_bus3077_L	208	wye-PQ	5
Load_3081	3Ø XFMR	T_bus3081_L	208	wye-PQ	2
Load_3083	1Ø CT XFMR	T_bus3083_L	120	wye-PQ	10
Load_3084	1Ø CT XFMR	T_bus3084_L	120	wye-PQ	3
Load_3085	1Ø CT XFMR	T_bus3085_L	120	wye-PQ	8
Load_3086	1Ø CT XFMR	T_bus3086_L	120	wye-PQ	5
Load_3087	1Ø CT XFMR	T_bus3087_L	120	wye-PQ	6
Load_3088	1Ø CT XFMR	T_bus3088_L	120	wye-PQ	7
Load_3089	1Ø CT XFMR	T_bus3089_L	120	wye-PQ	3
Load_3090	1Ø CT XFMR	T_bus3090_L	120	wye-PQ	7
Load_3091	1Ø CT XFMR	T_bus3091_L	120	wye-PQ	3
Load_3093	1Ø CT XFMR	T_bus3093_L	120	wye-PQ	10
Load_3094	1Ø CT XFMR	T_bus3094_L	120	wye-PQ	9
Load_3095	1Ø CT XFMR	T_bus3095_L	120	wye-PQ	11
Load_3096	1Ø CT XFMR	T_bus3096_L	120	wye-PQ	11

Continued on next page

Load Name	XMR Type	Bus	V (V)	Connection & Model	Customers
Load_3097	1Ø CT XFMR	T_bus3097_L	120	wye-PQ	5
Load_3098	1Ø CT XFMR	T_bus3098_L	120	wye-PQ	9
Load_3099	1Ø CT XFMR	T_bus3099_L	120	wye-PQ	7
Load_3101	1Ø CT XFMR	T_bus3101_L	120	wye-PQ	3
Load_3102	1Ø CT XFMR	T_bus3102_L	120	wye-PQ	5
Load_3103	1Ø CT XFMR	T_bus3103_L	120	wye-PQ	9
Load_3104	1Ø CT XFMR	T_bus3104_L	120	wye-PQ	2
Load_3105	1Ø CT XFMR	T_bus3105_L	120	wye-PQ	5
Load_3106	1Ø CT XFMR	T_bus3106_L	120	wye-PQ	9
Load_3108	1Ø CT XFMR	T_bus3108_L	120	wye-PQ	4
Load_3109	1Ø CT XFMR	T_bus3109_L	120	wye-PQ	5
Load_3110	1Ø CT XFMR	T_bus3110_L	120	wye-PQ	10
Load_3111	1Ø CT XFMR	T_bus3111_L	120	wye-PQ	11
Load_3112	1Ø CT XFMR	T_bus3112_L	120	wye-PQ	5
Load_3114	1Ø CT XFMR	T_bus3114_L	120	wye-PQ	9
Load_3115	1Ø CT XFMR	T_bus3115_L	120	wye-PQ	8
Load_3116	1Ø CT XFMR	T_bus3116_L	120	wye-PQ	8
Load_3117	1Ø CT XFMR	T_bus3117_L	120	wye-PQ	4
Load_3120	1Ø CT XFMR	T_bus3120_L	120	wye-PQ	3
Load_3121	1Ø CT XFMR	T_bus3121_L	120	wye-PQ	6
Load_3122	1Ø CT XFMR	T_bus3122_L	120	wye-PQ	3
Load_3123	1Ø CT XFMR	T_bus3123_L	120	wye-PQ	6
Load_3124	1Ø CT XFMR	T_bus3124_L	120	wye-PQ	3
Load_3125	1Ø CT XFMR	T_bus3125_L	120	wye-PQ	2
Load_3126	1Ø CT XFMR	T_bus3126_L	120	wye-PQ	5
Load_3127	1Ø CT XFMR	T_bus3127_L	120	wye-PQ	8
Load_3128	1Ø CT XFMR	T_bus3128_L	120	wye-PQ	4
Load_3129	1Ø CT XFMR	T_bus3129_L	120	wye-PQ	3
Load_3130	1Ø CT XFMR	T_bus3130_L	120	wye-PQ	5
Load_3131	1Ø CT XFMR	T_bus3131_L	120	wye-PQ	7
Load_3132	1Ø CT XFMR	T_bus3132_L	120	wye-PQ	5
Load_3134	1Ø CT XFMR	T_bus3134_L	120	wye-PQ	6
Load_3135	1Ø CT XFMR	T_bus3135_L	120	wye-PQ	6

Continued on next page

Load Name	XMR Type	Bus	V (V)	Connection & Model	Customers
Load_3136	1Ø CT XFMR	T_bus3136_L	120	wye-PQ	7
Load_3137	1Ø CT XFMR	T_bus3137_L	120	wye-PQ	9
Load_3138	1Ø CT XFMR	T_bus3138_L	120	wye-PQ	5
Load_3139	1Ø CT XFMR	T_bus3139_L	120	wye-PQ	1
Load_3141	1Ø CT XFMR	T_bus3141_L	120	wye-PQ	5
Load_3142	1Ø CT XFMR	T_bus3142_L	120	wye-PQ	5
Load_3143	1Ø CT XFMR	T_bus3143_L	120	wye-PQ	7
Load_3144	1Ø CT XFMR	T_bus3144_L	120	wye-PQ	3
Load_3145	1Ø CT XFMR	T_bus3145_L	120	wye-PQ	5
Load_3146	1Ø CT XFMR	T_bus3146_L	120	wye-PQ	5
Load_3147	1Ø CT XFMR	T_bus3147_L	120	wye-PQ	17
Load_3148	1Ø CT XFMR	T_bus3148_L	120	wye-PQ	8
Load_3149	1Ø CT XFMR	T_bus3149_L	120	wye-PQ	4
Load_3150	1Ø CT XFMR	T_bus3150_L	120	wye-PQ	4
Load_3151	1Ø CT XFMR	T_bus3151_L	120	wye-PQ	4
Load_3152	1Ø-CT XFMR	T_bus3152_L	120	wye-PQ	3
Load_3153	1Ø-CT XFMR	T_bus3153_L	120	wye-PQ	8
Load_3154	1Ø-CT XFMR	T_bus3154_L	120	wye-PQ	4
Load_3155	1Ø-CT XFMR	T_bus3155_L	120	wye-PQ	4
Load_3157	1Ø-CT XFMR	T_bus3157_L	120	wye-PQ	12
Load_3158	1Ø-CT XFMR	T_bus3158_L	120	wye-PQ	7
Load_3159	1Ø-CT XFMR	T_bus3159_L	120	wye-PQ	10
Load_3160	1Ø-CT XFMR	T_bus3160_L	120	wye-PQ	4
Load_3161	1Ø-CT XFMR	T_bus3161_L	120	wye-PQ	5
Load_3162	1Ø-CT XFMR	T_bus3162_L	120	wye-PQ	3

Note: The hourly demand data of the 240-bus PDN for complete one complete year is downloaded from, https://wzy.ece.iastate.edu/Testsystem.html

Appendix B

NHTS Data

The data for NHTS for the year 2009 and 2017 is downloaded from the following link,
https://nhts.ornl.gov/downloads

Appendix C

NASA Data for Wind-speed and Solar-irradiance

The data for the complete one year of solar irradiance and windspeed is download from the following website, https://power.larc.nasa.gov/data-access-viewer/

Appendix D

Manufacturer's Datasheet for Vestas 500 kW WT

Table D.1: Specifications of Vestas V39 WT [9]

Parameter	Value
R	19.5 m
$P_{w,r}$	500 kW
v_r	15 m/s
v_{ci}	4 m/s
v_{co}	25 m/s

Appendix E

Manufacturer's Datasheet for SILFAB SOLAR 500kW SPV Module

Table E.1: Specifications of SIL-500 HM SPV Module [10]

Module Characteristics	**Value**
Peak Power (W)	500
Open Circuit Voltage (V), V_{OC}	45.78
Short Circuit Current (A), I_{SC}	13.48
Voltage at Maximum Power (V), V_{MPP}	38.8
Current at Maximum Power (A), I_{MPP}	12.89
Voltage Temperature Coefficient (V°/C), C_V	-0.28%
Current Temperature Coefficient (A°/C), C_I	+0.064%
Nominal Cell Operating Temperature (°C), N_{OT}	45
Module Efficiency	21%